TRANSIENT CONDUCTION AND RADIATION IN A SEMI-TRANSPARENT PHASE CHANGE MEDIUM IN AN ANNULUS

by

Kwang S. Kim

B.S.M.E., Hanyang University, Seoul, Korea, 1978
M.S.M.E., University of Kansas, Lawrence, Kansas, 1982

Submitted to the Department of Mechanical Engineering and the Faculty of the Graduate School of the University of Kansas in partial fulfillment of the requirements for the degree of Doctor of Philosophy.

Dissertation Committee:

Redacted Signature

Redacted Signature

Redacted Signature

Redacted Signature

Dissertation Defended: 3/18/86

TABLE OF CONTENTS

ABSTRACT

The effect of thermal radiation on the solidification of an absorbing, emitting, isotropically scattering infinite and finite, semi-transparent gray medium bounded between two concentric cylinders is investigated. The conservation of energy principle employing enthalpy and temperature as dependent variables is coupled with a set of moment equations which are derived from the radiative transfer equations and Marshak type boundary conditions by applying P-1 differential approximations.

The transient temperature distribution, interface location of a semi-transparent phase change medium, and the local radiative radial and axial heat flux has been obtained by using a Gauss-Seidel iterative numerical scheme for some typical geometric dimensions and parameters. The numerical results for the one-dimensional axisymmetric case of pure conduction are verified by comparison with an analytical approximation where the change in the internal energy in the solid phase is neglected.

The results for an optically thick cylindrical medium are obtained, analyzed, and displayed in graphs.

NOMENCLATURE

a	absorption coefficient, m^{-1}
A	area, m^2
B	medium emissive power, $n^2\sigma T^4$, W/m^2
C	specific heat, J/kg K
C^*	speed of electromagnetic radiation propogation in a vacuum, m/s
Fr	dimensionless radial radiative flux, $q_r/\sigma T_r^4$
Fz	dimensionless axial radiative flux, $q_z/\sigma T_r^4$
g	acceleration of gravity, m/s^2
h	specific enthalpy, J/kg
h_s	specific enthalpy of solid at fusion temperature, J/kg
h_{sl}	latent of fusion, J/kg
h^*	Planck's constant, 1.381×10^{-23} J/K
I	intensity of radiation, W/m^2
I_r	reference intensity of radiation, W/m^2
I_ν	spectral intensity of radiation, W/m^2
$I_{b\nu}$	spectral Planck's function, or black body intensity, W/m^2
K	thermal conductivity, W/m K
K_s	thermal conductivity of solid at fusion temperature, W/m K
K_1, K_2	thermal conductivity of element surfaces at
K_3, K_4	$\tau = \tau_i + \frac{\delta\tau}{2}$, $\tau = \tau_i - \frac{\delta\tau}{2}$, $\eta = \eta_i + \frac{\delta\eta}{2}$, and $\eta = \eta_i - \frac{\delta\eta}{2}$ respectively, W/m K
L	dimensionless solid/liquid interface, ℓ/r_I
ℓ	radius of solid/liquid interface, m
$\ell_r, \ell_\theta, \ell_z$	directional cosines, $\sin\gamma\cos\varphi$, $\sin\gamma\sin\varphi$, $\cos\gamma$, respectively

$\vec{n}$	unit normal vector
n	index of refraction
N	conduction/radiation paramenter, $K_s \beta/4\sigma T_r^3$
p	pressure, $kg/m\ s^2$
q	integrated radiative heat flux vector, W/m^2
q_r	integrated radial radiative heat flux, W/m^2
q_z	integrated axial radiative heat flux, W/m^2
r	radial distance, m
$\vec{r}$	spatial direction vector, see Fig. 3.2, m
r_I	radius of inner cylinder, m
r_o	radius of outer cylinder, m
R	dimensionless radius, r/r_I
s	distance measured along beam of radiation, see Fig. 3.2, m
S	dimensionless parameter, $K_s T_r/4\ \alpha_s\ \rho_s\ hsl$
t	time, s
T	temperature, K
T_I	inside wall temperature, K
T_f	fusion temperature, K
T_r	reference temperature, K
T_o	outside wall temperature, K
u	specific internal energy, J/kg
v	volume, m^3
$\forall$	integration volume, m^3
z	axial distance, m
Z	dimensionless axial distance
α	thermal diffusivity, m^2/S
α_s	thermal diffusivity of solid at fusion temperature, m^2/S

β	extinction coefficient, $a+\omega$, m^{-1}
β^*	polar angle, see Fig. 3.4
γ	polar angle, angle from normal of area
ε_w	surface emissivity
η	axial optical coordinate variable, $(a+\omega)z$
Θ	dimensionless temperature
λ	scattering parameter, $\omega/(a+\omega)$
ν	frequency, s^{-1}
ξ	dimensionless time, $\alpha_s t\, \beta^2$
ρ	density of medium, kg/m^3
ρ_s	density of solid at fusion temperature, kg/m^3
σ	Stefan-Boltzmann constant, $W/m^2\, K^4$
τ	radial optical coordinate variable, $(a+\omega)r$
τ^*	optical depth in s-direction
φ	azimuthal angle for the intensity direction
Φ, Φ_w	dimensionless Planck functions $B/\pi I_r$ and $B_w/\pi I_r$, respectively
ψ	dimensionless intensity of radiation, I/I_r
ψ_o	dimensionless zeroth moment of intensity
ψ_r	dimensionless first moment of intensity in r-direction
ψ_z	dimensionless first moment of intensity in z-direction
ω	scattering coefficient, m^{-1}
ω^*	single scattering albedo, $\omega/(a+\omega)$
Ω	solid angle, steradian

SUBSCRIPTS

b	black
f	fusion
i	spatial location
I	inner
l	liquid
m	time level
o	outer
r	radial
s	solid
w	wall
z	axial
ν	frequency dependent

LIST OF FIGURES

Figures

Figures

Figures

Figures

Figures

Figures

Figures

ACKNOWLEDGEMENTS

I first express my deepest gratitude to my advisor, Dr. Bedru Yimer for his invaluable assistance, encouragement, and comments in the completion of this work.

I also extend my sincere appreciation to the members of my committee: Dr. Louis Burmeister, Dr. Richard Johnson, Dr. Chuan Lan, and Dr. Hillel Unz. Unlimited computing time on a Harris computer was provided by the School of Engineering, University of Kansas. The Departments of Mathematics and Mechanical Engineering have financially supported me during the course of the research.

Finally, I thank my wife, Kyung Jin, my son, Alfred Junghyun, and my parents for their motivation and support. The completion of this research would not have been possible without the patience and help of all the people mentioned.

CHAPTER 1

INTRODUCTION AND OBJECTIVES

1.1 INTRODUCTION

Because of the recent energy crisis and increase in energy prices, energy management has become an enduring concern. One of the many ways to manage energy is to store excess energy for use at a later time when it becomes necessary. Hence, efficient and reliable energy storage systems are of great interest. One of the energy storage methods is to use a phase change material as a thermal energy storage medium to store and release large amounts of thermal energy in the form of latent heat. The formation of fine quality crystals [3] is also an important phenomenon in which energy transfer analysis with phase change plays an important role.

Energy transfer problems in which one material is transformed into another or into another phase with generation or absorption of heat have been studied theoretically and experimentally for more than a century. Nearly all of these studies, however, have dealt with opaque materials and hence, the contribution of thermal radiation within the media has been ignored. Some of the investigators [3 - 9] over the past fifteen years have proved that for the range of parameters encountered in the solidification and melting of many optical materials, such as the weakly absorbing semi-transparent and partially transparent diathermanous solids, the internal radiant transfer has a significant effect, and neglecting it in the analysis leads to considerable error in predicted temperature distribution, interface position, and energy flux. More applications of this nature arise in areas such as freezing or melting of a solid, the growing of large

synthetic crystals and vapor films, the burning of solid propellants, the heating and cooling of spacecraft and aircraft windows and nuclear reactor fuel elements, converting energy in different solar devices, and others.

The analysis of combined energy transfer by conduction and radiation in participating materials is sufficiently complex so that numerical solutions are almost always required. As a result of the nonlinearity of these problems, some advanced and approximate analytical techniques have been used to obtain closed form solutions for a limited range of geometries and conditions. Although several investigators have dealt with the restricted one-dimensional Stefan problem that includes combined conductive and radiative transfer, little study, if any, has been devoted to the two-dimensional Stefan problem for a concentric cylindrical geometry.

Computations involving two-dimensional radiative fluxes with participating media are formidable. The difficulties arise for the following reasons. Quadruple integrals must be computed with respect to (1) physical distance, (2) optical thickness, (3) solid angle, and (4) wave length in order to obtain the local radiative flux. Even with the total band absorptance introduced, integrals with respect to (2) and (3) remain inevitable. Therefore, it has been necessary to develop some approximate methods for multi-dimensional analysis and possible parameterization studies.

1.2 OBJECTIVE OF INVESTIGATION

The objective of the present investigation is to develop and solve a two-dimensional radial and axial mathematical model to

determine the transient temperature distribution and interface location of a semi-transparent phase change medium bounded by two finite concentric cylinders when internal energy transfer occurs simultaneously by conduction and radiation for the solid region. The axial and radial local radiative heat fluxes and heat extraction rates from the inside pipe for different parameters are computed in order to observe the effect of radiation on the phase change medium of the system. In order to accomplish this objective, the classical Stefan problem [1,2] is to be reformulated to include the presence of internal radiative transfer, and then is to be solved by iterative numerical finite difference schemes using the appropriate thermal boundary/interface conditions. Because of the general lack of property data for the high solidification temperature materials, it is impossible to determine input parameters and properties specifically for a given substance. However, the approximate values of latent heat, conductivity, and specific heat with other several parameters for the solidification of fluorite (melting temperature of around 1700 K) are good enough to analyze and show the radiative effect on the present model. The gray medium will be assumed to be in local thermodynamic equilibrium (LTE), homogeneous, and isotropic with constant index of refraction within a given phase. This is a reasonable approximation in engineering applications [49].

The system, initially at the fusion temperature, is considered to be suddenly brought into intimate contact with the cold temperature at the inside cylinder. The walls of the enclosure are considered to be gray and diffuse and maintained at constant temperatures at the inside

and outside cylinder. The interface surface is to be assumed to be a diffuse gray surface and both base surfaces of the finite concentric cylinder are considered to be perfectly insulated. A schematic of the present physical system is shown in Figure 1, representing a heat pipe or thermal energy storage system (HP/TES system) for example.

CHAPTER 2

LITERATURE SURVEY

2.1 STEFAN PROBLEM WITH CONDUCTION AND RADIATION

Even though the solidification and melting of materials by heat transfer has been of importance in many technical fields and a subject of interest for over a century, considerable effort has been devoted to the Stefan problem with combined conductive and radiative transfer only over the past fifteen years.

Abrams and Viskanta [3,4] used explicit finite difference methods to investigate the effects of energy transfer for the range of dimensionless parameters governing phase change that is encountered in the melting and solidification of semi-transparent crystals. Consideration was limited to the one-dimensional radiative and conductive energy transfer in a region of finite thickness and of infinite lateral extent with physical assumptions, such as the absence of natural convection, the absence of scattering, isotropic media with uniform index of refraction for each phase, diffuse, parallel, and planar interfaces and boundaries, and so on. They found that radiation can significantly affect the dynamics of the solidification and melting of many optical materials; neglect of radiation can cause the temperature profile within the liquid to assume a shape which promotes unstable interfacial growth, a finding which is contrary to the idea that radiation always exerts a "stabilizing influence."

Habib [5,6] employed the approximate heat balance integral method to study the effect of the radiative heat transfer on the solidification rate and on the temperature distribution in the solid

phase of semi-transparent planar and infinite cylindrical media. The heat balance integral method of approximate analytical solution was developed by Goodman [11]. Habib used the trial temperature profile as the combination of polynomial and logarithmic functions. The constants in the trial function were determined from the boundary and the interfacial conditions. The significance of the radiative contribution to the process of phase change on the solidification rate and on the temperature distribution in the solid phase was presented with the results for the cases of absorbing, opaque, and non-participating media.

Ozisik [7] investigated the effects of radiation on the melting rate of an absorbing, emitting, scattering, semi-infinite, semi-transparent, homogeneous medium with reflective boundaries by solving the phase change and the radiative transfer problems simultaneously. Seki, Sugawara, and Fukusako [8] observed the phenomenon of back-melting caused by radiant energy penetrating through the ice layer. They experimentally found that the behavior of radiation transfer in a cloudy ice layer depends a great deal on the density of the cloudy ice, including air bubbles which produce scattering of radiation. They also showed that the melting rate of an ice layer can be predicted numerically by using the band model of extinction coefficient for the cloudy ice assumed.

The combined radiation and conduction problems with phase change for one-dimensional solidification of a semi-transparent, semi-infinite, gray, homogeneous and isotropic material with constant thermophysical and optical properties was solved by Chan and Albeirutty [9]. The B-splines collocation method with optimum

choice of collocation points was used to solve a non-linear integro-differential equation that can hardly be solved by using the available analytical methods in the literature. This method employed the unknown n-coefficients of the approximating polynomial that were evaluated by requiring that the integro-differential equation be satisfied at n-2 collocation points. This procedure reduced the nonlinear partial differential equation to a set of nonlinear ordinary differential equations.

Ortega, Benard, and Gobin [10] presented the results of experiments using paraffin wax as a storage medium in a storing wall (Trombe wall) leading to a study of the influence of various heat transfer modes (radiation, convection, conduction) on the melting process and the storage efficiency. The experiments showed a linear correlation between the volume of the liquid phase and the stored energy. The amount of energy stored by the element during the storage process was measured by calorimetry.

A more general solidification and melting one-dimensional model was recently proposed by Chan and Cho [12] which accounts for the existence of a two phase zone in which partial phase change can occur. The two phase zone was attributed to internal solidification or melting (as opposed to surface solidification or melting) induced by internal thermal radiation. Diaz and Viskanta [13] developed an analytical model for predicting radiative and thermal conditions during radiation induced phase change, as well as liquid/solid interface displacement with time. Energy equations are written separately for the two phases and required to meet simultaneous temperature and energy balance considerations at a common boundary, the liquid/solid

interface. Experimental simulations were conducted, using a high intensity tungsten filament lamp to melt both horizontal and vertical slabs of a low fusion temperature material (n-octadecane).

According to the literature surveyed, most of the approximate analytical methods and numerical methods that have been developed were used to solve one-dimensional Stefan planar problems including radiation and conduction with restrictive boundary conditions and physical optical properties. The energy balance has been separately applied for each phase and the proper boundary and interfacial conditions that couple the two phases. Temperature has been used as the dependent variable.

One of the techniques used to solve the Stefan problem is the "enthalpy method" which involves both temperature and enthalpy as the dependent variables. It was used by Shamsundar and Sparrow [14] to solve a pure conduction problem of a two-dimensional solidifying liquid that was initially at the fusion temperature. In this approach, the energy balance can be applied over the whole domain that covers both solid and liquid phases. Reformulation of the describing equations in terms of the enthalpy (i.e., the sum of the sensible and latent heats) removes the need to directly trace the position of the moving boundary and, hence, eliminates the numerical problems associated with the discontinuity of the temperature gradient. The use of the enthalpy model to solve the Stefan problem, including combined radiative and conductive transfer, has not been reported.

2.2 STEFAN PROBLEM

The formulation of the Stefan problem in one dimension has been known for more than a century. Hence, the Stefan literature has been concerned primarily with methods of solution rather than formulation.

During the past years, however, considerable effort [15-18] has been devoted to formulate and solve the two-dimensional Stefan problem even though the analysis of phase change problems in multi-dimensional regions is complicated and there is no obvious method to assess the reliability of the predictions. When radiation is present, the energy equation is nonlinear and the situation is much more complex than for pure conduction. Comprehensive surveys on moving interface problems appear in references [19-21].

The most popular approximate techniques used in the literature include pertubation, variational, heat balance integral, and series solution methods. As one of the simplest approaches, Goodman [22] employed the "integral method." This method requires assumption of a functional form of the solution which contains undetermined time-dependent coefficients. The assumed function is substituted into the governing differential equation which, together with the imposed boundary conditions, leads to one or more ordinary differential equations. Solutions of these equations, accomplished numerically in general, yield the undetermined coefficients.

Nonlinear differential equations can be solved by the "pertubation technique" which employsthe unknown function in the form of asymptotic expansions [23]. Yan and Huang [24] obtained pertubation solutions for the one-dimensional phase change problem in a finite region subject to convection and radiative boundary conditions

at the fixed boundary. Yen and Chung [25] used Biot's variational method to develop approximate analytical solutions for the location of the interface and temperature distribution for the one-dimensional phase change problem. The variational method reduces the more complicated nonlinear problem to a much simpler initial value problem which is then more easily solved using standard numerical techniques (e.g., Yen and Chung used the Runge-Kutta method).

In the other approach, the energy equation can be converted into general integral equations through the use of Green's functions [26]; the latter are solved numerically. The advantage of the integral formulation is that the solution can be obtained by the method of successive substitutions [27], which is an exact method in the sense that results can be computed within an arbitrary degree of accuracy. The disadvantage of this method is the excessive computing time requirement [28]. Abrams [3] formulated the integral equation for the one-dimensional Stefan problem, constant thermal conductivity and specific heat, and the same density in two phases, including radiation, by using Green's functions. However, practically speaking, the scarcity in the literature of numerical solutions to much simpler problems, strongly suggested that a numerical approach lacked feasibility in his formulation.

Yimer [21] formulated and developed the transient conductive analysis of phase change material contained within two coaxial cylinders with and without fins. The powerful enthalpy model together with the finite difference scheme was employed to compute the temperature distribution, interfacial location, and heat flux subject to various boundary conditions.

More recently, some of the work for the Stefan problem included natural convection effects along with conduction. Comprehensive reviews concerning natural convection effects are found in references [29,30]. Yao and Chen [31] demonstrated the increasing effect of natural convection on the melting process around a heated horizontal cylinder by using the regular pertubation series.

Saitoh and Hirose [32] obtained the transient aspects for natural convection flow, temperature profiles and melting interfaces inside a horizontal circular cylinder capsule, in which n-octadecane or water was used as a phase change material, by using an explicit finite difference scheme. A numerical procedure was developed by Chan and Schoukri [33] to analyze two-dimensional freezing with natural convection at the solid/liquid interface. The problem was divided into two parts. The first part solved the natural convection flow in the phase change medium using a well-established finite difference method, the simplified marker and cell technique. The second part calculated the local freezing rate using a local one-dimensional energy balance model. The two parts were coupled at the solid/liquid interface.

Rieger, Projahn, Bareiss, and Beer [34] investigated the melting process of a phase change material enclosed in a horizontal, isothermal circular tube by using a numerical mapping technique and allowing the melting front to be recorded photographically with time. Computations and experiments were performed for Rayleigh numbers in the range $10^5 \leq Ra \leq 10^6$.

2.3 COMBINED RADIATIVE AND CONDUCTIVE TRANSFER

Simultaneous heat transfer by conduction and radiation in semi-transparent participating media is a subject of considerable technological application which has received a great amount of attention particularly in connection with gray analysis [35-39]. Comprehensive surveys on combined conductive and radiative problems in participating media through 1975 appear in references [3,40]. The planar geometry with one-dimensional energy transfer has been the subject of much study and continues to serve as a standard of comparison. Radiative transfer with conduction has been studied in other one-dimensional geometries, but very little has been done with multi-dimensional geometries.

Viskanta and Hirleman [41] presented an analytical solution for the steady-state temperature distribution in a plate of semi-transparent solid which is irradiated on one side by beam (collimated) and diffuse fluxes. The validity of neglecting the interaction of conduction with radiation in the solid was examined by comparing the heat transfer rates predicted with those based on an approximate approach. The importance of radiation on the temperature distribution in a semi-transparent planar solid was reported by Amlin and Korpela [42].

The first-order differential approximation [42-47] of radiation was combined with conduction analysis to investigate the temperature profiles in a plane slab and a rectangular region. The coupled non-linear partial differential equations were solved numerically by either a standard implicit (backward difference in time and central in space) or an implicit alternating direction method. The effects of

Planck number, boundary emissivity, surface reflectivity, external temperature, and optical thickness were reported.

Heat transfer by simultaneous conduction and radiation in an absorbing, emitting, and anisotropically-scattering material was theoretically investigated by Yuen and Wang [48]. Consideration was given to a one-dimensional system bounded by two parallel gray, diffuse, and isothermal walls. Assuming a physical model of linear anisotropic scattering, the resulting integral-differential equation was solved by a successive approximation technique similar to the method of undetermined parameters.

Viskanta and Kim [49] presented a model for predicting conduction and radiation heat transfer across an irradiated plane layer of semi-transparent material at high temperature. A model for the prediction of radiative transfer was too complicated for design calculations. The validity and accuracy of the model was established by comparing the predictions with those reported in the literature.

Fernandes and Francis [50] formulated and solved the problem of transient combined conduction and radiation in a gray absorbing, emitting, and scattering medium of infinite cylindrical geometry. The medium was bounded by gray diffuse surfaces at known temperatures. The problem was solved by the Galerkin finite element method using linear interpolating functions. The transient terms were handled using the Crank-Nicolson scheme with the time steps chosen to avoid temperature fluctuations at early times.

Tsai and Chan [51] investigated the transient temperature distribution of two semi-infinite media at different temperatures that are suddenly brought into contact. The effect of thermal radiation in

the hot medium was considered. Solutions were obtained by a hybrid technique, using an explicit fourth-order Runge-Kutta method for the space variable. A variable grid spacing system utilizing hyperbolic sine functions was incorporated to extend the computational boundary as well as to minimize the computation time and the number of nodal points.

A one-dimensional combined conduction and radiation heat transfer problem between two isothermal parallel plates, where the intervening medium may absorb, emit, and isotropically scatter radiation, was considered by Ratzel and Howell [52] using the P-1 and P-3 differential approximations for the intensity distribution. The P-1 and P-3 methods yielded results for combined conduction-radiation problems which are in close agreement with "exact" solutions for one-dimensional planar problems.

Tong, Birkebak, and Enoch [53] considered the effect of thermal radiation with conduction and convection in vertical rectangular enclosures containing a porous medium, radiation having been neglected in previous publications. The enclosure was considered to be tall enough so that one-dimensional radiation exchange could be assumed to take place between the two vertical surfaces. It was further assumed that the fluid is non-participative in the radiative transfer process whereas the solid matrix emits, absorbs, and scatters thermal radiation. Shih and Chen [54] presented a modified version of the flux method, called the discretized intensity method, in which the intensity, a variable more primitive than the flux, was introduced to solve a two-dimensional system enclosing radiative and conductive media of unit depth. This method bypasses the unnecessary use of the

integro-differential energy transport equation and accounts for the dimensionality of the radiative fluxes.

Chung and Kim [55] presented a two-dimensional analysis of combined conductive, convective, and radiative heat transfer using finite elements. The standard Galerkin finite element could be used if the product of Reynolds number and Prandtl number was equal to or less than 1000. It was shown that the two-dimensional radiation function in terms of space surface and volume integrals could be efficiently performed via Gaussian quadrature applied to isoparametric finite elements. Numerical results were demonstrated for a diverging and converging channel with restrictive boundary conditions.

Rassaque, Howell, and Klein [56] presented the first numerical solution of the exact equations of coupled radiative/conductive heat transfer and temperature distribution inside a medium, and of the heat flux distribution at all the diffuse gray walls of a two-dimensional rectangular enclosure with the medium having uniform absorbing/emitting properties, using the finite element method. The drawback of this method, as for most others, is that for very low values of wall emissivity and conduction/radiation parameter, it requires a substantial amount of time to achieve convergence.

Very recently, a modified finite difference approach to the problem of transient combined conduction and radiation in an absorbing and emitting infinite annular medium was presented by Gordaninejad and Francis [57]. The energy equation was formulated in a finite difference format using the explicit form of the time derivative. Simpson's method with the Gauss quadrature (five points) was used to approximate the integrals.

2.4 MULTI-DIMENSIONAL AND CYLINDRICAL RADIATIVE TRANSFER

It has been seen that due to the complexity of coupled radiative and conductive heat transfer problems in the two-dimensional geometry, most of the work that has been reported in this area is confined to the one-dimensional planar radiative case. Nevertheless, since general and accurate solutions of the radiative transfer equation (RTE) are required now more than ever, especially for multi-dimensional geometries, a wide variety of solution methods have been developed.

Crosbie and Liesenbardt [58], in their study on the two-dimensional radiative transfer, have presented a comprehensive overview of a number of methods that were used to solve the RTE for various physical situations. Most works for multi-dimensional radiative transfer used some approximations [59-65] (i.e., the diffusion approximation, the discrete ordinates and Fourier transform methods, and the six flux approximation). The stochastic models such as Monte Carlo technique [66,67] and Hottel's zonal method [68-70] have been employed.

An extensive survey of the latest multi-dimensional rectangular radiative transfer models was reported by Howell [71]. Very recently, the radiative transfer in a three-dimensional rectangular enclosure containing radiatively participating gases and particles was studied using the spherical harmonics approximation by Viskanta and Menguc [72]. Inhomogeneities in the radiative properties of the medium as well as in the radiation characteristics of the boundaries were allowed in order to obtain the numerical solution of the model

equations by using a finite difference scheme. The third order spherical harmonics (P-3) approximation was stated as the optimum choice for general multi-dimensional radiative transfer calculations, both from the accuracy and the computational effort points of view [71,73].

Radiative heat transfer in a cylindrical geometry arises in numerous problems but has received relatively little attention due to its complexities [40]. Starting from the basic RTE, Kuznetsov [74] and Kesten [75] analyzed radiative transfer in an infinitely long cylindrical medium bounded by the opaque black walls. In this analysis the radiative heat flux was expressed in terms of a second-order integral equation. Kesten's results are presented in two different forms, the latter of which appears to be incorrect due to an integral transformation error. Later, Habib and Greif [76], in presenting an analysis on nongray gas effects, used the erroneous equation of Kesten [75] in their calculations and reported a discrepancy between their results and Kesten's. They also developed a kernel approximation which used a total band absorptance model for radiation.

Nakra and Smith [77] studied the interaction of radiative transfer with convection for slug flow in an absorbing-emitting gas in a circular tube with an isothermal black wall. They used the zone method for their numerical calculations.

Heaslet and Warming [78] developed analytical and numerical methods for predicting radiative transfer for a homogeneous medium of one-dimensional cylindrical geometry. Although their formulation accounted for isotropic scattering, they did not present any exact

results for scattering media. Echigo, et al. [79] used Heaslet and Warming's [78] radiation model to study the effect of radiative transfer in laminar and turbulent flow of gas particulate suspensions in circular tubes. In their analysis, the medium was assumed to be gray and non-scattering.

The first systematic approach for the exact calculation of multi-dimensional radiative heat flux in a cylindrical emitting-absorbing non-isothermal medium with non-isothermal black bounding walls was described by Dua and Cheng [80]. Numerical results were presented for the case of isothermal media bounded by piecewise isothermal walls. Bagazitoglu and Higenyi [81] introduced a higher-order differential approximation, applying it to infinite concentric cylinders. The series expansion of the angular distribution of radiative intensity needed by the boundary conditions was extended to include the number of terms in the P-3 approximation. They [82] also used the P-1 differential approximation, whose accuracy turns out to be very good for optically thick medium, to analyze an axially symmetric radiation field for a gray medium within a finite, cylindrical enclosure. The medium emits, absorbs, and isotropically scatters radiant energy and was subject to a specified heat generation. Numerical solutions were obtained for the one-dimensional radiative heat flux and emissive power distribution. It was found that the accuracy of the differential approximation is of the same order for the axially symmetric and one-dimensional problems.

An exact solution for radiative transfer in a gray, emitting, absorbing and linear-anisotropically scattering medium of one-dimensional cylindrical geometry had been developed by Azad and Modest

[83]. The exact results were compared with two approximate models, viz. (1) the differential approximation, (2) a kernel approximation. The first model reduced to the correct optically thick and thin limits and also yields reasonable results in the optically intermediate range. The second model produced excellent results for the optically thin regions and by appropriate choice of two constants it could also yield good approximations for the radiative flux at larger values of optical thickness. In addition, the results showed that in many engineering applications scattering might be neglected without significant loss of accuracy.

The basic RTE in three-dimensional space was expressed in terms of three commonly used coordinate systems, namely, Cartesian, cylindrical and spherical coordinates by Ou and Liou [84]. The concept of a transformation matrix was applied to the transformation processes between the Cartesian system and two other systems. The spherical harmonic method was then applied to decompose the RTE into a set of coupled partial differential equations for all three systems in terms of partial differential operators with the vacuum boundary conditions (no inward diffuse intensity). The analytical solutions in terms of infinite series were obtained.

The P-N method was used to compute the partial heat fluxes relevant to radiative transfer in an anisotropically scattering plane-parallel medium with specularly and diffusely reflecting boundaries by Siewert, Benassi, and Cotta [85]. They made use of exact particular solutions and the spherical harmonics method to compute the partial heat fluxes for the same class of problems.

Crosbie and Farrel [86] recently developed the first exact formulations for the source function, flux, and scattered intensity normal to the surface in cylindrical coordinates for a three-dimensional, absorbing, emitting, isotropically scattering medium exposed to both diffuse and collimated radiation. The collimated and diffuse radiation incident on the one side of three-dimensional geometry was used without taking into account boundary reflections.

2.5 SUMMARY

It is concluded from the objective of this investigation and the current state of the problem or related areas (unsteady combined conductive and radiative heat transfer, Stefan problems, and cylindrical radiative transfer) that of prime interest in the present investigation is the applications of the "enthalpy method" with the divergence of the radiative flux vector. The mathematical formulation of the problem with boundary and interfacial conditions is to be developed, as is approximate numerical method to determine the radiative heat flux, which can be coupled with the principle of energy conservation that employs enthalpy, temperature, and radiative heat flux as dependent variables.

CHAPTER 3

ANALYTICAL APPROACH

The energy balance including radiant heat flux for a control volume is considered by employing the "enthalpy model." The general radiative transfer equation for arbitrary geometry is used to develop exact expressions for the radiative intensity distribution of a two-dimensional finite concentric cylindrical geometry with given boundary conditions. This exact formulation has not been reported in the literature.

3.1 THE LAW OF CONSERVATION OF ENERGY

In developing the describing equations, a method that uses the enthalpy along with the temperature as dependent variables is employed. In this approach, the energy equation is applied once over the complete domain covering both phases. The location of the solid/liquid interface is eliminated from the formulation and is obtained as one of the results of the solution after the temperature distribution is found. The equivalence between the enthalpy model and the conventional form of the energy conservation equations where temperature is the sole dependent variable is shown by Shamsundar and Sparrow [14].

The development assumes no energy source, no pressure variation, and no external work done on the control volume. Convection within the fluid is neglected. Applying the law of conservation of energy to a control volume, the net rate of energy increase of a control volume is equated to the net rate at which heat is conducted and radiated into the control volume through its surface area.

$$\frac{d}{dt}\iiint_{\forall} \rho u d\forall = \iint_{A} K \text{ grad } T\cdot\vec{n}\, dA - \iint_{A} \vec{q}\cdot\vec{n}\, dA + \cancel{e}^{\,0} + \cancel{\mu}^{\,0} \qquad (3.1)$$

$$\left[\begin{array}{c}\text{net rate of energy}\\ \text{increase of control volume}\end{array}\right] = \left[\begin{array}{c}\text{net rate at which}\\ \text{heat is conducted}\end{array}\right] + \left[\begin{array}{c}\text{net rate at which}\\ \text{heat is radiated}\end{array}\right]$$

$$+ \left[\begin{array}{c}\text{heat}\\ \text{generation}\end{array}\right]^{\,0} + \left[\begin{array}{c}\text{dissipated heat}\\ \text{by viscous effects}\end{array}\right]^{\,0}$$

where e is the local heat source, and μ is the heat production rate by viscous dissipation. When the internal energy (u) is replaced by the difference between enthalpy and pressure and assuming that

$$\frac{d}{dt}\iiint p\, dv = 0$$

Equation (3.1) takes the form

$$\frac{d}{dt}\iiint_{\forall} \rho h d\forall = \iint_{A} K \text{ grad } T\cdot\vec{n}\, dA - \iint_{A} \vec{q}\cdot\vec{n}\, dA \qquad (3.2)$$

The above Equation (3.2) includes the conventional interface condition, and the verification is shown in Appendix A.

In the analysis of the two-dimensional case with radial and axial variations, the region of interest ($r_I \leq r \leq r_o$, $0 \leq z \leq z^*$) is subdivided into smaller elements. Each element is a concentric ring of width δr and depth δz (See Figure 3.1).

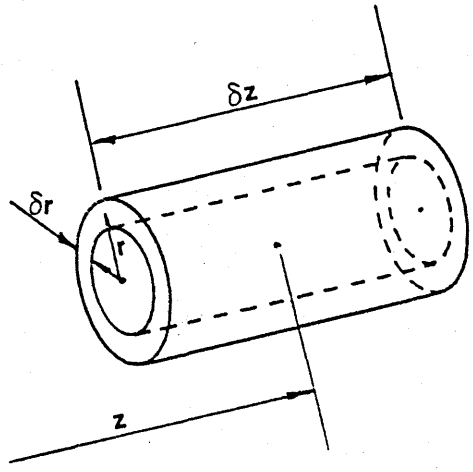

Figure 3.1 Two-Dimensional Element

Then the average values of the enthalpies, the temperatures, and the radiant heat fluxes at the nodal points (r, z) at the centers of the elements are studied as function of time. Assuming the temperature to be uniform over an element, Equation (3.2) for an element takes the form

$$\frac{d}{dt} \int_{r-\frac{\delta r}{2}}^{r+\frac{\delta r}{2}} \int_{z-\frac{\delta z}{2}}^{z+\frac{\delta z}{2}} (\rho h) 2\pi r \delta z \delta r = K_1 \frac{\partial T}{\partial r}\Big)_{r+\frac{\delta r}{2}} \cdot 2\pi\left(r + \frac{\delta r}{2}\right) \delta z$$

$$- K_2 \frac{\partial T}{\partial r})_{r-\frac{\delta r}{2}} \cdot 2\pi(r - \frac{\delta r}{2})\delta z + K_3 \frac{\partial T}{\partial z})_{z+\frac{\delta z}{2}} \cdot 2\pi r \delta r - K_4 \frac{\partial T}{\partial z})_{z-\frac{\delta z}{2}} \cdot 2\pi r \delta r$$

$$- q_r)_{r+\frac{\delta r}{2}} \cdot 2\pi(r + \frac{\delta r}{2})\delta z + q_r)_{r-\frac{\delta r}{2}} \cdot 2\pi(r - \frac{\delta r}{2})\delta z - q_z)_{z+\frac{\delta z}{2}}$$

$$\cdot 2\pi r \delta r + q_z)_{z-\frac{\delta z}{2}} \cdot 2\pi r \delta r \qquad (3.3)$$

3.2 INTEGRAL EQUATION FORMULATION AND RADIATIVE FLUX

The equation of radiative transfer theory is derived by making a radiant energy balance on an elementary solid angle and accounting for all phenomenological transformations experienced by the radiation as it passes through a participating medium [40,66,86]. The spectral intensity I_ν ($\vec{r},\vec{s}$) defining the radiation field is governed by the equation of transfer in the radiant direction along $\vec{s}$, i.e.

$$\frac{1}{C^*} \frac{\partial I_\nu}{\partial t} + s \cdot \nabla I_\nu = -\beta_\nu I_\nu + a_\nu n^2 I_{b\nu} + \frac{\omega_\nu}{4\pi} \int_{\Omega_i} I_\nu \zeta(\nu, \Omega, \Omega_i)\, d\Omega_i \qquad (3.4)$$

$$\left[\begin{array}{l}\text{local and spatial} \\ \text{changes in intensity}\end{array}\right] = \left[\begin{array}{l}\text{loss by absorption and} \\ \text{scattering}\end{array}\right]$$

$$+ \left[\text{gain by emission}\right] + \left[\begin{array}{l}\text{gain by scattering} \\ \text{into s-direction}\end{array}\right]$$

where $\zeta(\nu,\Omega,\Omega_i)$ is the phase function whose physical interpretation is the scattered intensity in a direction, divided by the intensity

that would be scattered in that direction if the scattering were isotropic, and $I_{b\nu}$ (T) is Planck's function

$$I_{b\nu}(T) = \frac{2\pi h^* \nu^3}{C^{*2}} \cdot \left[\exp\left(\frac{h\nu}{KT}\right) - 1\right]^{-1} \tag{3.5}$$

When the coordinate s is placed along the direction $\vec{s}$, the directional derivative $(\vec{s} \cdot \nabla) I_\nu$ becomes dI_ν/ds (see Figure 3.2). For most applications, it is usually assumed that a steady state condition prevails since the speed of propagation C^* is very large. Then equation (3.4) becomes

$$\frac{dI_\nu}{d\tau^*_\nu} + I_\nu(\tau^*_\nu) = S^*_\nu(\tau^*_\nu, \Omega) \tag{3.6}$$

where τ^*_ν is the optical depth or opacity when both scattering and absorption are present, or $\tau^*_\nu = \int^S \beta_\nu ds'$, and the source function $S^*_\nu(\tau^*_\nu, \Omega)$ is employed as

$$S^*_\nu(\tau^*_\nu, \Omega) = (1 - \omega^*) n^2_\nu I_{b\nu}(\tau^*_\nu) + \frac{\omega^*}{4\pi} \int_{\Omega_i = 4\pi} I_\nu(\tau^*_\nu, \Omega_i) \zeta(\nu, \Omega, \Omega_i)\, d\Omega_i \tag{3.7}$$

Equation (3.6) is an integro-differential equation since I_ν is within the integral of the source function. The integration over the solid

angle $d\Omega_i$ is an integration of the intensity at s over all possible directions.

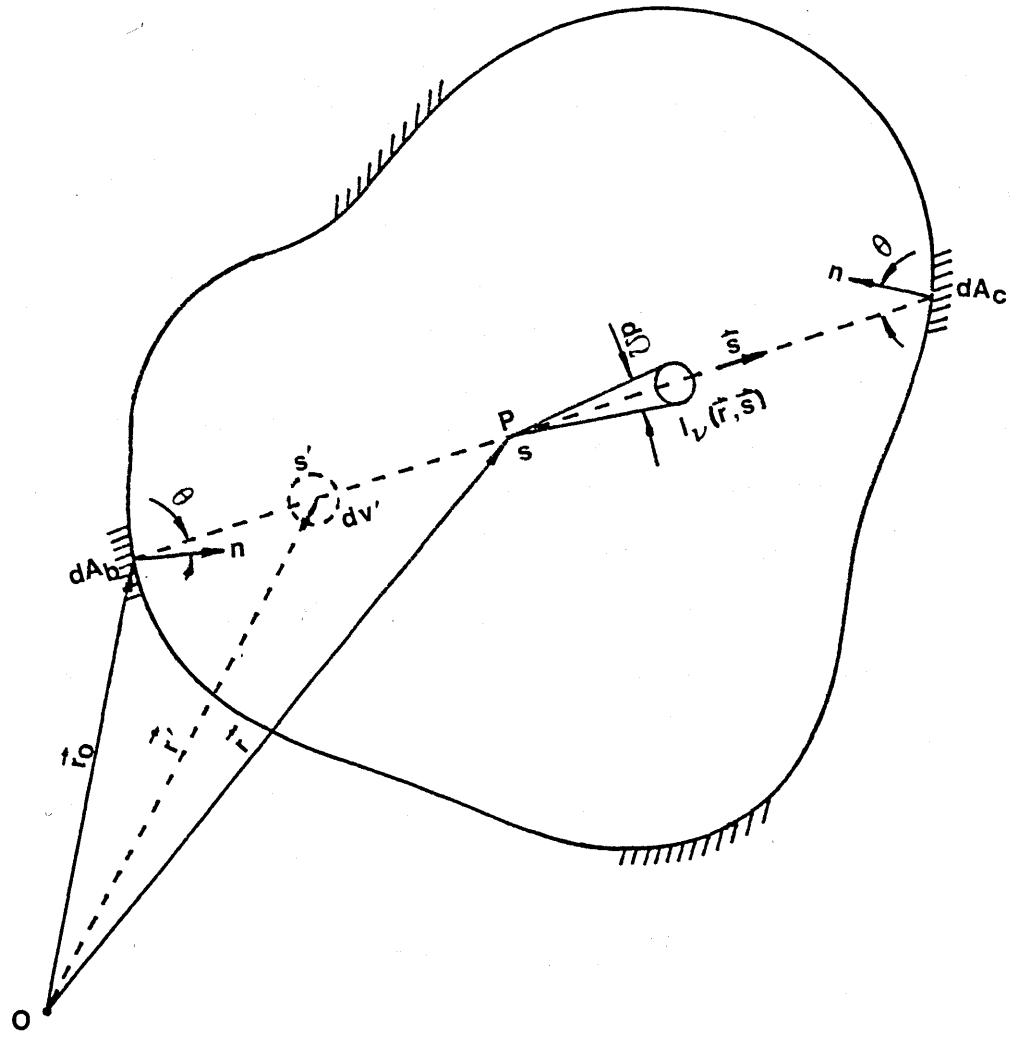

Figure 3.2 Radiative Intensity In an Arbitrary Geometry

By use of the integrating factor exp τ_ν^*, Equation (3.6) is integrated over an optical thickness from $\tau_{\nu b}^* = \int_0^{s_b} \beta_\nu ds'$ to $\tau_\nu^* = \int_0^{s} \beta_\nu ds'$, i.e.,

$$I_\nu(\tau_\nu^*) = I_\nu(\tau_{\nu b}^* , \Omega_b) \exp [- (\tau_\nu^* - \tau_{\nu b}^*)]$$

$$+ \int_{\tau_{\nu b}^*}^{\tau_\nu^*} S_\nu^* (\tau_\nu^{*'} , \Omega) \exp [- (\tau_\nu^* - \tau_\nu^{*'})] \, d\tau_\nu^{*'} \qquad (3.8)$$

where $\tau_\nu^{*'}$ is a dummy variable of integration, $I_\nu (\tau_{\nu b}^*, \Omega_b)$ is the intensity incident on the medium at S_b, and Ω_b defines the angular dependency with respect to the inward drawn normal to the boundary. $I_\nu (\tau_\nu^*)$ can be determined if the source function $S_\nu^* (\tau_\nu^*, \Omega)$ is known. By substitution of Equation (3.8) for the intensity into the definition for the source function, Equation (3.7), an integral equation for the source function is obtained, i.e.

$$S_\nu^*(\tau_\nu^* ,\Omega) = (1-\omega^*) n_\nu^{*2} I_{b\nu} (\tau_\nu^*) + \frac{\omega^*}{4\pi} \int_{4\pi} I_\nu(\tau_{\nu b}^*,\Omega_b) \, \zeta(\nu,\Omega.\Omega_b) \cdot$$

$$\exp [- (\tau_\nu^* - \tau_{\nu b}^*)] \, d\Omega_b + \frac{\omega^*}{4\pi} \int_{4\pi} \int_{\tau_{\nu b}^*}^{\tau_\nu^*} S_\nu^*(\tau_\nu^{*'} , \Omega_i) \cdot$$

$$\zeta(\nu,\Omega,\Omega_i) \exp [- (\tau_\nu^* - \tau_\nu^{*'})] \, d\tau_\nu^{*'} \, d\Omega_i \qquad (3.9)$$

For the special case of constant absorption coefficient a_ν and neglecting a scattering effect ($\omega_\nu = 0$), Equation (3.8) reduces to

$$I_\nu(s) = I_\nu(s_b,\Omega_b) \exp\left[-a_\nu (s - s_b)\right] + a_\nu n_\nu^2 \int_{s_b}^{s} I_{b\nu}[T(s')] \exp\left[-a_\nu \cdot (s - s')\right] ds' \tag{3.10}$$

The absence of scattering applies to the physical situation where the solid phases are either all single crystals or consist of polycrystals which are small compared to the wave lengths of the incident radiant energy. The scattering of thermal radiation by de-gassed liquids is expected to be negligible.

The net radiative heat flux in the s direction is

$$q(s) = q^+(s) - q^-(s)$$

where $q^+(s)$, the component of the flux in the positive s direction, is given by

$$q^+(S) = \int_0^\infty \int_0^{2\pi} I_\nu(s_b',\Omega_b') \exp\left[-a_\nu (s - s_b')\right] \mu' \, d\Omega' \, d\nu + a_\nu n_\nu^2 \int_0^\infty \int_0^{2\pi} \int_{s_b'}^{s} I_{b\nu}\left[T(s')\right] \exp\left[-a_\nu (s - s')\right] \mu' ds' d\Omega' d\nu \tag{3.11}$$

and $q^-(s)$, the negative s component, is given by

$$q^-(s) = \int_0^\infty \int_0^{2\pi} I_\nu(s_c', \Omega_c') \exp\left[-a_\nu(s - s_c')\right] \mu' d\Omega' d\nu$$

$$+ a_\nu n_\nu^2 \int_0^\infty \int_0^{2\pi} \int_{s_c'}^{s} I_{b\nu}\left[T(s')\right] \exp\left[-a_\nu(s - s')\right] \mu' ds' d\Omega' d\nu \qquad (3.12)$$

The components of the flux along with the hemispheres of integration are shown in Figure 3.3. The hemisphere indicated in Equation (3.11) is the one marked by "+" in the figure and the hemisphere for Equation (3.12) is the one indicated by "-". In either relationship, Θ' is measured from the s direction so that $\mu' = \cos\Theta' > 0$.

In order to determine the exact radiative flux from Equation (3.11) and Equation (3.12), knowledge of the radiosities and intensities, $I_\nu(s_b', \Omega_b')$ and $I_\nu(s_c', \Omega_c')$, are necessary for special geometry, interfacial condition, and different boundary conditions. These functions, in turn, depend upon the emission coefficient, $n_\nu^2 a_\nu(s)$ $I_{b\nu}[T(s,t)]$, the directional distribution of intensity incident upon the system from the surroundings, if any, and the manner in which the interfaces and boundaries reflect and transmit radiation. The emission coefficient involves $I_{b\nu}$, which depends on temperature distribution of a participating medium and, hence, must be obtained by solving the energy equation.

For finite concentric cylinders with the prescribed given conditions in the cylindrical coordinate system, the previous considerations to determine the exact radiative flux using Equation (3.11) and

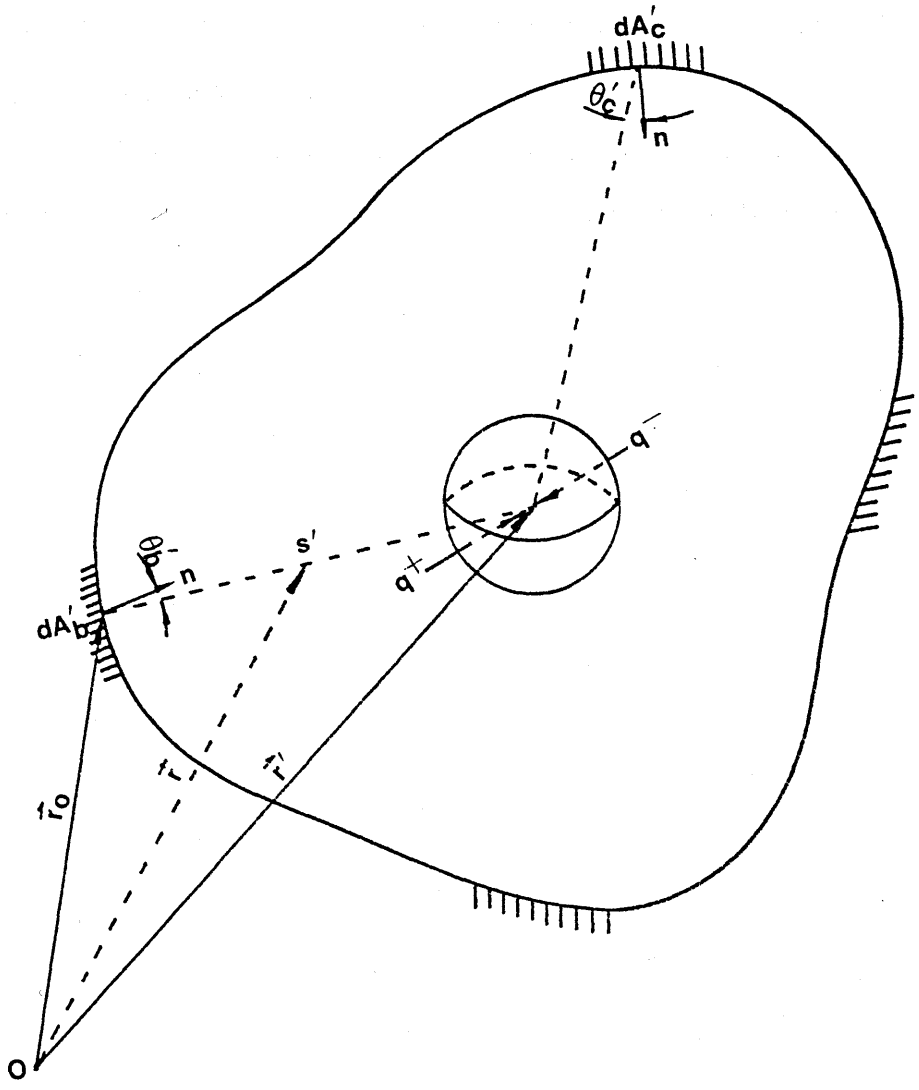

Figure 3.3 Components of Radiative Heat Flux

Equation (3.12) with proper boundary conditions suggest that the exact treatment of the RTE in multi-dimensional non-planar enclosures is very difficult and time consuming because of the long distance nature of radiation, the curvature or corner effects of boundary surfaces, and the simultaneous treatment of the energy equation with the integrated form of the equation of transfer.

For an infinite cylindrical annulus of inside radius r_I and outside radius r_o illustrated in Figure 3.4, the radial local radiative flux can be obtained from Viskanta and Anderson [40] as

$$q_\nu(r) = \frac{4r_o}{r} \left\{ \int_0^{\sin^{-1}(r_I/r_o)} \left[\left(q^i_{1d\nu}/\pi \right) \varphi_1(r) + \left(q^i_{2d\nu}/\pi \right) \varphi_2(r) + \varphi_3(r) \right] \cos\beta^* \, d\beta^* + \int_{\sin^{-1}(r_I/r_o)}^{\sin^{-1}(r/r_o)} \left[\left(q^i_{2d\nu}/\pi \right) \psi_2(r) + \psi_3(r) \right] \cos\beta^* \, d\beta^* \right\} \tag{3.13}$$

where

$$\varphi_1(r) = D_3\left[\gamma(r, r_I)\right]$$

$$\varphi_2(r) = -D_3\left[\gamma(r_o, r)\right]$$

$$\varphi_3(r) = \int_{r_o}^{r} \frac{n^2 I_{b\nu}(r')}{F(r', \beta^*)} D_2\left[\gamma(r, r')\right] dr'$$

$$+ \int_{r_o}^{r} \frac{n_\nu^2 I_{b\nu}(r')}{F(r',\beta^*)} D_2 \left[\gamma(r',r)\right] dr'$$

$$\psi_2(r) = D_3 \left[2\gamma(r, r_o \sin\beta^*) + \gamma(r_o,r)\right] - D_3 \left[\gamma(r_o,r)\right]$$

$$\psi_3(r) = \int_{r_o\sin\beta^*}^{r} \frac{n_\nu^2 I_{b\nu}(r')}{F(r',\beta^*)} D_2 \left[\gamma(r,r')\right] dr'$$

$$- \int_{r}^{r_o} \frac{n_\nu^2 I_{b\nu}(r')}{F(r',\beta^*)} D_2 \left[\gamma(r',r)\right] dr'$$

$$+ \int_{r_o\sin\beta^*}^{r_o} \frac{n_\nu^2 I_{b\nu}(r')}{F(r',\beta^*)} \left\{ D_2 \left[\gamma(r,r_o\sin\beta^*)\right] + D_2 \left[\gamma(r',r_o\sin\beta^*)\right]\right\} dr'$$

$$Dn(x) = \int_{1}^{\infty} \frac{e^{-x\xi} d\xi}{\xi^n(\xi^n-1)^{\frac{1}{2}}} = \int_{o}^{1} \frac{\mu^{n-1}\, e^{-x/\mu} d\mu}{(1-\mu^2)^{\frac{1}{2}}}$$

$$\gamma(b,a) = \int_{a}^{b} d\eta / F(\eta,\beta^*)$$

$$F(r',\beta^*) = \left[r'^2 - r_o \sin^2\beta^*\right]^{\frac{1}{2}} / r' a_\nu$$

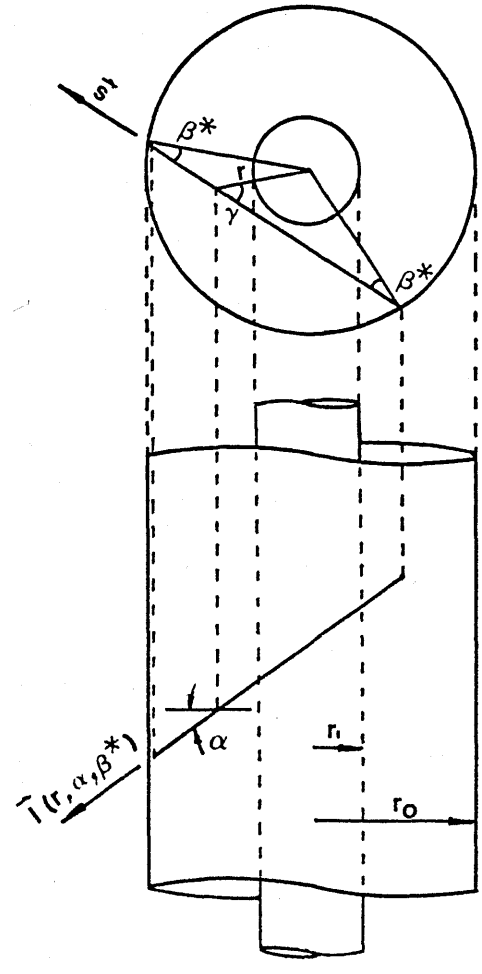

Figure 3.4 Geometrical Coordinates in Infinitely Long Cylindrical Annulus

Since q_d^i represents a diffuse flux leaving (reflected plus transmitted, or emitted if the boundary is opaque) the boundary of the cylinder, the radiative flux is not completely defined until q_{1d}^i and q_{2d}^i are specified. This can be accomplished by making radiant energy balances for the cylindrical annulus at surfaces 1 and 2. When the

inner and outer surfaces are assumed to be gray diffuse and maintained at constant temperatures, the radiant energy balances at both surfaces yields the following boundary conditions

$$q^{i}_{1d} = \text{Emitted} + \text{Reflected}$$
$$= \varepsilon_1 \sigma T_I^4 + (1 - \varepsilon_1)\, q\,(r_I) \tag{3.14}$$

$$q'_{2d} = \text{Emitted} + \text{Reflected}$$
$$= \varepsilon_2 \sigma T_o^4 + (1 - \varepsilon_2)\, q\,(r_o) \tag{3.15}$$

These two boundary conditions in Equation (3.14) and (3.15) are substituted into Equation (3.13) (see Appendix B).

3.3 SPHERICAL HARMONICS APPROXIMATION

In some applications, the radiation, conduction, and/or convection within a fluid may equally become significant, and their interaction alters the temperature distribution in the medium making the analysis additionally complicated. Therefore, various approximate methods have been developed. Among the methods for solving the transport equations, the Monte Carlo technique [66] and Hottel's zone method [68-70] are either very difficult or computationally expensive, even when the simplification of a gray medium is introduced [72,82].

Usually some approximations such as the moment, spherical harmonics, discrete ordinates methods, or some hybrid formulations are preferable to calculate radiative heat flux in multi-dimensional enclosures when the flow field must also be considered since they are

compatible with finite difference schemes [72]. It has been shown by Krook [88] that the moment method, the discrete ordinate method, and the spherical harmonics method are closely related and completely equivalent. The approximate describing equations for these methods are similar, but the physical boundary conditions are different. The spherical harmonics approximation, which is as elegant as it is tedious, takes its power from its strong mathematical base. It can be easily used with the finite difference schemes required for flow field calculations and can yield quite accurate radiative heat flux predictions, especially for optical thickness greater than unity [81]. This method was first suggested by Jeans [89] in connection with the problem of radiative transfer in stars. A general description of the method of spherical harmonics can be found in the books by Kourganoff [93] for radiative transfer application, and by Davidson [94] for neutron transport applications.

Assuming that a gray medium is isotropically scattering (phase function $\zeta(\Omega, \Omega_i) = 1.0$) and in local thermodynamic equilibrium within a finite cylindrical enclosure (see Figure 3.5), the describing radiative transport Equation (3.4) is given in the cylindrical coordinate system by Uesugi and Tsujita [91] and is rewritten in the dimensionless form

$$\ell_r \frac{\partial \psi}{\partial \tau} - \frac{1}{\tau} \ell_{\Theta^*} \left(\frac{\partial \psi}{\partial \varphi} - \frac{\partial \psi}{\partial \Theta^*} \right) + \ell_z \frac{\partial \psi}{\partial \eta} + \psi = (1-\omega^*)\Phi + \frac{\omega^*}{4\pi} \int_{\Omega} \psi' \, d\Omega' \qquad (3.16)$$

where

$$\psi = I/I_r$$

$$I = \int_0^\infty I_\nu d\nu$$

$$\Phi = B/\pi I_r$$

$$B = \int_0^\infty B_\nu d\nu = n^2 \sigma T^4$$

$$\tau = (a + \omega)r$$

$$\eta = (a + \omega)z$$

$\omega^* = \omega/(a + \omega)$ and I_r is a reference intensity of radiation.

One way of developing the differential approximation of Equation (3.16) is by expanding the intensity in a series of orthogonal functions--Chebyshev polynomials or spherical harmonics. Chebyshev polynomials are limited to one-dimensional problem; hence, spherical harmonics are widely used. Then the radiation intensity distribution is expanded in an orthogonal series of spherical harmonics of the form

$$\psi(\vec{r},\gamma,\varphi) = \sum_{n=0}^{\infty} \sum_{m=0}^{n} \frac{2n+1}{4\pi} P_n^m (\cos\gamma) \left[A_n^m (\vec{r}) \cos m\varphi + D_n^m (\vec{r}) \sin m\varphi \right] \tag{3.17}$$

where $A_n^m (\vec{r})$ and $D_n^m (\vec{r})$ are position-dependent coefficients to be determined and $P_n^m (\cos\gamma)$ are the associated Legendre polynomials of the first kind, defined by

$$P_n^m (\cos\gamma) = \frac{1}{2^n n!} (1 - \cos^2\gamma)^{\frac{m}{2}} \frac{d^{m+n}}{d(\cos\gamma)^{m+n}} (\cos^2\gamma - 1)^n \tag{3.18}$$

$\ell_z = \cos\gamma$

$\ell_r = \sin\gamma\cos\varphi$

$\ell_\theta = \sin\gamma\sin\varphi$

$d\Omega = \sin\gamma\, d\gamma\, d\varphi$

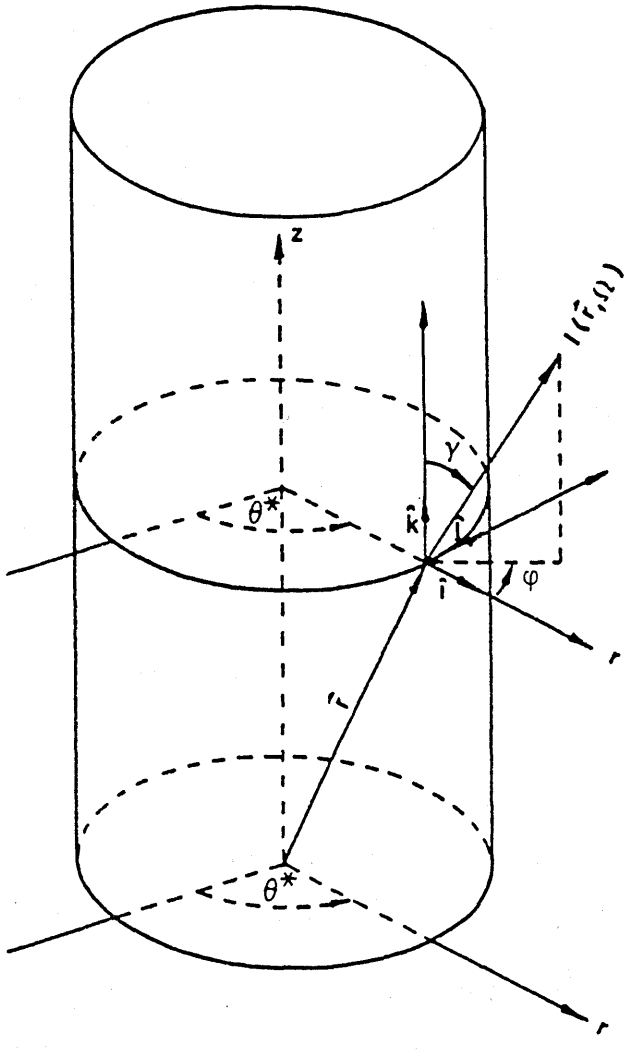

Figure 3.5 Cylindrical Coordinate System

The intensity distribution is approximated by truncating the series after a finite set of terms, n=1 and n=3 for the P-1 and P-3 approximations, respectively. Since the angular distribution of intensity for the axisymmetric case is invariant with respect to rotation about the axial axis or to a reflection in a plane through the axial axis, the P-N approximation reduces to the even function of angle φ.

$$\psi(r,z,\gamma,\varphi) = \sum_{n=0}^{N} \sum_{m=0}^{n} \frac{2n+1}{4\pi} P_n^m (\cos\gamma) A_n^m (r,z) \cos m\varphi \qquad (3.19)$$

In the case of an infinitely long cylinder, the intensity distribution must be invariant under a reflection through every plane perpendicular to the z-axis, along with invariance under a rotation about the z-axis. Thus another symmetry property modifies Equation (3.19) into the equation [95]

$$\psi(r,\gamma,\varphi) = \sum_{n=0}^{N} \sum_{m=0}^{n} \frac{2n+1}{8\pi} \left[1 + (-1)^{n+m}\right] P_n^m (\cos\gamma) A_n^m (r) \cos m\varphi \qquad (3.20)$$

The spatial coefficients A_n^m in Equations (3.19) and (3.20) can be expressed in terms of moments of intensity by multiplying both sides of each of the equations by powers of ℓ_r, ℓ_{θ^*} and ℓ_z individually or in a combination and integrating over a solid angle of 4π. Various moments of intensity are defined as follows

$$\psi_{o(r)} = \int_{\Omega} \psi(r,\Omega)\, d\Omega$$

$$\psi_{s_i}(r) = \int_{\Omega} \psi(r,\Omega)\, \ell_{s_i}\, d\Omega$$

$$\psi_{s_i s_j}(r) = \int_{\Omega} \psi(r,\Omega)\, \ell_{s_i} \ell_{s_j}\, d\Omega$$

$$\psi_{s_i s_j s_k}(r) = \int_{\Omega} \psi(r,\Omega) \ell_{s_i s_j s_k}\, d\Omega \qquad (3.21)$$

where $i, j, k = 1, 2, 3$; $s_1 = r$, $s_2 = \theta^*$, $s_3 = z$

In Equation (3.21), ψ_o, the zeroth moment of intensity, divided by the speed of light, gives radiation energy density; ψ_{s_i}, the first moment of intensity, is the radiative energy flux in the i^{th} coordinate direction; and $\psi_{s_i s_j}$, which is the second moment of intensity, divided by the speed of light can be shown to be the radiation stress. Higher moments of intensity do not have a direct physical interpretation.

For the P-1 approximation of an axisymmetric case, the angular distribution in Equation (3.19) becomes

$$\psi(r,z,\gamma,\varphi) = \frac{1}{4\pi} P_o^o(\cos\gamma)\, A_o^o(r,z) + \frac{3}{4\pi} P_1^o(\cos\gamma)\, A_1^o(r,z) + \frac{3}{4\pi} P_1^1(\cos\gamma)\, A_1^1(r,z) \cos\varphi \qquad (3.22)$$

Since $\ell_r = \sin\gamma \cos\varphi$, $\ell_{\theta^*} = \sin\gamma \sin\varphi$, $\ell_z = \cos\gamma$, and $d\Omega = \sin\gamma\, d\gamma d\varphi$ along with the definition of the associated Legendre polynomials of the first kind in Equation (3.18), the multiplication of ℓ_r and ℓ_z and integration over solid angle 4π in both sides of Equation (3.22) yields

$$\psi_o = A_o^o - \frac{3}{4\pi} A_1^o \cdot (2\pi) \int_1^{-1} \cos\gamma\, d(\cos\gamma) - \frac{3}{4\pi}$$

$$\cdot A_1^1 \int_0^{2\pi} \int_1^{-1} \cos\varphi \, (1 - \cos^2\gamma)^{\frac{1}{2}} \, d(\cos\gamma) \, d\varphi$$

$$A_0^0 = \psi_0 \tag{3.23}$$

and

$$\psi_r = -\frac{1}{4\pi} \psi_0 \int_0^{2\pi} \int_1^{-1} \cos\varphi \, \sin\gamma \, d(\cos\gamma) \, d\varphi$$

$$-\frac{3}{4\pi} A_1^0 \int_0^{2\pi} \int_1^{-1} \cos\varphi \cos^2\gamma \cdot d(\cos\gamma) \, d\varphi$$

$$+\frac{3}{4\pi} A_1^1 \int_0^{2\pi} \int_0^{\pi} \cos^2\varphi \sin^3\gamma \, d\gamma \, d\varphi$$

$$A_1^1 = \psi_r \tag{3.24}$$

Then

$$\psi_z = \frac{1}{4\pi} \cdot A_0^0 \int_0^{2\pi} \int_0^{\pi} \sin\gamma \cos\gamma \, d\gamma \, d\varphi$$

$$-\frac{3}{4\pi} A_1^0 \int_0^{2\pi} \int_1^{-1} \cos^2\gamma \, d(\cos\gamma) \, d\varphi$$

$$-\frac{3}{4\pi} A_1^1 \int_0^{2\pi} \int_1^{-1} (1 - \cos^2\gamma)^{\frac{1}{2}} \cos\varphi \, \cos\gamma \, d(\cos\gamma) \, d\varphi$$

$$A_1^0 = \psi_z \tag{3.25}$$

Thus the intensity distribution in terms of moments of intensity by P-1 approximation turns out to be

$$\psi(r,z,\gamma,\varphi) = \frac{1}{4\pi}\,\psi_o + \frac{3}{4\pi}\cos\gamma\,\psi_z + \frac{3}{4\pi}\sin\gamma\cos\varphi\,\psi_r \tag{3.26}$$

Equation (3.26) is multiplied by ℓ_r^2, $\ell_r\ell_z$ and ℓ_z^2 in both sides and integrated over solid angle 4π to yield the "closure condition" as

$$\psi_{rr} = \frac{1}{4\pi}\,\psi_o \int_{4\pi} \ell_r\ell_r\,d\Omega + \frac{3}{4\pi}\,\psi_z \int_{4\pi} \cos\gamma\,\ell_r\ell_r\,d\Omega$$

$$+ \frac{3}{4\pi}\,\psi_r \int_{4\pi} \sin\gamma\,\cos\varphi\cdot\ell_r\ell_r\,d\Omega$$

$$\psi_{rr} = \frac{1}{3}\,\psi_o$$

Similarly, by employing the Kronecker delta δij, the "closure condition" is rewritten as

$$\psi_{s_i s_j} = \int_{\Omega} \psi \ell_{s_i} s_j\,d\Omega = \frac{1}{3}\,\psi_o \delta_{ij} \tag{3.27}$$

To develop the moment differential equations for the axisymmetric finite cylinder case with isotropic scattering, the describing radiative transfer Equation (3.16) reduces to

$$\ell_r \frac{\partial\psi}{\partial\tau} - \frac{1}{\tau}\,\ell_{\theta*}\frac{\partial\psi}{\partial\varphi} + \ell_z \frac{\partial\psi}{\partial\eta} + \psi = (1-\omega^*)\,\Phi + \frac{\omega^*}{4\pi}\,\psi_o \tag{3.28}$$

To integrate both sides of Equation (3.28) over solid angle 4π, the second term in the left hand side must be carried by using the integration by parts technique. Then

$$-\frac{1}{\tau}\int_{4\pi} \ell_{\Theta^*}\ \frac{\partial\psi}{\partial\varphi}\ d\Omega = -\frac{1}{\tau}\int_0^{\pi}\int_0^{2\pi} \frac{\partial\psi}{\partial\varphi}\ \ell_{\Theta^*}\ \sin\gamma\ d\varphi\ d\gamma$$

using

$$u = \ell_{\Theta} \quad , \quad du = \ell_r\ d\varphi$$

$$dv = \frac{\partial}{\partial\varphi}(\psi\ \sin\gamma)\ d\varphi \quad , \quad v = \psi\sin\gamma$$

$$-\frac{1}{\tau}\int_0^{\pi}\int_0^{2\pi} \frac{\partial\psi}{\partial\varphi}\ \ell_{\Theta^*}\ \sin\gamma\ d\varphi\ d\gamma = -\psi\ell_{\Theta^*}\ \sin\gamma\ \Big)_{\varphi=0}^{2\pi}$$

$$+\frac{1}{\tau}\int_0^{\pi}\int_0^{2\pi} \psi\ell_r\ \sin\gamma\ d\varphi\ d\gamma - \frac{1}{\tau}\int_{4\pi}\ell_{\Theta^*}\frac{\partial\psi}{\partial\varphi}\ d\Omega = \frac{\psi_r}{\tau} \qquad (3.29)$$

Once the other terms are integrated by using the definition of moments of intensity and interchanging integration with differentiation, Equation (3.28) becomes

$$\frac{\psi_r}{\tau} + \frac{\partial\psi_r}{\partial\tau} + \frac{\partial\psi_z}{\partial\eta} = (1 - \omega^*)\ (4\pi\Phi - \psi_o) \qquad (3.30)$$

The multiplication of ℓ_r, ℓ_z and integration over solid angle 4π in Equation (3.28) by employing the same techniques used to develop Equation (3.30) yields

$$\frac{\partial\psi_{rr}}{\partial\tau} + \frac{1}{\tau}\left(\psi_{rr} - \psi_{\Theta^*\Theta^*}\right) + \frac{\partial\psi_{rz}}{\partial\eta} = -\psi_r \qquad (3.31)$$

$$\frac{\psi_{rz}}{\tau} + \frac{\partial \psi_{rz}}{\partial \tau} + \frac{\partial \psi_{zz}}{\partial \eta} = -\psi_z \tag{3.32}$$

Using the "closure condition" of Equation (3.27), Equations (3.31) and (3.32) produce the directional radiative heat flux in terms of intensity, respectively, as

$$\psi_r = -\frac{1}{3}\frac{\partial \psi_o}{\partial \tau} \tag{3.33}$$

$$\psi_z = -\frac{1}{3}\frac{\partial \psi_o}{\partial \eta} \tag{3.34}$$

Substituting Equations (3.33) and (3.34) into Equation (3.30), the differential equation

$$\frac{\partial^2 \psi_o}{\partial \tau^2} + \frac{1}{\tau}\frac{\partial \psi_o}{\partial \tau} + \frac{\partial^2 \psi_o}{\partial \eta^2} = 3(1-\omega^*)(\psi_o - 4\pi\Phi) \tag{3.35}$$

is obtained. The results obtained in Equations (3.33), (3.34), and (3.35) are the same as those obtained by Higenyi [96]. Similarly, for an infinite cylindrical symmetry, the radial heat flux and the moment differential equation within an emitting, absorbing, isotropically scattering and gray phase change medium are obtained; these are

$$\psi_r = -\frac{1}{3}\frac{d\psi_o}{d\tau} \tag{3.36}$$

$$\frac{d^2 \psi_o}{d\tau^2} + \frac{1}{\tau}\frac{d\psi_o}{d\tau} = 3(1-\omega^*)(\psi_o - 4\pi\Phi) \tag{3.37}$$

The exact radiative boundary conditions for a general case of opaque, diffusively emitting, diffusively and specularly reflecting surfaces take the form

$$\psi(r,\Omega)\,)_{si,n} = F_{si,n}(r,\Omega) \qquad \begin{matrix} si = r,\theta^*,z \\ n = 1,2 \end{matrix} \tag{3.38}$$

where

$$F_{si}(r,\Omega) = \{\, \varepsilon_w \Phi_w(r) + \rho_{sw}\psi'(r,\Omega) + \frac{\rho_{dw}}{\pi} \int_a \psi'(r,\Omega)\ell_{si}\, d\Omega \,\}\,)_{s_{i,n}}$$

or

$$\left[\begin{matrix}\text{net radiative intensity} \\ \text{at r in } \Omega \text{ direction}\end{matrix}\right] = \left[\begin{matrix}\text{intensity due} \\ \text{to surface emission}\end{matrix}\right] + \left[\begin{matrix}\text{intensity due to} \\ \text{specular reflection}\end{matrix}\right]$$

$$+ \left[\begin{matrix}\text{intensity due to} \\ \text{diffuse reflection}\end{matrix}\right]$$

Since the above exact boundary condition of Equation (3.38) is not appropriate for use with a specified P-N approximation, Marshak [97] and Mark [98] proposed two different approaches. Mark's method seeks to satisfy Equation (3.38) at discrete solid angles, the angles being obtained from a constraint appropriate to a particular approximation. Marshak's conditions require, at each boundary surface, a balance of the first (N+1)/2 half odd moments of intensity as calculated from both sides of Equation (3.38). The extension of Mark's conditions to cylindrically symmetric and multi-dimensional problems is not established. Moreover, it has been stated that Marshak's boundary condition yields more accurate results for lower order spherical harmonic approximations. The reason for this is that for the lower order approximations, the average intensity leaving the

boundaries can represent the intensity distribution more realistically. Marshak's boundary conditions for multi-dimensional cylindrical geometry are obtained by taking the integral of the intensity over the appropriate hemisphere such that

$$\int_{\Omega} \psi(r,\Omega^{n}_{si})\, \ell^{2k-1}_{si}\, d\Omega \Big)_{si,n} = \int_{\Omega} F\,(r,\, \Omega^{m}_{si})\, \ell^{2k-1}_{si}\, d\Omega \Big)_{s_i,n} \qquad (3.39)$$

where

$$F\,(r,\Omega^{m}_{si}) = \varepsilon_{w}\Phi_{w}\,(r) + \rho_{sw}\;\psi(r,\Omega^{m}_{si}) + \frac{\rho_{dw}}{\pi}\int_{\Omega} \psi(r,\Omega^{m}_{si})\, \ell_{si}\, d\Omega$$

$$n = 1,2$$

$$i = 1,2,3$$

$$s_1 = r, \quad s_2 = \theta^{*}, \quad s_3 = z$$

$$k = 1,2, \ldots., (N+1)/2$$

$$m = 3 - n$$

and

$$\psi(r,\Omega^{n}_{z}) = \psi(r,\gamma_{n},\varphi);\ \gamma_1 = \gamma,\ \gamma_2 = \pi - \gamma$$

$$\psi(r,\Omega^{n}_{r}) = \psi(r,\gamma,\varphi_{n});\ \varphi_1 = \varphi,\ \varphi_2 = \pi - \varphi$$

Higenyi [96] applied this general Marshak type boundary conditions to a finite cylindrical geometry and developed the pairs of boundary conditions for a P-N differential approximation. Neglecting the specularly reflected term in the P-1 approximation, the substitution

of Equation (3.26) into Equation (3.39) yields the boundary conditions

$$\psi_o \pm Ei \frac{\partial \psi_o}{\partial \tau^*} = 4\pi\Phi_{wi} \quad , \tau^* = \tau, \eta \qquad (3.40)$$

$$Ei = \frac{2}{3} \frac{2-\epsilon_{wi}}{\epsilon_{wi}} \quad , i = 1,2,3,4$$

for the axisymmetric two-dimensional case. To express Equation (3.40) in terms of the zeroth moment of intensity, Equations (3.33) and (3.34) are substituted into Marshak type boundary conditions. Similarly, Equation (3.39) is transformed into the differential equations

$$\psi_o \pm Ei \frac{d\psi_o}{d\tau} = 4\pi\Phi_{wi} \quad , \quad i = 1,2 \qquad (3.41)$$

for cylindrical symmetry one-dimensional case. Then Equations (3.35) and Equation (3.40) are coupled with Equation (3.3) because the temperature distribution of a medium must be determined in terms of a dimensionless Planck function term Φ.

CHAPTER 4

NUMERICAL APPROACH

The principle of the conservation of energy and the moment differential equations are to be reformulated into finite difference form. The region of interest is subdivided into a number of small elements--for example, infinite lateral concentric rings of width δr for a cylindrical symmetric one-dimensional problem and finite annular rings of width δr and depth δz for a cylindrical two-dimensional problem. Then the average value of the enthalpies and temperatures at the nodal points (r) or (r,z), placed at the centers of the elements, are studied as function of time. And the moment differential equations, which yield the intensities and the radiative heat flux of each element within an absorbing, emitting, and isotropic scattering medium with reflected and emitted boundary and moving interfacial conditions are simultaneously solved with the energy equation at each time step.

4.1 AXISYMMETRIC TWO-DIMENSIONAL FORMULATION

Since it is advantageous and convenient to use the dimensionless form as a means of identifying pertinent dimensionless variables, the following forms of dimensionless variables are introduced in Equation (3.3);

$$H = \frac{1}{\rho_s \delta v} \iiint_{\forall} \frac{\rho(h-h_s)}{h_{sl}} \delta v$$

$$\Theta = \frac{C_s(T-T_f)}{h_{sl}} = \frac{K_s}{\alpha_s \rho_s} \frac{(T-T_f)}{h_{sl}}$$

$$\tau = r(a+\omega) \quad , \quad \eta = z(a+\omega)$$

$$\xi = \alpha_s (a+\omega)^2 \, t \quad , \quad F_{si} = \frac{q_{si}}{\sigma T r^4} = \frac{\psi_{si}}{\pi} \quad , \quad si = r,z, \tag{4.1}$$

where

H = dimensionless enthalpy

Θ = dimensionless temperature

τ = dimensionless radial optical coordinate

η = dimensionless axial optical coordinate

ξ = dimensionless time

F = dimensionless radiative heat flux.

By employing the above dimensionless variables given above, Equation (3.3) becomes

$$\rho_s h_{sl} \, 2\pi r \delta r \delta z \, \frac{d}{dt} \left[\frac{1}{\rho_s 2\pi r \delta r \delta z} \int_{r-\frac{\delta r}{2}}^{r+\frac{\delta r}{2}} \int_{z-\frac{\delta z}{2}}^{z+\frac{\delta z}{2}} \frac{\rho(h-h_s)}{h_{sl}} \, 2\pi r \delta z \delta r \right]$$

$$= \left\{ K_1 \frac{\partial}{\partial r} \left[\frac{K_s}{\alpha_s \rho_s h_{sl}} (T-T_f) \right] \right\}_{r+\frac{\delta r}{2}} 2\pi (r + \tfrac{\delta r}{2}) \, \delta z$$

$$- K_2 \frac{\partial}{\partial r} \left[\frac{K_s}{\alpha_s \rho_s h_{sl}} (T-T_f) \right]_{r-\frac{\delta r}{2}} 2\pi (r - \tfrac{\delta r}{2}) \, \delta z$$

$$+ K_3 \frac{\partial}{\partial z} \left[\frac{K_s}{\alpha_s \rho_s h_{sl}} (T-T_f) \right]_{z+\frac{\delta z}{2}} 2\pi r \delta r$$

$$- K_4 \frac{\partial}{\partial z} \left[\frac{K_s}{\alpha_s \rho_s h_{sl}} (T - T_f) \right]_{z - \frac{\delta z}{2}} 2\pi r \delta r \Big\} \frac{\alpha_s \rho_s h_{sl}}{K_s}$$

$$+ \Big\{ - \frac{q_r}{\sigma T r^4} \Big)_{r + \frac{\delta r}{2}} \cdot 2\pi (r + \frac{\delta r}{2}) \delta z + \frac{q_r}{\sigma T r^4} \Big)_{r - \frac{\delta r}{2}} \cdot 2\pi (r - \frac{\delta r}{2}) \delta z$$

$$- \frac{q_z}{\sigma T r^4} \Big)_{z + \frac{\delta z}{2}} \cdot 2\pi r \delta r + \frac{q_z}{\sigma T r^4} \Big)_{z - \frac{\delta z}{2}} \cdot 2\pi r \delta r \Big\} \sigma T r^4 , \qquad (4.2)$$

$$K_s \delta\tau \frac{dH}{d\xi} = \Big\{ K_1 (1 + \frac{\delta\tau}{2\tau}) \frac{\partial\theta}{\partial\tau} \Big)_{\tau + \frac{\delta\tau}{2}} - K_2 (1 - \frac{\delta\tau}{2\tau}) \frac{\partial\theta}{\partial\tau} \Big)_{\tau - \frac{\delta\tau}{2}}$$

$$+ K_3 \frac{\delta\tau}{\delta\eta} \frac{\partial\theta}{\partial\eta} \Big)_{\eta + \frac{\delta\eta}{2}} - K_4 \frac{\delta\tau}{\delta\eta} \frac{\partial\theta}{\partial\eta} \Big)_{\eta - \frac{\delta\eta}{2}} \Big\} + \Big\{ - (1 + \frac{\delta\tau}{2\tau}) F_r \Big)_{\tau + \frac{\delta\tau}{2}}$$

$$+ (1 - \frac{\delta\tau}{2\tau}) F_r \Big)_{\tau - \frac{\delta\tau}{2}} - \frac{\delta\tau}{\delta\eta} F_z \Big)_{\eta + \frac{\delta\eta}{2}} + \frac{\delta\tau}{\delta\eta} F_z \Big)_{\eta - \frac{\delta\eta}{2}} \Big\} \cdot \frac{S}{N} \cdot K_s$$

(4.3)

where

$N = K_s \beta / 4\sigma T r^3$; conduction and radiation parameter

$S = K_s \, Tr / 4\alpha_s \rho_s h_{sl}$; parameter

$\beta = a + \omega$; extinction coefficient

T_r ; reference temperature in absolute value.

Enthalpy and temperature for different phases of pure substance are related as

$$h - h_s = C(T-T_f) = \frac{K}{\rho\alpha}\ (T-T_f) \quad \text{for} \quad T < T_f \tag{4.4}$$

$$h - h_s = \frac{K}{\rho\alpha}\ (T-T_f) + h_{sl} \quad \text{for} \quad T > T_f \tag{4.5}$$

To obtain expressions that relate enthalpy with temperature for an element, Equations (4.4) and (4.5) are substituted into Equation (4.1) as

$$H = \frac{1}{\rho_s \delta v} \iiint \frac{\rho(h-h_s)}{h_{sl}}\ \delta v = \frac{K(T-T_f)}{\alpha \rho_s h_{sl} \delta v} \cdot \delta v$$

$$= \frac{K\alpha_s}{\alpha K_s}\ \Theta \quad ,$$

$$\Theta = \frac{\alpha K_s}{K\alpha_s}\ H \qquad \text{for} \quad H < 0 \quad \text{(solid)} \tag{4.6}$$

Similarly,

$$\Theta = \frac{\alpha K_s}{K\alpha_s}\ (H - 1) \qquad \text{for} \quad H > 1 \ \text{(liquid)} \tag{4.7}$$

When the dimensionless enthalpy takes values between 0 and 1,

$$\Theta = 0 \qquad \text{for} \quad 0 \leq H \leq 1 \ \text{(during phase change)} \tag{4.8}$$

For different boundary conditions, Equation (4.3) may be modified to satisfy specific boundary conditions at a boundary

element. Then Equation (4.3) must be solved simultaneously with moment differential Equations (3.33), (3.34), and (3.35) whose Marshak type boundary conditions were derived in Equation (3.40). These equations are summarized here for completeness as

$$\frac{\partial^2 \psi_o}{\partial \tau^2} + \frac{1}{\tau} \frac{\partial \psi_o}{\partial \tau} + \frac{\partial^2 \psi_o}{\partial \eta^2} = 3(1 - \omega^*)(\psi_o - 4\pi\Phi) \tag{3.35}$$

$$F_r = \psi_r/\pi = -\frac{1}{3\pi} \frac{\partial \psi_o}{\partial \tau} \tag{4.9}$$

$$F_z = \psi_z/\pi = -\frac{1}{3\pi} \frac{\partial \psi_o}{\partial \eta} \tag{4.10}$$

4.2 CYLINDRICAL SYMMETRIC ONE-DIMENSIONAL FORMULATION

If variations in the angular direction and along the longitudinal axis of the system are neglected, the analysis reduces to the cylindrical symmetric one-dimensional case. Thus, Equation (4.3) reduces to

$$K_s \delta\tau \frac{dH}{d\xi} = K_1 \left(1 + \frac{\delta\tau}{2\tau}\right) \frac{\partial \Theta}{\partial \tau}\Bigg)_{\tau + \frac{\delta\tau}{2}} - K_2 \left(1 - \frac{\delta\tau}{2\tau}\right) \frac{\partial \Theta}{\partial \tau}\Bigg)_{\tau - \frac{\delta\tau}{2}}$$

$$+ \left\{ -\left(1 + \frac{\delta\tau}{2\tau}\right) F_r \Big)_{\tau + \frac{\delta\tau}{2}} + \left(1 - \frac{\delta\tau}{2\tau}\right) F_r \Big)_{\tau - \frac{\delta\tau}{2}} \right\} \cdot \frac{S}{N} \cdot K_s \tag{4.11}$$

The moment differential equations were derived as

$$\frac{d^2 \psi_o}{d\tau^2} + \frac{1}{\tau} \frac{d\psi_o}{d\tau} = 3(1 - \omega^*)(\psi_o - 4\pi\Phi) \tag{3.37}$$

$$F_r = \psi_r/\pi = -\frac{1}{3\pi} \frac{d\psi_o}{d\tau} \tag{4.12}$$

whose Marshak type boundary conditions are given in Equation (3.41).

4.3 FINITE DIFFERENCE FORMULATION

The principle of conservation of energy which employs enthalpy in its describing equation and the moment differential equations developed in the previous sections are first written in the finite difference form given below. In the finite difference formulations time derivatives are represented by backward differences whereas spatial derivatives are represented by forward and central differences (see Figure 2). Imaginary nodes are generated on the outside of each boundary so that the boundary condition equations can be included [92].

4.3.1 Axisymmetric Two-Dimensional Case

When the value of the dimensionless enthalpy is below zero, the finite difference representation of the principle of conservation of energy takes the form

$$A^{m-1}_{i,j}\ H^{m}_{i,j} = YH^{m-1}_{i,j} + b^{m-1}_{i,j}\ \Theta^{m}_{i+1,j} + a^{m-1}_{i,j}\ \Theta^{m}_{i-1,j} + d^{m-1}_{i,j}\ \Theta^{m}_{i,j+1}$$

$$+ e^{m-1}_{i,j}\ \Theta^{m}_{i,j-1} + \{ f_i F^{m}_{r,i+1,j} + g_i F^{m}_{r,i-1,j} + P_i F^{m}_{r,i,j}$$

$$- DTZ \cdot F^{m}_{z,i,j+1} + DTZ \cdot F^{m}_{z,i,j-1} \} \cdot \frac{S}{N} \cdot K_s \qquad (4.13)$$

and

$$\Theta^{m}_{i,j} = \frac{H^{m}_{i,j}}{D^{m-1}_{i,j}} \quad \text{for} \quad H^{m}_{i,j} < 0 \qquad (4.14)$$

where

$$A^{m-1}_{i,j} = \{ K_s \frac{(\delta\tau)^2}{\delta\xi} + \frac{1}{D^{m-1}_{i,j}} [(1 + \frac{\delta\tau}{2\tau})\ K^{m-1}_{1,i,j} + (1 - \frac{\delta\tau}{2\tau})\ K^{m-1}_{2,i,j}$$

$$+ (\frac{\delta\tau}{\delta\eta})^2\ K^{m-1}_{3,i,j} + (\frac{\delta\tau}{\delta\eta})^2\ K^{m-1}_{4,i,j}]\}$$

$$Y = K_s \frac{(\delta\tau)^2}{\delta\xi} \quad , \quad D_{i,j}^{m-1} = \frac{K_{i,j}^{m-1} \alpha_s}{\alpha_{i,j}^{m-1} K_s}$$

$$P_i = - \frac{(\delta\tau)^2}{2\tau_i} \quad , \quad DTZ = \frac{(\delta\tau)^2}{2\delta\eta}$$

$$b_{i,j}^{m-1} = (1 + \frac{\delta\tau}{2\tau}) K_{1,i,j}^{m-1}$$

$$a_{i,j}^{m-1} = (1 - \frac{\delta\tau}{2\tau}) K_{2,i,j}^{m-1}$$

$$d_{i,j}^{m-1} = (\frac{\delta\tau}{\delta\eta})^2 K_{3,i,j}^{m-1}$$

$$e_{i,j}^{m-1} = (\frac{\delta\tau}{\delta\eta})^2 K_{4,i,j}^{m-1}$$

$$f_i = - \frac{\delta\tau}{2} (1 + \frac{\delta\tau}{2\tau_i})$$

$$g_i = \frac{\delta\tau}{2} (1 - \frac{\delta\tau}{2\tau_i})$$

For the range of dimensionless enthalpy values between 0 and 1, the describing equations in finite difference form can be written as

$$\textcircled{Y}H_{i,j}^m = YH_{i,j}^{m-1} + b_{i,j}^{m-1} \Theta_{i+1,j}^m + a_{i,j}^{m-1} \Theta_{i-1,j}^m + d_{i,j}^{m-1} \Theta_{i,j+1}^m$$

$$+ e_{i,j}^{m-1} \Theta_{i,j-1}^m + \{ f_i F_{r,i+1,j}^m + g_i F_{r,i-1,j}^m + P_i F_{r,i,j}^m$$

$$- DTZ F_{z,i,j+1}^m + DTZ F_{z,i,j-1}^m \} \frac{S}{N} \cdot K_s \qquad (4.15)$$

and

$$\Theta_{i,j}^m = 0 \quad \text{for} \quad 0 \leq H_{i,j}^m \leq 1 \qquad (4.16)$$

When the values of the dimensionless enthalpy are above 1, the finite difference representations

$$A^{m-1}_{i,j}\ H^{m}_{i,j} = YH^{m-1}_{i,j} + b^{m-1}_{i,j}\ \Theta^{m}_{i+1,j} + a^{m-1}_{i,j}\ \Theta^{m}_{i-1,j} + A^{m-1}_{i,j} - Y$$

$$+ d^{m-1}_{i,j}\ \Theta^{m}_{i,j+1} + e^{m-1}_{i,j}\ \Theta^{m}_{i,j-1} + \{ f_i F^{m}_{r,i+1,j} + g_i F^{m}_{r,i-1,j}$$

$$+ P_i F^{m}_{r,i,j} - DTZ \cdot F^{m}_{z,i,j+1} + DTZ\ F^{m}_{z,i,j-1} \} \frac{S}{N} \cdot K_s \qquad (4.17)$$

and

$$\Theta^{m}_{i,j} = \frac{H^{m}_{i,j} - 1}{D^{m-1}_{i,j}} \quad \text{for} \quad H^{m}_{i,j} > 1 \qquad (4.18)$$

are obtained.

If the system initially is at a uniform temperature above the fusion temperature or at the fusion temperature without internal thermal radiation, then

$$\Theta^{o}_{i,j} = \Theta_I \quad \text{for all } i,j \qquad (4.19)$$

$$H^{o}_{i,j} = 1 + D^{o}_{i,j}\ \Theta^{o}_{i,j} \quad \text{for all } i,j \qquad (4.20)$$

$$F^{o}_{r,i,j} = F^{o}_{z,i,j} = 0 \quad \text{for all } i,j \qquad (4.21)$$

where

Θ_I = initial dimensionless temperature

When the inside and outside cylinder of the cylindrical annulus are maintained at constant temperatures with the insulated end

surfaces, the thermal boundary conditions in terms of dimensionless temperatures become

$$\Theta^m_{1,j} = \Theta_i \qquad \text{at } r = r_I \qquad \text{for all } j$$

$$\Theta^m_{M,j} = \Theta_o \qquad \text{at } r = r_o \qquad \text{for all } j$$

$$\Theta^m_{i,-1} = \Theta^m_{i,2} \qquad \text{at } z = 0 \qquad \text{for all } i$$

$$\Theta^m_{i,N-1} = \Theta^m_{i,-N} \qquad \text{at } z = z^* \qquad \text{for all } i \tag{4.22}$$

The dimensionless enthalpy must be again incorporated with the dimensionless temperatures depending upon the values of enthalpies. For boundary elements with different conditions from Equation (4.22), such as a convective boundary condition or an appropriate heat extraction or supply, Equations (4.13), (4.15), and (4.17) may be modified to include the specific boundary conditions.

The finite difference formulation of the moment differential equations then reduces to

$$AA^{m-1}_{i,j} \quad \psi^m_{o,i,j} = \left(1 + \frac{\delta\tau}{2\tau_i}\right) \psi^m_{o,i+1,j} + \left(1 - \frac{\delta\tau}{2\tau_i}\right) \psi^m_{o,i-1,j}$$

$$+ \left(\frac{\delta\tau}{\delta\eta}\right)^2 \psi^m_{o,i,j+1} + \left(\frac{\delta\tau}{\delta\eta}\right)^2 \psi^m_{o,i,j-1} + BB^{m-1}_{i,j} \quad \Phi^m_{i,j} \tag{4.23}$$

$$F^m_{r,i,j} = - \frac{1}{6\pi\delta\tau} \left(\psi^m_{o,i+1,j} - \psi^m_{o,i-1,j}\right) \tag{4.24}$$

$$F^m_{z,i,j} = - \frac{1}{6\pi\delta\eta} \left(\psi^m_{o,i,j+1} - \psi^m_{o,i,j-1}\right) \tag{4.25}$$

where

$$AA_{i,j}^{m-1} = \{ 2 + 2 \left(\frac{\delta\tau}{\delta\eta}\right)^2 + 3(\delta\tau)^2 (1 - \omega_{i,j}^{*\,m-1}) \}$$

$$BB_{i,j}^{m-1} = 12\pi(\delta\tau)^2 (1 - \omega_{i,j}^{*m-1})$$

For boundary elements, the finite difference representation of Marshak type boundary conditions must be substituted into Equation (4.23), (4.24), and (4.25) to satisfy the thermal radiative boundary conditions. Then, at the inside cylinder of the system, the radiative intensity and heat flux are modified into

$$DD_{1,j}^{m-1} \quad \psi_{o,1,j}^{m} = 2\,\psi_{o,2,j}^{m} + \frac{D3_j^m}{D1}\left(1 - \frac{\delta\tau}{2\tau_1}\right) + \left(\frac{\delta\tau}{\delta\eta}\right)^2 \psi_{o,1,j+1}^{m} + \left(\frac{\delta\tau}{\delta\eta}\right)^2 \psi_{o,1,j-1}^{m} + BB_{1,j}^{m-1} \quad \Phi_{1,j}^{m} \tag{4.26}$$

$$F_{r,1,j}^{m} = -\frac{1}{6\pi D1 \cdot \delta\tau}\left(\psi_{o,1,j}^{m} - D3_j^m\right) \tag{4.27}$$

$$F_{z,1,j}^{m} = -\frac{1}{6\pi\delta\eta}\left(\psi_{o,1,j+1}^{m} - \psi_{o,1,j-1}^{m}\right) \tag{4.28}$$

where

$$DD_{1,j}^{m-1} = AA_{1,j}^{m-1} + \frac{1}{D1}\left(1 - \frac{\delta\tau}{2\tau_1}\right)$$

$$D1 = \frac{E_1}{2\delta\tau}$$

$$D3_j^m = 4\pi\,\Phi_{w1,j}^{m}, \qquad E_i = \frac{2}{3}\left(\frac{2 - \varepsilon_{wi}}{\varepsilon_{wi}}\right)$$

When the system is initially at the fusion temperature and it is being solidified from the inside cylinder, neglecting thermal radiative penetration into the liquid region leads to the modification of intensity and heat flux at solid/liquid interface as being given in the following paragraphs.

The number of radial nodes at S/L interface is obtained from Figure 4.1:

$$LL = i \quad \text{when} \quad \delta\tau^* \leq \frac{\delta\tau}{2}$$

$$LL = i + 1 \quad \text{when} \quad \delta\tau^* > \frac{\delta\tau}{2} \tag{4.29}$$

Then

$$FF^{m-1}_{LL,j}\ \psi^{m}_{o,LL,j} = \left(1 + \frac{\delta\tau}{2\tau_L}\right) \frac{F2^m_j}{F1} + 2\,\psi^{m}_{o,LL-1,j} + \left(\frac{\delta\tau}{\delta\eta}\right)^2 \psi^{m}_{o,LL,j+1}$$

$$+ \left(\frac{\delta\tau}{\delta\eta}\right)^2 \psi^{m}_{o,LL,j-1} + BB^{m-1}_{LL,j}\ \Phi^{m}_{LL,j} \tag{4.30}$$

$$F^{m}_{r,LL,j} = \frac{1}{6\pi F1 \cdot \delta\tau}\left(\psi^{m}_{o,LL,j} - F2^m_j\right) \tag{4.31}$$

$$F^{m}_{z,LL,j} = -\frac{1}{6\pi\delta\eta}\left(\psi^{m}_{o,LL,j+1} - \psi^{m}_{o,LL,j-1}\right) \tag{4.32}$$

where

$$FF^{m-1}_{LL,j} = AA^{m-1}_{LL,j} + \left(1 + \frac{\delta\tau}{2\tau_L}\right) \frac{1}{F1}$$

$$F2^m_j = 4\pi\,\Phi^{m}_{w2,j}$$

$$F1 = \frac{E_2}{2\delta\tau}$$

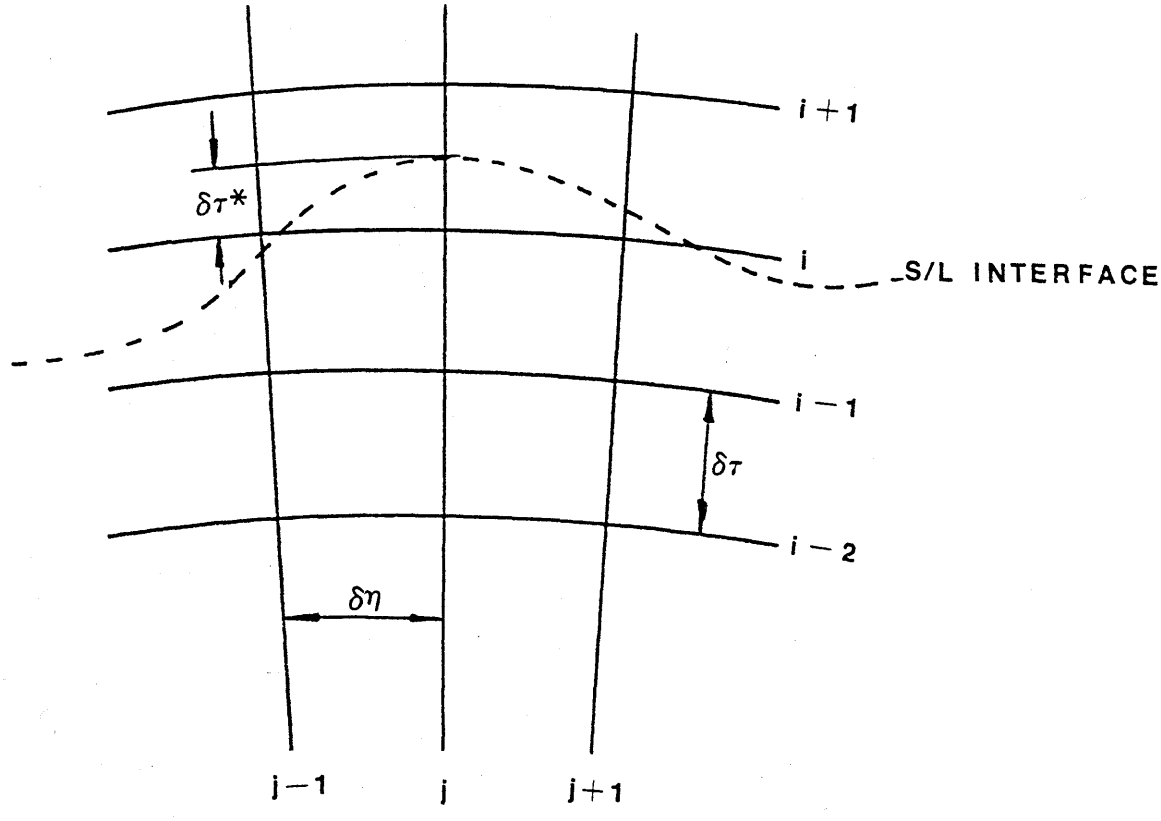

Figure 4.1 Moving S/L Interface at Fixed Meshes

At the left end of the base surface the moment differential equations take the forms

$$GG_{i,1}^{m-1}\ \psi_{o,i,1}^{m} = (1 + \frac{\delta\tau}{2\tau_i})\ \psi_{o,i+1,1}^{m} + (1 - \frac{\delta\tau}{2\tau_i})\ \psi_{o,i-1,1}^{m}$$

$$+ 2\ (\frac{\delta\tau}{\delta\eta})^2\ \psi_{o,i,2}^{m} + \frac{G3_i^m}{G1}\ (\frac{\delta\tau}{\delta\eta})^2 + BB_{i,1}^{m-1}\ \Phi_{i,1}^{m} \qquad (4.33)$$

$$F_{r,i,1}^{m} = -\frac{1}{6\pi\delta\tau}\ (\psi_{o,i+1,1}^{m} - \psi_{o,i-1,1}^{m}) \qquad (4.34)$$

$$F_{z,i,1}^{m} = -\frac{1}{6\pi G1 \cdot \delta\eta}\ (\psi_{o,i,1}^{m} - G3_i^m) \qquad (4.35)$$

where

$$GG_{i,1}^{m-1} = AA_{i,1}^{m-1} + (\frac{\delta\tau}{\delta\eta})^2\ \frac{1}{G1}$$

$$G3_i^m = 4\pi\Phi_{w3,i,1}^{m}$$

$$G1 = \frac{E_3}{2\delta\eta}$$

At the right end of the base surface, the finite difference representation of the moment differential equations becomes

$$PP_{i,N}^{m-1}\ \psi_{o,i,N}^{m} = (1 + \frac{\delta\tau}{2\tau_i})\ \psi_{o,i+1,N}^{m} + (1 - \frac{\delta\tau}{2\tau_i})\ \psi_{o,i-1,N}^{m}$$

$$+ 2\ (\frac{\delta\tau}{\delta\eta})^2\ \psi_{o,i,N-1}^{m} + (\frac{\delta\tau}{\delta\eta})^2\ \frac{P3_i^m}{P1} + BB_{i,N}^{m-1}\ \Phi_{i,N}^{m} \qquad (4.36)$$

$$F_{r,i,N}^{m} = -\frac{1}{6\pi\delta\tau}\ (\psi_{o,i+1,N}^{m} - \psi_{o,i-1,N}^{m}) \qquad (4.37)$$

$$F_{z,i,N}^{m} = \frac{1}{6\pi P1 \cdot \delta\eta}\ (\psi_{o,i,N}^{m} - P3_i^m) \qquad (4.38)$$

where

$$PP_{i,N}^{m-1} = AA_{i,N}^{m-1} + \left(\frac{\delta\tau}{\delta\eta}\right)^2 \cdot \frac{1}{P1}$$

$$P3_i^m = 4\pi\, \Phi_{w4,i,N}^m$$

$$P1 = \frac{E_4}{2\delta\eta}$$

4.3.2 Cylindrical Symmetric One-Dimensional Case

For the cylindrical symmetric one-dimensional case, Equations (4.13) through (4.22) reduce to

$$A_i^{m-1}\, H_i^m = YH_i^{m-1} + b_i^{m-1}\, \Theta_{i+1}^m + a_i^{m-1} + \Theta_{i-1}^m + \{ f_i\, F_{r,i+1}^m + P_i\, F_{r,i}^m + g_i\, F_{r,i-1}^m \} \cdot \frac{S}{N} \cdot K_s \qquad (4.39)$$

and

$$\Theta_i^m = \frac{H_i^m}{D_i^{m-1}} \qquad \text{for} \qquad H_i^m < 0 \qquad (4.40)$$

$$YH_i^m = YH_i^{m-1} + b_i^{m-1}\, \Theta_{i+1}^m + a_i^{m-1}\, \Theta_{i-1}^m + \{ f_i\, F_{r,i+1}^m + P_i\, F_{r,i}^m + g_i\, F_{r,i-1}^m \} \cdot \frac{S}{N} \cdot K_s \qquad (4.41)$$

and

$$\Theta_i^m = 0 \qquad \text{for} \qquad 0 \leq H_i^m \leq 1 \qquad (4.42)$$

$$A_i^{m-1} H_i^m = YH_i^{m-1} + b_i^{m-1} \Theta_{i+1}^m + a_i^{m-1} \Theta_{i-1}^m + A_i^m - Y$$

$$+ \{f_i F_{r,i+1}^m + P_i F_{r,i}^m + g_i F_{r,i-1}^m\} \cdot \frac{S}{N} K_s \qquad (4.43)$$

and

$$\Theta_i^m = \frac{H_i^m - 1}{D_i^{m-1}} \qquad \text{for} \qquad H_i^m > 1 \qquad (4.44)$$

For boundary nodal points whose conditions are different from those given in Equation (4.22), Equations (4.39), (4.41)), and (4.43) must be modified to satisfy the appropriate boundary conditions. For a case where a constant heat flux is extracted from an opaque inner surface of the cylinder, Equation (4.11) on boundary element is modified as

$$K_s \delta\tau \frac{dH}{d\xi} = K_1 \left(1 + \frac{\delta\tau}{2\tau}\right) \left.\frac{\partial\Theta}{\partial\tau}\right)_{\tau_1 + \frac{\delta\tau}{2}} - \text{Ste} \cdot K_s - \frac{S}{N} \cdot K_s \left(1 + \frac{\delta\tau}{2\tau}\right) F_r \Big)_{\tau_1 + \frac{\delta\tau}{2}} \qquad (4.45)$$

where

$$\text{Ste} = \frac{q''}{\alpha_s \rho_s h_{sl} \beta} = \text{Stefan Number}$$

The finite difference representations of Equation (4.45) are obtained, depending upon the phase status of a boundary element, as :

$$A_1^{(m-1)^*} H_1^m = YH_1^{m-1} + b_1^{m-1} \Theta_2^m - \text{Ste} \cdot K_s \cdot \delta\tau + \frac{S}{N} \cdot K_s \{ f_1 (F_{r,1}^m + F_{r,2}^m) \} \qquad (4.46)$$

and

$$\Theta_1^m = \frac{H_1^m}{D_1^{m-1}} \qquad \text{for} \qquad H_1^m < 0$$

$$YH_1^m = YH_1^{m-1} + b_1^{m-1}\,\Theta_2^m - Ste \cdot K_s \cdot \delta\tau + \frac{S}{N}K_s\{\, f_1\,(F_{r,1}^m + F_{r,2}^m)\,\} \tag{4.47}$$

and

$$\Theta_1^m = 0 \qquad \text{for} \qquad 0 \leq H_1^m \leq 1$$

$$A_1^{(m-1)^*} H_1^m = YH_1^{m-1} + b_1^{m-1}\,\Theta_2^m + \frac{b_1^{m-1}}{D_1^{m-1}} - Ste \cdot K_s \cdot \delta\tau$$

$$+ \frac{S}{N}K_s\{\, f_1\,(F_{r,1}^m + F_{r,2}^m)\,\} \tag{4.48}$$

and

$$\Theta_1^m = \frac{H_1^m - 1}{D_1^{m-1}} \qquad \text{for} \qquad H_1^m > 1$$

where

$$A_1^{(m-1)^*} = A_1^{m-1} - \frac{a_1^{m-1}}{D_1^{m-1}}$$

Equations (3.37) and (4.12) are discretized in a manner similar to that employed in the previous section to obtain

$$AA_i^{m-1}\,\psi_{o,i}^m = (1 + \frac{\delta\tau}{2\tau_i})\,\psi_{o,i+1}^m + (1 - \frac{\delta\tau}{2\tau_i})\,\psi_{o,i-1}^m + BB_i^{m-1}\,\Phi_i^m \tag{4.49}$$

$$F_{r,i}^m = -\frac{1}{6\pi\delta\tau}\,(\psi_{o,i+1}^m - \psi_{o,i-1}^m) \tag{4.50}$$

For nodes on the inner surface of the cylinder the substitution of the Marshak type boundary condition into Equation (4.49) yields

$$DD_1^{m-1}\ \psi_{o,1}^m = 2\psi_{o,2}^m + \frac{D3}{D1}\ (1 - \frac{\delta\tau}{2\tau_1}) + BB_1^{m-1}\ \Phi_1^m \qquad (4.51)$$

$$F_{r,1}^m = -\frac{1}{6\pi D1 \cdot \delta\tau}\ (\psi_{o,1}^m - D3) \qquad (4.52)$$

At the solid/liquid interface, the finite difference formulation of the moment differential equation is carried out by using the same discretization as used in Equation (4.30) to obtain

$$FF_1^{m-1}\ \psi_{o,LL}^m = (1 + \frac{\delta\tau}{2\tau_L})\ \frac{F2}{F1} + 2\ \psi_{o,LL-1}^m + BB_1^{m-1}\ \Phi_{LL}^m \qquad (4.53)$$

$$F_{r,LL}^m = \frac{1}{6\pi F1 \cdot \delta\tau}\ (\psi_{o,LL}^m - F2) \qquad (4.54)$$

4.4 METHOD OF SOLUTION

The implicit finite difference equations developed in the previous section, together with the initial and appropriate boundary conditions, form a set of non-linear simultaneous algebraic equations for the unknown temperatures, enthalpies, radiative intensities, and radiative heat flux. In these equations enthalpies at time level m-1 are known and the temperatures, radiative intensities, and radiative heat flux may be evaluated by using appropriate governing equations.

The Gauss-Seidel iterative method with successive over-relaxation [92] is used to solve the non-linear simultaneous difference equations. This iterative method is attractive because it needs little computer memory and it works.

For the axisymmetric two-dimensional case, the right hand side of Equation (4.13) is first calculated by using the most recently evaluated enthalpy values and then Equations (4.14), (4.23), (4.24), and (4.25) are used to compute the corresponding temperature values, radiative intensities, and radiative heat fluxes. After the sign of $H_{i,j}$ is determined from the previous iteration, the new value of $H_{i,j}$ is then computed using the appropriate equations (Equations (4.13), (4.15) or (4.17)) applicable for the different range of enthalpy values. This value of $H_{i,j}$ is then modified by the over-relaxation factor as

$$H^{m}_{i,j} = ORF \cdot H^{ml}_{i,j} + (1 - ORF)\, H^{mo}_{i,j} \qquad (4.55)$$

where

ORF = over-relaxation factor

$H^{m}_{i,j}$ = new value

$H^{ml}_{i,j}$ = value calculated using Equations (4.13), (4.15), or (4.17) depending on the range of enthalpy values

$H^{mo}_{i,j}$ = value calculated on previous iteration

In the successive over relaxation scheme, the speed of convergence is significantly improved. It should be noted that for ORF = 1, the procedure is identical to the Gauss-Seidel method, and for a choice of ORF in the range $1 < ORF < 2$, the convergence is more rapid.

The dimensionless temperature is correspondingly modified and the radiative intensity and radiative heat flux are computed from the temperature distribution in Equations (4.23), (4.24), and (4.25).

The process described above is repeated for all nodes until the change in $H^{m}_{i,j}$ between successive iterations satisfy a convergence criterion.

$$\sum_{i=1}^{M}\sum_{j=1}^{N}\frac{\left|H_{i,j}^{m}-H_{i,j}^{mo}\right|}{\left|H_{i,j}^{m}\right|} < ERR \qquad (4.56)$$

where

ERR = allowable error tolerance.

The procedure is then initiated for a new time and the number of time steps is extended as long as is required. The whole numerical procedure is diagrammed in Figure 4.2.

When the enthalpy distribution has been calculated with sufficient accuracy, the temperature, radiative intensity, and radiative heat flux distribution is obtained. The position of the solid/liquid interface is also determined from the enthalpy distribution. The location of the interface is where the value of the dimensionless enthalpy is zero. This interface location is used as one of the boundary surfaces when the internal thermal radiative transfer is taken into account. The total conductive and radiative dimensionless heat flux at the inner surface of the cylinder at any time m is evaluated by

$$\left(F_{t,1}\right)_{\text{total}} = \left(\frac{q_{c,1}}{\sigma T_r^4}\right)_{\text{conductive}} + \left(F_{r,1}\right)_{\text{radiative}} \qquad (4.57)$$

where

$$q_{c,1} = -\frac{\alpha_s \rho_s \beta h_{s1}}{K_s} \cdot K_1 \left(\frac{\partial \Theta}{\partial \tau}\right)_{\tau_1} = \text{conductive heat flux at the inner wall}$$

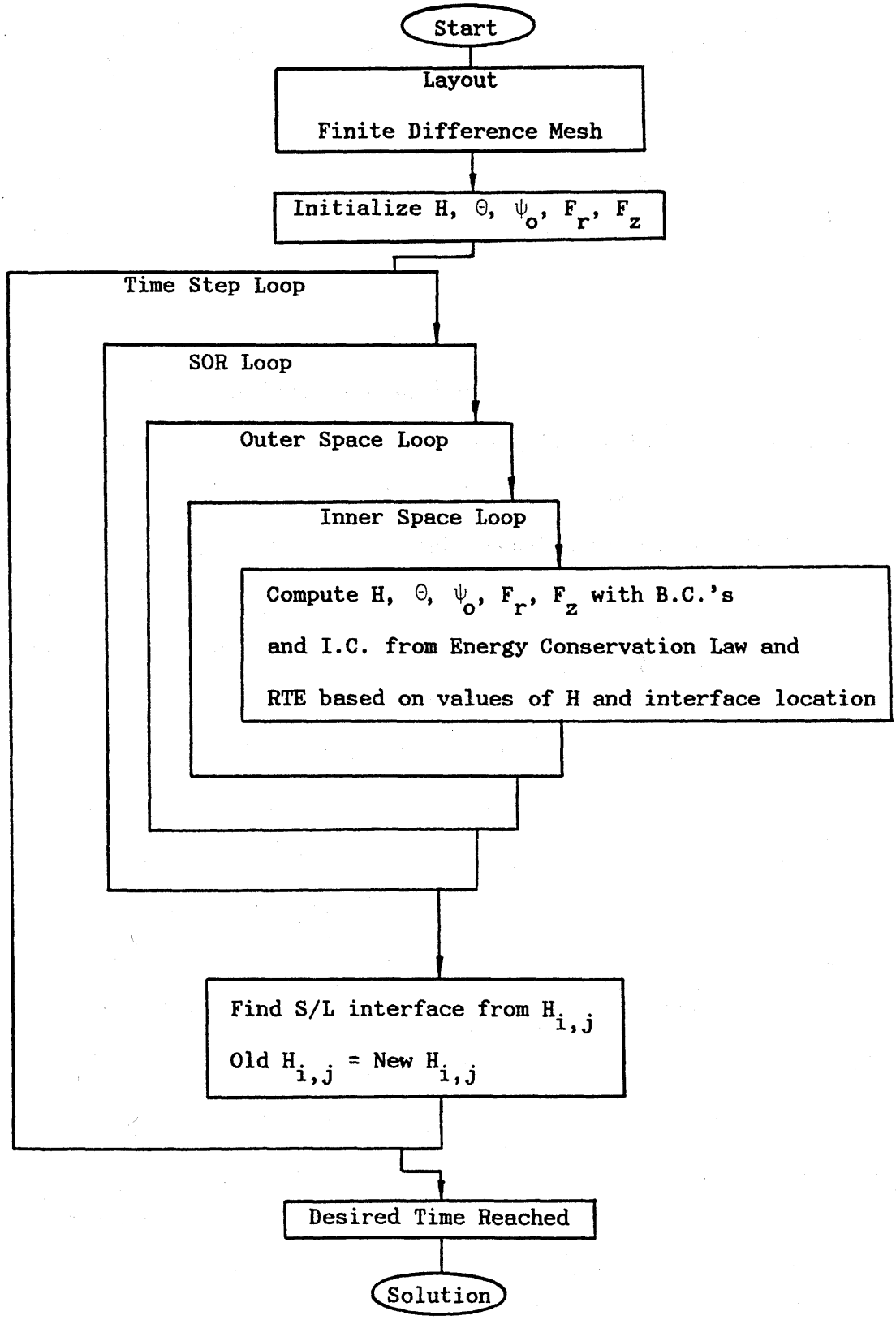

Figure 4.2 Numerical Schematic Procedure of Axisymmetric Two-Dimensional Case

$F_{t,l})_{total}$ = total dimensionless conductive and radiative heat flux at the inner wall

The total volume solidified at any time is also obtained by summing all the masses of the solid elements in phase change material.

4.5 APPROXIMATE ANALYTICAL SOLUTION

Since the conductive heat transfer problem involving change of phase is non-linear, the coupled radiative transfer with conduction in a phase change medium yields more non-linearity. Due to the non-linearity introduced by the moving boundary and the higher power of temperature as well as the effects of refraction and reflection and the directional and spectral nature of radiation, both the exact and approximate analytical treatments and experimental investigations are limited and difficult [40,90].

In order to assess the numerical results for the present system, whose exact or approximate solutions are not reported in the literature, approximate analytical solutions for the one-dimensional axisymmetric heat conduction equation were obtained after making simplifying assumptions. The system initially was assumed to be at the fusion temperature and the liquid phase remained at this temperature throughout the process. Further, the change in internal energy in the solid phase was neglected. This assumption is reasonable when the latent heat of the phase change material is much larger than the sensible heat.

With the assumptions given above, the governing heat conduction equations for the cylindrical symmetric one-dimensional case in dimensionless form reduce to

$$\frac{\partial^2 \Theta_s}{\partial R^2} + \frac{1}{R} \frac{\partial \Theta_s}{\partial R} = 0 \qquad \text{for} \qquad 1 < R < L \tag{4.58}$$

$$\Theta_\ell = 0 \qquad \text{for} \qquad L \leqq R \leqq R_o \tag{4.59}$$

$$\beta^2 r_I^2 \frac{dL}{d\xi} = \frac{\partial \Theta_s}{\partial R} \qquad \text{for} \qquad R = L \tag{4.60}$$

The boundary conditions are

$$\Theta_s(R) = \Theta_1 \qquad \text{for} \qquad R = 1 \tag{4.61}$$

$$\Theta_s(R) = 0 \qquad \text{for} \qquad R = L \tag{4.62}$$

$$L(\xi) = 1 \qquad \text{for} \qquad \xi = 0 \tag{4.63}$$

The classical solutions of Equations (4.58) and (4.60) that satisfy the above boundary conditions are

$$\Theta_s(R) = \Theta_1 \left(1 - \frac{\ln R}{\ln L}\right) \tag{4.64}$$

$$\frac{L^2}{2} \ln L - \frac{1}{4} L^2 - J = 0 \tag{4.65}$$

where

$$R = \frac{r}{r_I} \quad , \quad L = \frac{\ell}{r_I} \quad , \quad \Theta_s = \frac{K_s}{\alpha_s \rho_s} \frac{(T_s - T_f)}{h_{sl}}$$

$$J = -\left(\frac{\Theta_1}{\beta^2 r_I^2} \cdot \xi + \frac{1}{4} \right)$$

The numerical solutions for pure conduction obtained using the enthalpy approach were compared with the approximate analytical solutions given by the simultaneous solution of Equations (4.64) and (4.65). In Figure 3 it may be seen that the analytical solution predicts slightly smaller values of temperature distribution than the numerical solution does. It may also be seen in Figure 4 that the interface radius predicted by the numerical solution is slightly smaller than that predicted by the analytical solution. The slight differences between the two solutions are due to the small amount of heat coming from the change in the internal energy of the solid phase which was included in the numerical solution and neglected in the approximate analytical solution. The difference between two solutions became smaller as the latent heat of fusion of the phase change medium increased.

Then the numerical results at the center nodes in radial or axial direction for two-dimensional problem were compared with those of one-dimensional case. The temperature and interface are compared in Figures 35 through 40 and 67 through 73. The agreement between the one- and the two-dimensional case is generally very close and, hence, reassuring.

When the internal thermal radiation is coupled with conduction for a solid region with a moving interface, the radiation effects on the temperature distribution of the phase change medium at any time and steady state conditions are in agreement with those reported in the literature for a semi-transparent medium without phase change. This is expected because the difference between the phase change

problem and the problem without phase change is at the solid/liquid interface where the latent heat of fusion is included for the phase change medium.

CHAPTER 5

NUMERICAL RESULTS AND DISCUSSION

The results of the present investigation are obtained from numerical experiments performed upon the cylindrical symmetric one- and the axisymmetric two-dimensional solidification problems. Since no prior work of the present problem has appeared in the literature, the general objective of these experiments is to gain a quantitative understanding of the effects of radiative transfer upon the dynamics of the phase change process.

Even though the computer programs (see Appendix C) have been developed to account for the temperature dependent conductivities and gray optical properties, those properties are assumed independent of temperature except for the first one-dimensional case where the conductivities are linearly dependent on temperatures for the solid region, and, for simplicity, only a liquid phase at the fusion temperature is assumed to be initially present.

Since a large number of independent parameters are involved to illustrate the effects of radiation heat transfer in a phase change material, results for various combinations of those parameters have been obtained.

For the present investigation, the various combinations of different conductivities, inside and outside temperature ratios, wall and solid/liquid interface emissivities, and scattering coefficients have been employed for an optically thick medium ($a \approx 4.572\ m^{-1}$).

In order to avoid an inaccurate characteristic of the P-1 approximation for an optically thin medium, the internal thermal radiation has been taken into account just after the radial optical thickness,

a ($\ell - r_I$), became greater than 1.5. This approximation may be justified for some real situations since the optical thickness or temperature difference of a medium between the inner cylinder and the interface becomes small enough to neglect an attenuation of radiation or a net radiative heat transfer at the beginning of solidification.

In the numerical solutions using the iterative scheme, the convergence criterion was based on the average of the absolute magnitudes of the changes of the enthalpy variable at all the nodes. This criterion was presented in Equation (4.56) in Chapter 4.

For an allowable error tolerance value (ERR) of 0.00001, the results of two successive iterations agreed to three significant digits. The accuracy of the numerical results was then considered adequate. The second parameter, which is critical for the accuracy of the results, is the dimensionless time step. Different time steps were studied by trial and error in order to find suitable sizes. The other parameters examined were the radial and axial mesh sizes. Different spatial mesh sizes were used in order to investigate their influence on the accuracy of the results. As the mesh size decreases, it is necessary to reduce the time step appreciably , increasing the C.P.U. time significantly.

By trial and error, it was found for the final computer runs that the number of spatial meshes can be respectively taken as 40 in radial direction for one-dimensional and/or two-dimensional cases and 20 in the axial direction for the two-dimensional case at $d\xi = 0.001$ for the input data without losing the desired accuracy. Convergence has been achieved within ten interations at each time step for the combinations of different parameters given in the following two sections.

5.1 SOLIDIFICATION OF CYLINDRICAL ONE-DIMENSIONAL ANNULUS

The purposes of this numerical experiment are to determine and analyze the significance of the conduction-radiation interaction parameter N and the error incurred by neglecting radiative transfer in an example representative of the solidification of a semi-transparent medium in a concentric annulus. A liquid cylindrical medium, initially at the fusion temperature is suddenly brought into perfect contact with opaque inner surface of a cylinder. The temperature of the inner cylinder surface is less than the medium solidification temperature and is held constant, while the temperature of the outside cylinder is maintained at the fusion temperature. The thicknesses of the inside and outside cylinder walls are small enough to neglect conduction, and thermal radiative penetration into the liquid region from the solid region is assumed to be neglected. Both boundaries are diffuse gray and the phase change medium is gray with an isotropic scattering coefficient.

Because of the general lack of property data for the high solidification temperature materials, it is impossible to determine input parameters and properties specifically for a given substance. However, the thermal and optical properties used in this investigation are approximately for the situation of a fluorite, one of the high temperature melting/solidification semi-transparent materials [3,6]. The temperature of the inner cylinder TI has been maintained at 810.8K that is lower than the medium solidification temperature TF. The reference temperature TR in dimensionless variables has been taken same as TF.

In Figures 5 through 8, the effect of linear dependence of thermal conductivity on temperature is shown along with the constant thermal conductivity. A broken circle in Figure 8 indicates the points where the internal thermal radiation has been taken into account. The linearly temperature dependent conductivities do not significantly affect the thermal radiation effect on the analysis. However, it makes the problem more nonlinear. Thus, constant conductivities are used throughout the following results.

The first quantitative thermal radiation effects on the transient temperature distribution in the solid phase of the present model are shown in Figures 9 through 14. The three different conductivities are employed in Figures 9, 10, and 11 while the three different temperature ratios are used in Figures 12, 13 and 14 for some typical Stark numbers or the conduction-radiation parameters. In Figures 9 ($N = 0.304$) and 14 ($N = 0.176$), the temperature distribution becomes more "S"-shaped (steeper gradient near inner and outer boundary surfaces). This is expected for the smaller values of N since the medium near the hot wall emits more radiant energy than it absorbs, or vice versa, near the cold wall. The medium in the cold region is more affected by the thermal radiation of the medium in the hot region and/or the hot wall than the opposite case. It may also be seen that the relative importance of thermal radiation becomes greater as N decreases even though the temperature ratio (TI/TF) is constant.

Thus, the smaller the value of N the larger is the temperature gradient at the inner surface of the cylinder for the conduction component as compared with the pure conduction case which, in turn,

increases the conductive heat extraction rate to maintain the constant inside temperature, as clearly shown in Figures 15, 16, and 17. The different conduction-radiation parameters are used for the three different conductivities in Figure 15. The conductive heat extraction rate for the combined case is greater than that of the purely conductive heat transfer case where the internal thermal radiation has not been taken into account. The difference in conductive and purely conductive heat extraction rate as well as between the total heat extraction (conductive and radiative extraction) and the purely conductive heat extraction becomes slightly smaller as N decreases. It can also be seen that the conductive heat flux at the inner surface of the cylinder decreases with time, faster at earlier times, but the radiative flux becomes almost steady from the beginning of solidification [99].

However, for the different inside and fusion temperature ratios, the radiative heat transfer effect is significantly increased as N decreases as shown in Figures 16 and 17. For $TI/TF = 0.4$, it is noticed that the radiative heat flux decreases as the time increases. This shows the fact that the transient effect on the radiative flux becomes important for the higher temperature solidifying or melting semi-transparent materials. The total and conductive heat extraction rates for the combined case, being compared with the pure conduction, are greatly increased for $N < 1.0$. In Figure 18, the steady state heat fluxes at the inner cylinder are illustrated for black surfaces and different temperature ratios. It can be seen that although the magnitude of the radiative heat flux is small compared to the conductive heat flux the effect of taking radiation into account is

significant; the conductive flux component is much greater than when radiation is neglected. This effect is seen to increase with increasing temperature ratio. It should be noted that the difference between conduction and pure conduction is bigger than the absolute magnitude of radiative heat flux. And this radiative flux becomes greater than the purely conductive extraction for TF/TI > 3.5.

Figures 19 through 23 show the transient radiative heat flux distributions in the radial direction in the solid region. The magnitude of the radial radiative heat flux initially increases but then becomes smaller as time increases. It has a maximum value near the center except the case for ξ = 3.0 in Figure 22 and ξ = 1.5, 3.0 in Figure 23, where some net positive radiative heat flux has developed. There is no adequate explanation for the occurrence of the large positive radiative heat flux. It shows that the change of radiant intensity gradient does not follow the pattern of the other cases given in the figures. Recognizing that the divergence of the radiative flux vector is negative in the vicinity of the cold surface, it is clear that the rate of absorption of radiant energy per unit of the volume exceeds the rate of emission. By the opposite reasoning, the rate of emission of radiant energy exceeds the rate of absorption near the hot interface. This explains why the "S"-shaped temperature distributions are formed within the solid region. Figures 24 through 26 show an acceleration of the solid/liquid interface at different times when the thermal radiation has been taken into account in the semi-transparent phase change material. The different conductivities in Figure 24 and temperature ratios in Figures 25 and 26 are introduced to indicate the internal thermal

radiation effect on the dynamics of the solid/liquid interface. An acceleration of the interface is a consequence of the cooling of the liquid by radiation.

The radiative effect of different wall emissivities on the temperature, the radial radiative heat flux, the solid/liquid interface, and the heat flux at the inner cylinder is illustrated in Figures 27 through 30. In Figure 27, the slope of the temperature distribution decreases near the cold inner surface and increases near the hot interface with decrease in emissivity. The absolute magnitudes of the radial radiative heat flux and the heat extraction rate at the inner cylinder decreases as the emissivity decreases in Figures 28 and 30. An influence upon the solid/liquid interface location by the different emissivities is shown to be within three percent in Figure 29. The radiative effect of different scattering coefficient ω on above four cases for TI/TF = 0.5 and Ks = 3.462 W/mK has been found to be within 2% of values for ω = 0.5 and is shown in Figures 31 through 34 and hence, only single curves for the transient temperature distributions and the radial radiative heat fluxes appear in Figures 31 through 33.

5.2 SOLIDIFICATION OF FINITE CYLINDRICAL TWO-DIMENSIONAL ANNULUS

In the numerical experiments for the finite concentric cylindrical medium, both base surfaces of the finite concentric cylinders are assumed to be perfectly insulated. The length of the cylinder is taken the same as the radius of the outside cylinder radius (z/r_o = 1) except in Figures 40, 48, 50, and 58 where z/r_o is 0.5. In Figures 35 through 40, the transient temperature distributions in the

radial direction for different conduction-radiation parameters are illustrated at j =N/2 of the inside cylinder (see Figure 2) and compared with the results obtained in the numerical experiments for the infinite concentric cylindrical medium. Even though the difference of temperature distribution for the purely conductive case between one- and two- dimensional problems is negligible, the difference for the combined conduction and radiation case between the finite and the infinite concentric cylinders becomes greater as N decreases (see Figures 35 through 38). This suggests that the infinite one-dimensional analysis for the finite two-dimensional present model may lead to a significant error as radiative transfer becomes increasingly important. It can also be seen that the slopes of temperature profiles of the one-dimensional model near the inner cylinder becomes steeper than those of the two-dimensional analysis. An increase of the steepness produces a greater conductive heat extraction rate at the inner cylinder (see Figure 49). The effect of emissivities of the walls on temperature distribution is shown in Figure 39 where the temperature near the solid/liquid interface is mostly affected. This is also seen in the radial radiative heat flux at ξ = 8.0 in Figure 53. The change of length in the axial direction does not significantly affect the temperature distribution as shown by comparing Figures 35 and 40. This is because the magnitude of the axial radiative heat flux is less than one-tenth of the radial radiative heat flux for this case as will be shown in Figures 50 and 58.

The transient radial heat flux distribution in the axial direction is displayed in Figures 41 through 48 for different parameters. As the internal thermal radiation becomes more important, the total

heat extraction rate along the axial direction tends to be more non-uniform for the black surfaces as shown in Figures 41, 42, 43, and 45. However, more uniform heat flux distributions are established in Figures 44, 46, and 47 by employing lower surface emissivities. Compare Figures 43 and 44 and 45, 46, and 47. In Figure 48, the transient radial heat fluxes at the inner cylinder are displayed for $z/r_o = 0.5$, and it is seen that these are not greatly influenced by the change of the length (compare with Figure 41). The heat fluxes in the radial direction, at $j = N/2$, at the inner cylinder after steady state are plotted with respect to the temperature ratios, TF/TI's in Figure 49. The heat fluxes obtained for the finite annulus are then compared with those of the infinite model. The radial radiative heat flux for the infinite model (B) is overpredicted, being compared with the finite model (A), for TF/TI > 2.0, and the discrepancy between these two models increases as TF/TI increases. The difference of conductive heat extraction rates for the combined case between two analyses continually increases as TF/TI increases even though the radiative heat fluxes are close to each other until TF/TI = 2.0. The single line is used to show the purely conductive heat fluxes for two different models since the difference of the results obtained between the infinite and the finite analyses is not discernible. Note that the axial radiative heat flux has been included for the finite cylindrical problem while only the radial radiative heat flux has been considered for the one-dimensional problem.

Figures 50 through 56 show the transient radial radiative heat flux distributions at $j = N/2$ in the solid region. The employment of

gray surfaces produces a positive radial radiative heat flux at $\xi = 8.0$ shown in Figure 53 as is in the one-dimensional case. The positive quantities in Figure 53 mean that the radiative intensity has been increased in the negative r-direction near the solid/liquid interface. An increase of the positive divergence of the radiative flux vector near the interface yields, being compared to the rate of absorption, more emission rate of radiant energy per unit of the volume. A similar phenomenon has appeared in Figures 54, 55, and 56 for N = 0.176.

In Figures 57 through 66, the transient axial radiative heat flux distributions at $\ell/2$ are illustrated. It may be seen that the axial radiative heat flux for $z/r_o = 0.5$ in Figure 58 becomes slightly larger near both base surfaces than that of $z/r_o = 1.0$ shown in Figure 57. Symmetric axial radiative heat flux effects are obtained because of the symmetric geometry of the present model when the solid/liquid interface becomes a straight line (Figure 67). A schematic sketch of symmetric radiative heat flux is shown in Figure 5.1 where (A) represents the negative axial flux while (B) represents the positive axial flux shown in Figures 57 and 58. Probable reasons for the non-symmetric effect on the axial flux at $\xi = 20.0$ and 30.0 in Figure 59 are in the approximation of RTE with Marshak type boundary conditions or an error in the numerical computation. Figures 60 through 62 show the effects of varying wall and solid/liquid interface emissivities for N = 0.736. The symmetric effect on the solid/liquid interface can also be seen

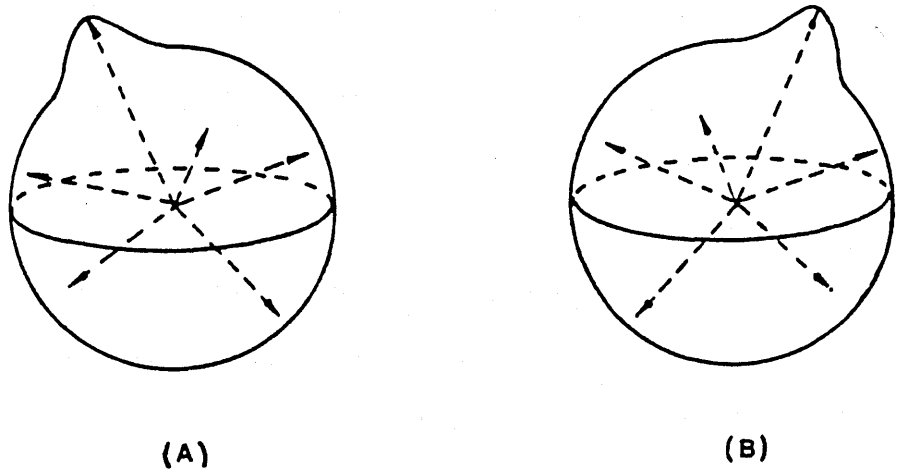

Figure 5.1 A Schematic Sketch of Symmetric Radiative Heat Flux

in Figures 70 (N = 0.736), 71 (N = 0.422) and 72 (N = 0.176). Figure 63 shows the transient axial radiative heat fluxes for N = 0.422. Figures 64, 65, and 66 show that the transient axial radiative heat fluxes may almost die out if the surface emissivities are diminished.

In Figures 67 through 72, the transient solid/liquid interfaces of the finite concentric cylindrical medium are compared with those of the infinite concentric cylindrical medium. The difference between one- and two-dimensional cases becomes larger as the time increases and the conduction-radiation parameter decreases. The movement of the solid/liquid interface locations by the infinite model is always predicted to be faster than those of the finite model for the various parameters. The effect of wall and solid/liquid interface emissivities on the interface is shown in Figure 73. The employment of black surface produces a faster solidification process than the gray cases.

CHAPTER 6

CONCLUSIONS AND RECOMMENDATIONS

6.1 CONCLUSIONS AND SUMMARY

The effect of internal thermal radiation on the solidification and energy transfer within an absorbing, emitting, isotropically scattering infinite and finite, semi-transparent gray phase change medium bounded by two concentric cylinders has been investigated. Since the exact treatment of a coupled heat transfer problem with radiation for a finite phase change cylindrical medium is complicated, it has been necessary to employ approximate methods which are generally good for multi-dimensional analysis and parameter studies.

In the present work, the principle of conservation of energy which employs enthalpy and temperature as dependent variables has been first coupled with a set of moment equations that are derived from the radiative transfer equations and Marshak type boundary conditions by applying P-1 differential approximations. The transient temperature distribution, interface location of a semi-transparent phase change medium, and the local radiative radial and axial heat fluxes have been obtained by using a Gauss-Seidel iterative numerical scheme for some typical cases.

The optically thick solid medium was in local thermodynamic equilibrium and gray, homogeneous, and isotropic assumptions were employed. Surfaces were assumed to be opaque and diffuse gray.

The computer programs were developed so that different boundary conditions could easily be incorporated--possibly with semi-transparent surfaces, and spatially dependent thermal and optical

properties except density variations within a medium. In the typical numerical experiments chosen in this investigation, the solid/liquid interface was quantitatively shown to accelerate more as the conduction/radiation parameter, N, became smaller, particularly less than 1. "S"-shaped temperature distributions (steeper near the inner and outer walls than in the central region) were obtained when the internal energy transfer occurs simultaneously by conduction and radiation.

As a result of the steeper temperature gradient near the inner cylinder for the combined energy transfer analysis, the conductive heat extraction rate at the inner cylinder has increased. The conductive and/or radiative heat extraction rates at the inner cylinder are plotted for different temperature ratios (TI/TF) or N in order to show the effect of varying the fusion temperature.

It was found that the transient solid/liquid interface and temperature distribution for the finite concentric cylinder (TI/TF = 0.5, r_I/r_o = 0.5, z/r_o = 1.0) was very close to that of an infinite cylinder when the conductive heat transfer was the only energy transfer mode. However, when the radiative transfer became increasingly important, it was shown that the infinite one-dimensional analysis for the finite two-dimensional model might lead to a significant error.

For a finite concentric annulus, the solid/liquid interface became almost a straight line when N was greater than 1 and at the early stages of solidification (see Figures 67 through 70). The axial radiative heat flux distributions were nearly symmetric with respect to the center line from both base surfaces when solid/liquid

interface is a straight line. The net axial radiative heat flux was then close to zero at the center because of the physically symmetric distance effect of the geometry and the assumptions of a gray, homogeneous, and isotropic medium together with gray diffuse opaque boundary surfaces. When different emissivities of the walls, temperature ratios (TF/TI), and conductivities were used for the coupled problem, there was some net radiative heat flux development where the change of radiant intensity gradient was somewhat different from the other cases. An increase of the positive divergence of the radiative flux vector near the interface yielded, being compared to the rate of absorption, more emission rate of radiant energy per unit of volume. More uniform radial radiative heat flux at the inner cylinder and a smaller magnitude of the axial radiative heat flux were obtained when the gray surfaces for some typical cases were employed.

In the numerical experiments using the iterative scheme, the allowable error tolerance value and the time step size were critical for the accuracy of the results. As the mesh size decreased by a factor of two, it was necessary to reduce the time step appreciably so that the C.P.U. time for the axisymmetric two-dimensional cases could be kept at a reasonable level. Therefore, the appropriate spatial mesh sizes for a specific time step were determined based upon two successive computer runs where the difference of these two results was within three percent in order to have an economical computing time.

6.2 FURTHER RECOMMENDED TOPICS

Although the objective of the present investigation has been accomplished, the following areas are recommended for further research.

1. The search must continue for simplified but meaningful methods that can determine the radiative heat flux for a non-planar multi-dimensional optically thin medium along with easy incorporation into the energy equation.

2. An appropriate model for nongray radiative transfer in semi-transparent phase change materials can be employed by including the weighted mean absorption coefficient that is analogous to the Planck and Rosseland mean approximations.

3. The effects of optical anisotropy and non-homogeneity of a semi-transparent medium on radiative transfer may be significant and need to be examined.

4. The radiative heat balance at the semi-transparent non-planar boundary surfaces and the solid/liquid interface must be developed. The effects of surface curvature on the refraction of incident radiation and on radiative transfer as well as heat transfer, temperature distribution, and solid/liquid interface location should be determined.

5. A convective effect can be included in the liquid region and an extension to three-dimensional geometry including angular direction is recommended.

6. Although experimental investigations, particularly at high temperature, are challenging and difficult because of the complicated and long distance nature of radiation for the coupling of radiation with other modes of energy transfer, it is recommended that some experiments which would verify the findings of this investigation be devised.

LIST OF REFERENCES

1. Carslaw, H.S., and Jaeger, J.C., "Conduction of Heat in Solids," Oxford University Press, Oxford, 1959.

2. Stefan, J., "Ueber die Theorie der Eisbildung, insbesondere über die Eisbildung im Polarmeere," Ann. Phy. Chem., Vol. 42, p. 269, 1891.

3. Abrams, M., "Energy Transfer During Melting and Solidification of Semi-Transparent Crystals," Ph.D. Thesis, Purdue University, Lafayette, Indiana, 1971.

4. Abrams, M., and Viskanta, R., "Effects of Radiative Heat Transfer Upon Melting and Solidification of Semi-Transparent Crystals," J. Heat Transfer, Vol. 96, pp. 184-190, 1974.

5. Habib, I.S., "Solidification of Semi-Transparent Materials by Conduction and Radiation," Int. J. Heat Mass Transfer, Vol. 14, pp. 2161-2164, 1971.

6. Habib, I.S., "Solidification of Semi-Transparent Cylindrical Medium by Conduction and Radiation," J. Heat Transfer, Vol. 95, pp. 37-41, 1973.

7. Cho, C., and Ozisik, M.N., "Effects of Radiation on Melting of Semi-Transparent Semi-Infinite Medium," Int. Heat Transfer Conf. 6th, pp. 373-378, 1978.

8. Seki, N., Sugawara, M., and Fukusako, S., "Back-Melting of Horizontal Cloudy Ice Layer with Radiative Heating," J. Heat Transfer, Vol. 101, pp. 90-95, 1979.

9. Chan, S.H., and Albeirutty, M.H., "B-Splines Collocation Solution of Combined Conduction-Radiation with Phase Change and

Moving Boundary," Int. Cong. on Numerical Method in Thermal Probs. 2nd., Venice, pp. 180-192, 1981.

10. Ortega, A.S., Benard, C., and Gobin, D., "Paraffin Trombe Wall for Space Heating," Build. Energy Manage. Consv. and Sol. Approaches, pp. 195-200, 1980.

11. Goodman, T.R., "Heat Balance Integral and Its Application to Problems Involving Change of Phase," Trans. ASME, pp. 335-342, 1958.

12. Chan, S.H., and Cho, D.H., "Melting and Solidification with Internal Radiative Transfer - Gerneralized Phase Change Model," Int. J. Heat Mass Transfer, Vol. 26, No. 4, pp. 621-633, 1983.

13. Diaz, L.A., "Radiation Induced Melting of Semi-Transparent Phase Change Material," Ph. D. Dissertation, Purdue University, 1983.

14. Shamsundar, N., and Sparrow, E.M., "Analysis of Multi-Dimensional Conduction Phase Change Via Enthalpy Model," ASME J. Heat Transfer, pp. 330-340, 1975.

15. Patel, P.D., "Interface Conditions in Heat Conduction Problems with Phase Change," AIAA J., Vol. 6, p. 2454, 1968.

16. Rathjen, K.A., and Jiji, L.M., "Heat Conduction with Melting or Freezing in Corner," Tran. ASME J. Heat Transfer, Vol. 93, pp. 101-109, 1971.

17. Koeger, P.G., and Ostrach, S., "Solution of Two-Dimensional Freezing Problems Including Convection Effects in Liquid Region," Int. J. Heat Transfer, Vol. 17, pp. 1191-1207, 1974.

18. Siegel, R., "Shape of Two-Dimensional Solidification Interface During Directional Solidification by Continuous Casting," ASME J. Heat Transfer, February, 1978.

19. Bankoff, S.G., "Heat Conduction or Diffusion with Change of Phase," Advances in Chemical Engineering, Drew, T., ed., Academic Press, pp. 75-150, N.Y., 1964.

20. Muehlbauer, J.C., and Sunderland, E.J., "Heating Conduction with Freezing or Melting," Appl. Mech. Rev., Vol. 18, pp. 951-959, 1965.

21. Yimer, B., "Transient Thermal Analysis of Phase Change Material Energy Storage System," Ph.D. Thesis, U. of Dayton, 1979.

22. Goodman, T.R., "Application of Integral Methods to Transient Nonlinear Heat Transfer," Advances in Heat Transfer, Vol. 1, Irvine, T.F. and Hartnett, J.P., eds., Academic Press, N.Y., pp. 51-122, 1964.

23. Van Dyke, M., "Pertubation Methods in Fluid Mechanics," Academic Press, 1964.

24. Yan, M.M., and Huang, P.N., "Pertubation Solution to Phase Change Problem Subject to Radiation and Convection," J. Heat Transfer, April, 1977.

25. Yen, L.T., and Chung B.T.F., "Variational Analysis of Freezing or Melting in Finite Medium Subject to Radiation and Convection," J. Heat Transfer, Vol. 101, pp. 592-597, 1979.

26. Tikhov, A.N., and Samarskii, A.A., "Equations of Mathematical Physics," Pergamon Press Oxford, 1963.

27. Indritz, J., "Method in Analysis," Macmillan, N.Y., 1963.

28. Chang, Y., and Kang, C., "Transient and Steady Heat Transfer in Conducting and Radiating Medium," AIAA J., Vol. 8, pp. 609-614, 1970.

29. Bathlet, A.G., and Viskanta, R., "An Experimental Investigation of Natural Convection in Melted Region Heated Horizontal Cylinder," J. Fluid Mechanics, Vol. 90, pp. 227-239, 1979.

30. Sparrow, E.M., and Schmidt, R.R., "Experiments on Role of Natural Convection in Melting of Solids," J. Heat Transfer, Vol. 100, pp. 11-16, 1978.

31. Yao, L.S., and Chen, F.F., "Effects of Natural Convection in Melted Region Around Heated Horizontal Cylinder," J. Heat Transfer, Vol. 102, pp. 667-672, 1980.

32. Saitoh, T. and Hirose, K., "High Rayleigh Number Solution to problems of Latent Heat Thermal Energy Storage in Horizontal Cylinder Capsule," J. Heat Transfer, Vol. 104, pp. 545-553, 1982.

33. Chan, A.M.C., and Shoukri, M., "Numerical Solution of Two-Dimensional Freezing Under Influence of Natural Convection in Liquid Phase," ASME Paper No. 82-WA/HT-10, 1982.

34. Rieger, H., Projahn, U., Bareiss, M., and Beer, H., "Heat Transfer During Melting Inside Horizontal Tube," J. Heat Transfer, Vol. 105, pp. 226-234, 1983.

35. Viskanta, R., and Grosh, R.J., "Heat Transfer by Simultaneous Conduction and Radiation in Absorbing Medium," J. Heat Transfer, Vol. 84, pp. 63-72, 1962.

36. Viskanta, R., "Heat Transfer by Conduction and Radiation in Absorbing and Scattering Materials," J. Heat Transfer, Vol. 87, pp. 143-150, 1965.

37. Lick, W., "Transient Energy Transfer by Radiation and Conduction," Int. J. Heat Mass Transfer, Vol. 8, pp. 119-127, 1965.

38. Chang, Y.P., "A Potential Treatment of Energy Transfer in Conducting and Emitting Medium," ASME Paper, No. 67-WA/HT-40, 1967.

39. Hazzak, A.S. and Beck, J.V., "Unsteady Combined Conduction-Radiation Energy Transfer Using a Rigorous Differential Method," Int. J. Heat Mass Transfer, Vol. 13, pp. 517-522, 1975.

40. Viskanta, R., and Anderson, E.E., "Heat Transfer in Semi-Transparent Solids," Adv. Heat Transfer, Vol. 11, pp. 317-441, 1975.

41. Viskanta, R., and Hirleman, E.D., "Combined Conduction-Radiation Heat Transfer Through Irradiated Semi-Transparent," J. Heat Transfer, Vol. 100, pp. 169-172, 1978.

42. Amlin, D.W., and Korpela, S., "Influence of Thermal Radiation of Temperature Distribution in Semi-Transparent Solid," J. Heat Transfer, Vol. 101, pp. 76-80, 1979.

43. Milne, E.A., "Thermodynamics of Stars," Handbuch Der Astrophysik, Vol. 3, pp. 65-255, 1930.

44. Eddington, A., The Internal Constitution of Stars, Dover, 1959.

45. Chandrasekhar, S., Radiative Transfer, Dover, 1960.

46. Cheng, P., "Study of Flow of Radiating Gas by Differential Approximation," Ph.D. Dissertation, Stanford University, 1965.

47. Cheng, P., "Exact Solutions and Differential Approximation for Multi-Dimensional Radiative Transfer in Cartesian Coordinate Configuration," Prog. & Astronaut, and Aeronaut., Vol. 31, p. 269, 1972.

48. Yuen, W.W., and Wong, L.W., "Heat Transfer by Conduction and Radiation in One-Dimensional Absorbing, Emitting, and

Anisotropically-Scattering Medium," J. Heat Transfer, Vol. 102, pp. 303-307, 1980.

49. Viskanta, R., and Kim, D.M., "Heat Transfer Through Irradiated, Semi-Transparent Layers at High Temperature," ASME J. Heat Transfer, Vol, 102, pp. 388-390, 1980.

50. Fernandes, R., and Francis, J., "Combined Conductive and Radiative Heat Transfer in Absorbing, Emitting, and Scattering Cylindrical Media," J. Heat Transfer, Vol. 104, pp. 594-601, 1982.

51. Tsai, C.F., and Chan, S.H., "Numerical Solution of Contact Interface Temperature with Internal Thermal Radiation and Conduction Effects," Numerical Heat Transfer, Vol. 5, pp. 359-365, 1982.

52. Ratzel, A.C. and Howell, J.R., "Heat Transfer by Conduction and Radiation in One-Dimensional Planar Media Using the Differential Approximation," ASME J. Heat Transfer, Vol. 104, pp. 388-391, 1982.

53. Tong, T.W., Birkebak, R.C., and Enoch, I.E., "Thermal Radiation, Convection, and Conduction in Porous Media Contained in Vertical Enclosures," J. Heat Transfer, Vol. 105, pp. 414-418, 1983.

54. Shih, T.M., and Chen, Y.N., "Descretized-Intensity Method Proposed for Two-Dimensional Systems Enclosing Radiative and Conductive Media," Numerical Heat Transfer, Vol. 6, pp. 117-134, 1983.

55. Chung, T.J., and Kim, J.Y., "Two-Dimensional, Combined-Mode Heat Transfer by Conduction, Convection, and Radiation in Emitting,

Absorbing, and Scattering Media-Solution by Finite Elements," J. Heat Transfer, Vol. 106, pp. 448-452, 1982.

56. Razzaque, M.M., Howell, J.R., and Dlein, D.E., "Coupled Radiative and Conductive Heat Transfer in Two-Dimensional Rectangular Enclosure with Gray Participating Media Using Finite Elements," J. Heat Transfer, Vol. 106, pp. 613-619, 1984.

57. Gordaninejad, F., and Francis, J., "A Finite Difference Solution to Transient Combined Conductive and Radiative Heat Transfer in Annular Medium," ASME J. Heat Transfer, Vol. 106, pp. 888-891, 1984.

58. Crosbie, A.L. and Linsenbardt, T.L., "Two-Dimensional Isotropic Scattering in Semi-Infinite Medium," Quant. Spectrpsc. Radiat. Transfer, Vol. 19, pp. 257-284, 1978.

59. Breig, W.F., and Crosbie, A.L., "Two-Dimensional Radiative Equilibrium," J. Math. Analysis and Applics., Vol. 46, No. 1, pp. 104-125, 1974.

60. Modest, M.F., "Two-Dimensional Radiative Equilibrium of Gray Medium in Planar Layer Bounded by Gray Nonisothermal Walls," ASME J. Heat Transfer, Vol. 96, No. 4, pp. 483-488, 1974.

61. Yuen, W.W., and Tien, C.L., "Successive Approximation Approach to Problems in Radiative Transfer with Differential Approximation," ASME J. Heat Transfer, Vol. 102, No. 1, pp. 86-91, 1980.

62. Glatt, L., and Olfe, D.B., "Radiative Equilibrium of Gray Medium in Rectangular Enclosure," J. Quant. Spectr. and Rad. Transf., Vol. 13, No. 9, pp. 881-895, 1973.

63. Yuen, W.W., and Wong, L.W., "Radiative Transfer in Rectangular Enclosure with Gray Medium," ASME Paper No. 80-HT-101, 1980.

64. Siddall, R.G., and Selcuk, N., "Evaluation of New Six-Flux Model for Radiative Transfer in Rectangular Enclosure," Trans. J. Chem. E., Vol. 57, No. 13, 1979.

65. Ratzel, A.C., "P-N Differential Approximation for Solution of One- and Two-Dimensional Radiation and Conduction Energy Transfer in Gray Participation Media," Ph.D. Dissertation, The University of Texas at Austin, 1981.

66. Siegel, R., and Howell, J.R., Thermal Radiation Heat Transfer, 2nd ed. McGraw-Hill, N.Y., 1981.

67. Taniguchi, H., "Radiative Heat Transfer of Gas in Three-Dimensional System Calculated by Monte Carlo Method," Bull JSME, Vol. 12, pp. 67-68, 1969.

68. Hottel, H.C., and Sarofim, A.F., Radiative Transfer, McGraw-Hill, N.Y., 1967.

69. Hottel, H.C., and Cohen, E.S., "Radiant Heat Exchange in Gas-Filled Enclosure: Allowance for Non-Uniformity of Gas Temperature," AICHE Journal, Vol. 4, No. 1, pp. 3-14, 1958.

70. Larsen, M., "Hottel Zone Code," developed for Ph.D. Research at Univ. of Texas at Austin, Aug. 1981.

71. Howell, J.R., "Radiative Transfer in Multi-Dimensional Geometries," ASME Paper No. 83-HT-32, 1983.

72. Meuguc, M.P. and Viskanta, R., "Radiative Transfer in Three-Dimensional Rectangular Enclosures," ASME Paper No. 84-HT-35, 1984.

73. Fletcher, J.K., "The Solution of Multi-Group Neutron Transport Equation Using Spherical Harmonics," Nuclear Science and Engineering, Vol. 84, pp. 271-288, 1982.

74. Kuznetsov, Y.S., "Temperature Distribution in Infinite Cylinder and Sphere in a State of Non-Monochromatic Radiation Equilibrium," USSR Comput. Math. Phys. 2, pp. 230-254, 1963.

75. Kesten, A.S., "Radiant Heat Flux Distribution in Cylindrically-Symmetric Nonisothermal Gas with Temperature Dependent Absorption Coefficient," J. Quant. Spectrosc. Radiat. Transfer, Vol. 8, pp. 419-434, 1968.

76. Habib, I.S., and Greif, R., "Nongray Radiative Transport in Cylindrical Media," ASME J. Heat Transfer, pp. 29-32, 1970.

77. Nakra, N.K., and Smith, T.F., "Combined Radiation-Convection for Real Gas," ASME J. Heat Transfer, Vol. 99, pp. 60-65, 1977.

78. Heaslet, M.A., and Warming, R.F., "Theoretical Predictions of Radiative Transfer in Homogeneous Cylindrical Medium," J. Quant. Spectrosc. Radiat. Transfer, Vol. 6, pp. 751-774, 1966.

79. Echigo, R., Hasegawa, S., and Tamehiro, H., "Radiative Heat Transfer by Flowing Multi-Phase Medium-Part II. An Analysis on Heat Transfer of Laminar Flow in Entrance Region of Circular Tube," Int. J. Heat Mass Transfer, Vol. 15, pp. 2595-2610, 1972.

80. Dua, S.S., and Cheng, P., "Multi-Dimentional Radiative Transfer in Non-Isothermal Cylindrical Media with Non-Isothermal Bounding Walls," Int. J. Heat Mass Transfer, Vol. 18, pp. 245-259, 1975.

81. Bayazitoglu, Y., and Higenyi, J., "Higher-Order Diferential Equations of Radiative Transfer: P-3 Approximation," AIAA Journal, Vol. 17, No. 4, pp. 424-431, 1979.

82. Bayazitoglu, Y., and Higenyi, J., "Differential Approximation of Radiative Heat Transfer in Gray Medium-Axially Symmetric Radiation Field," J. Heat Transfer, Vol. 102, pp. 719-723, 1980.

83. Azad, F.H., and Modest, M.F., "Evaluation of Radiative Heat Flux in Absorbing, Emitting and Linear-Anisotropically Scattering Cylindrical Media," J. Heat Transfer, Vol. 103, pp. 350-356, 1981.

84. Ou, S.C. and Liou, K.N., "Generalization of Spherical Harmonic Method to Radiataive Transfer in Multi-Dimensional Space," J. Quant. Spectrosc. Radiat. Transfer, Vol. 28, No. 4, pp. 271-288, 1982.

85. Benassi, M., Cotta, R.M., and Siewert, C.E., "The P-N Method for Radiative Transfer Problems with Reflective Boundary Conditions," J. Quant. Spectrosc. Radiat. Transfer, Vol. 30, No. 6, pp. 547-553, 1983.

86. Crosbie, A.L. and Farrell, J.B., "Exact Formulation of Multiple Scattering in Three-Dimensional Cylindrical Geometry," J. Quant. Spectrosc. Radiat. Transfer, Vol. 31, No. 5, pp. 397-416, 1984.

87. Desosto, S., "Coupled Radiation, Conduction and Convection in Entrance Flow," Int. J. Heat Mass Transfer, Vol. 11, pp. 245-259, 1975.

88. Krook, M., "On the Solution of Equation of Transfer, I," Astrophys. J., Vol. 122, pp. 488-497, 1955.

89. Jeans, J.H., "Equations of Radiative Transfer of Energy," Monthly Notices Rev. Astron. Soc., Vol. 78, pp. 28-36, 1917.

90. Ozisik, N.M., "Radiative Transfer and Interactions with Conduction and Convection," Wiley-Interscience, N.Y., 1973.

91. Uesugi, A., and Tsujita, J., "Difuse Reflection of Searchlight Beam by Slab, Cylindrical and Spherical Media," Astronomical Society of Japan Publication, Vol. 21, pp. 370-383, 1969.

92. Carnahan, B., Luther, H.A., and Wilkes, J.O., Applied Numerical Methods, (John Wiley & Inc.), 1969.

93. Kourganoff, V., "Basic Methods in Transfer Problems," Dover Publications, N.Y., 1963.

94. Davidson, B., "Neutron Transport Theory," Oxford University Press, London, 1958.

95. Case, K.M. and Zweifel, P.F., "Linear Transport Theory," Addison-Wesley Publishing Co., 1967.

96. Higenyi, J.K.D., "Higher Order Diferential Approximation of Radiative Energy Transfer in Cylindrical Gray Medium," Ph.D. Dissertation, Rice University, 1980.

97. Marshak, R.E., "Note on the Spherical Harmonics Method as Applied to the Milne Problem for a Sphere," Phys. Review, Vol. 71, pp. 443-446, 1947.

98. Mark, J.C., "The Spherical Harmonics Method, Parts I and II," National Research Council of Canada, Atomic Energy Reports, No. MT92 (1944) and MT97 (1945).

99. Chang, Y.P. and Smith, R.S., Jr., "Steady and Transient Heat Transfer By Radiation and Conduction In a Medium Bounded By Two Coaxial Cylindrical Surfaces," Int. J. Heat Mass Transfer, Vol 13, pp. 69-80, 1970.

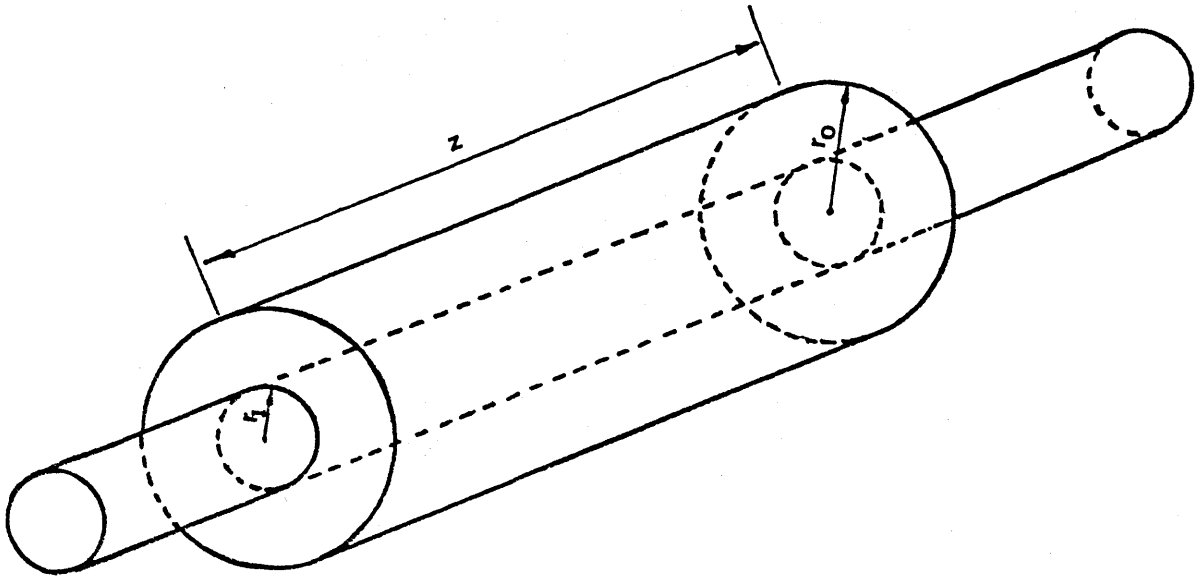

Figure 1 A SCHEMATIC OF THE PHYSICAL SYSTEM

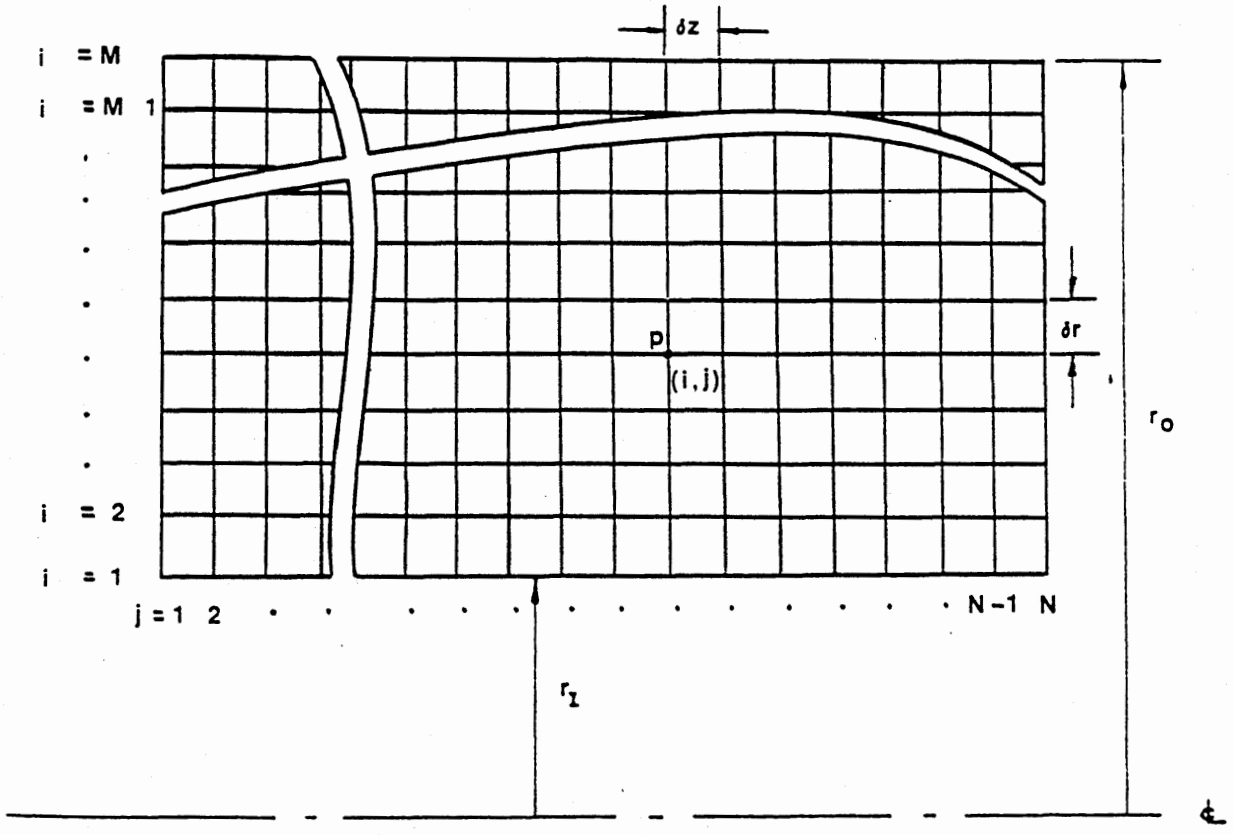

Figure 2 MESH LAYOUT OF FINITE CONCENTRIC CYLINDRICAL MEDIUM

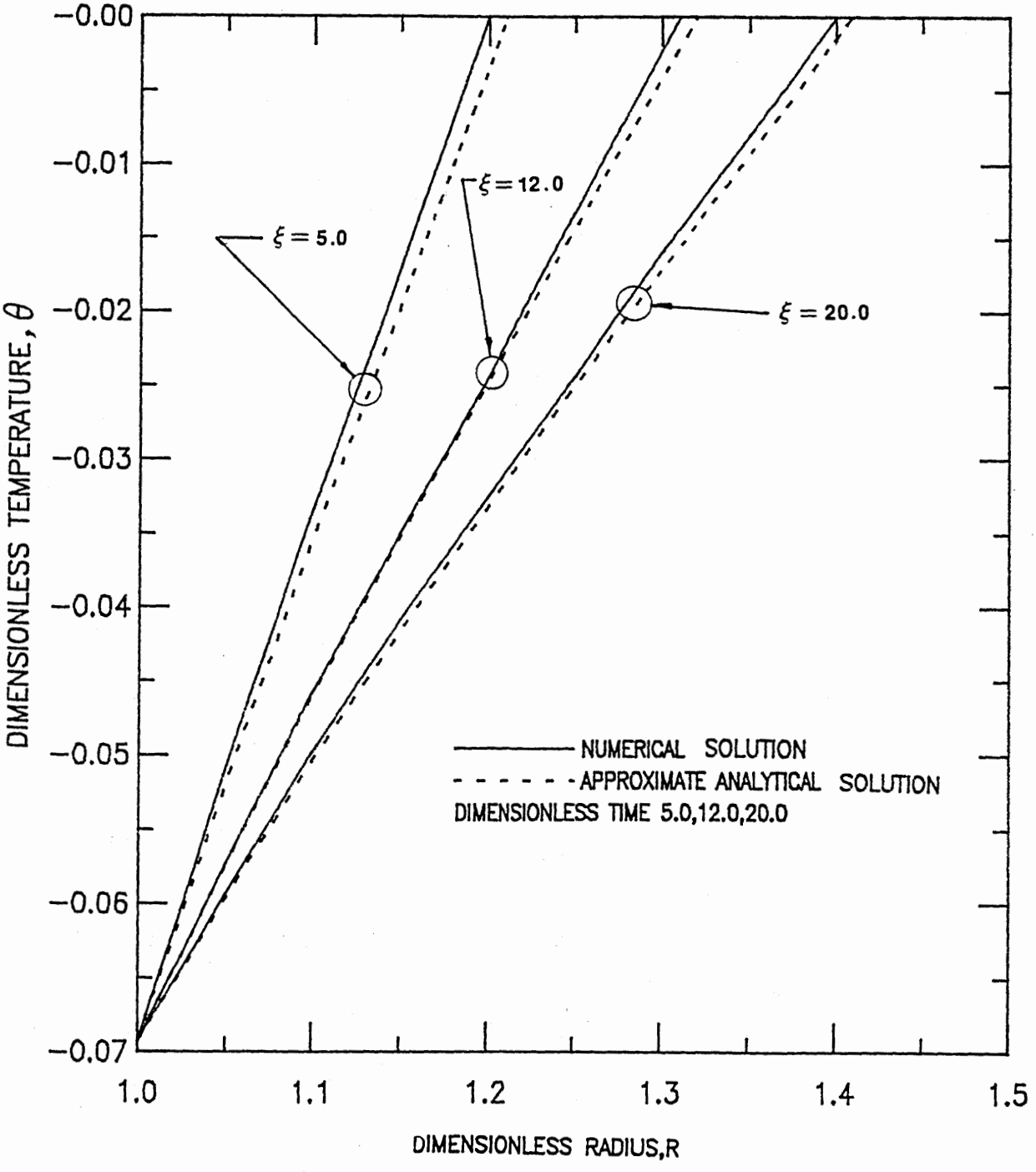

Figure 3 TRANSIENT DIMENSIONLESS TEMPERATURE VS. DIMENSIONLESS RADIUS

TI/TF=0.714,a=4.572 /m,ri/ro=0.5,Ks=7.114W/mK
Hsl=1395.6kJ/kg, ρ=2803.2kg/m^3, αs=0.0307m^2/hr

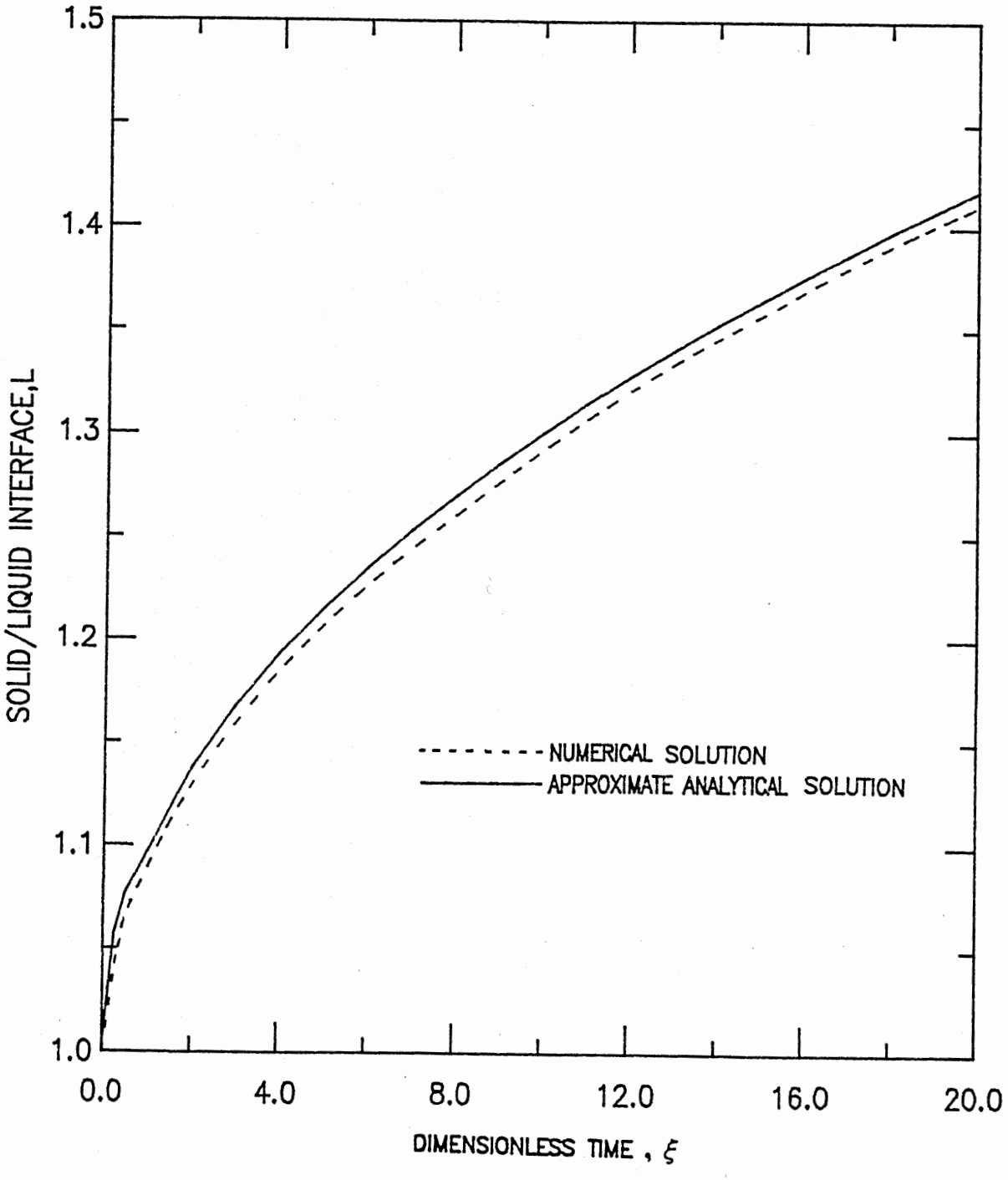

Figure 4 SOLID/LIQUID INTERFACE VS. DIMENSIONLESS TIME

Tl/TF=0.714,a=4.572 /m,ri/ro=0.5,Ks=7.114W/mK
Hsl=1395.6kJ/kg, ρ=2803.2kg/m^3, α_s=0.0307m^2/hr

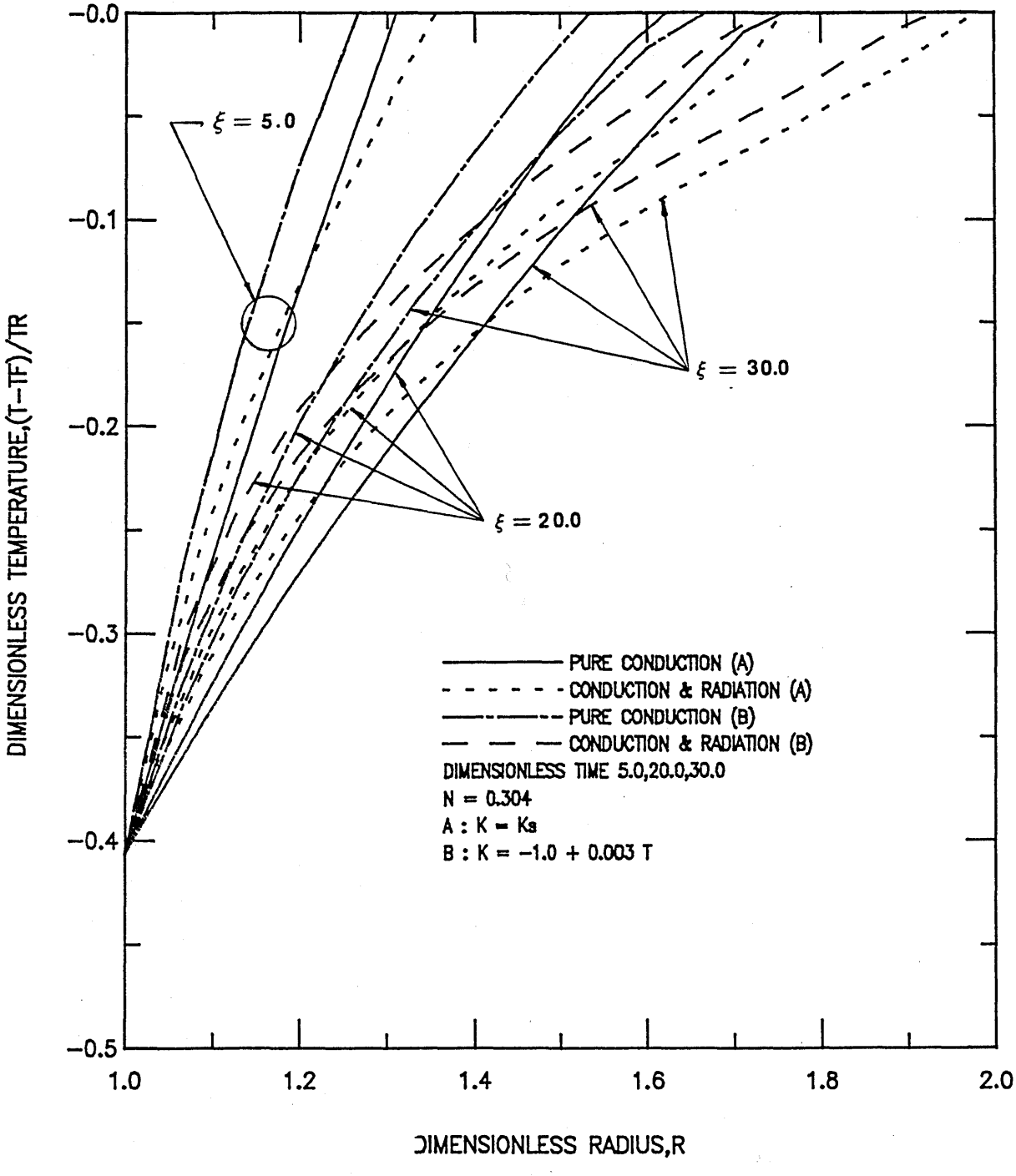

Figure 5 TRANSIENT DIMENSIONLESS TEMPERATURE VS. DIMENSIONLESS RADIUS

TI/TF=0.5, εw1= εw2=1.0, ω =0.5, a=4.572 /m, ri/ro=0.5
Hsl=465.2kJ/kg, ρ=2803.2kg/m^3, αs=0.0307m^2/hr, Ks=3.462W/mK

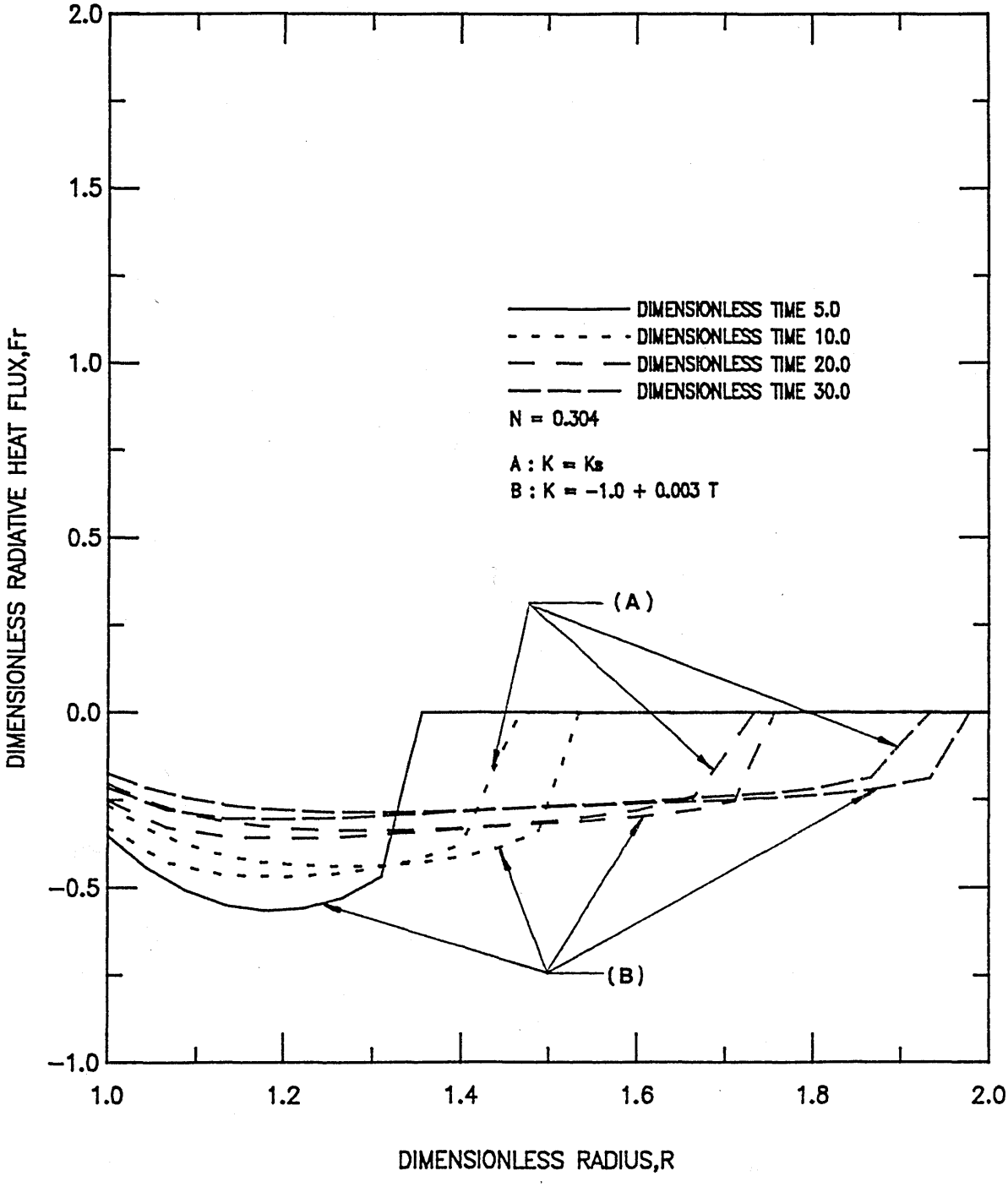

Figure 6 TRANSIENT DIMENSIONLESS RADIATIVE FLUX VS. DIMENSIONLESS RADIUS

Tl/TF=0.5, $\varepsilon w1 = \varepsilon w2 = 1.0$, $\omega = 0.5$, $a = 4.572$ /m, ri/ro=0.5
Hsl=465.2kJ/kg, $\rho = 2803.2 kg/m^3$, $\alpha s = 0.0307 m^2/hr$, Ks=3.462W/mK

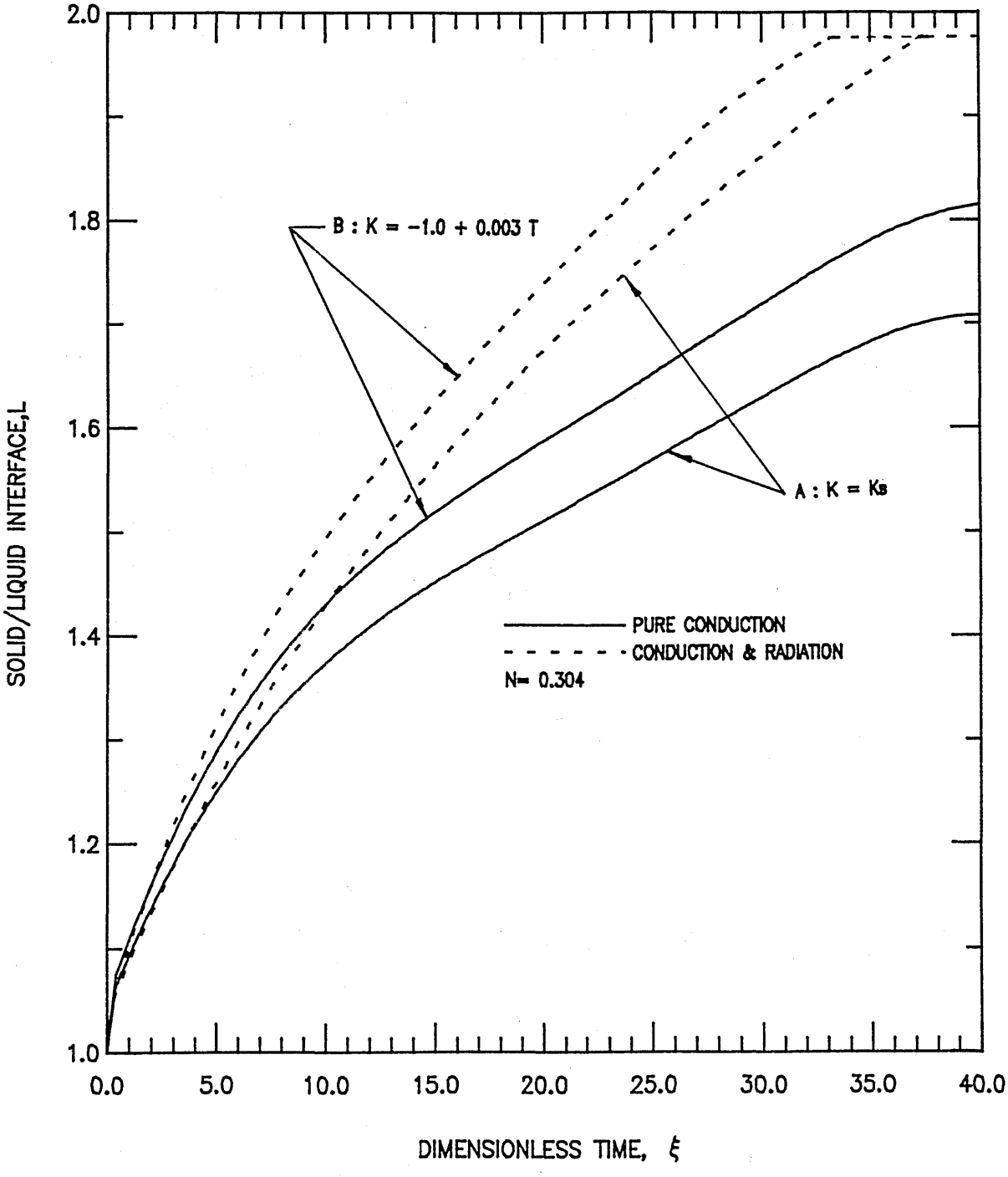

Figure 7 SOLID/LIQUID INTERFACE VS. DIMENSIONLESS TIME

Ti/TF=0.5, εw1= εw2=1.0, ω =0.5, a=4.572 /m, ri/ro=0.5
Hsl=465.2kJ/kg, ρ=2803.2kg/m^3, αs=0.0307m^2/hr, Ks=3.462W/mK

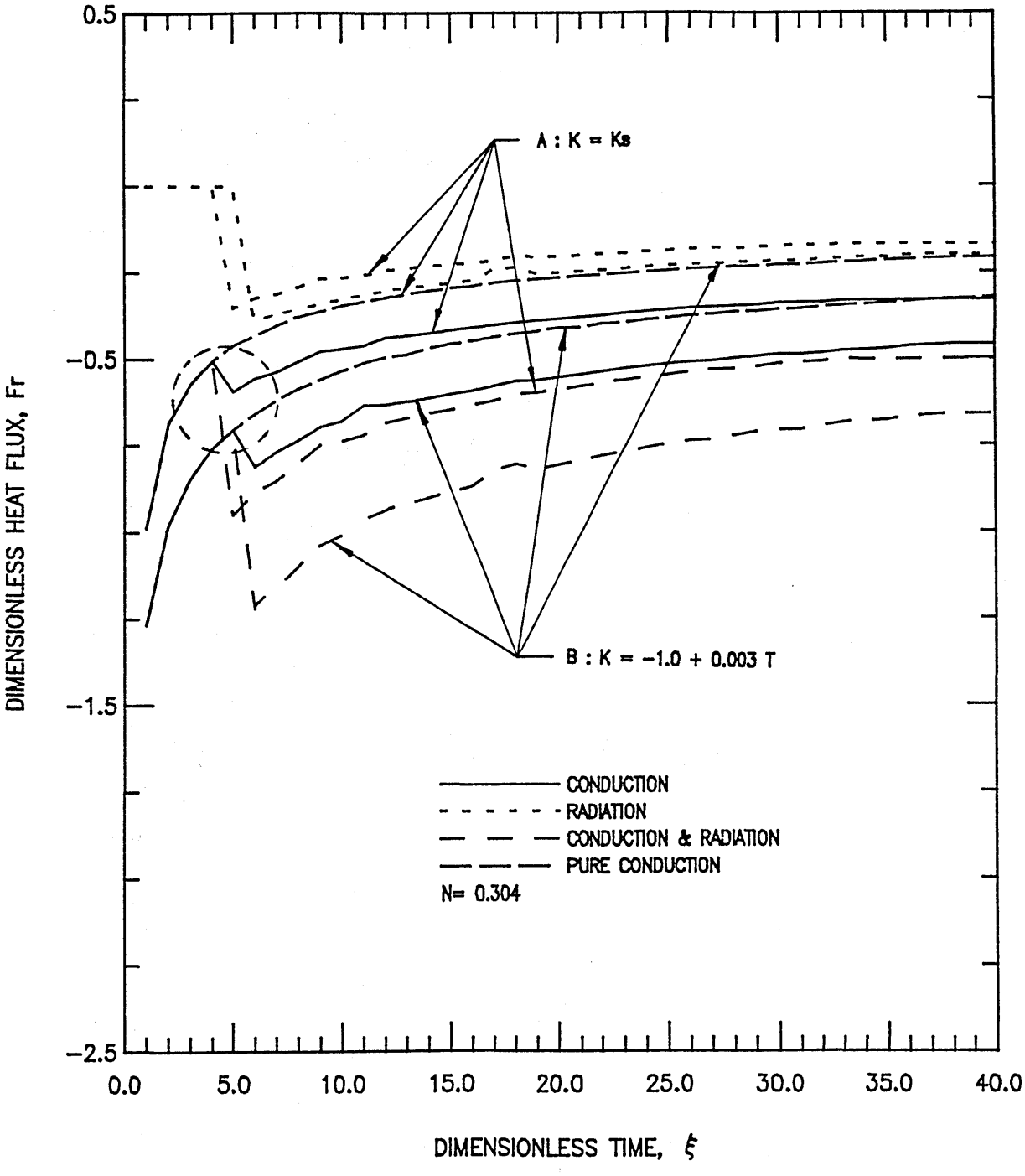

Figure 8 TRANSIENT HEAT FLUX AT INSIDE CYLINDER

TI/TF=0.5, εw1= εw2=1.0, ω=0.5,a=4.572 /m,ri/ro=0.5
Hsl=465.2kJ/kg, ρ =2803.2kg/m^3, αs=0.0307m^2/hr,Ks=3.462W/mK

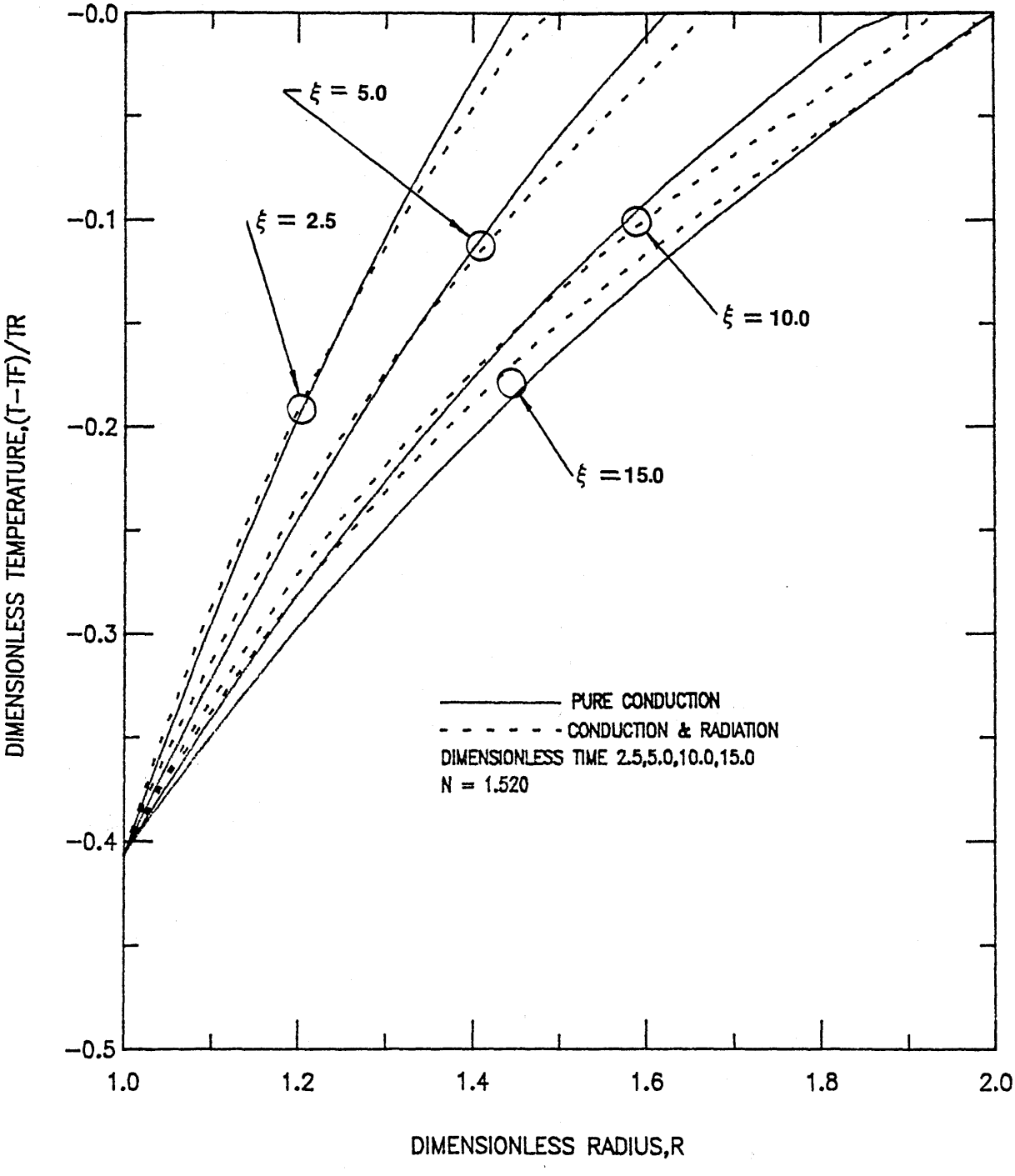

Figure 9 TRANSIENT DIMENSIONLESS TEMPERATURE VS. DIMENSIONLESS RADIUS

TI/TF=0.5, εw1= εw2=1.0, ω=0.5,a=4.572 /m,ri/ro=0.5
Hsl=465.2kJ/kg, ρ=2803.2kg/m^3, αs=0.0307m^2/hr,Ks=17.307W/mK

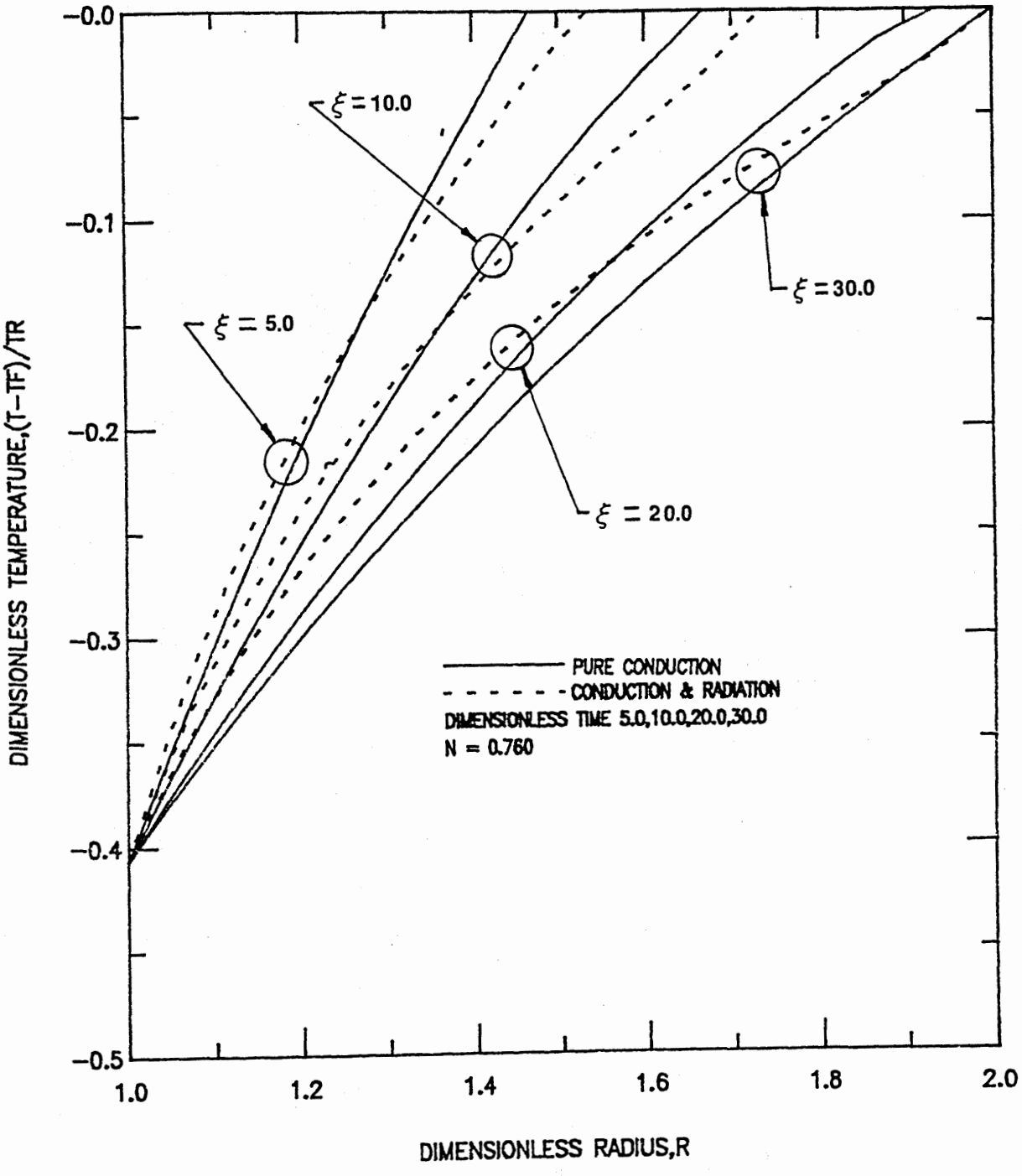

Figure 10 TRANSIENT DIMENSIONLESS TEMPERATURE VS. DIMENSIONLESS RADIUS

TI/TF=0.5, εw1= εw2=1.0, ω =0.5, a=4.572 /m, ri/ro=0.5
Hsl=465.2kJ/kg, ρ=2803.2kg/m^3, αs=0.0307m^2/hr, Ks=8.654W/mK

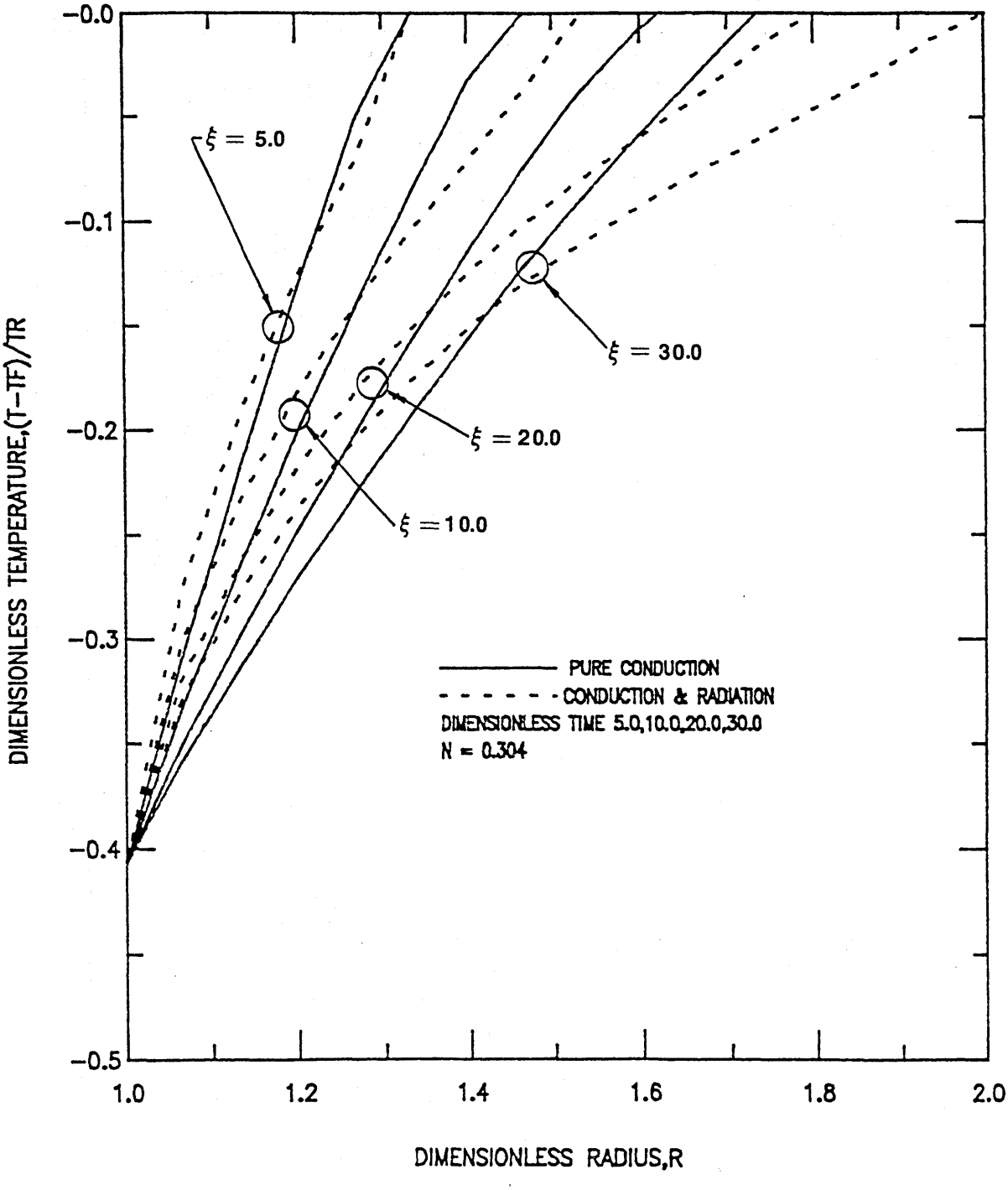

Figure 11 TRANSIENT DIMENSIONLESS TEMPERATURE VS. DIMENSIONLESS RADIUS

TI/TF=0.5, εw1= εw2=1.0,ω =0.5,a=4.572 /m,ri/ro=0.5
Hsl=465.2kJ/kg, ρ=2803.2kg/m^3, αs=0.0307m^2/hr,Ks=3.462W/mK

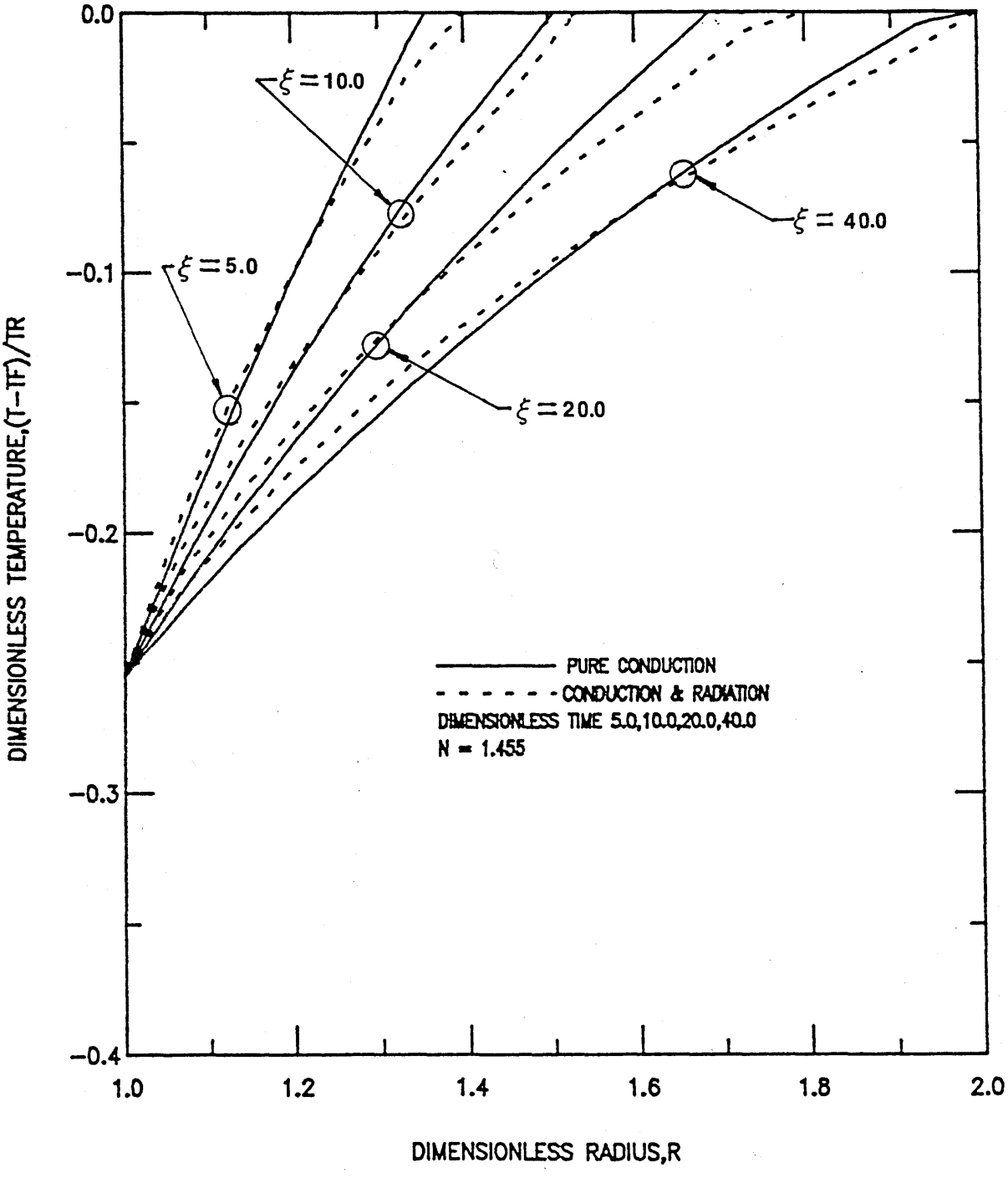

Figure 12 TRANSIENT DIMENSIONLESS TEMPERATURE VS. DIMENSIONLESS RADIUS

TI/TF=0.667, εw1= εw2=1.0, ω=0.0,a=4.572 /m,ri/ro=0.5
Hsl=465.2kJ/kg, ρ=2803.2kg/m^3, αs=0.0307m^2/hr,Ks=8.654W/mK

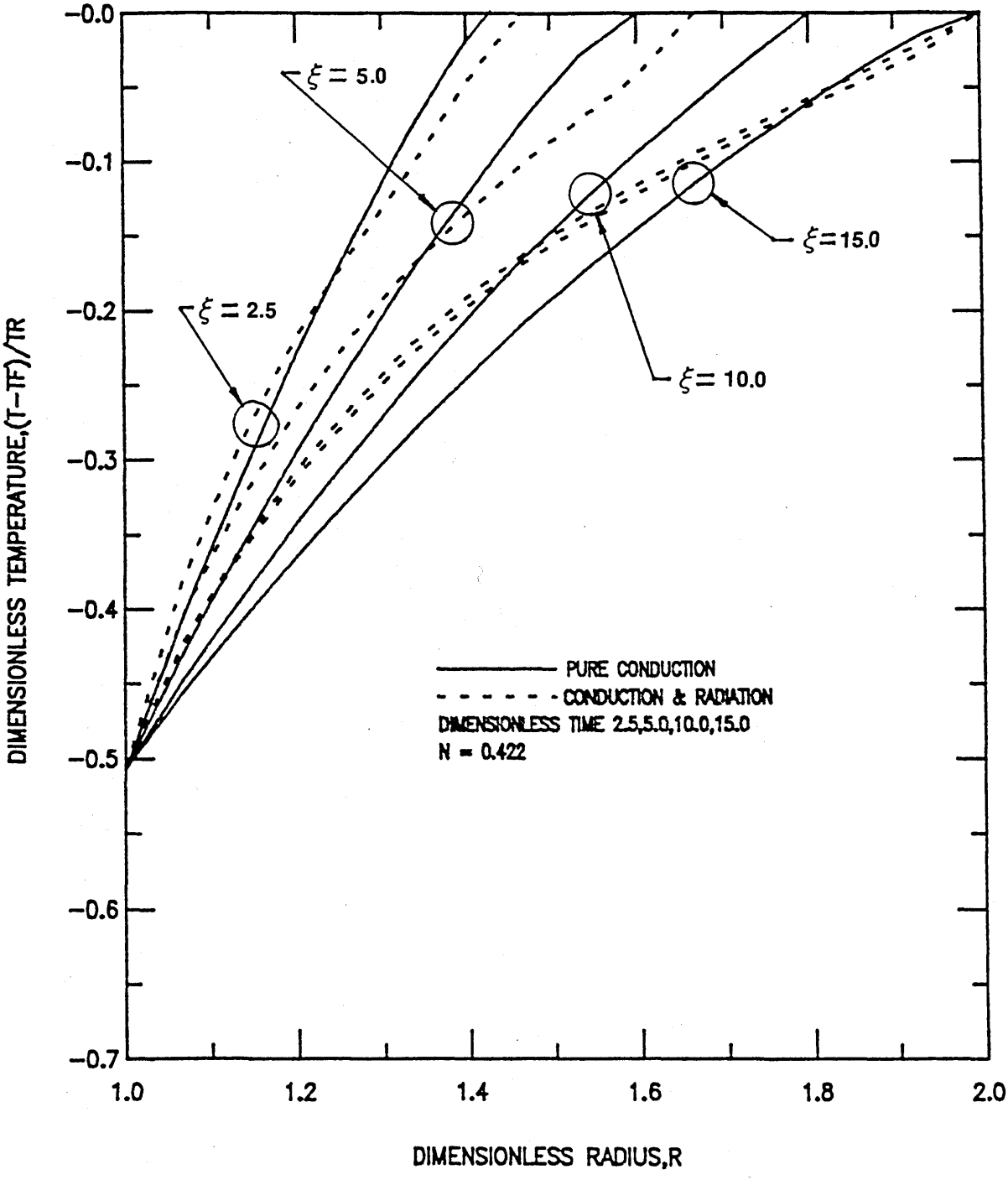

Figure 13 TRANSIENT DIMENSIONLESS TEMPERATURE VS. DIMENSIONLESS RADIUS

TI/TF=0.4, εw1= εw2=1.0, ω=0.0,a=4.572 /m,ri/ro=0.5
Hsl=465.2kJ/kg, ρ=2803.2kg/m^3, αs=0.0307m^2/hr,Ks=8.654W/mK

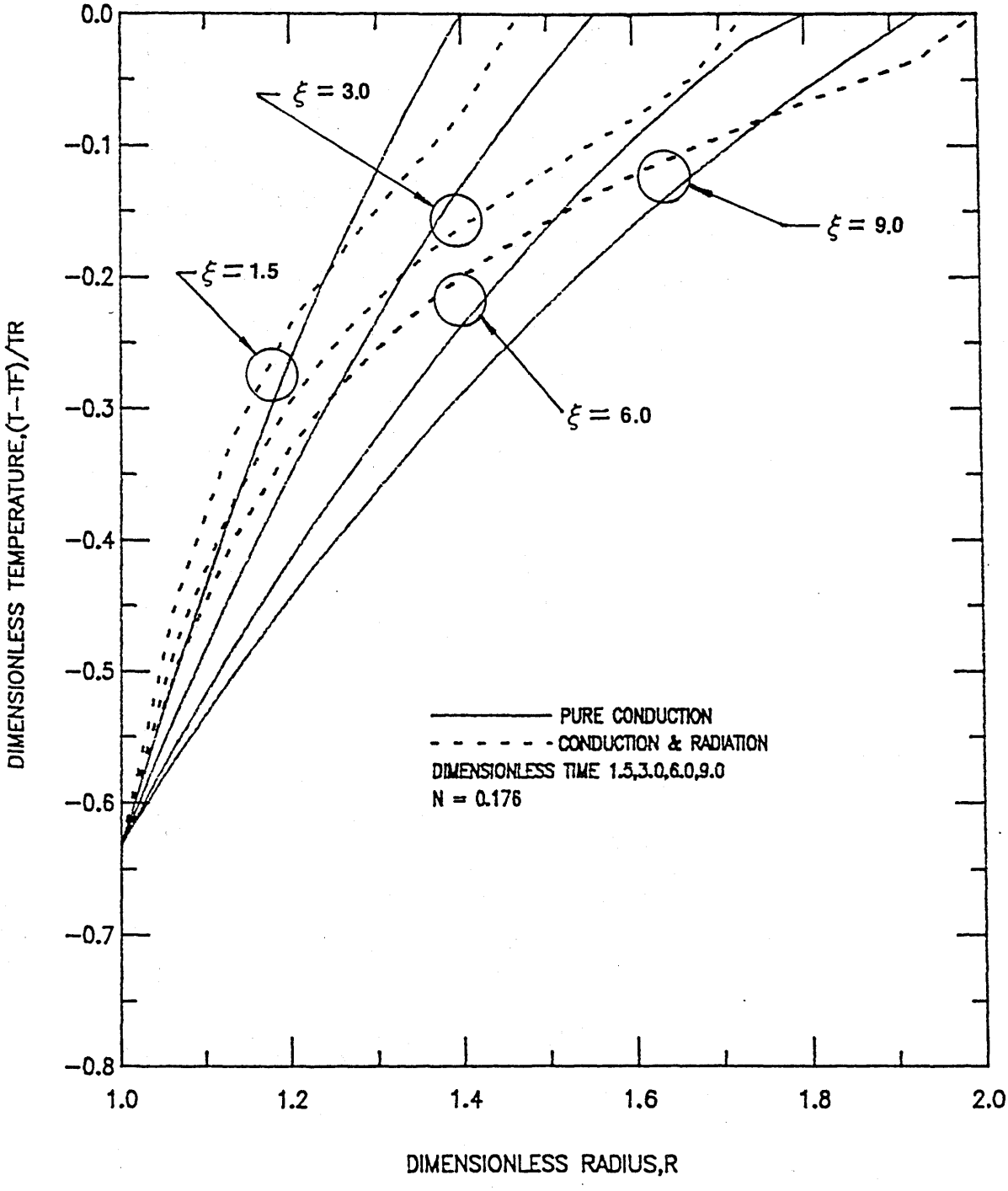

Figure 14 TRANSIENT DIMENSIONLESS TEMPERATURE VS. DIMENSIONLESS RADIUS

TI/TF=0.286, εw1= εw2=1.0, ω =0.0, a=4.572 /m, ri/ro=0.5
Hsl=465.2kJ/kg, ρ=2803.2kg/m^3, αs=0.0307m^2/hr, Ks=8.654W/mK

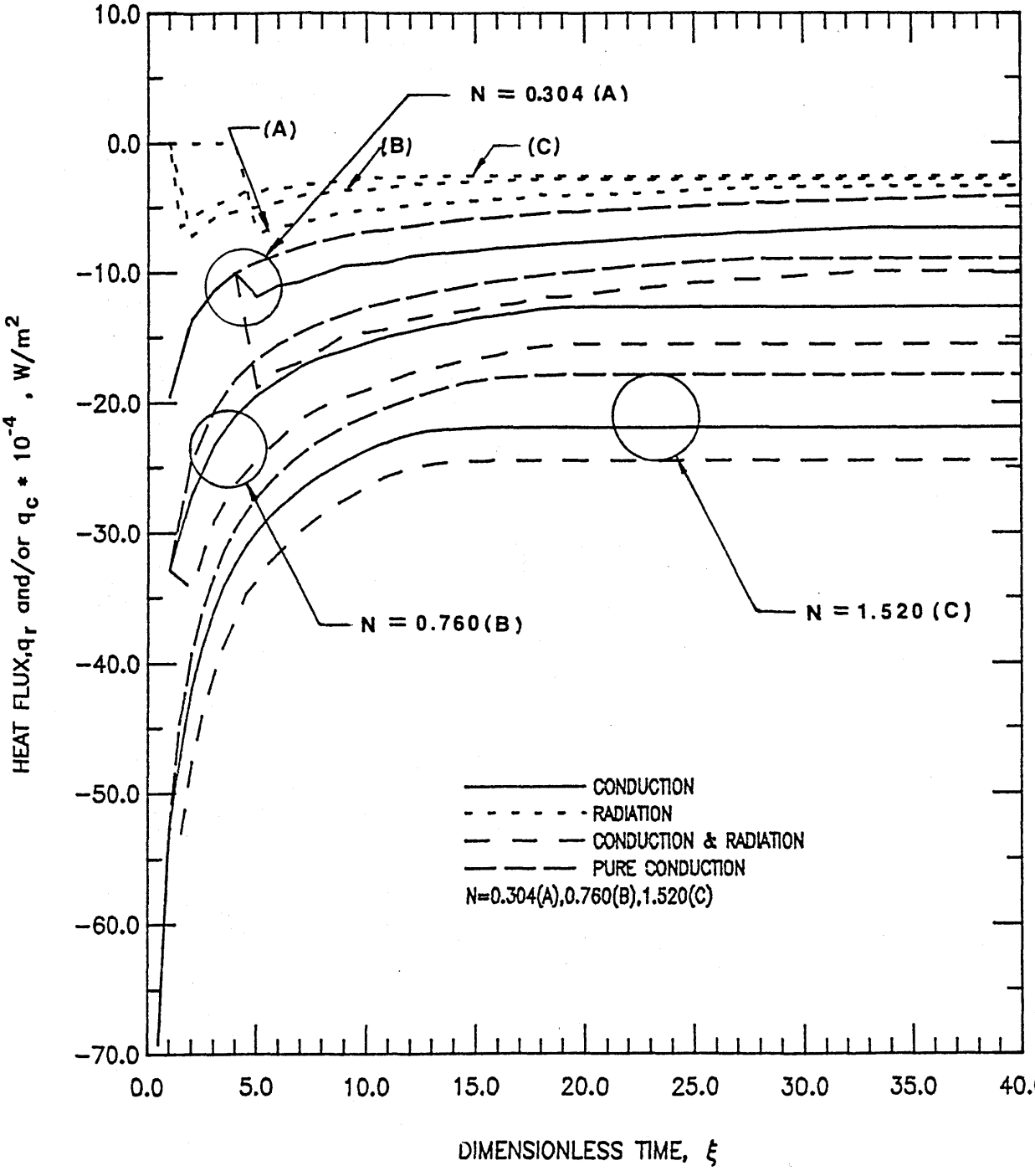

Figure 15 TRANSIENT HEAT FLUX AT INSIDE CYLINDER

Tl/TF=0.5, $\varepsilon w1 = \varepsilon w2 = 1.0$, $\omega = 0.5$, a=4.572 /m, ri/ro=0.5
Hsl=465.2kJ/kg, $\rho = 2803.2 kg/m^3$, $\alpha s = 0.0307 m^2/hr$
Ks=3.462(A),8.654(B),17.307(C)W/mK

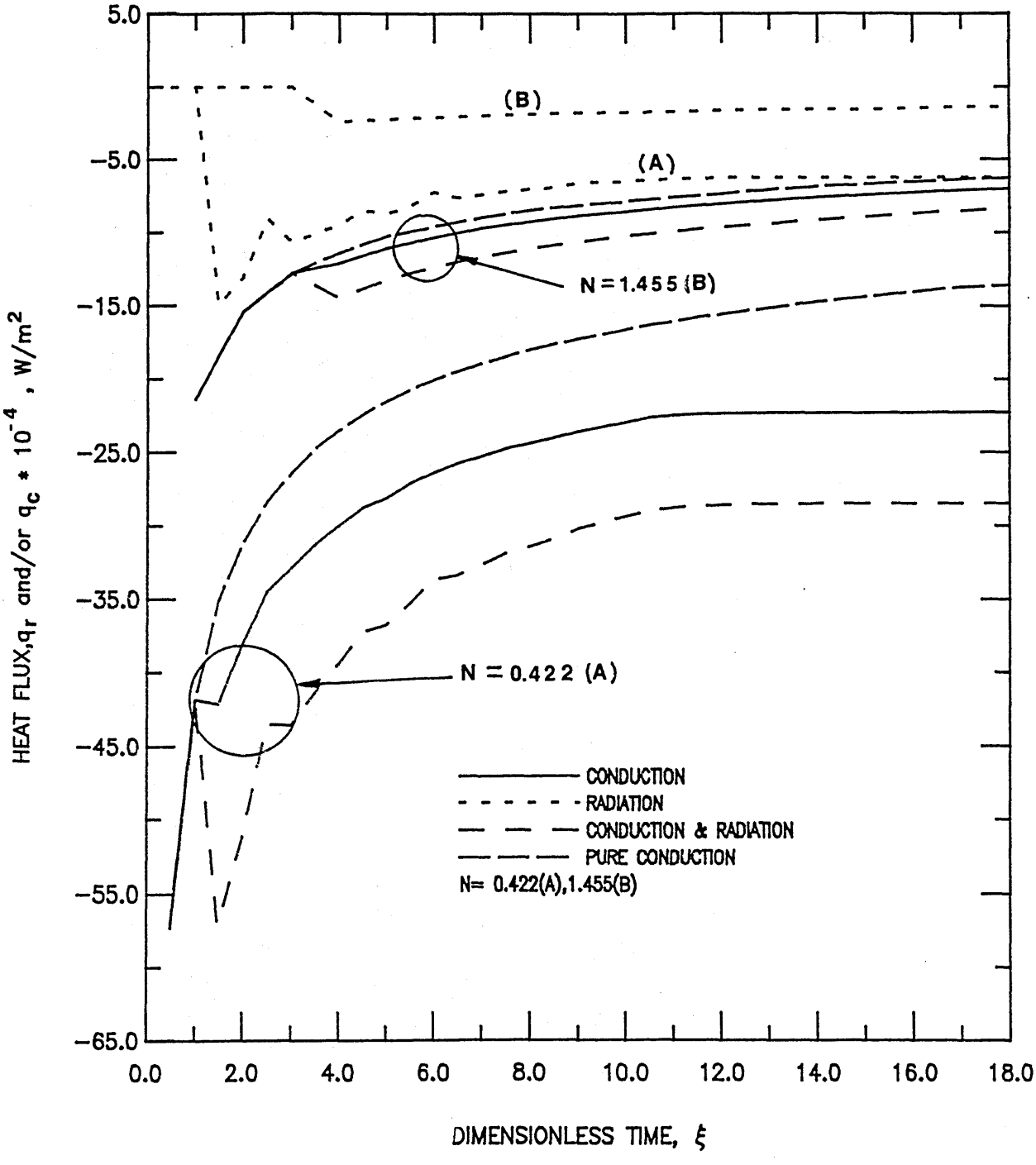

Figure 16 TRANSIENT HEAT FLUX AT INSIDE CYLINDER

Ti/TF=0.4(A),0.667(B), $\varepsilon w1 = \varepsilon w2 = 1.0$, $\omega = 0.0$, $a = 4.572$ /m
ri/ro=0.5, Hsl=465.2kJ/kg, $\rho = 2803.2$kg/m^3, $\alpha s = 0.0307$m^2/hr
Ks=8.654 W/mK

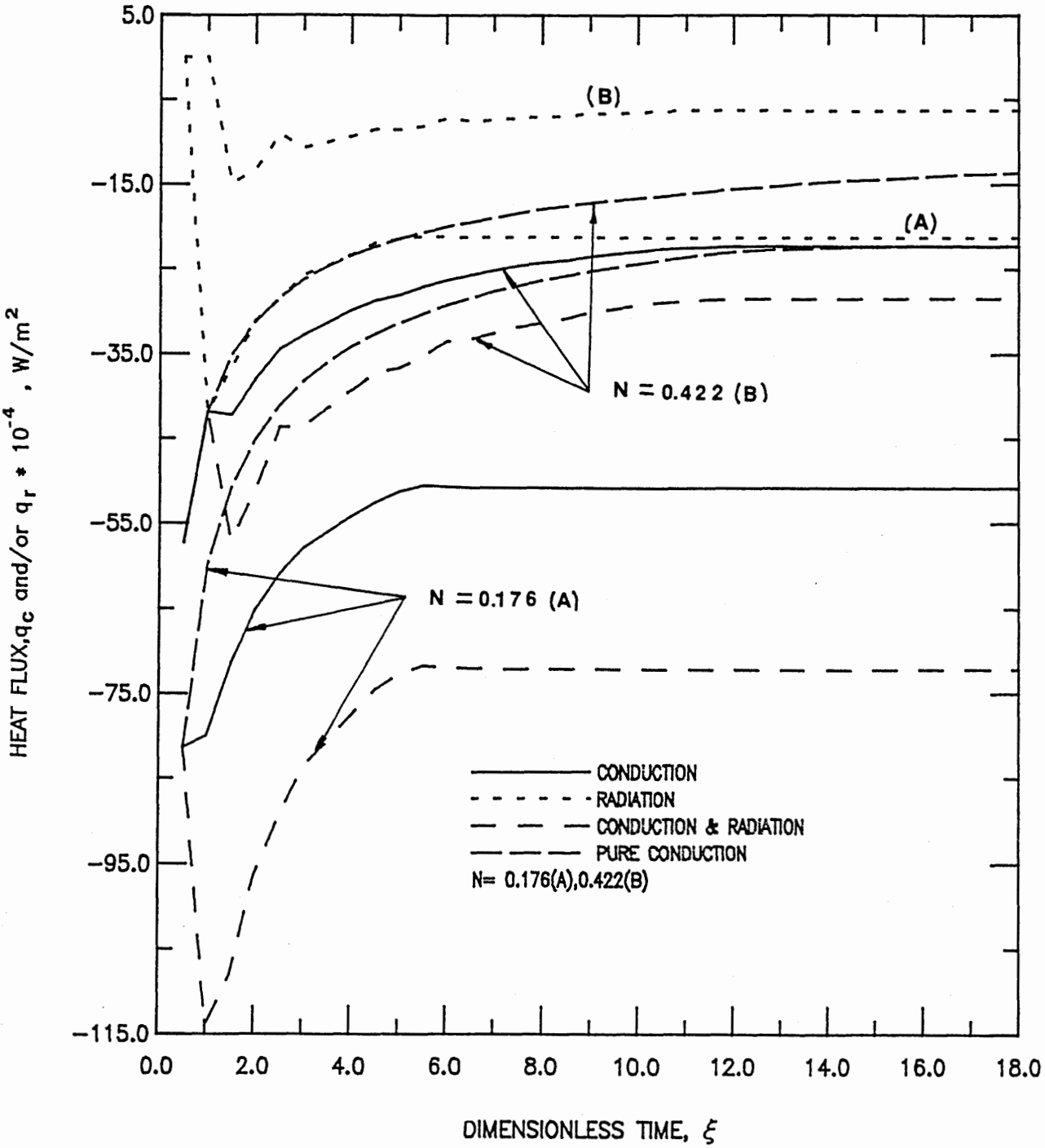

Figure 17 TRANSIENT HEAT FLUX AT INSIDE CYLINDER

Ti/Tf=0.286(A),0.4(B), $\varepsilon w1 = \varepsilon w2 = 1.0$, $\omega = 0.0$, $a = 4.572$ /m
ri/ro=0.5, Hsl=465.2kJ/kg, ρ =2803.2kg/m^3, $\alpha s = 0.0307$m^2/hr
Ks=8.654 W/mK

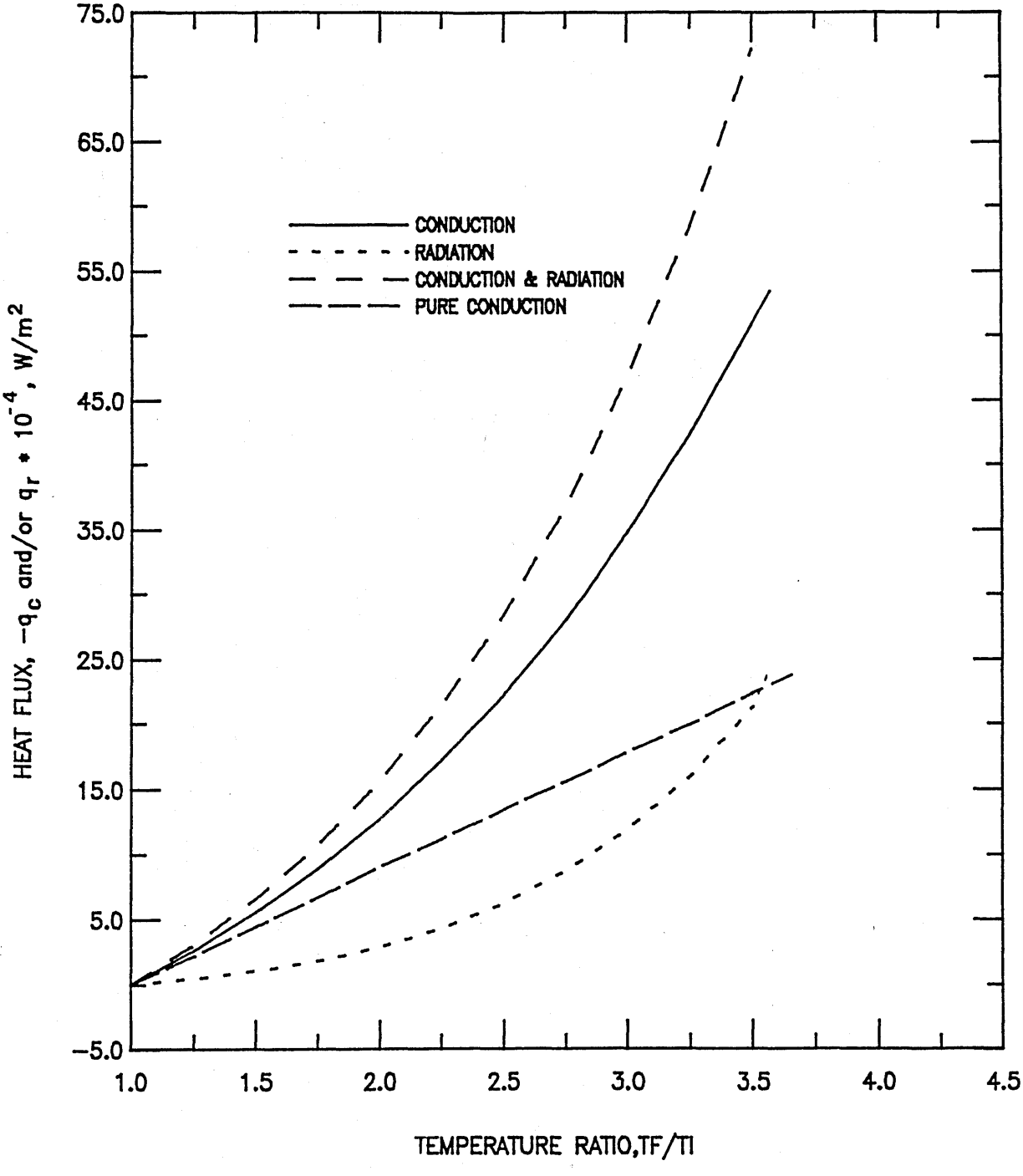

Figure 18 STEADY STATE HEAT FLUX AT INSIDE CYLINDER VS. TEMPERATURE RATIO

$\varepsilon w1 = \varepsilon w2 = 1.0$, $\omega = 0.0$, $a = 4.572$ /m, $ri/ro = 0.5$
$Hsl = 465.2 kJ/kg$, $\rho = 2803.2 kg/m^3$, $\alpha s = 0.0307 m^2/hr$, $Ks = 8.654 W/mK$

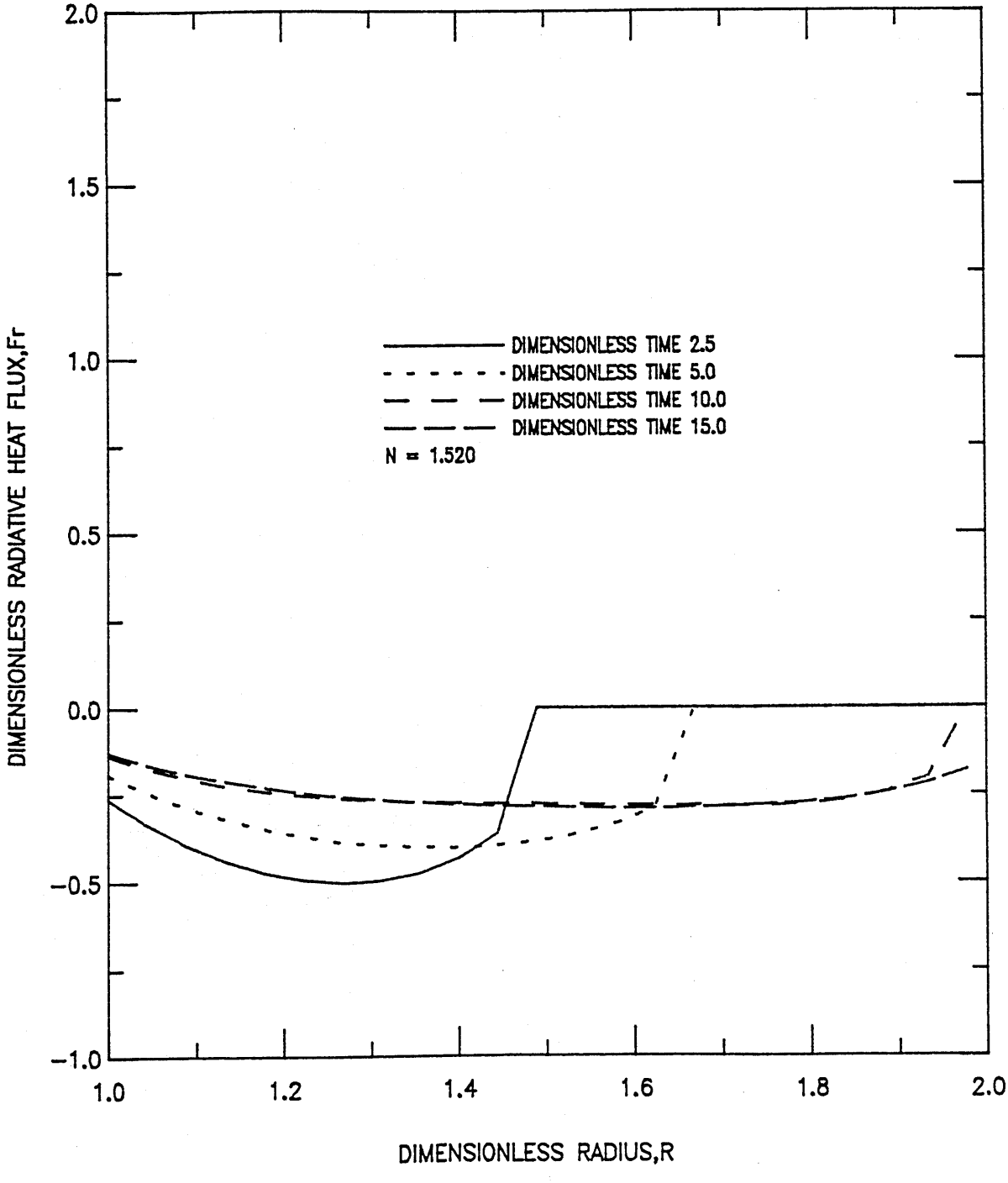

Figure 19 TRANSIENT DIMENSIONLESS RADIATIVE FLUX VS. DIMENSIONLESS RADIUS

Tl/TF=0.5, $\varepsilon w1 = \varepsilon w2 = 1.0$, $\omega = 0.5$, $a = 4.572$ /m, ri/ro=0.5
Hsl=465.2kJ/kg, $\rho = 2803.2 kg/m^3$, $\alpha s = 0.0307 m^2/hr$, Ks=17.307W/mK

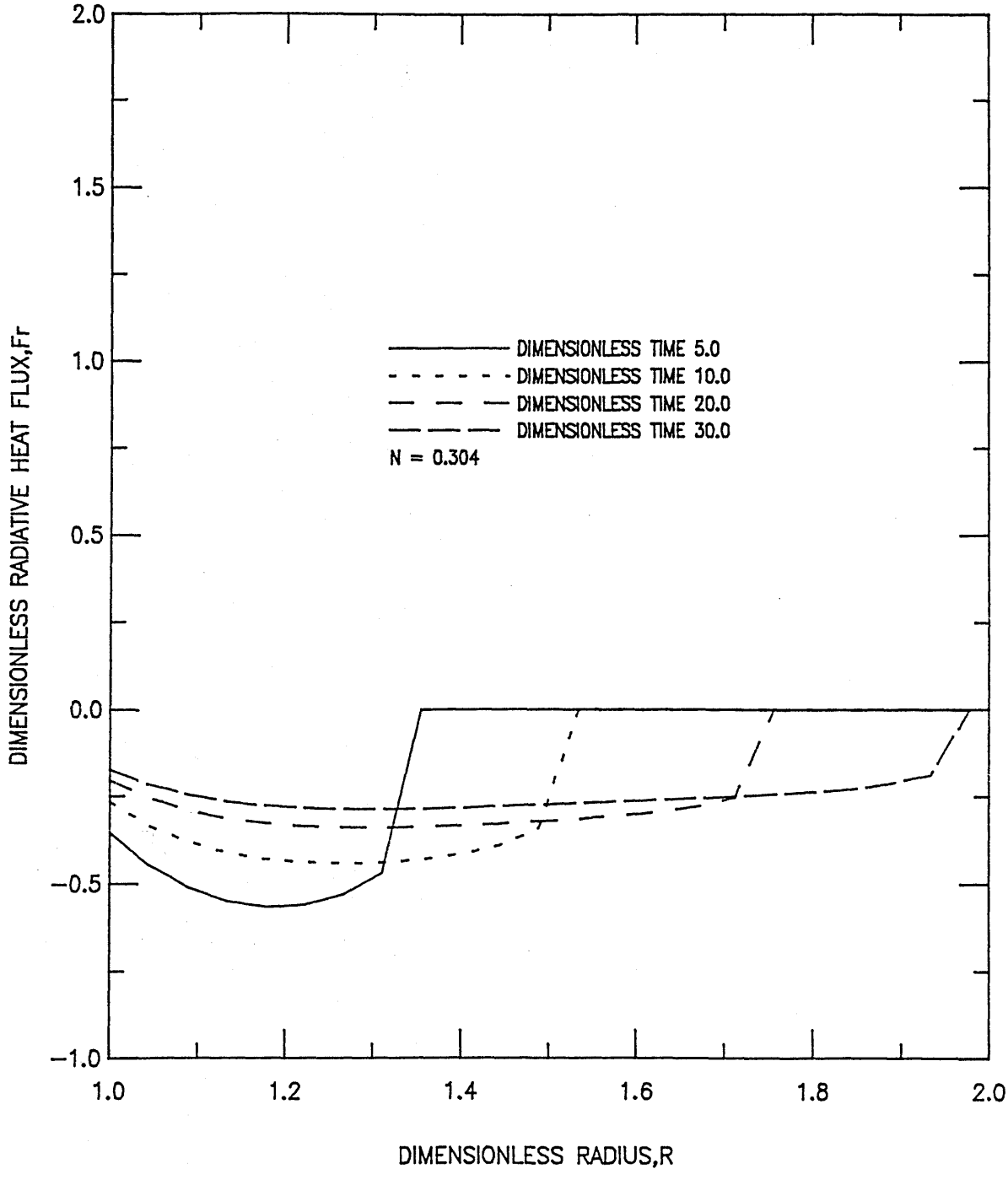

Figure 20 TRANSIENT DIMENSIONLESS RADIATIVE FLUX VS. DIMENSIONLESS RADIUS

Tl/TF=0.5, $\varepsilon w1 = \varepsilon w2 = 1.0$, $\omega = 0.5$, $a = 4.572$ /m, ri/ro=0.5
Hsl=465.2kJ/kg, $\rho = 2803.2 kg/m^3$, $\alpha s = 0.0307 m^2/hr$, Ks=3.462W/mK

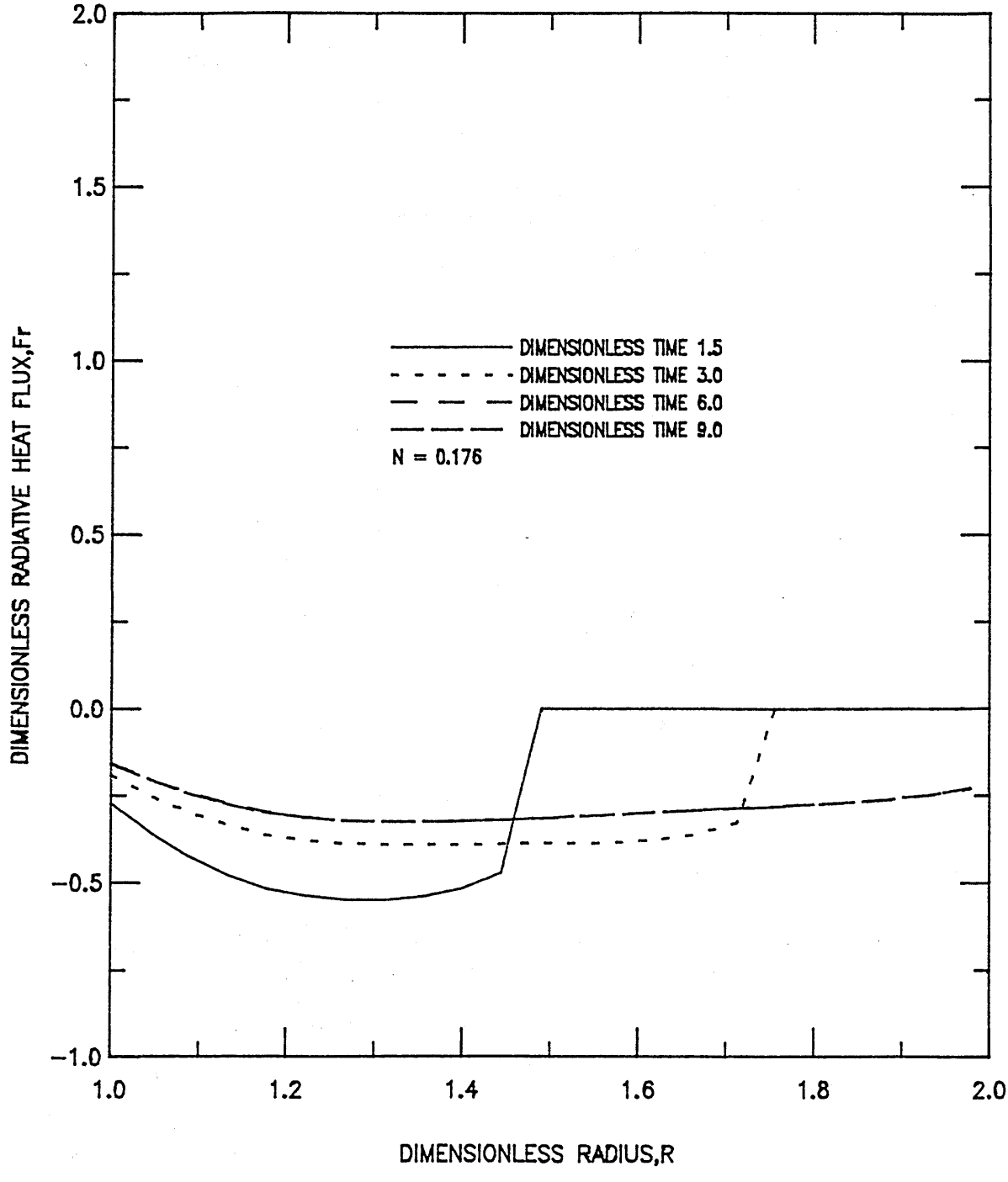

Figure 21 TRANSIENT DIMENSIONLESS RADIATIVE FLUX VS. DIMENSIONLESS RADIUS

Tl/TF=0.286, $\varepsilon w1 = \varepsilon w2 = 1.0$, $\omega = 0.0$, $a = 4.572$ /m, ri/ro=0.5
Hsl=465.2kJ/kg, $\rho = 2803.2 kg/m^3$, $\alpha s = 0.0307 m^2/hr$, Ks=8.654W/mK

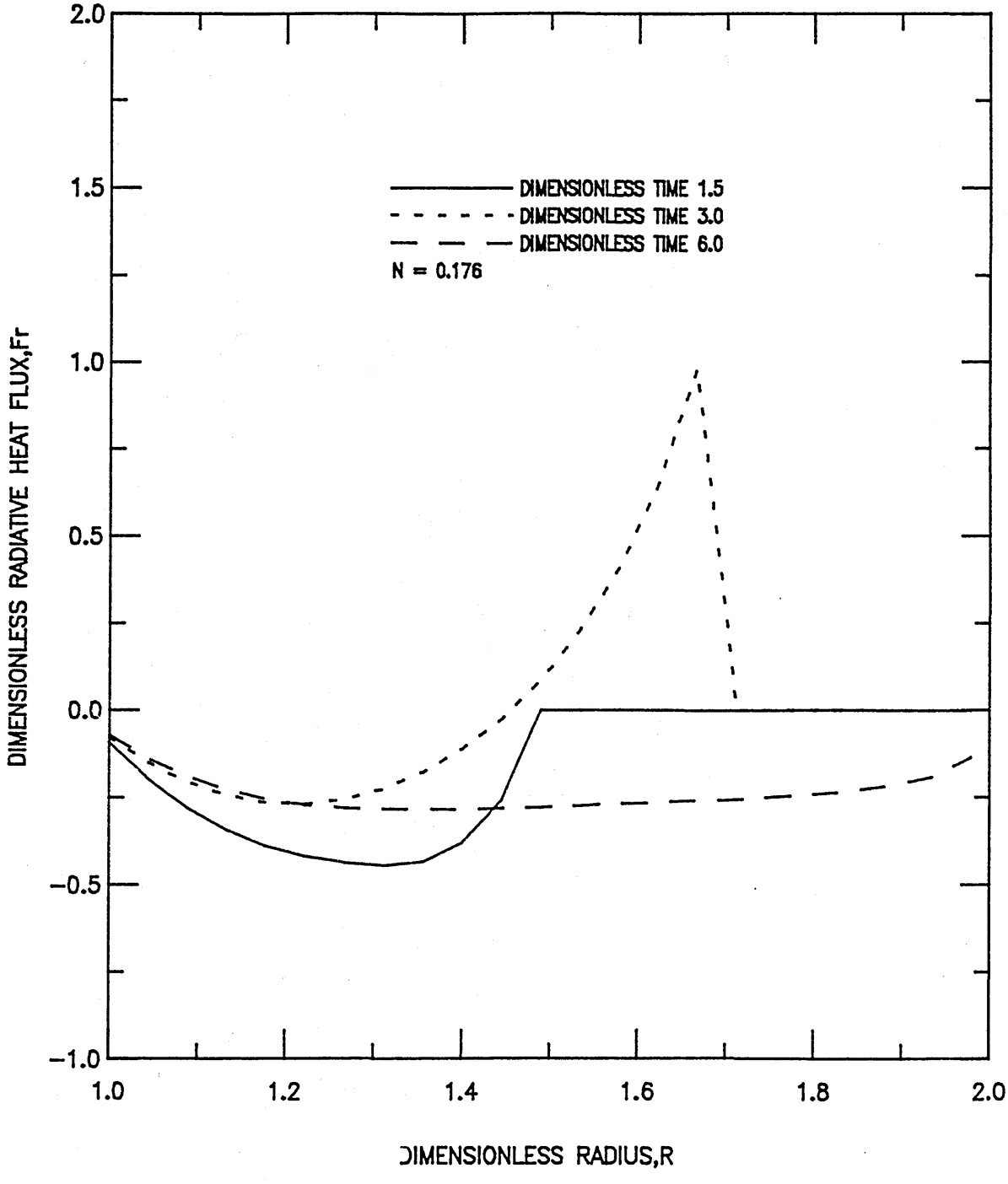

Figure 22 TRANSIENT DIMENSIONLESS RADIATIVE FLUX VS. DIMENSIONLESS RADIUS

Ti/TF=0.286, εw1= εw2=0.5, ω=0.0,a=4.572 /m,ri/ro=0.5
Hsl=465.2kJ/kg, ρ=2803.2kg/m^3, αs=0.0307m^2/hr,Ks=8.654W/mK

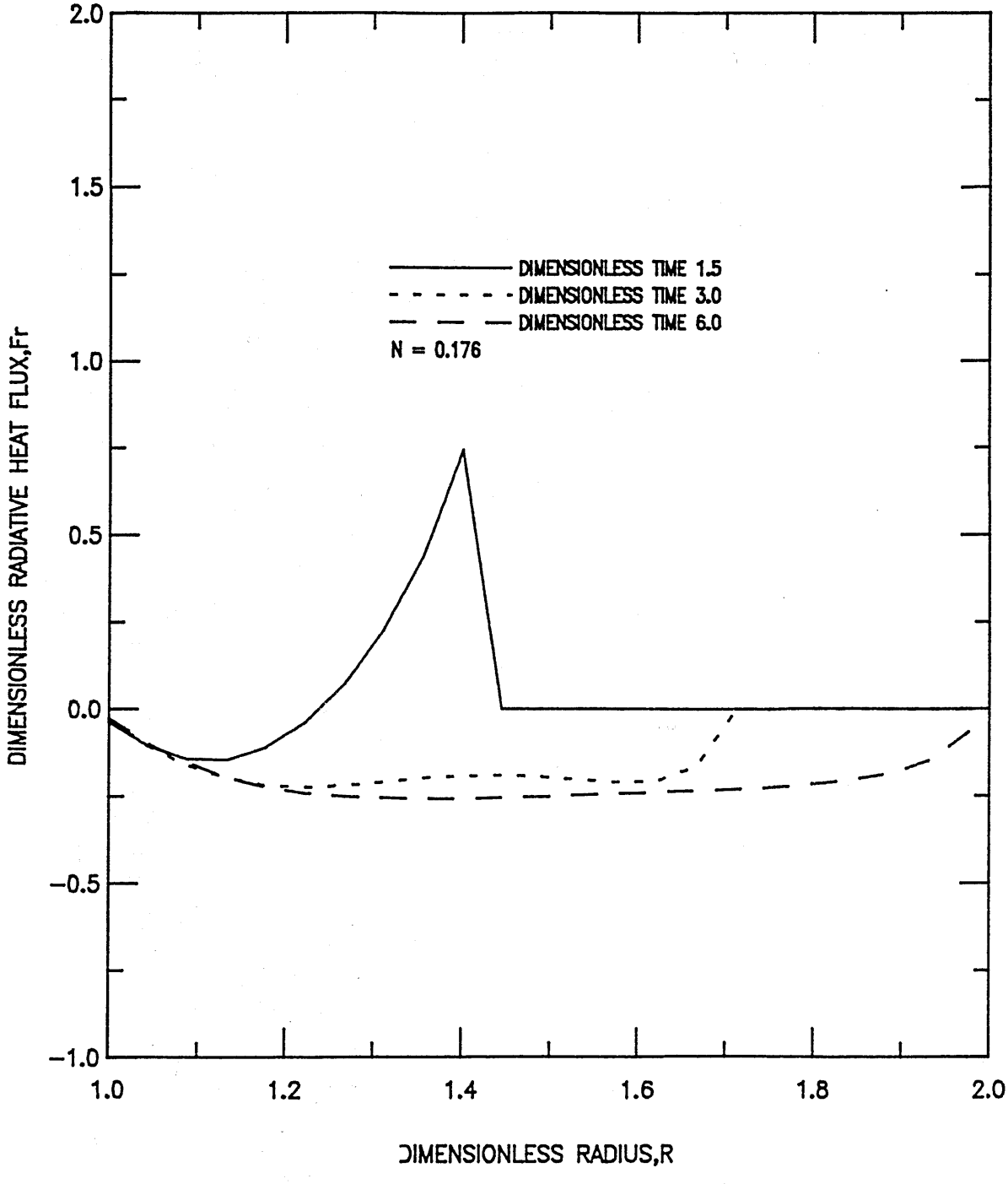

Figure 23 TRANSIENT DIMENSIONLESS RADIATIVE FLUX VS. DIMENSIONLESS RADIUS

Tl/TF=0.286, $\varepsilon w1 = \varepsilon w2 = 0.2$, $\omega = 0.0$, $a = 4.572$ /m, ri/ro=0.5
Hsl=465.2kJ/kg, $\rho = 2803.2 kg/m^3$, $\alpha s = 0.0307 m^2/hr$, Ks=8.654W/mK

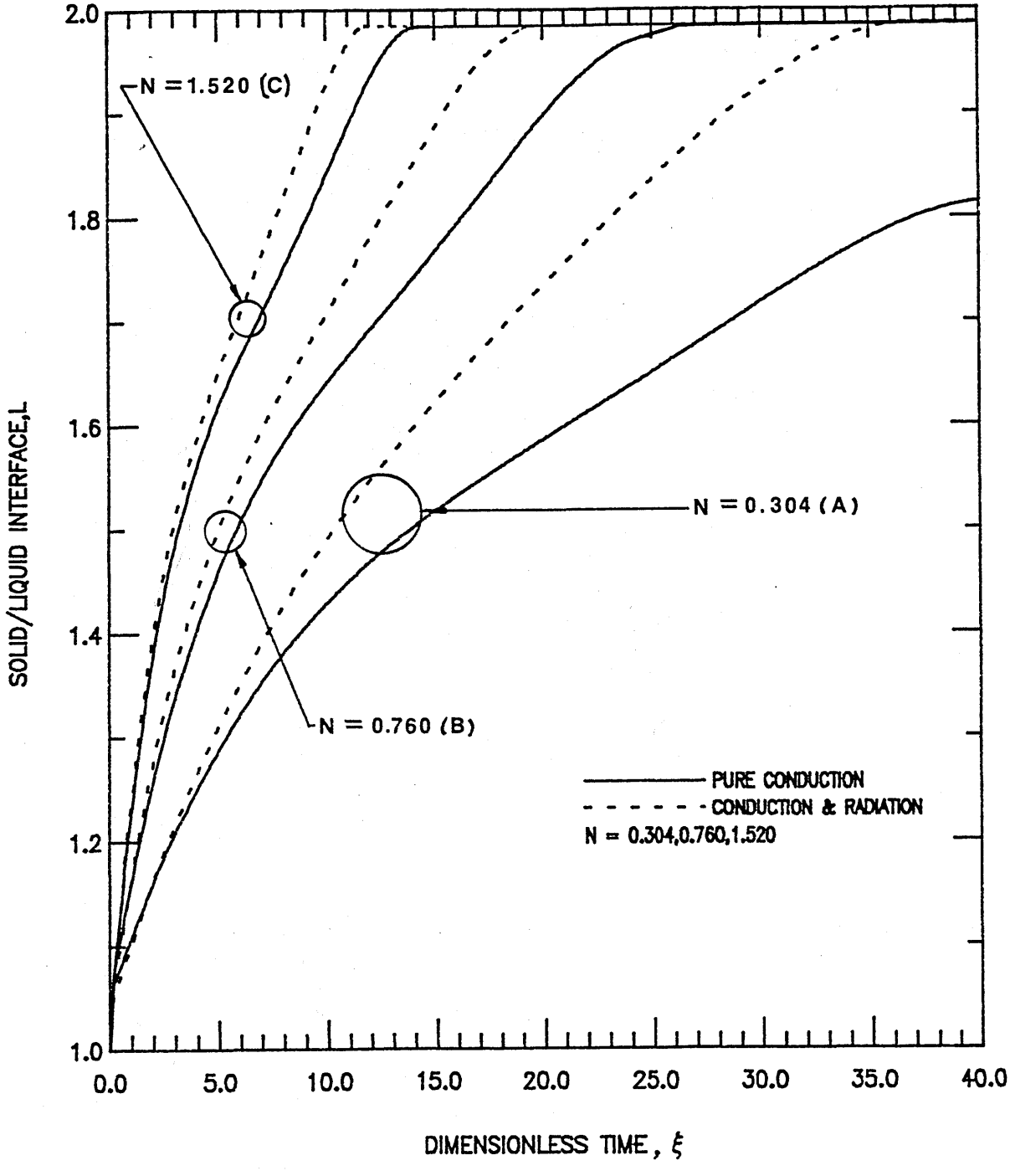

Figure 24 SOLID/LIQUID INTERFACE VS. DIMENSIONLESS TIME

TI/TF=0.5, $\varepsilon w1 = \varepsilon w2 = 1.0$, $\omega = 0.5$, a=4.572 /m, ri/ro=0.5
Hsl=465.2kJ/kg, $\rho = 2803.2 kg/m^3$, $\alpha s = 0.0307 m^2/hr$
Ks=3.462(A),8.654(B),17.307(C)W/mK

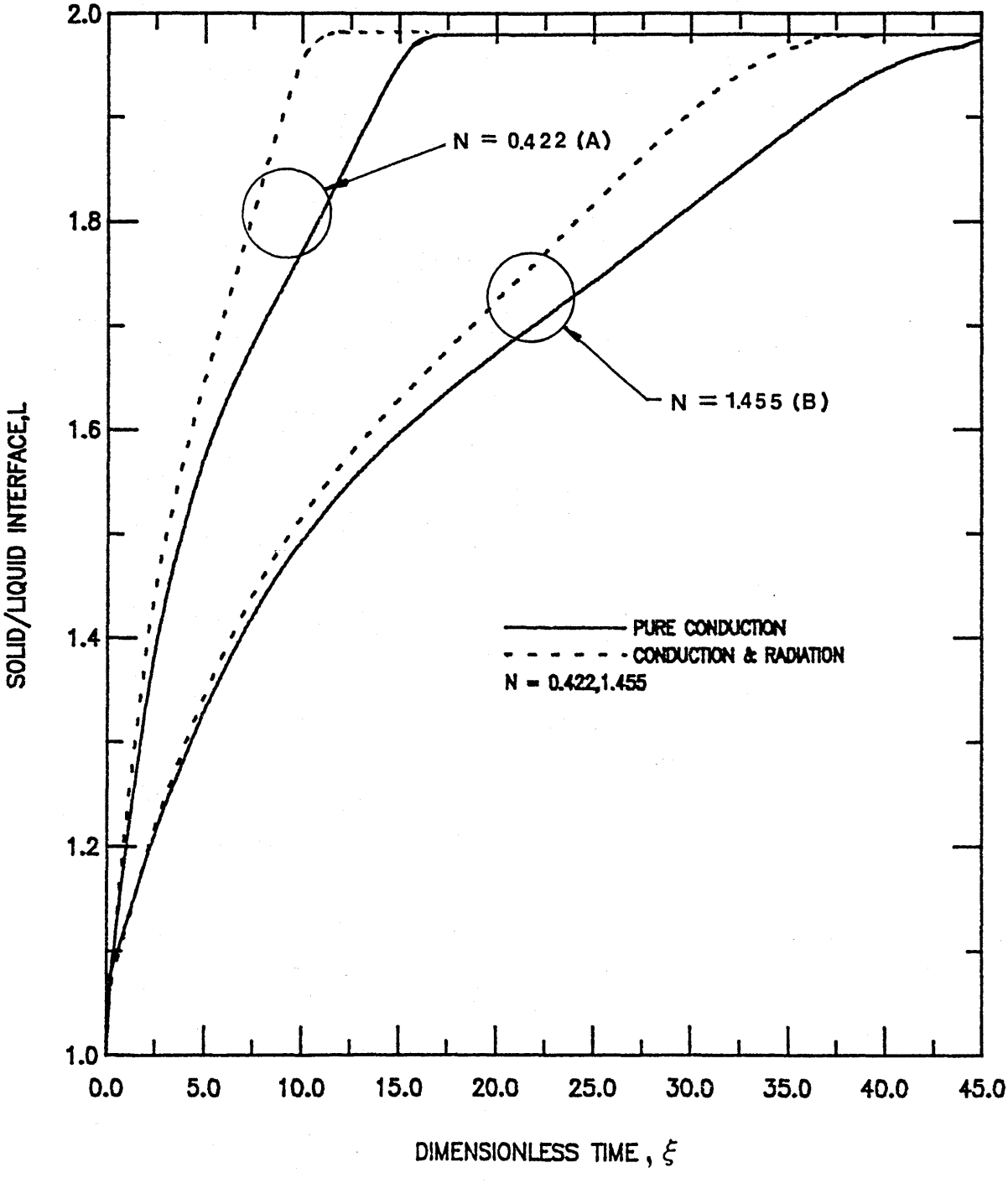

Figure 25 SOLID/LIQUID INTERFACE VS. DIMENSIONLESS TIME

TI/TF=0.4(A),0.667(B), εw1= εw2=1.0, ω =0.0,a=4.572 /m,ri/ro=0.5
Hsl=465.2kJ/kg, ρ=2803.2kg/m^3, αs=0.0307m^2/hr,Ks=8.654W/mK

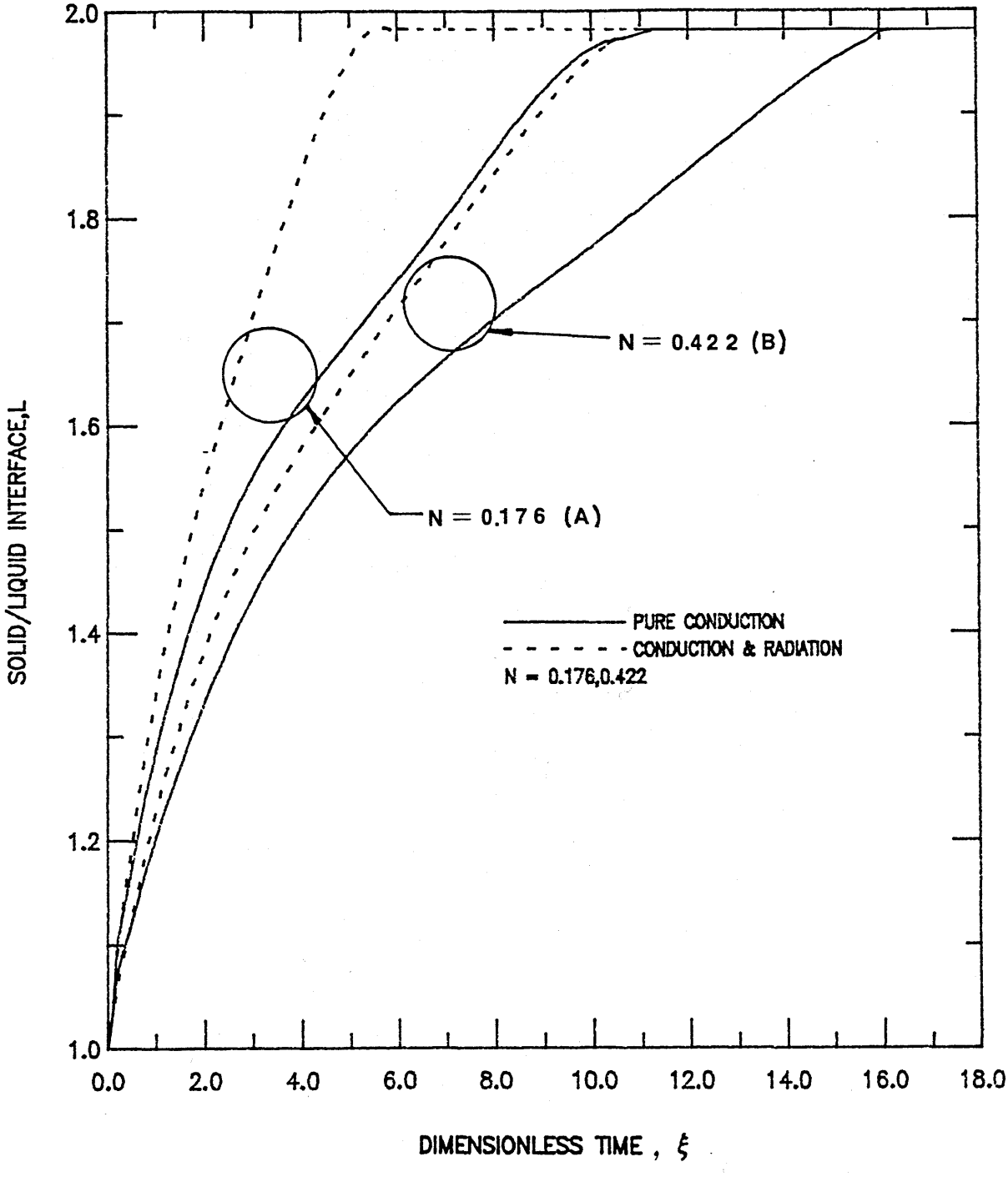

Figure 26 SOLID/LIQUID INTERFACE VS. DIMENSIONLESS TIME

Ti/Tf=0.286(A),0.4(B), $\varepsilon w1 = \varepsilon w2 = 1.0$, $\omega = 0.0$, $a = 4.572$ /m, ri/ro=0.5
Hsl=465.2kJ/kg, $\rho = 2803.2 kg/m^3$, $\alpha s = 0.0307 m^2/hr$, Ks=8.654W/mK

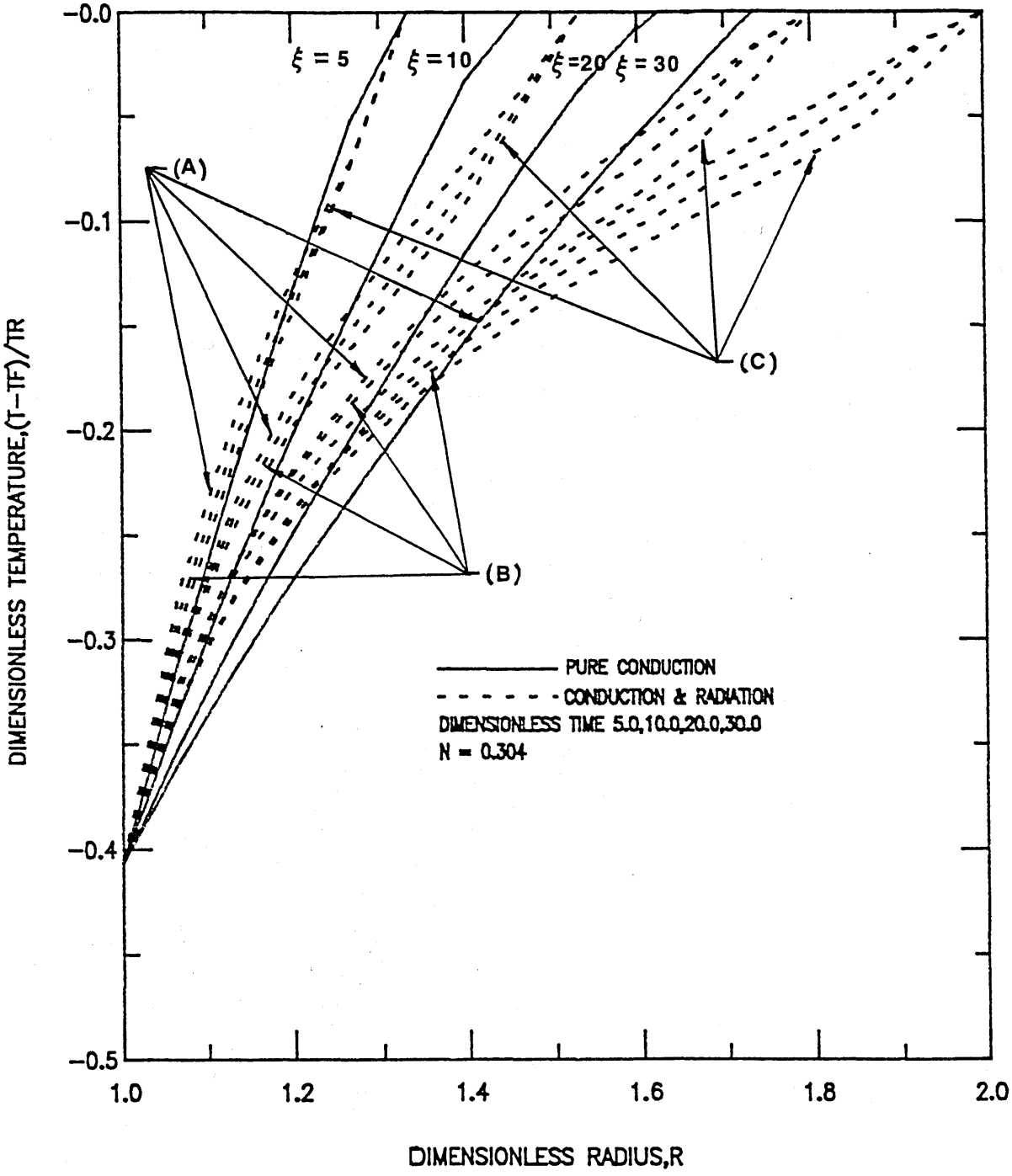

Figure 27 TRANSIENT DIMENSIONLESS TEMPERATURE VS. DIMENSIONLESS RADIUS

TI/TF=0.5, $\varepsilon w1 = \varepsilon w2 = 1.0(A), 0.5(B), 0.2(C), \omega = 0.5$
$a = 4.572$ /m, ri/ro=0.5, Hsl=465.2kJ/kg
$\rho = 2803.2 kg/m^3$, $\alpha s = 0.0307 m^2/hr$, Ks=3.462W/mK

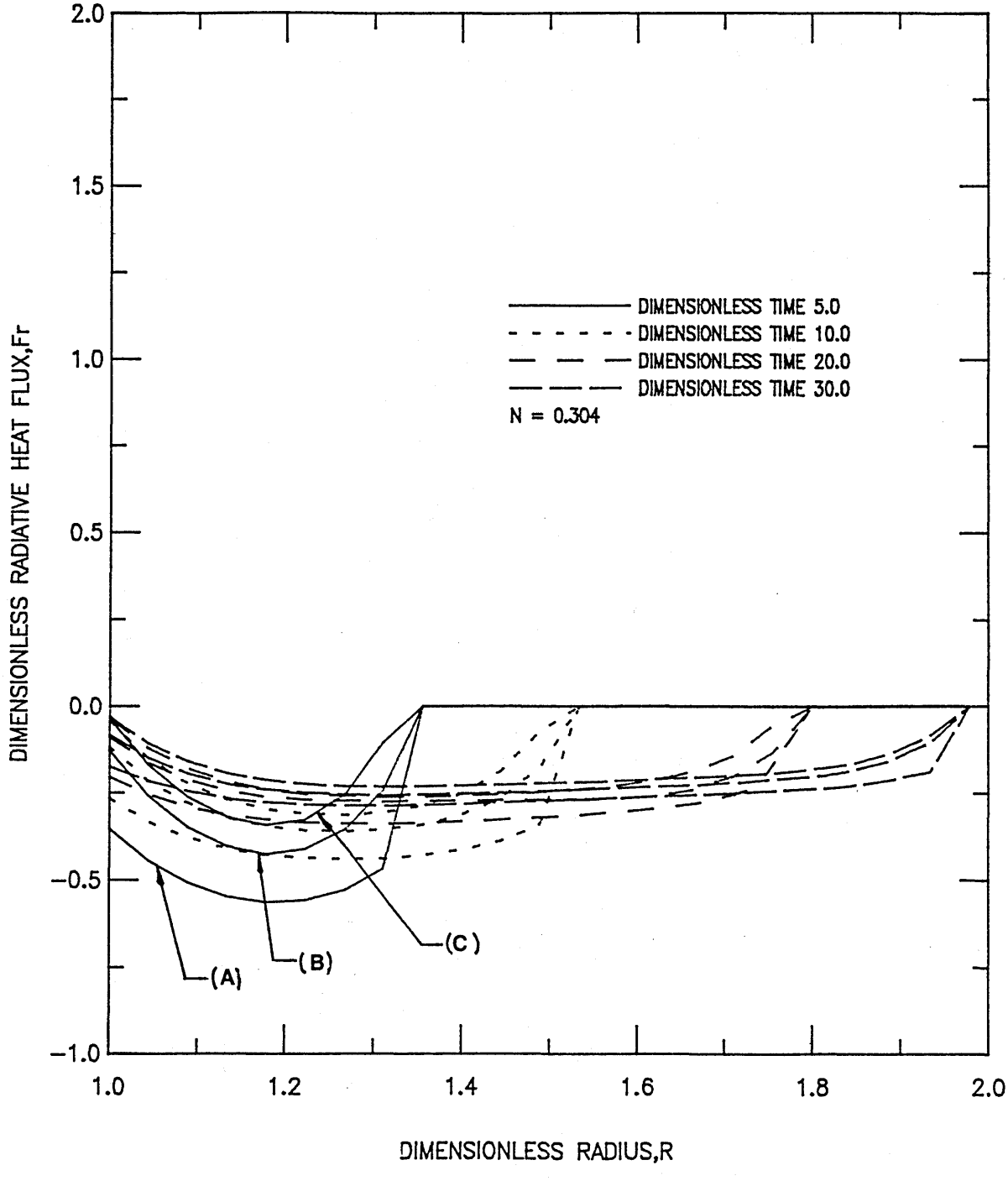

Figure 28 TRANSIENT DIMENSIONLESS RADIATIVE FLUX VS. DIMENSIONLESS RADIUS

TI/TF=0.5, $\varepsilon w1 = \varepsilon w2 = 1.0(A), 0.5(B), 0.2(C)$, $\omega = 0.5$
$a = 4.572$ /m, ri/ro=0.5, Hsl=465.2kJ/kg
$\rho = 2803.2 kg/m^3$, $\alpha s = 0.0307 m^2/hr$, Ks=3.462W/mK

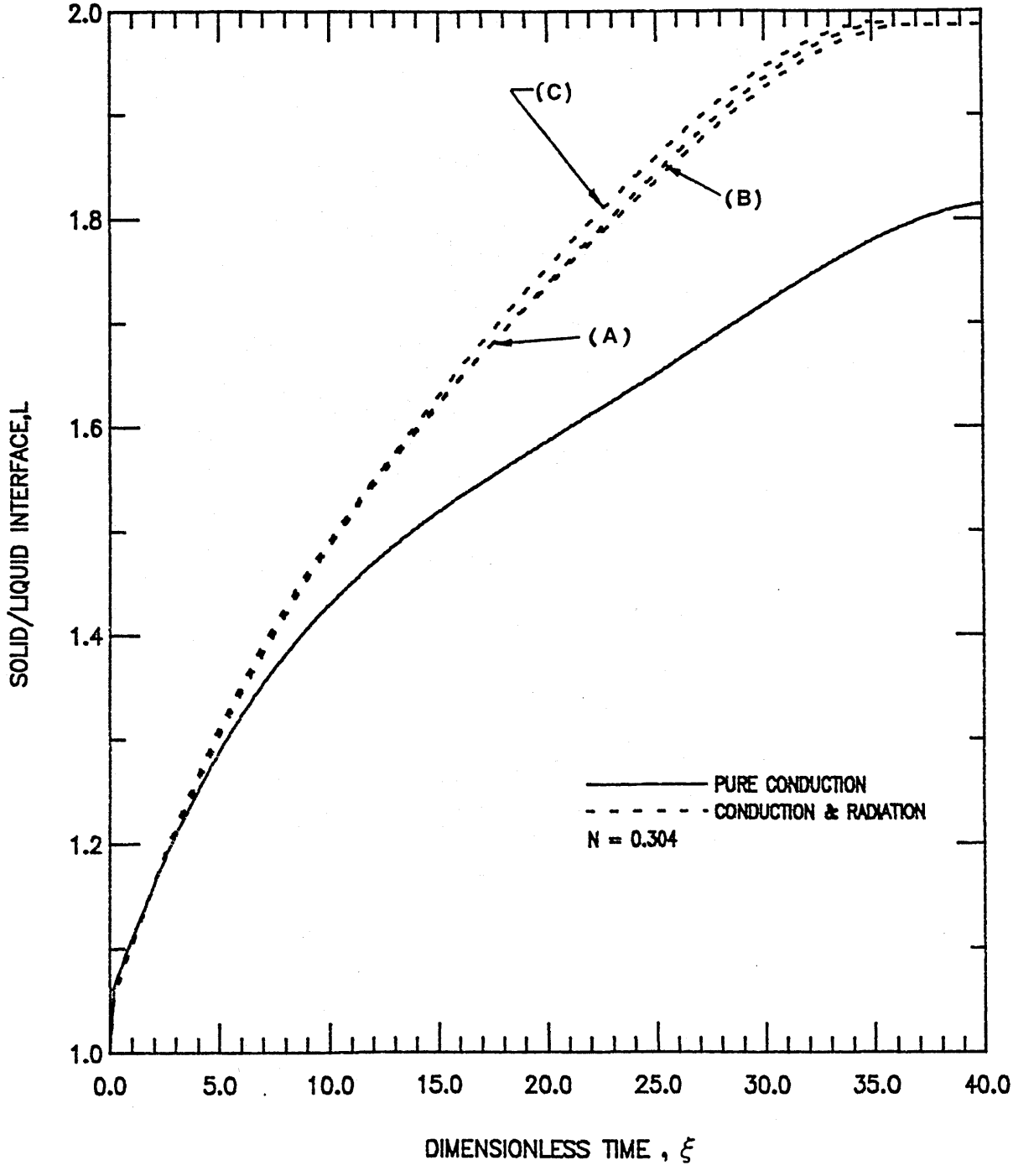

Figure 29 SOLID/LIQUID INTERFACE VS. DIMENSIONLESS TIME

TI/TF=0.5, εw1= εw2=1.0(A),0.5(B),0.2(C), ω=0.5
a=4.572 /m,ri/ro=0.5,Hsl=465.2kJ/kg
ρ =2803.2kg/m^3, αs=0.0307m^2/hr,Ks=3.462W/mK

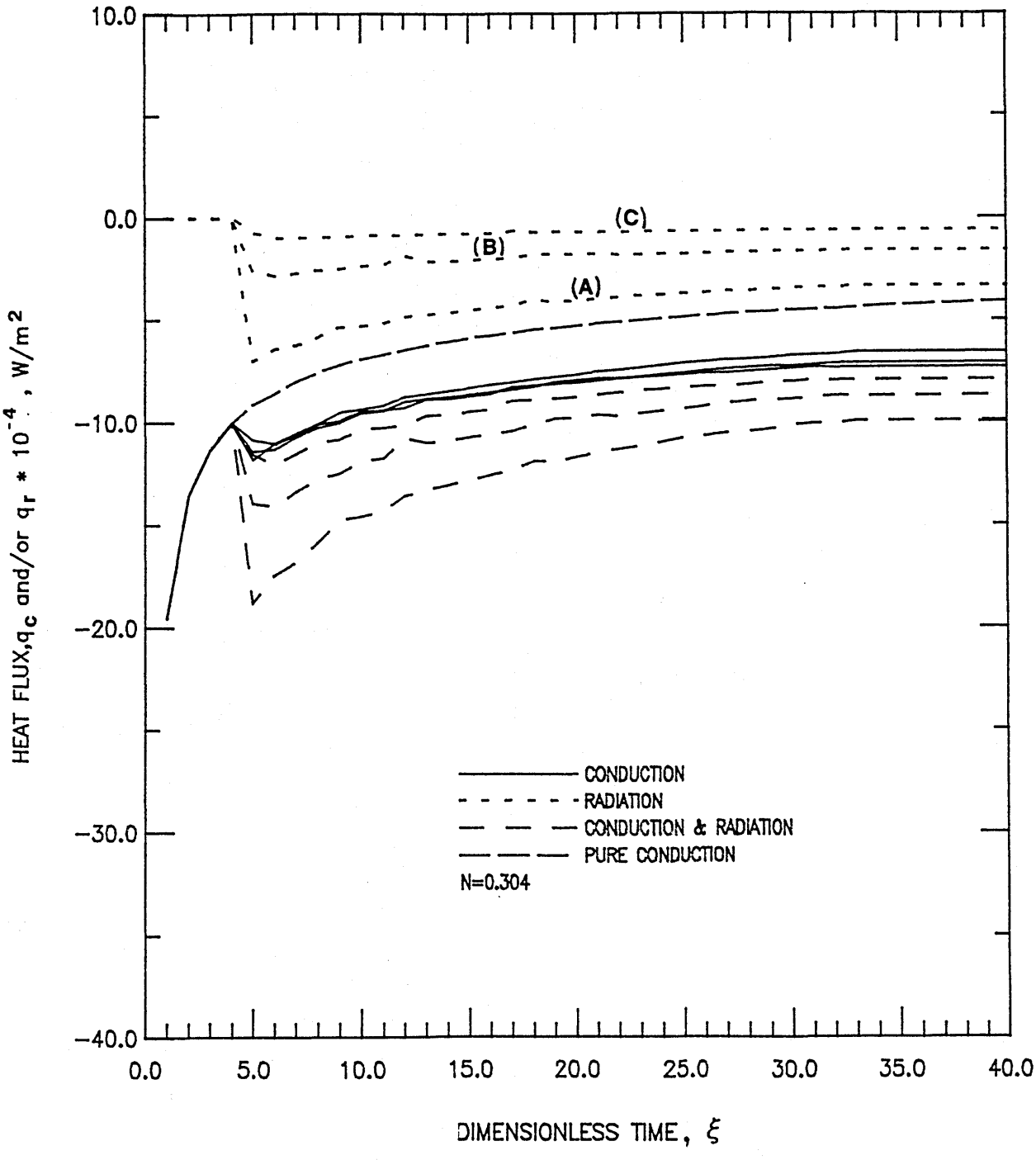

Figure 30 TRANSIENT HEAT FLUX AT INSIDE CYLINDER

TI/TF=0.5, $\varepsilon w1 = \varepsilon w2 = 1.0(A), 0.5(B), 0.2(C)$, $\omega = 0.5$
a=4.572 /m,ri/ro=0.5,Hsl=465.2kJ/kg
ρ=2803.2kg/m^3, αs=0.0307m^2/hr,Ks=3.462 W/mK

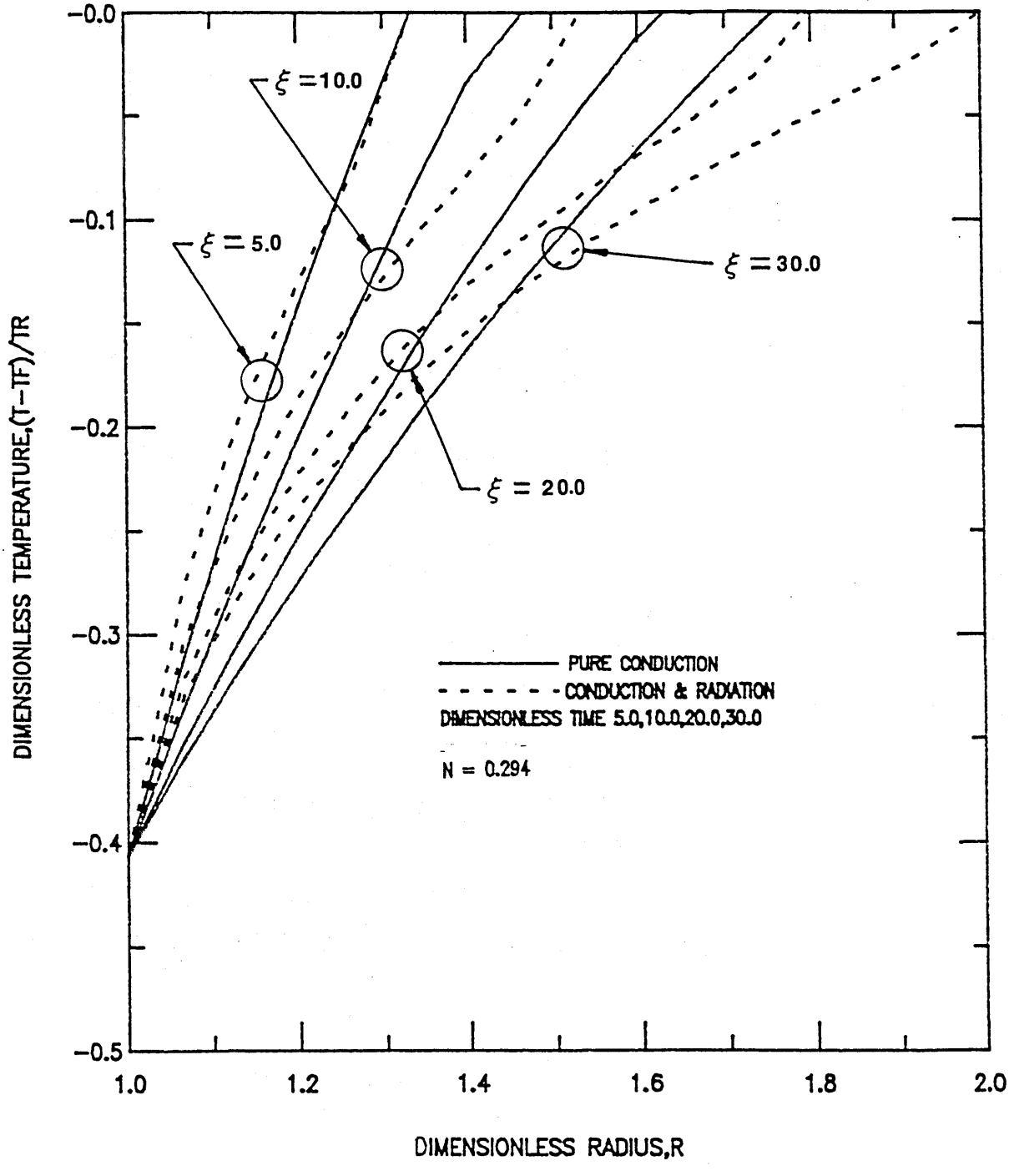

Figure 31 TRANSIENT DIMENSIONLESS TEMPERATURE VS. DIMENSIONLESS RADIUS

Tl/TF=0.5, εw1= εw2=1.0, ω =0.0,a=4.572 /m,ri/ro=0.5
Hsl=465.2kJ/kg, ρ=2803.2kg/m^3, αs=0.0307m^2/hr,Ks=3.462W/mK

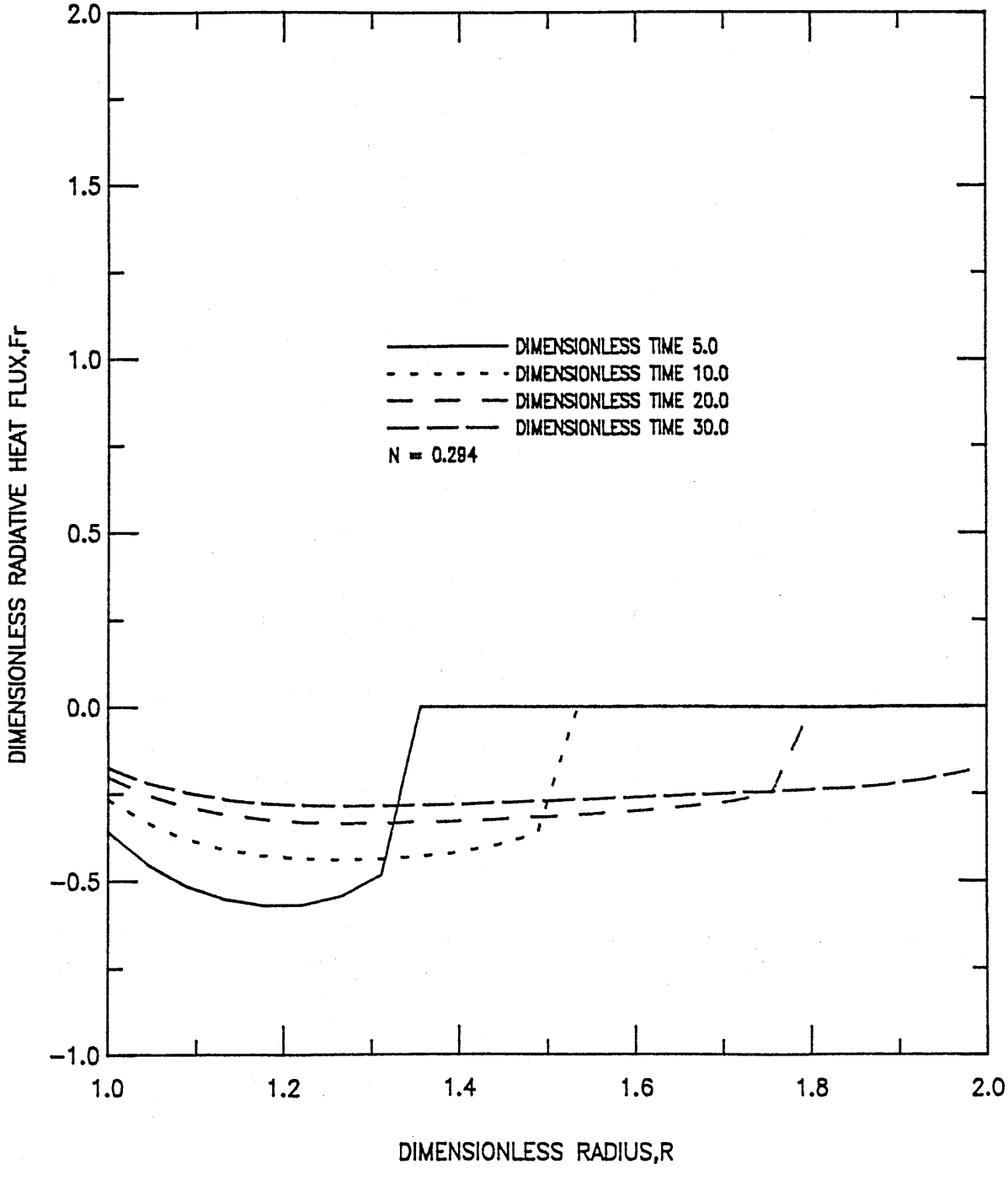

Figure 32 TRANSIENT DIMENSIONLESS RADIATIVE FLUX VS. DIMENSIONLESS RADIUS

TI/TF=0.5, $\varepsilon w1 = \varepsilon w2 = 1.0$, $\omega = 0.0$, $a = 4.572$ /m, ri/ro=0.5
Hsl=465.2kJ/kg, $\rho = 2803.2 kg/m^3$, $\alpha s = 0.0307 m^2/hr$, Ks=3.462W/mK

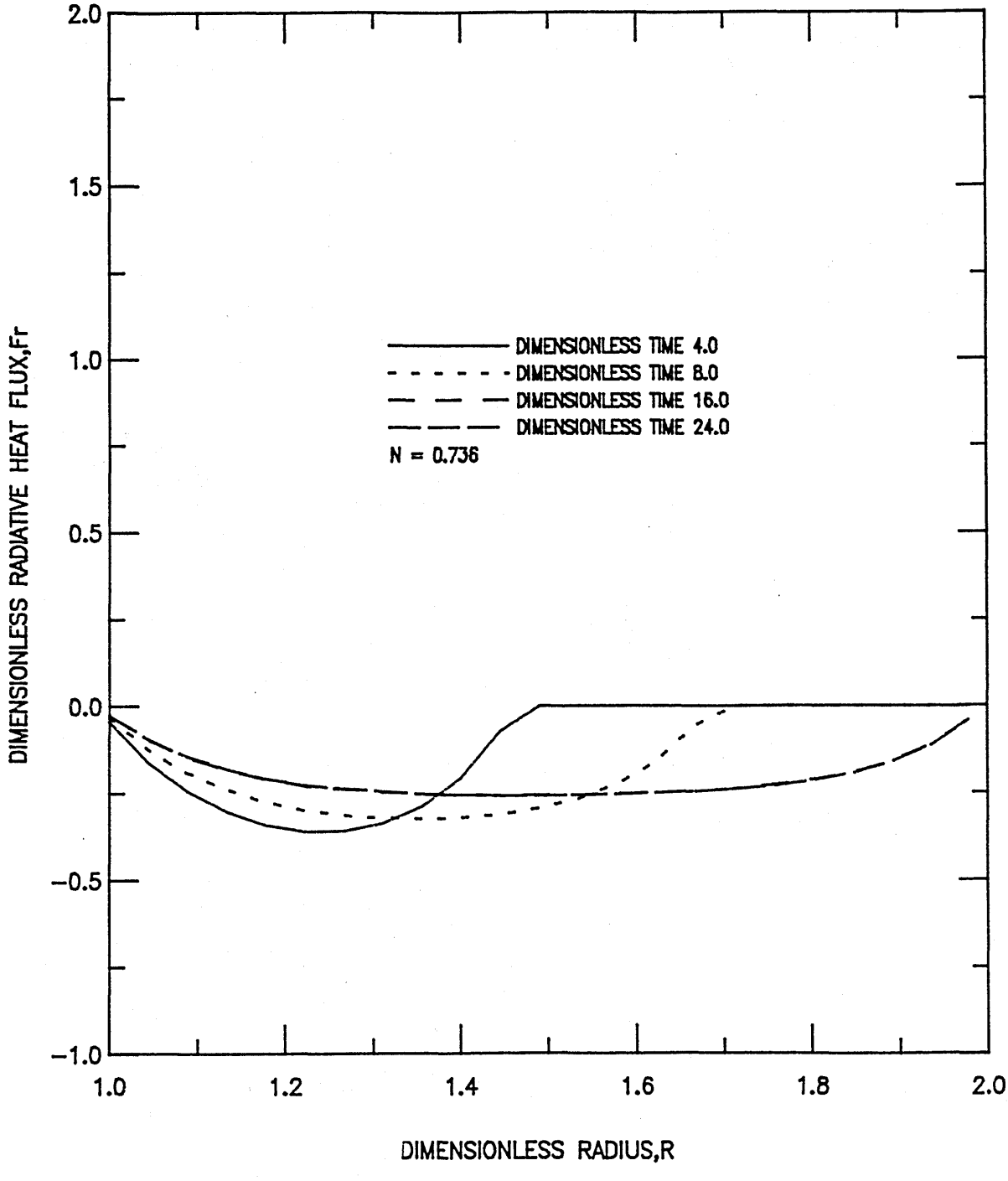

Figure 33

TRANSIENT DIMENSIONLESS RADIATIVE FLUX VS. DIMENSIONLESS RADIUS

Tl/TF=0.5, $\varepsilon w1 = \varepsilon w2 = 0.2$, $\omega = 0.0$, $a = 4.572$ /m, ri/ro=0.5
Hsl=465.2kJ/kg, $\rho = 2803.2 kg/m^3$, $\alpha s = 0.0307 m^2/hr$, Ks=8.654W/mK

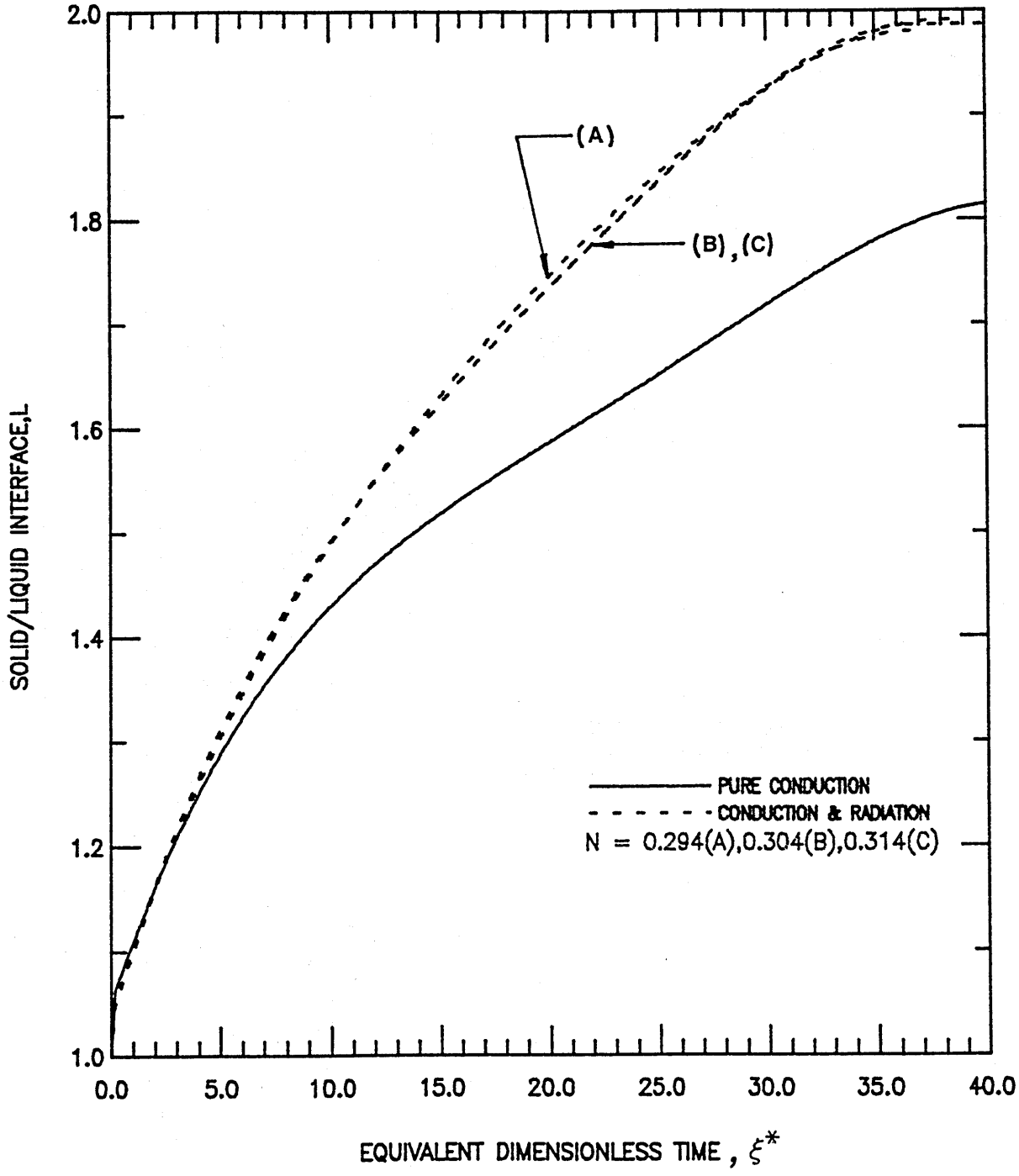

Figure 34 SOLID/LIQUID INTERFACE VS. DIMENSIONLESS TIME

TI/TF=0.5, εw1= εw2=1.0,ω =0.0(A),0.5(B),1.0(C),a=4.572 /m
ri/ro=0.5,Hsl=465.2kJ/kg, ρ=2803.2kg/m^3, αs=0.0307m^2/hr
Ks=3.462W/mK

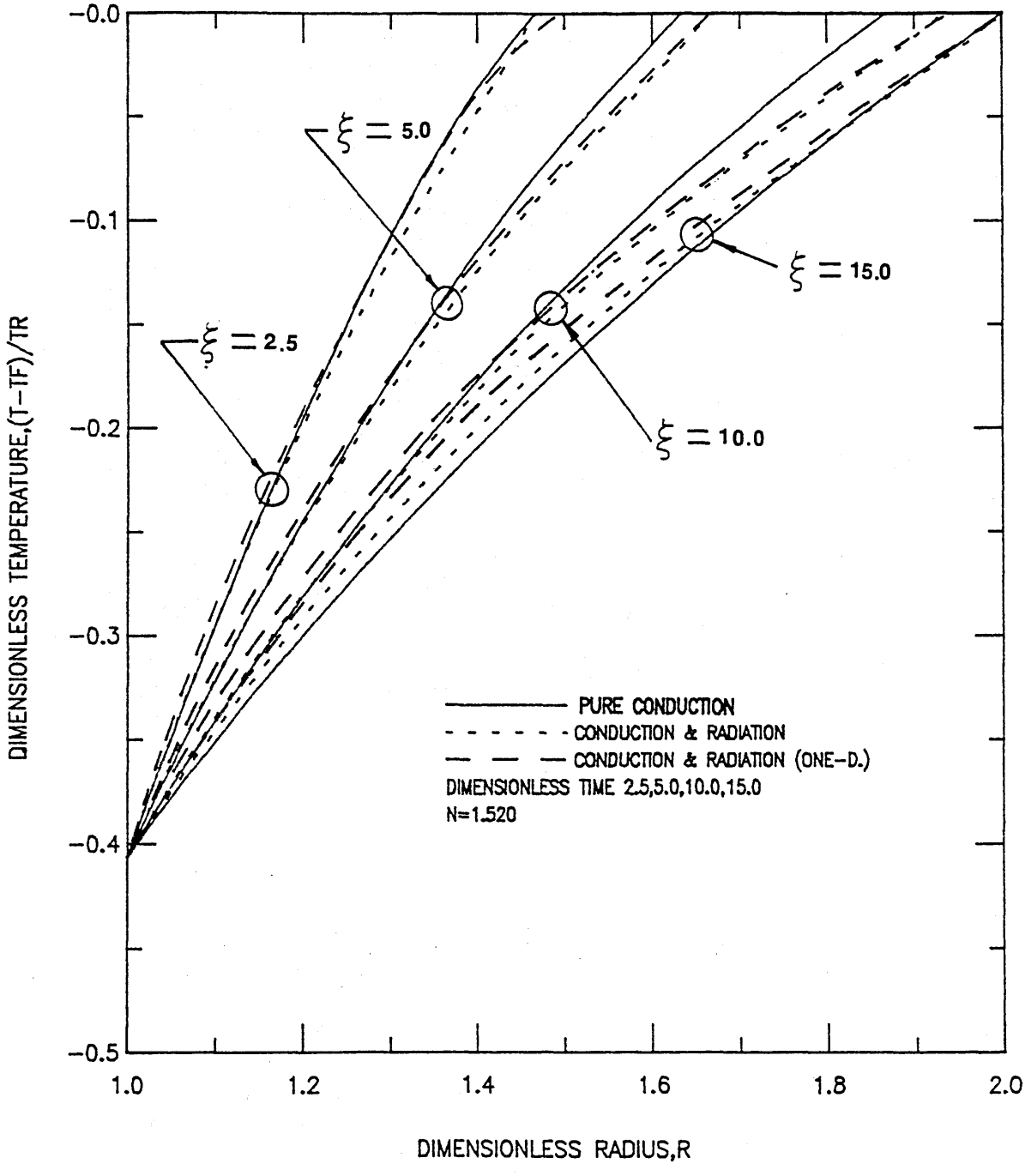

Figure 35 DIMENSIONLESS TEMPERATURE VERSUS DIMENSIONLESS RADIUS AT J=N/2

TI/TF=0.5, εw1= εw2=1.0, εw3= εw4=1.0,a=4.572 /m
ω =0.5,ri/ro=0.5,z/ro=1.0,Hsl=465.2kJ/kg
Ks=17.307W/mK, ρ=2803.2kg/m^3, αs=0.0307m^2/hr

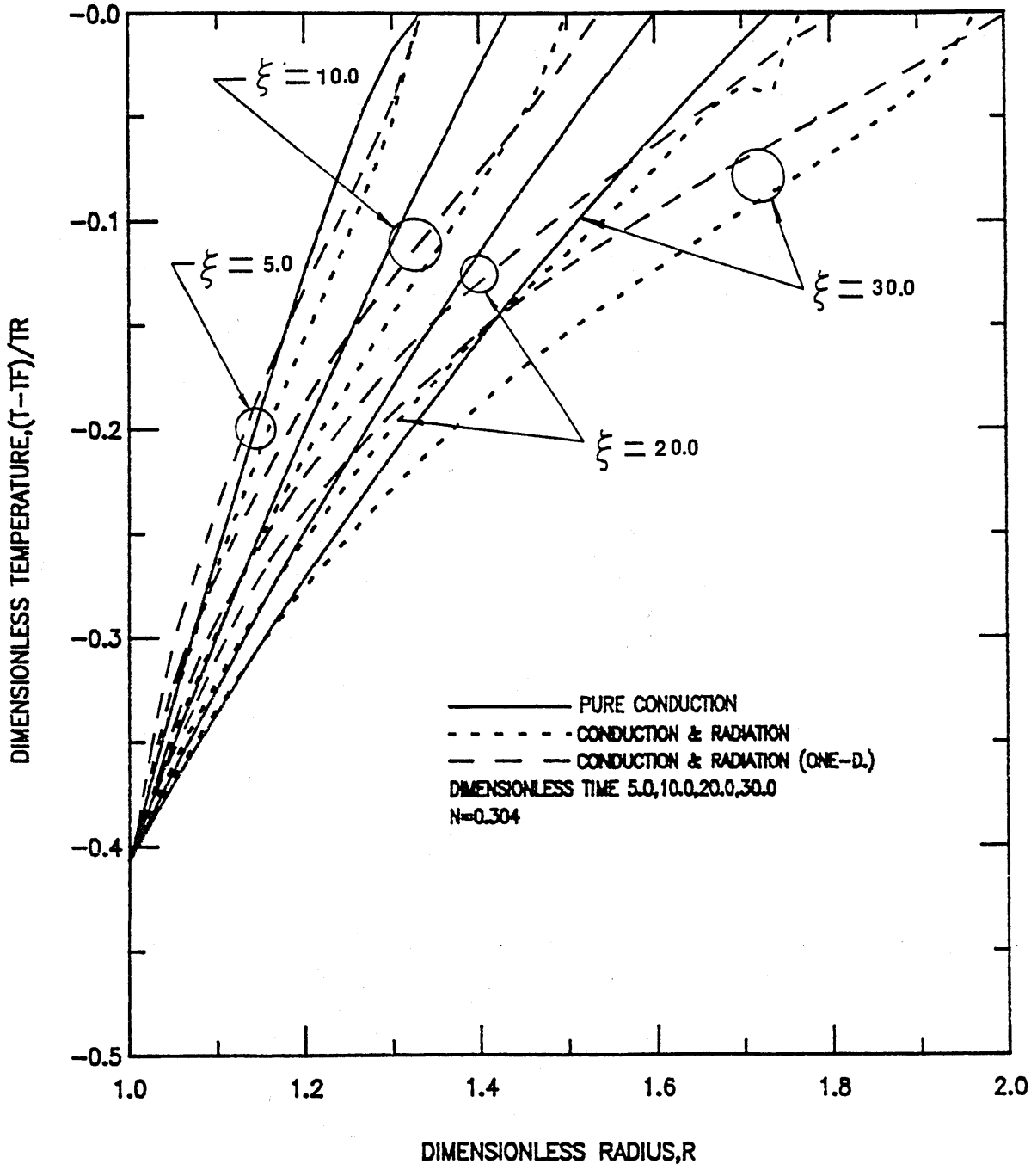

Figure 36 DIMENSIONLESS TEMPERATURE VERSUS DIMENSIONLESS RADIUS AT J=N/2

TI/TF=0.5, εw1= εw2=1.0, εw3= εw4=1.0,a=4.572 /m
ω =0.5,ri/ro=0.5,z/ro=1.0,Hsl=465.2kJ/kg
Ks=3.462W/mK, ρ=2803.2kg/m^3, αs=0.0307m^2/hr

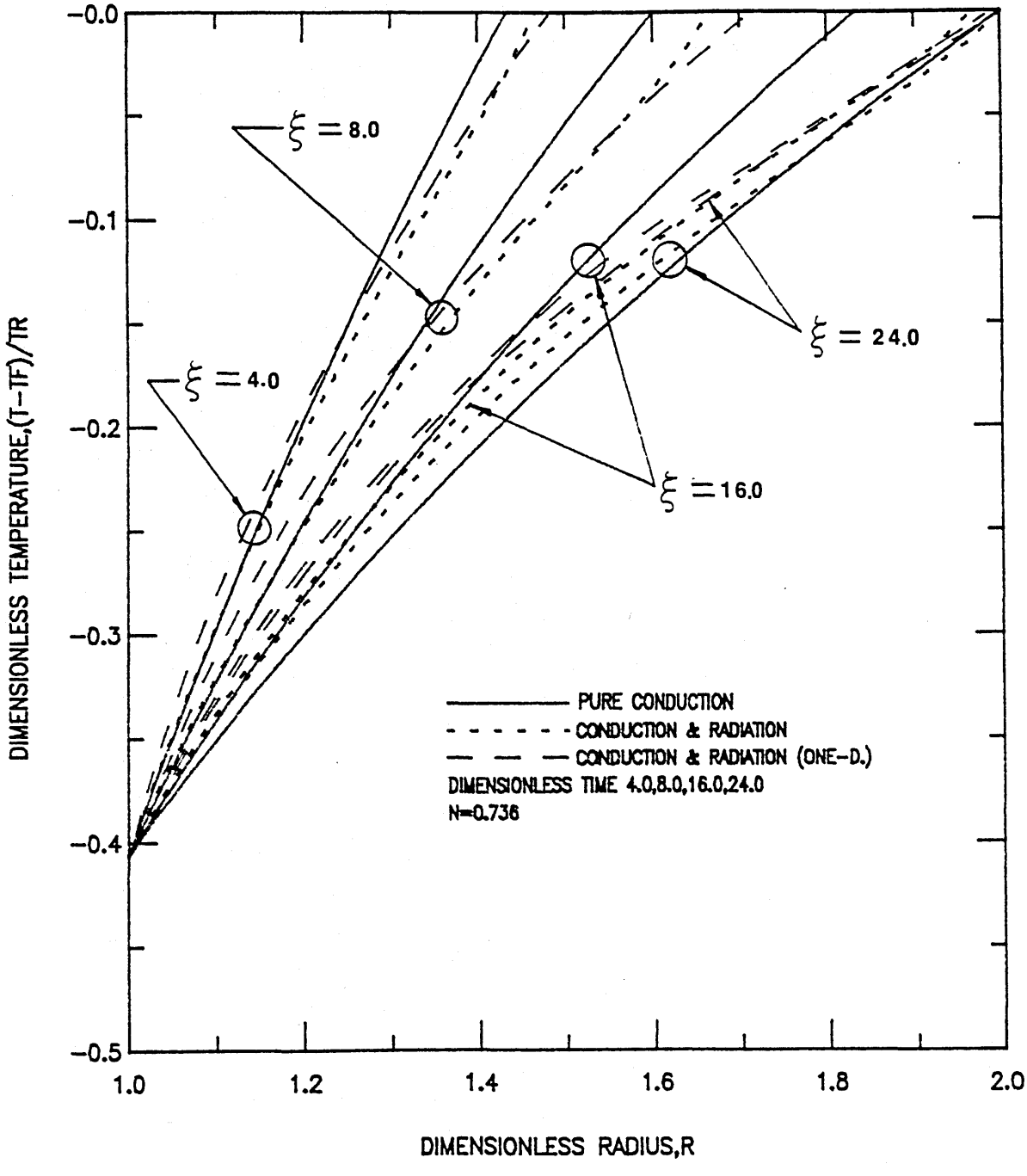

Figure 37 DIMENSIONLESS TEMPERATURE VERSUS DIMENSIONLESS RADIUS AT J=N/2

TI/TF=0.5, εw1= εw2=1.0, εw3= εw4=1.0,a=4.572 /m
ω=0.0,ri/ro=0.5,z/ro=1.0,Hsl=465.2kJ/kg
Ks=8.654W/mK, ρ=2803.2kg/m^3, αs=0.0307m^2/hr

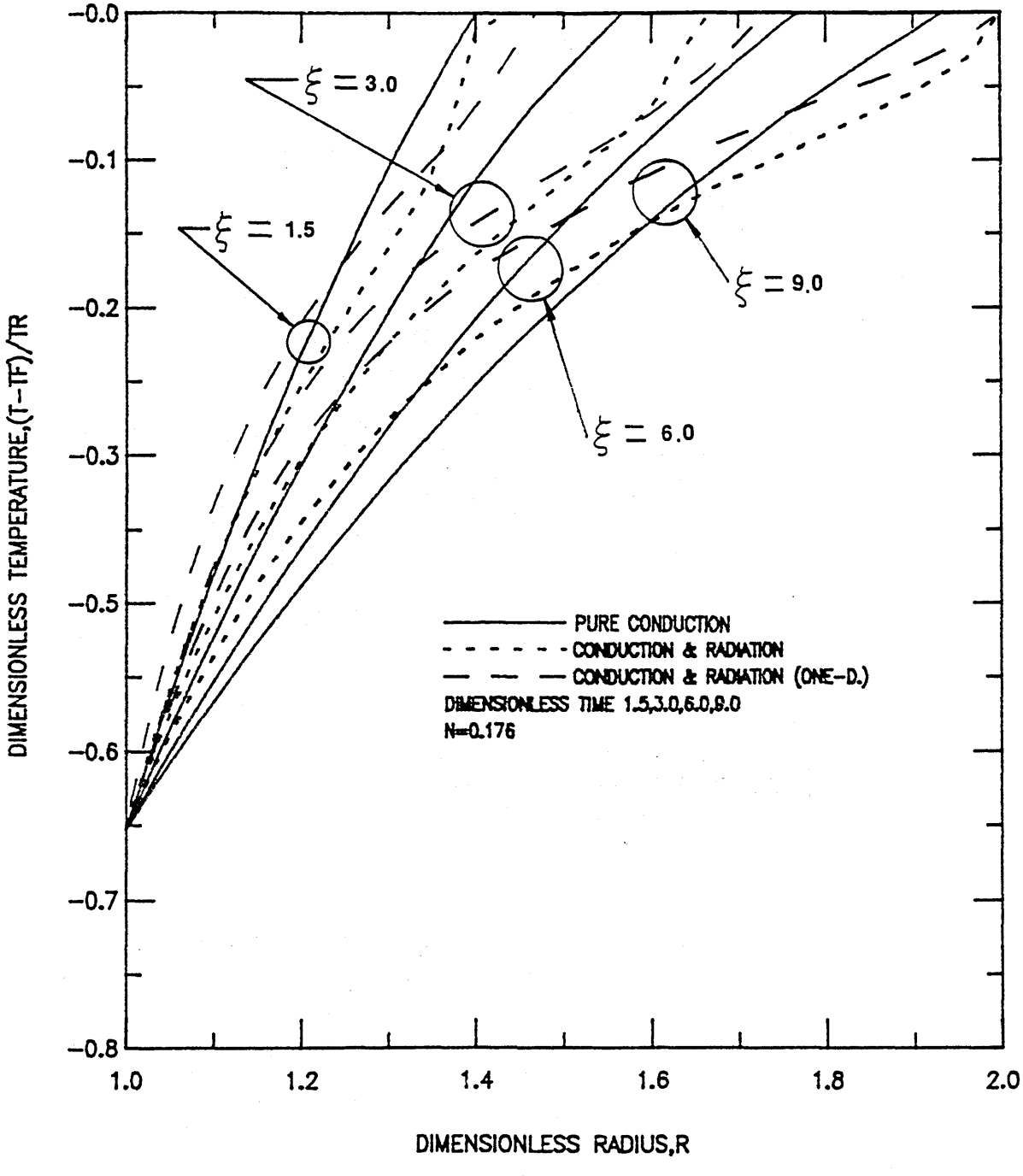

Figure 38 DIMENSIONLESS TEMPERATURE VERSUS DIMENSIONLESS RADIUS AT J=N/2

TI/TF=0.286, εw1= εw2=1.0, εw3= εw4=1.0,a=4.572 /m
ω=0.0,ri/ro=0.5,z/ro=1.0,Hsl=465.2kJ/kg
Ks=8.654W/mK, ρ=2803.2kg/m^3, αs=0.0307m^2/hr

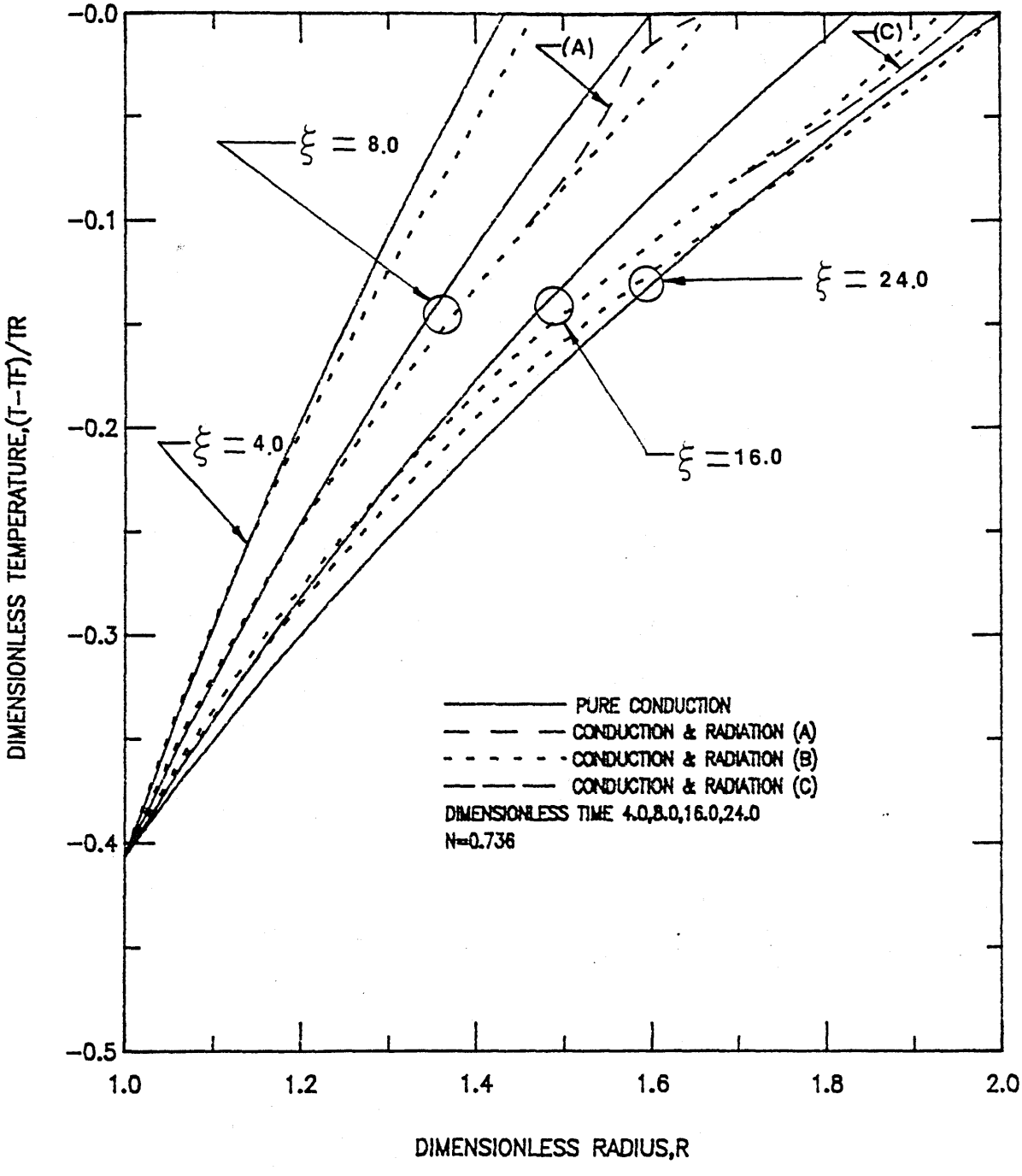

Figure 39 DIMENSIONLESS TEMPERATURE VERSUS DIMENSIONLESS RADIUS AT J=N/2

TI/TF=0.5, $\varepsilon w1 = \varepsilon w2$=0.2(A),0.5(B),1.0(C),Ks=8.654W/mK
a=4.572 /m, ω=0.0,ri/ro=0.5,z/ro=1.0,Hsl=465.2kJ/kg
$\epsilon w3 = \varepsilon w4$=0.2(A),0.5(B),1.0(C), ρ=2803.2kg/m^3, αs=0.0307m^2/hr

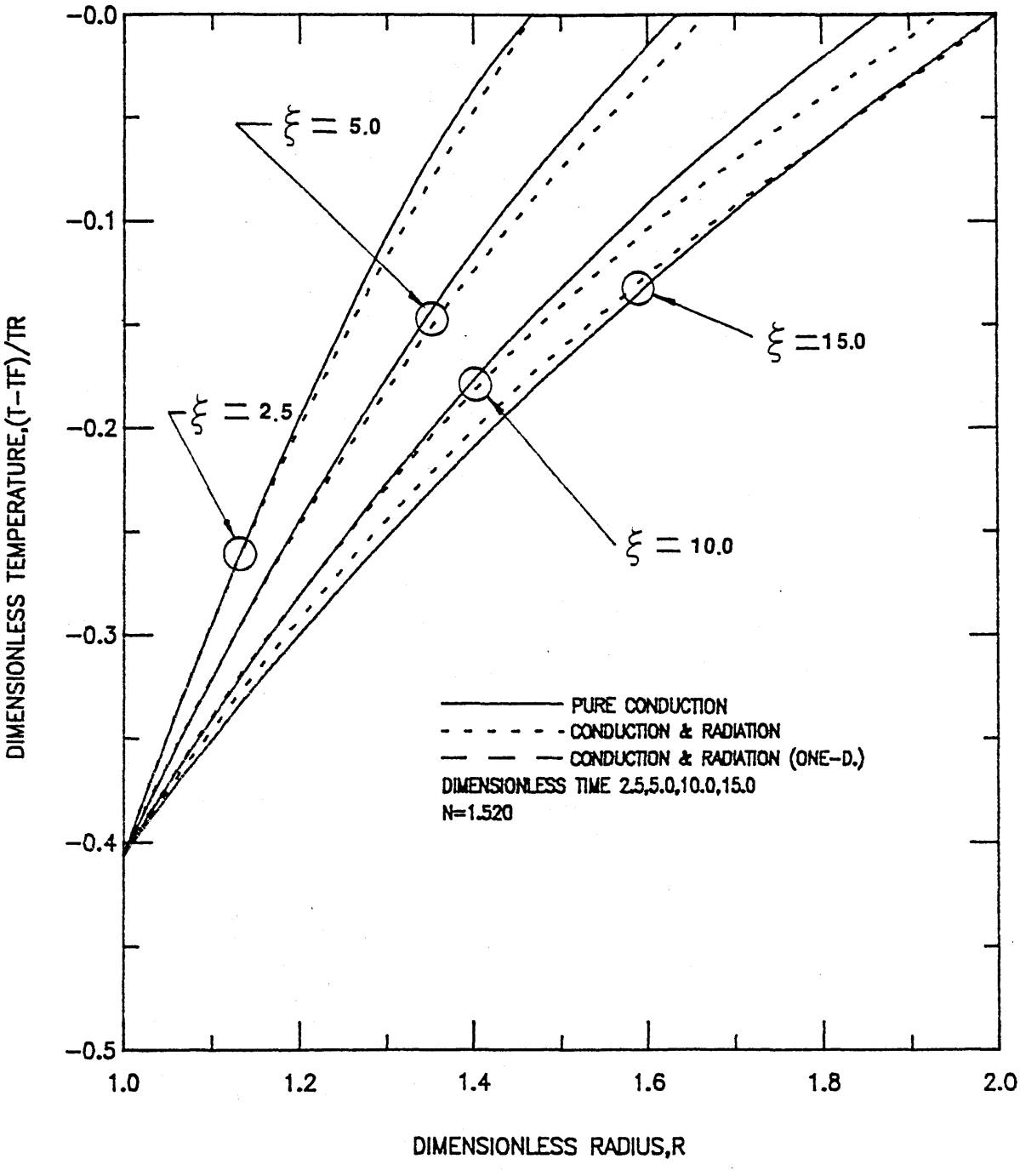

Figure 40 DIMENSIONLESS TEMPERATURE VERSUS DIMENSIONLESS RADIUS AT J=N/2

TI/TF=0.5, εw1= εw2=1.0, εw3= εw4=1.0,a=4.572 /m
ω=0.5,ri/ro=0.5,z/ro=0.5,Hsl=465.2kJ/kg
Ks=17.307W/mK, ρ=2803.2kg/m^3, αs=0.0307m^2 /hr

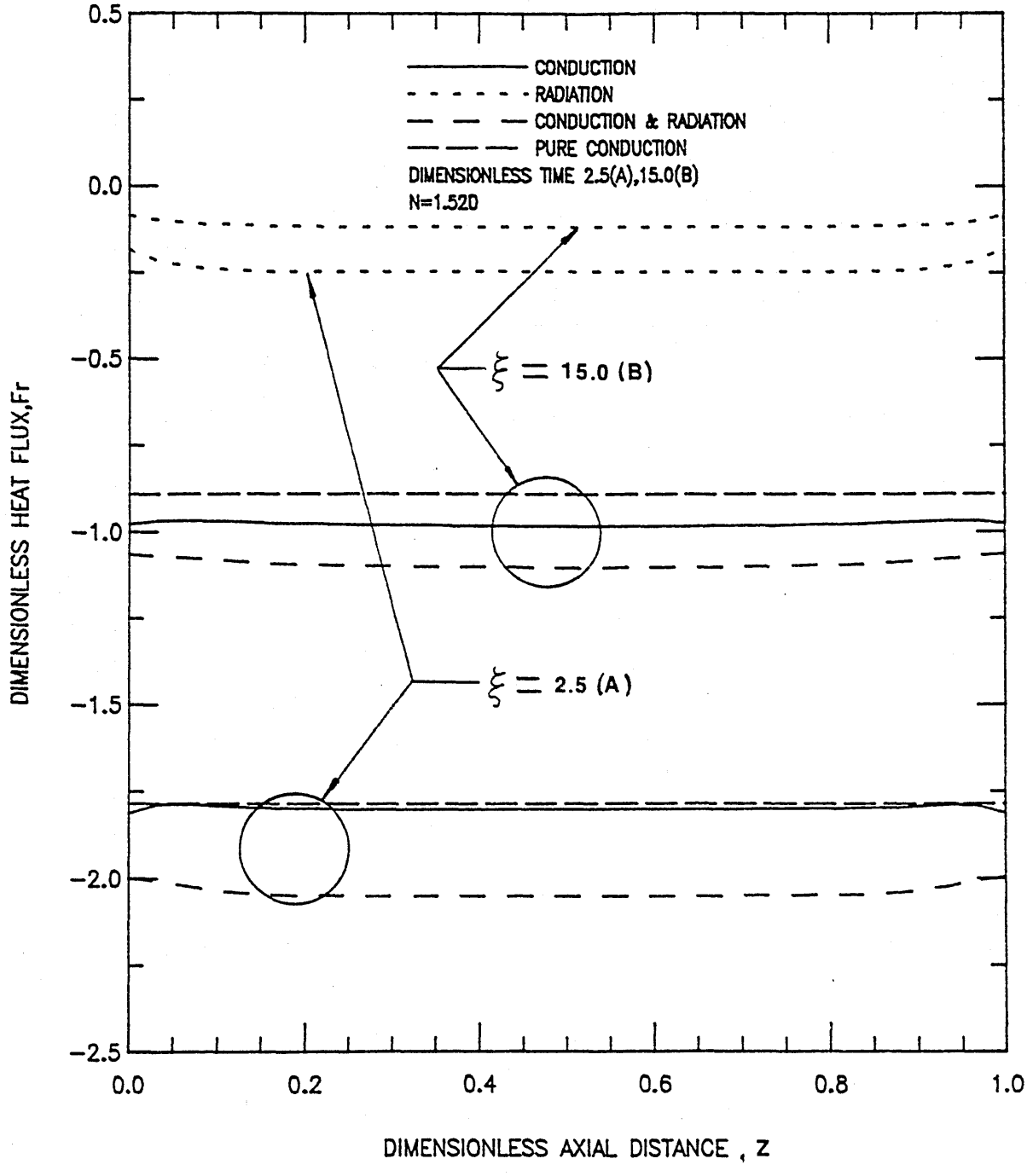

Figure 41 HEAT FLUX AT INSIDE CYLINDER VS. DIMENSIONLESS AXIAL DISTANCE

$T_I/T_F=0.5$, $\varepsilon_{w1}=\varepsilon_{w2}=1.0$, $\varepsilon_{w3}=\varepsilon_{w4}=1.0$, $a=4.572$ /m
$\omega=0.5$, $r_i/r_o=0.5$, $z/r_o=1.0$, $H_{sl}=465.2$kJ/kg
$K_s=17.307$W/mK, $\rho=2803.2$kg/m^3, $\alpha_s=0.0307$m^2/hr

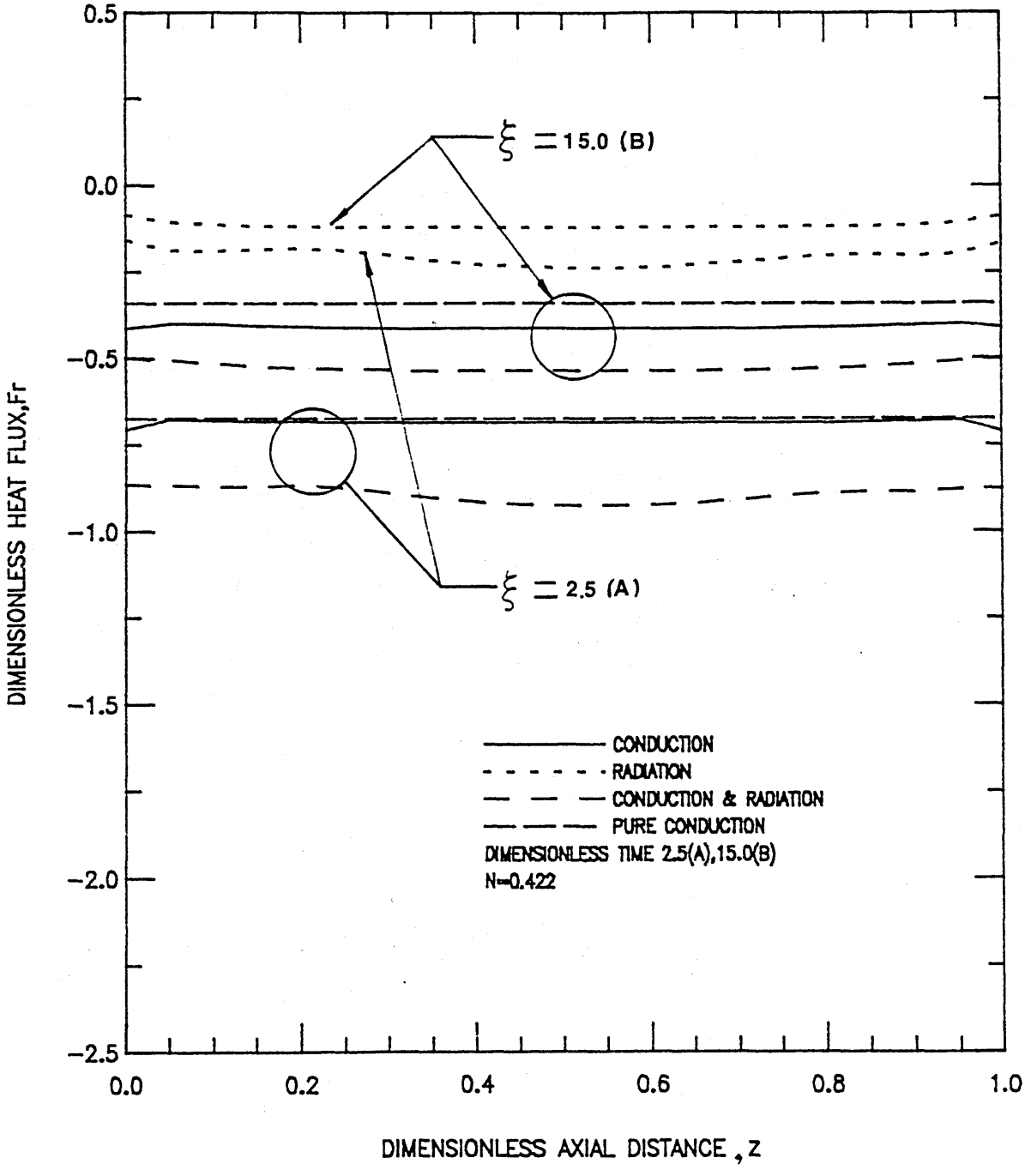

Figure 42 HEAT FLUX AT INSIDE CYLINDER VS. DIMENSIONLESS AXIAL DISTANCE

TI/TF=0.4, εw1= εw2=1.0, εw3= εw4=1.0,a=4.572 /m
ω =0.0,ri/ro=0.5,z/ro=1.0,Hsl=465.2kJ/kg
Ks=8.654W/mK, ρ=2803.2kg/m^3, αs=0.0307m^2/hr

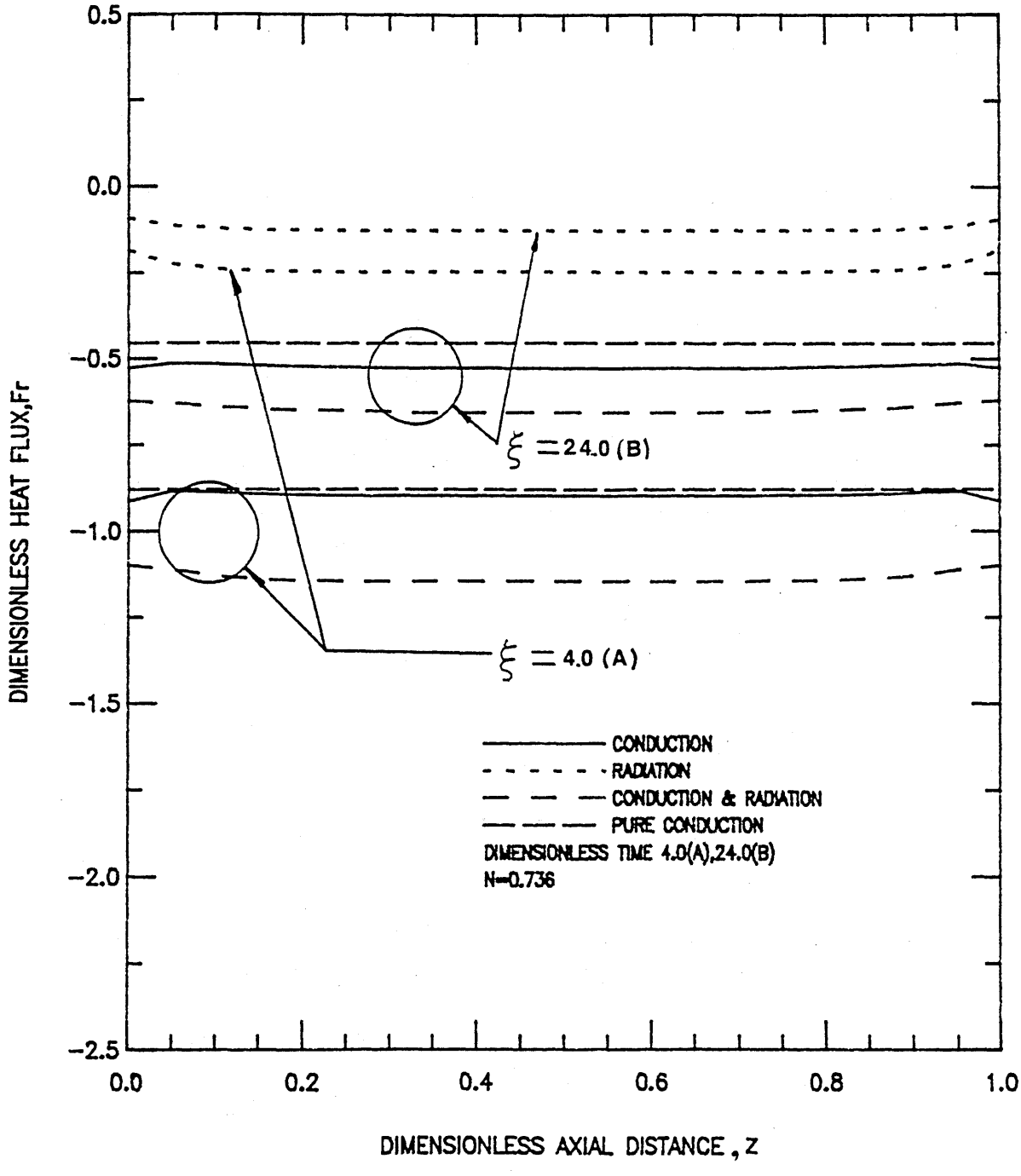

Figure 43 HEAT FLUX AT INSIDE CYLINDER VS. DIMENSIONLESS AXIAL DISTANCE

TI/TF=0.5, $\varepsilon w1 = \varepsilon w2 = 1.0$, $\varepsilon w3 = \varepsilon w4 = 1.0$, $a = 4.572$ /m
$\omega = 0.0$, $ri/ro = 0.5$, $z/ro = 1.0$, $Hsl = 465.2$kJ/kg
$Ks = 8.654$W/mK, $\rho = 2803.2$kg/m^3, $\alpha s = 0.0307$m^2/hr

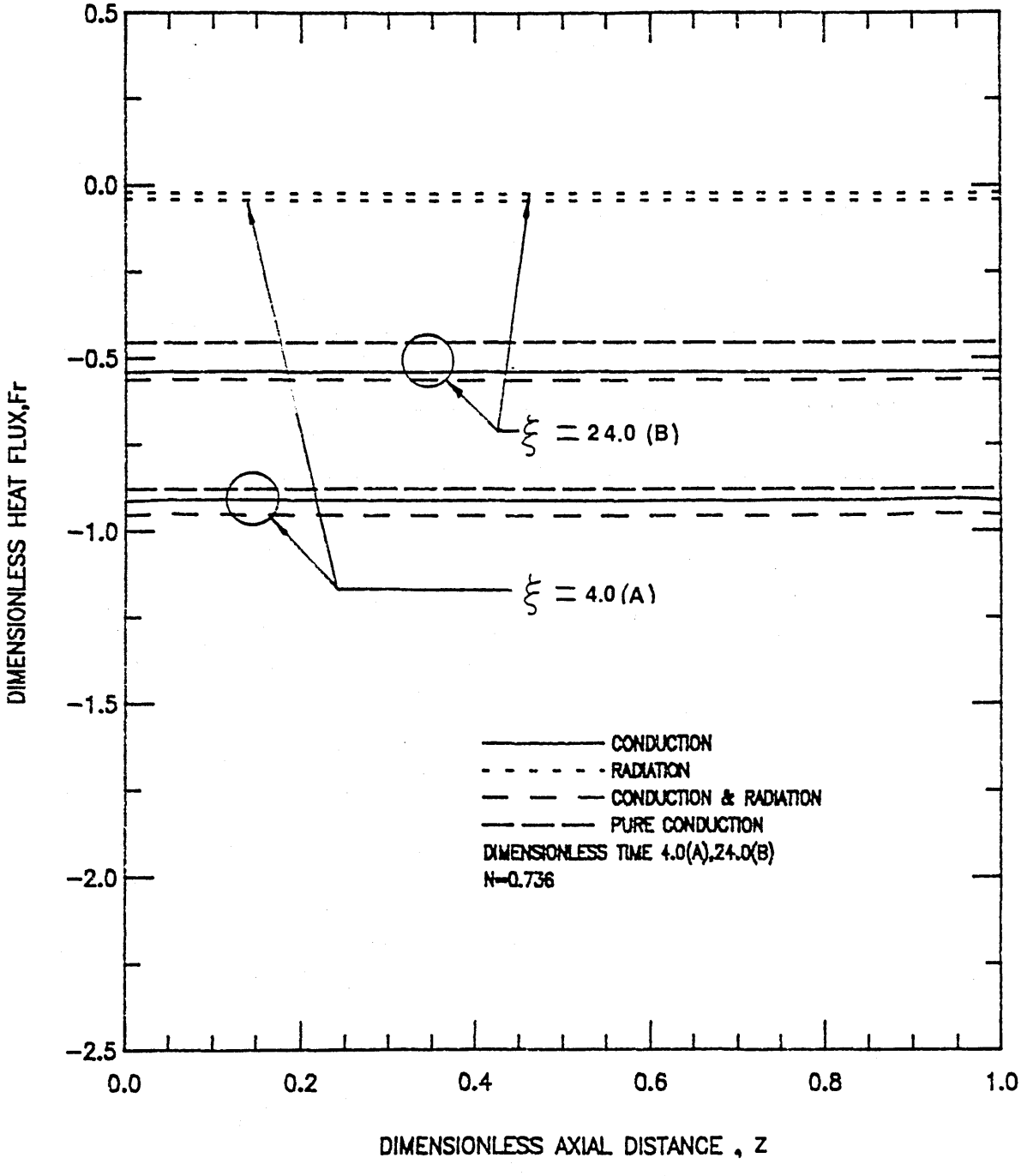

Figure 44 HEAT FLUX AT INSIDE CYLINDER VS. DIMENSIONLESS AXIAL DISTANCE

TI/TF=0.5, $\varepsilon w1 = \varepsilon w2 = 0.2$, $\varepsilon w3 = \varepsilon w4 = 0.2$, $a = 4.572$ /m
$\omega = 0.0$, $ri/ro = 0.5$, $z/ro = 1.0$, $Hsl = 465.2$kJ/kg
$Ks = 8.654$W/mK, $\rho = 2803.2$kg/m^3, $\alpha s = 0.0307$m^2/hr

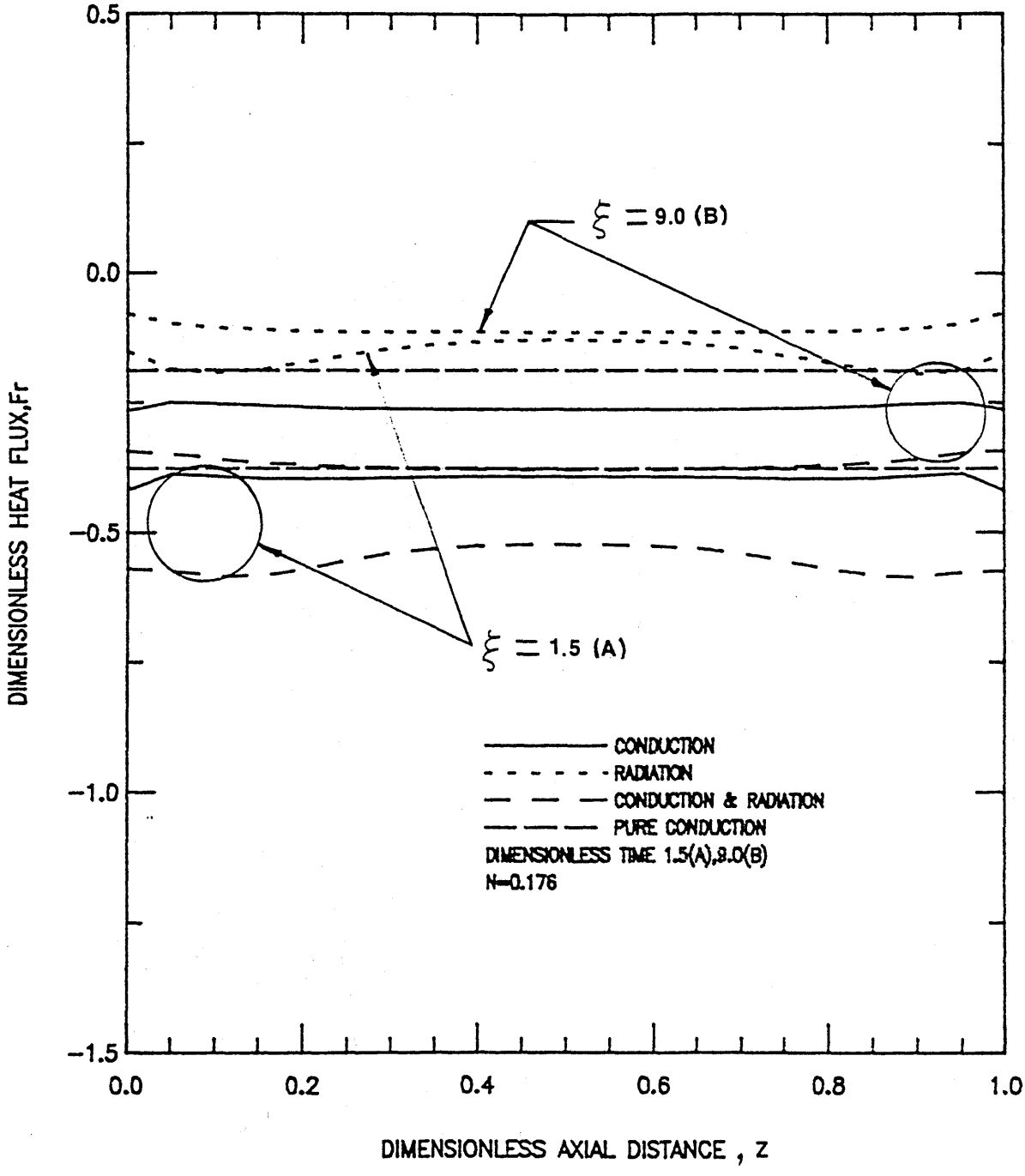

Figure 45 HEAT FLUX AT INSIDE CYLINDER VS. DIMENSIONLESS AXIAL DISTANCE

Ti/Tf=0.286, $\varepsilon w1 = \varepsilon w2 = 1.0$, $\varepsilon w3 = \varepsilon w4 = 1.0$, $a = 4.572$ /m
$\omega = 0.0$, $ri/ro = 0.5$, $z/ro = 1.0$, $Hsl = 465.2$kJ/kg
$Ks = 8.654$W/mK, $\rho = 2803.2$kg/m^3, $\alpha s = 0.0307$m^2/hr

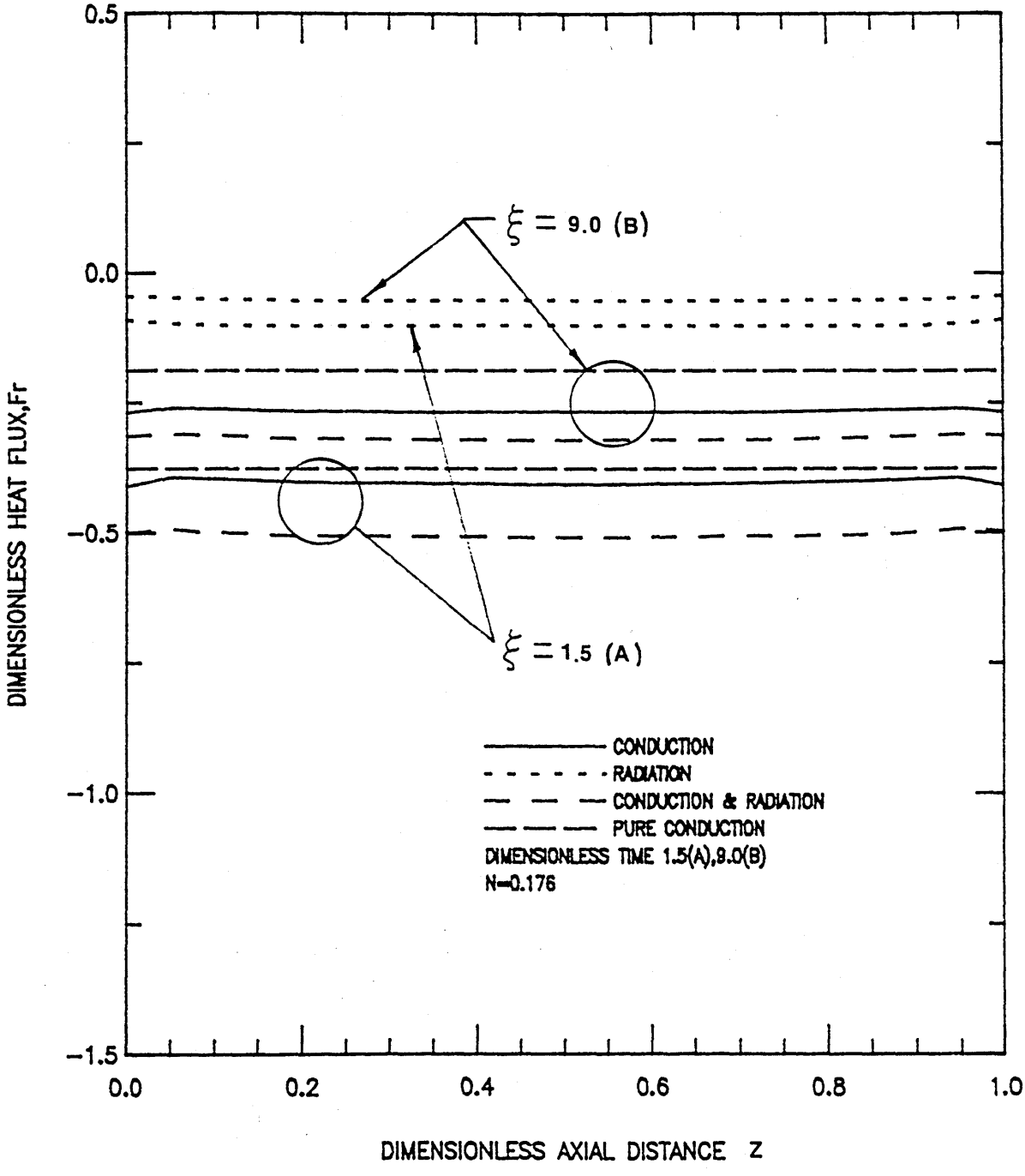

Figure 46 HEAT FLUX AT INSIDE CYLINDER VS. DIMENSIONLESS AXIAL DISTANCE

TI/TF=0.286, εw1= εw2=0.5, εw3= εw4=0.5,a=4.572 /m
ω=0.0,ri/ro=0.5,z/ro=1.0,Hsl=465.2kJ/kg
Ks=8.654W/mK, ρ=2803.2kg/m^3, αs=0.0307m^2/hr

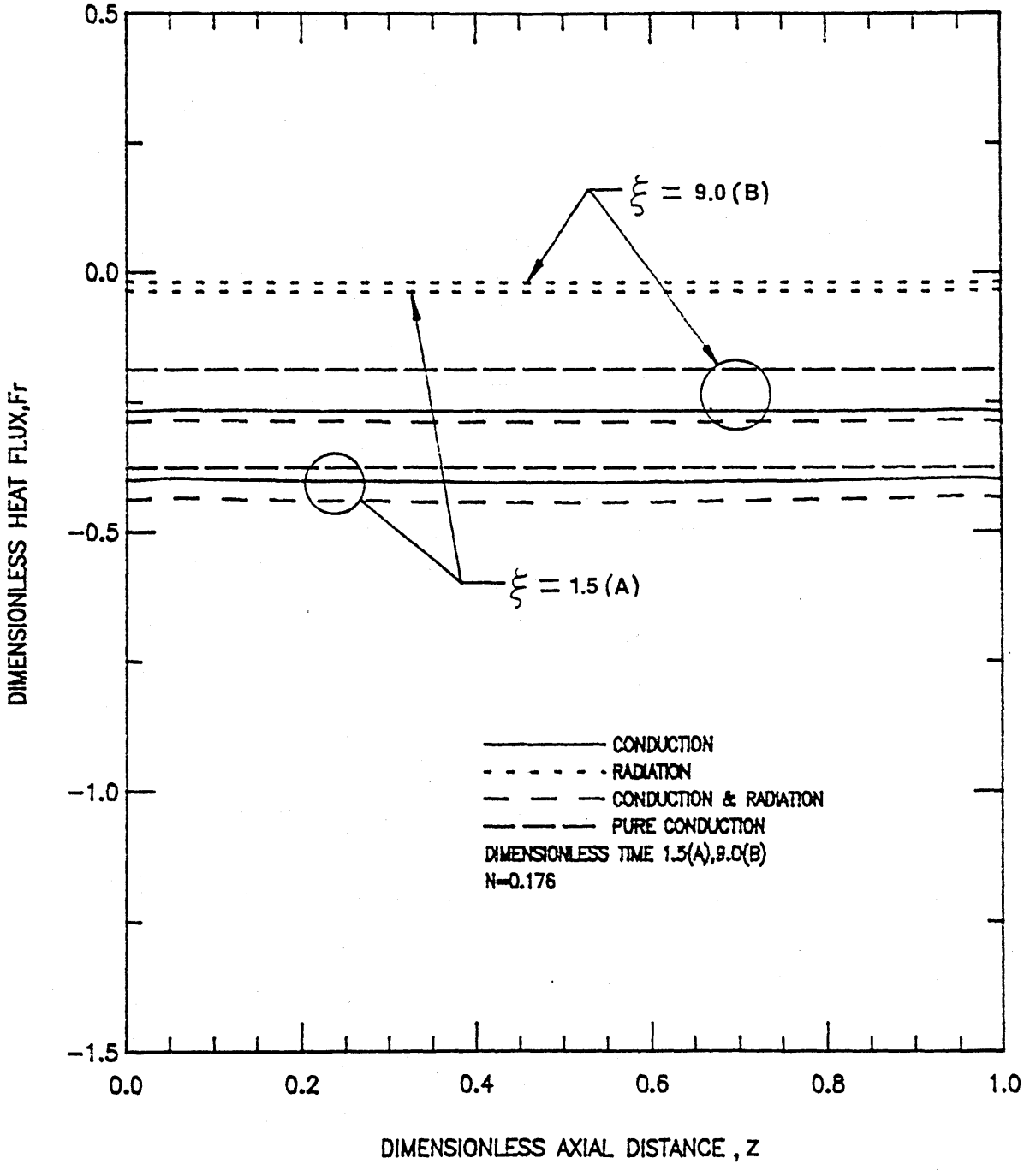

Figure 47. HEAT FLUX AT INSIDE CYLINDER VS. DIMENSIONLESS AXIAL DISTANCE

TI/TF=0.286, εw1= ε w2=0.2, εw3= εw4=0.2,a=4.572 /m
ω=0.0,ri/ro=0.5,z/ro=1.0,Hsl=465.2kJ/kg
Ks=8.654W/mK, ρ=2803.2kg/m ^{3}, αs=0.0307m ^{2}/hr

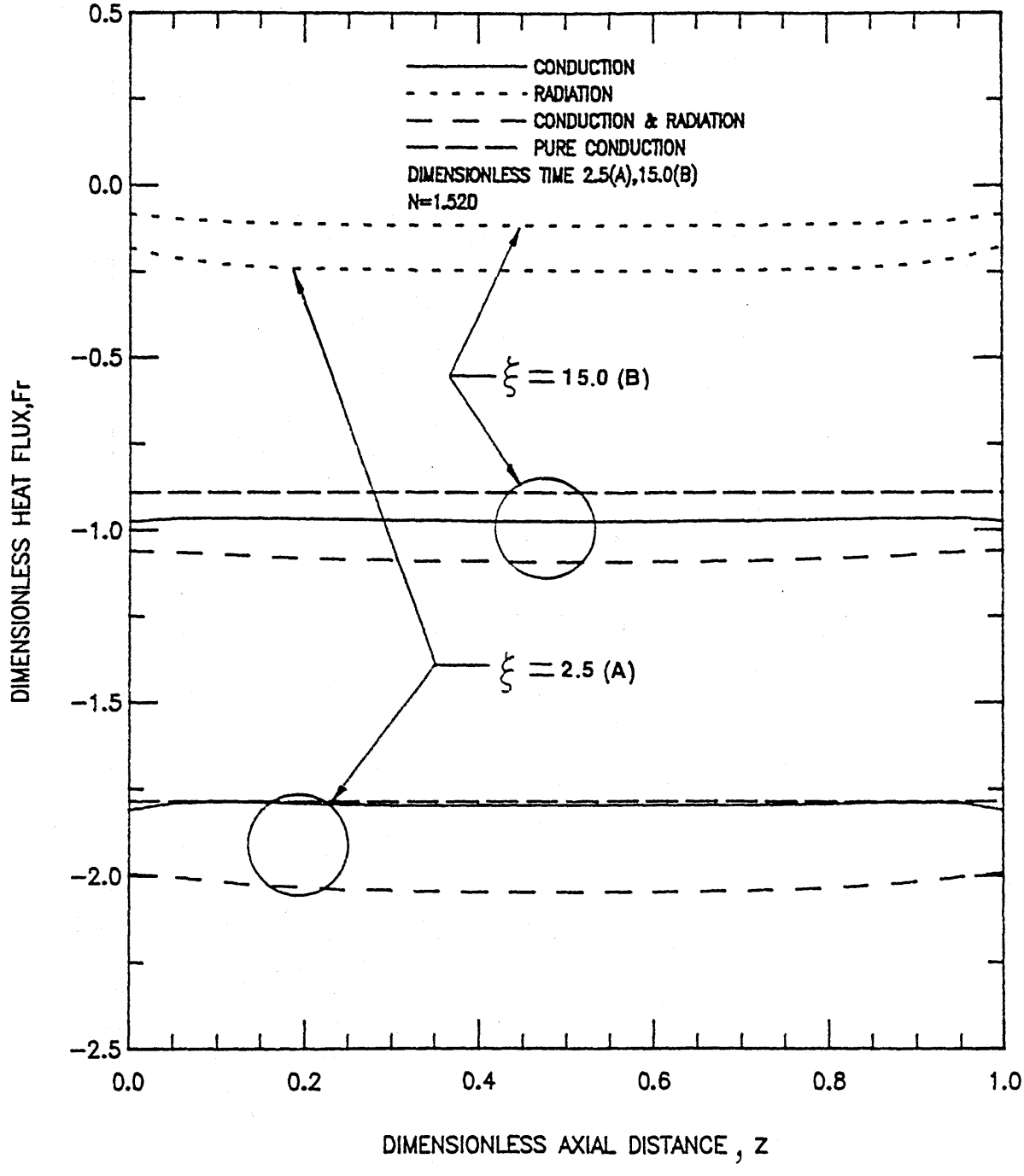

Figure 48 HEAT FLUX AT INSIDE CYLINDER VS. DIMENSIONLESS AXIAL DISTANCE

Ti/Tf=0.5, $\varepsilon w1 = \varepsilon w2 = 1.0$, $\varepsilon w3 = \varepsilon w4 = 1.0$, $a = 4.572$ /m
$\omega = 0.5$, ri/ro=0.5, z/ro=0.5, Hsl=465.2kJ/kg
Ks=17.307W/mK, $\rho = 2803.2 kg/m^3$, $\alpha s = 0.0307 m^2/hr$

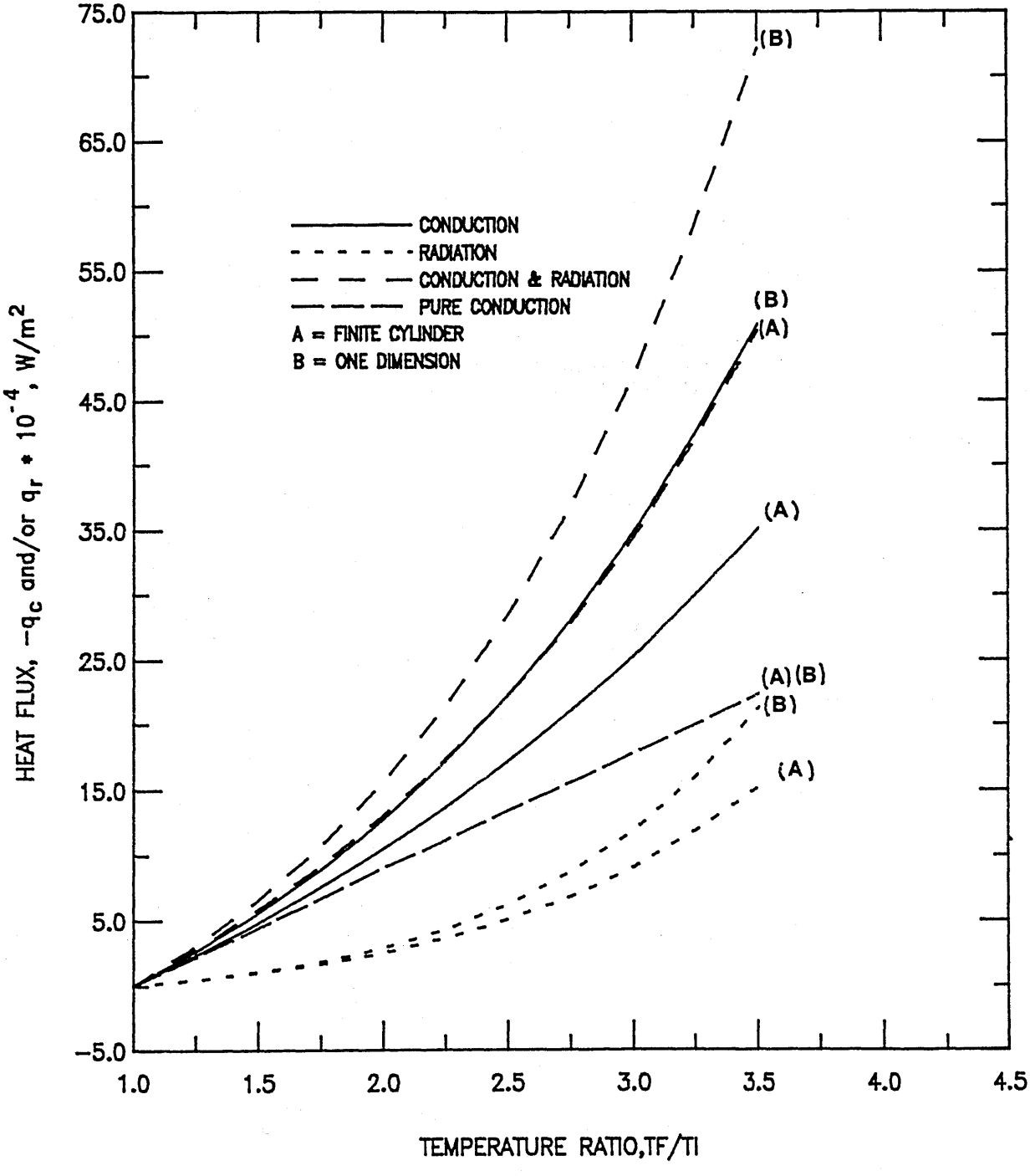

Figure 49

STEADY STATE HEAT FLUX AT INSIDE CYLINDER VS. TEMPERATURE RATIO
(HEAT FLUX FOR FINITE ANNULUS IS AT J/2)

$\epsilon w1 = \epsilon w2 = 1.0$, $\epsilon w3 = \epsilon w4 = 1.0$, $\omega = 0.0$, $a = 4.572$ /m, ri/ro=0.5
Hsl=465.2kJ/kg, ρ =2803.2kg/m^3, $\alpha s = 0.0307 m^2/hr$, Ks=8.654W/mK

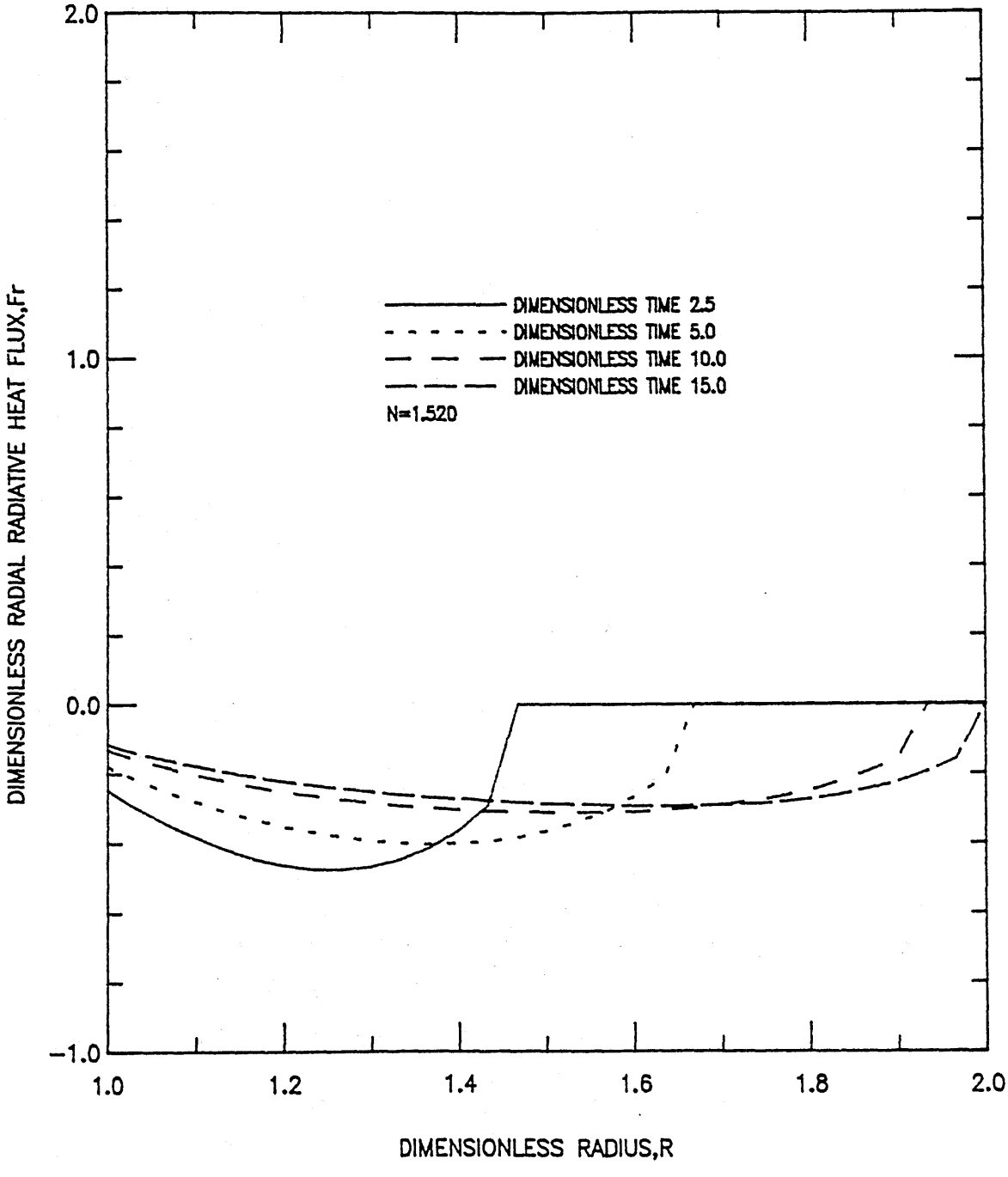

Figure 50 RADIAL RADIATIVE FLUX VS. DIMENSIONLESS RADIUS AT J=N/2

TI/TF=0.5, $\varepsilon w1 = \varepsilon w2 = 1.0$, $\varepsilon w3 = \varepsilon w4 = 1.0$, a=4.572 /m
ω=0.5,ri/ro=0.5,z/ro=0.5,Hsl=465.2kJ/kg
K_S=17.307W/mK, ρ=2803.2kg/m^3, α_S=0.0307m^2 /hr

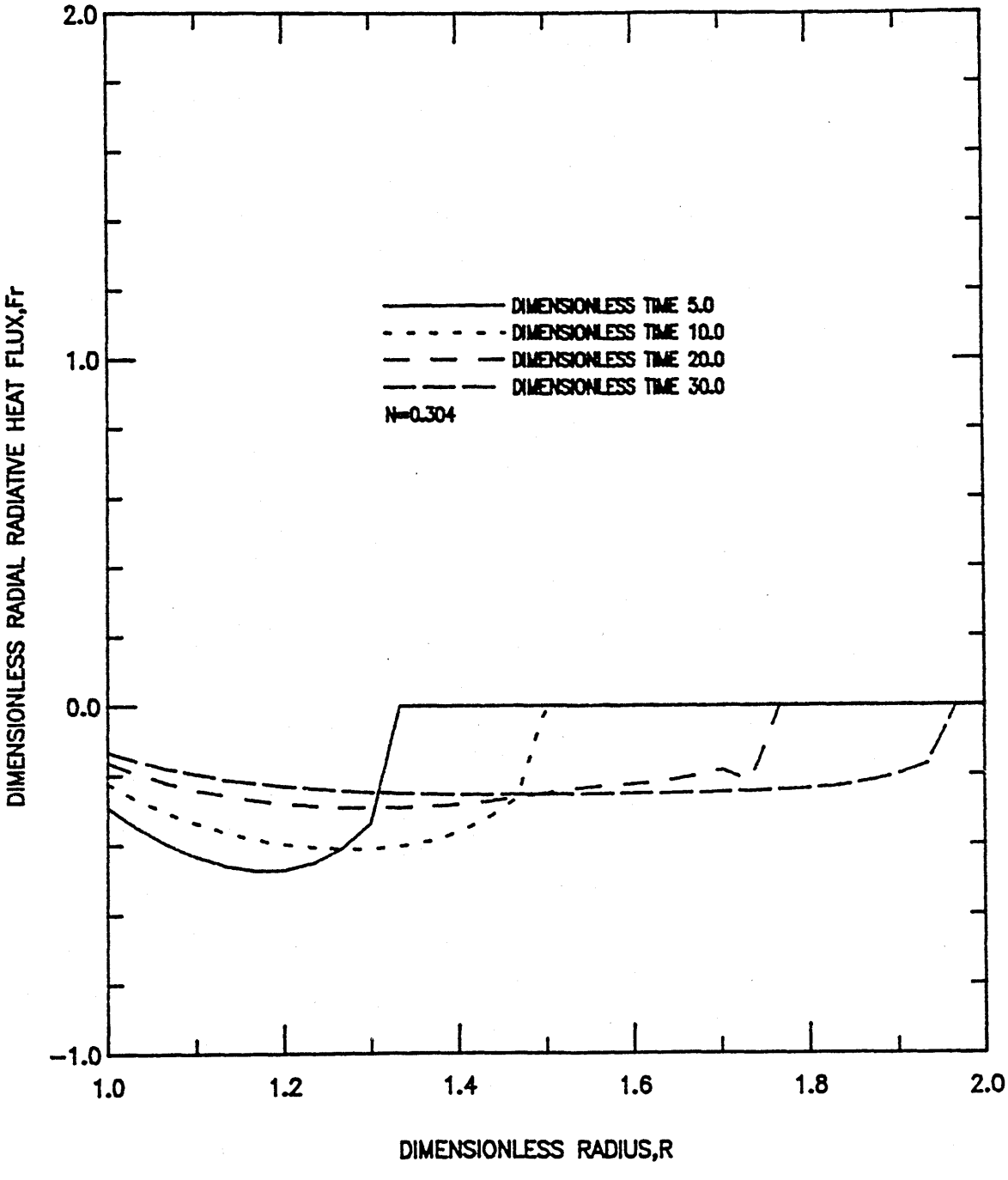

Figure 51 RADIAL RADIATIVE FLUX VS. DIMENSIONLESS RADIUS AT J=N/2

TI/TF=0.5, $\varepsilon w1 = \varepsilon w2 = 1.0$, $\varepsilon w3 = \varepsilon w4 = 1.0$, $a = 4.572$ /m
$\omega = 0.5$, ri/ro=0.5, z/ro=1.0, Hsl=465.2kJ/kg
Ks=3.462W/mK, $\rho = 2803.2 kg/m^3$, $\alpha s = 0.0307 m^2/hr$

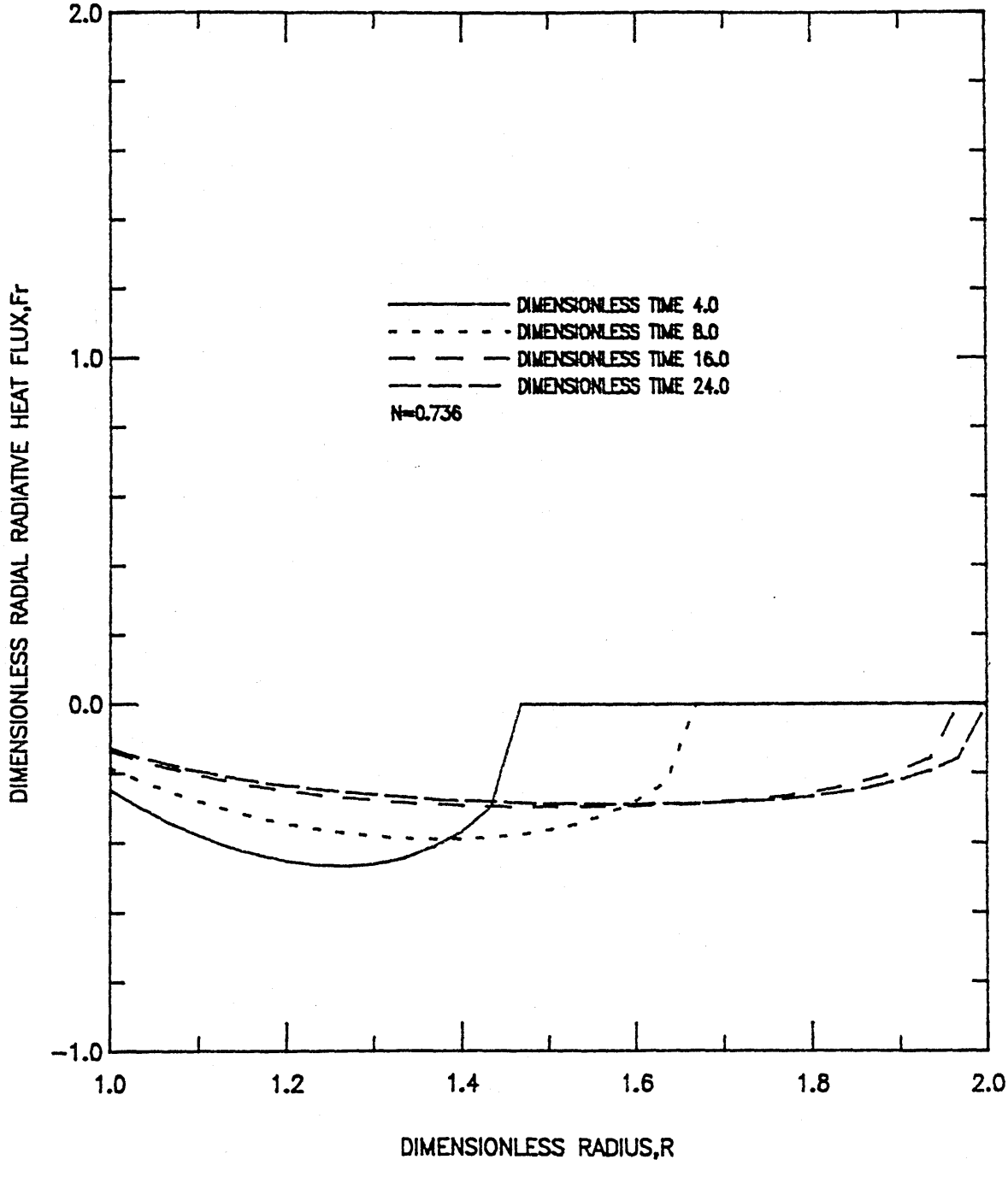

Figure 52 RADIAL RADIATIVE FLUX VS. DIMENSIONLESS RADIUS AT J=N/2

TI/TF=0.5, $\varepsilon w1 = \varepsilon w2 = 1.0$, $\varepsilon w3 = \varepsilon w4 = 1.0$, $a = 4.572$ /m
$\omega = 0.0$, ri/ro=0.5, z/ro=1.0, Hsl=465.2kJ/kg
Ks=8.654W/mK, $\rho = 2803.2 kg/m^3$, $\alpha s = 0.0307 m^2/hr$

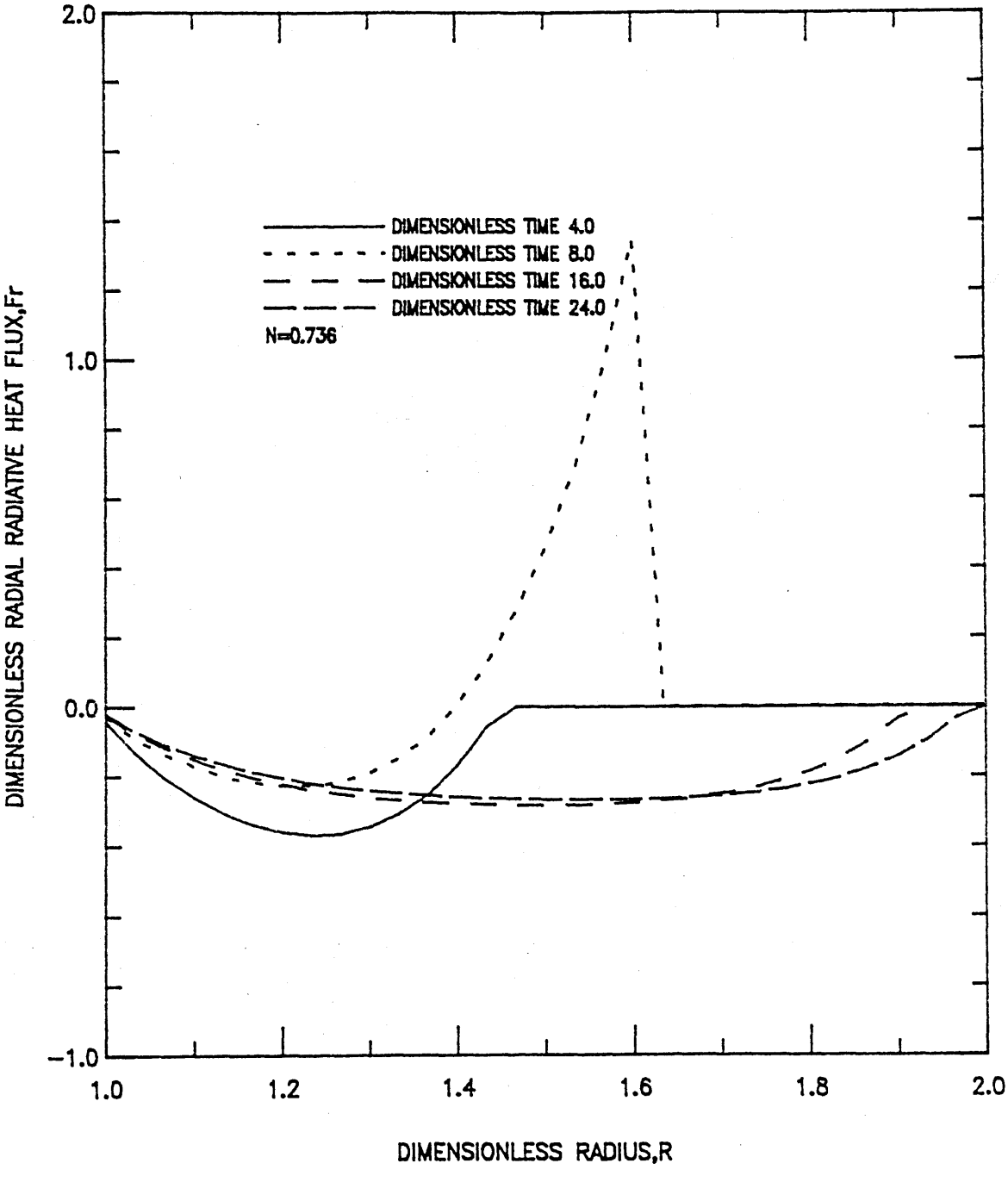

Figure 53 RADIAL RADIATIVE FLUX VS. DIMENSIONLESS RADIUS AT J=N/2

TI/TF=0.5, εw1= εw2=0.2, εw3= εw4=0.2,a=4.572 /m
ω=0.0,ri/ro=0.5,z/ro=1.0,Hsl=465.2kJ/kg
Ks=8.654W/mK, ρ=2803.2kg/m^3, αs=0.0307m^2/hr

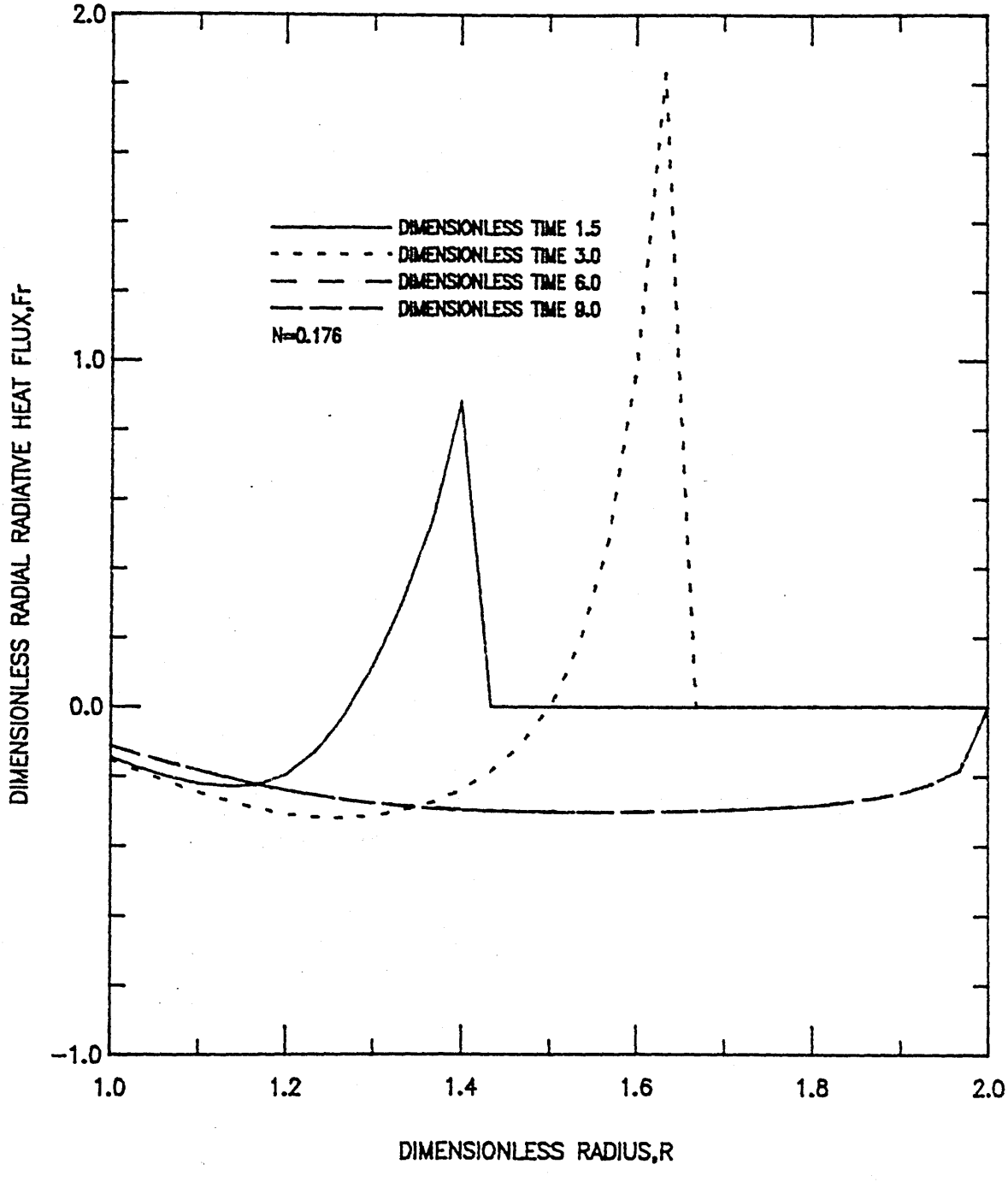

Figure 54 RADIAL RADIATIVE FLUX VS. DIMENSIONLESS RADIUS AT J=N/2

TI/TF=0.286, εw1= εw2=1.0, εw3= εw4=1.0,a=4.572 /m
ω =0.0,ri/ro=0.5,z/ro=1.0,Hsl=465.2kJ/kg
Ks=8.654W/mK, ρ=2803.2kg/m^3, αs=0.0307m^2/hr

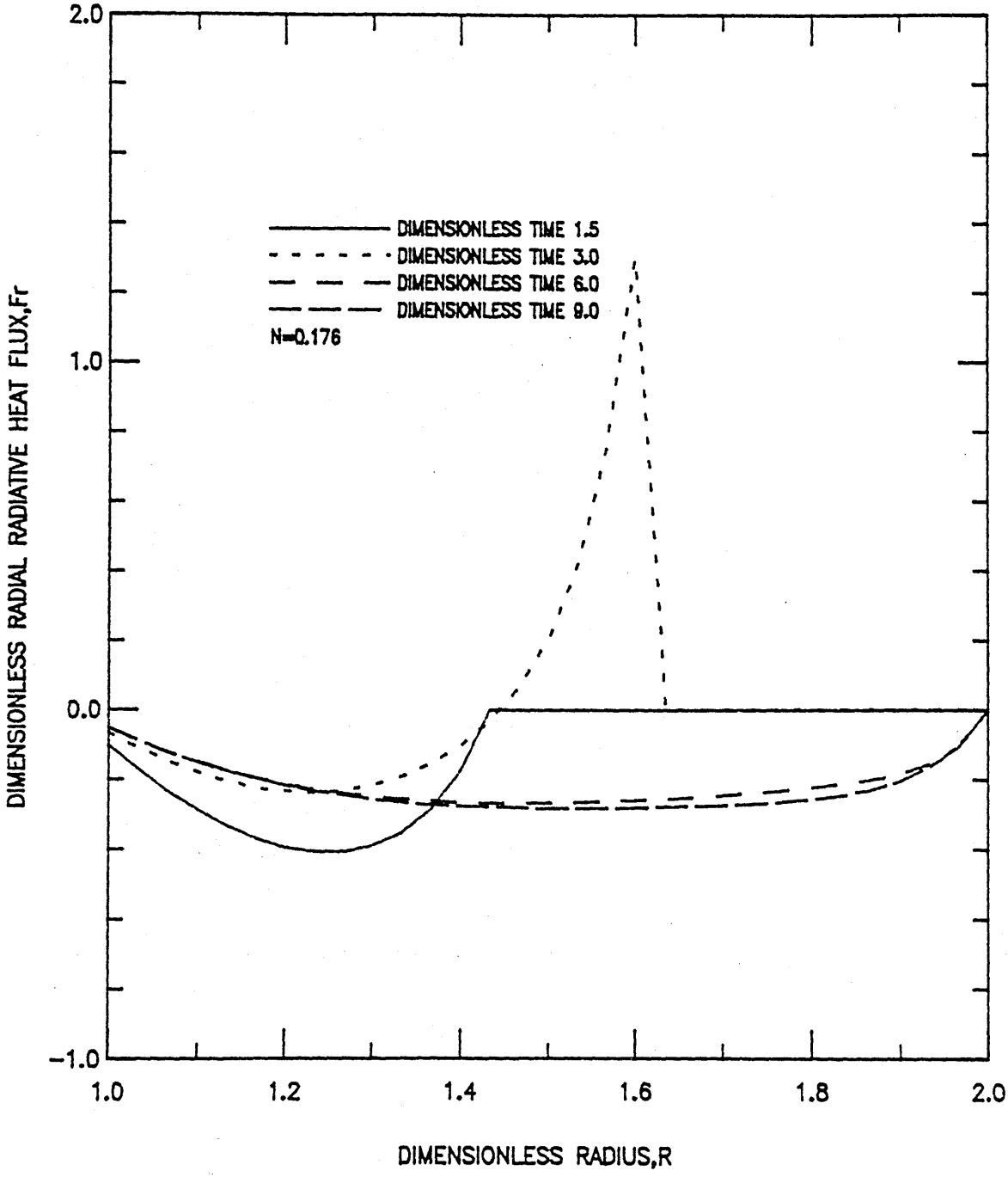

Figure 55 RADIAL RADIATIVE FLUX VS. DIMENSIONLESS RADIUS AT J=N/2

TI/TF=0.286, εw1= εw2=0.5, εw3= εw4=0.5,a=4.572 /m
ω=0.0,ri/ro=0.5,z/ro=1.0,Hsl=465.2kJ/kg
Ks=8.654W/mK, ρ=2803.2kg/m^3, αs=0.0307m^2/hr

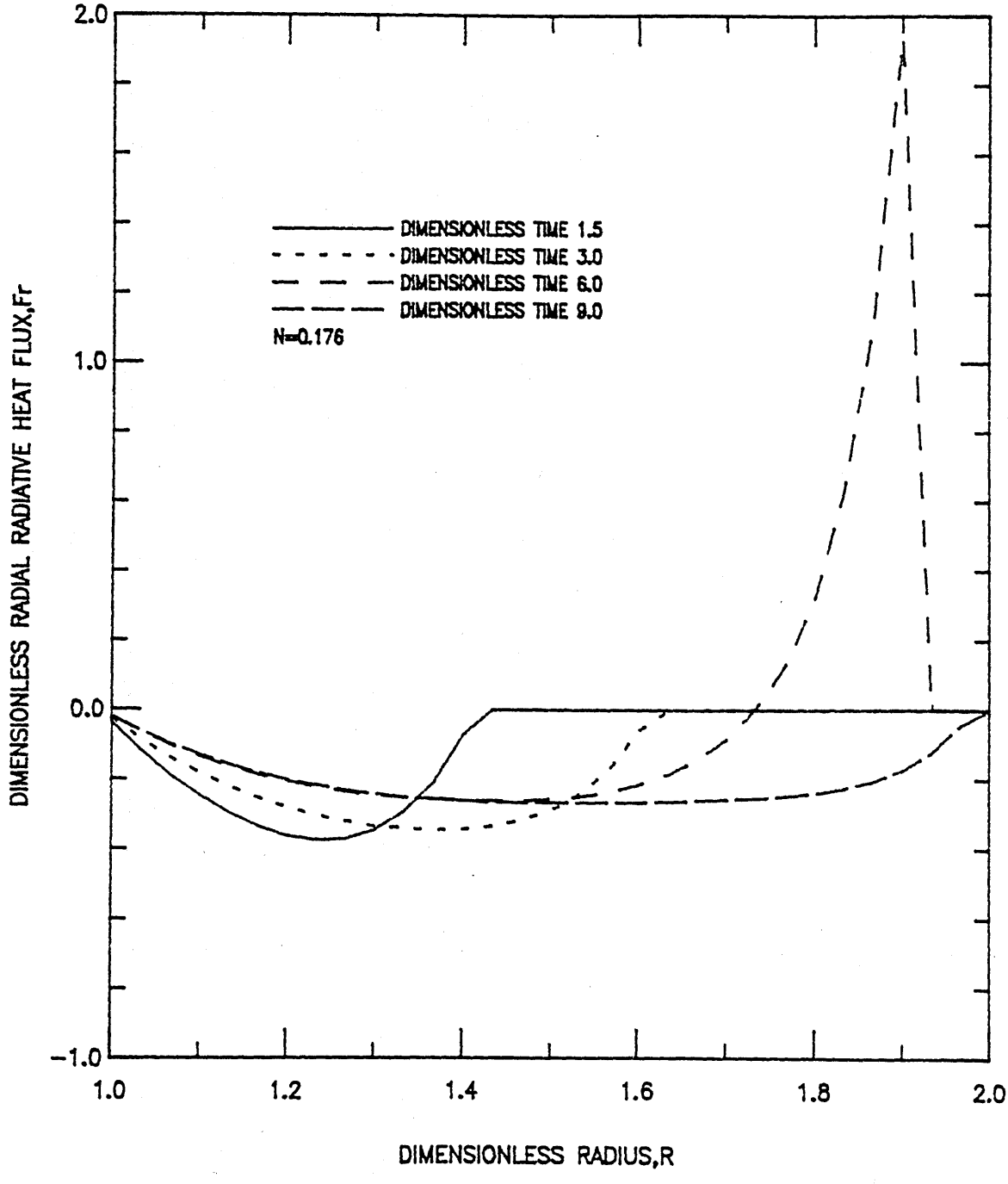

Figure 56 RADIAL RADIATIVE FLUX VS. DIMENSIONLESS RADIUS AT J=N/2

TI/TF=0.286, εw1= εw2=0.2, εw3= εw4=0.2,a=4.572 /m
ω=0.0,ri/ro=0.5,z/ro=1.0,Hsl=465.2kJ/kg
Ks=8.654W/mK, ρ=2803.2kg/m^3, αs=0.0307m^2/hr

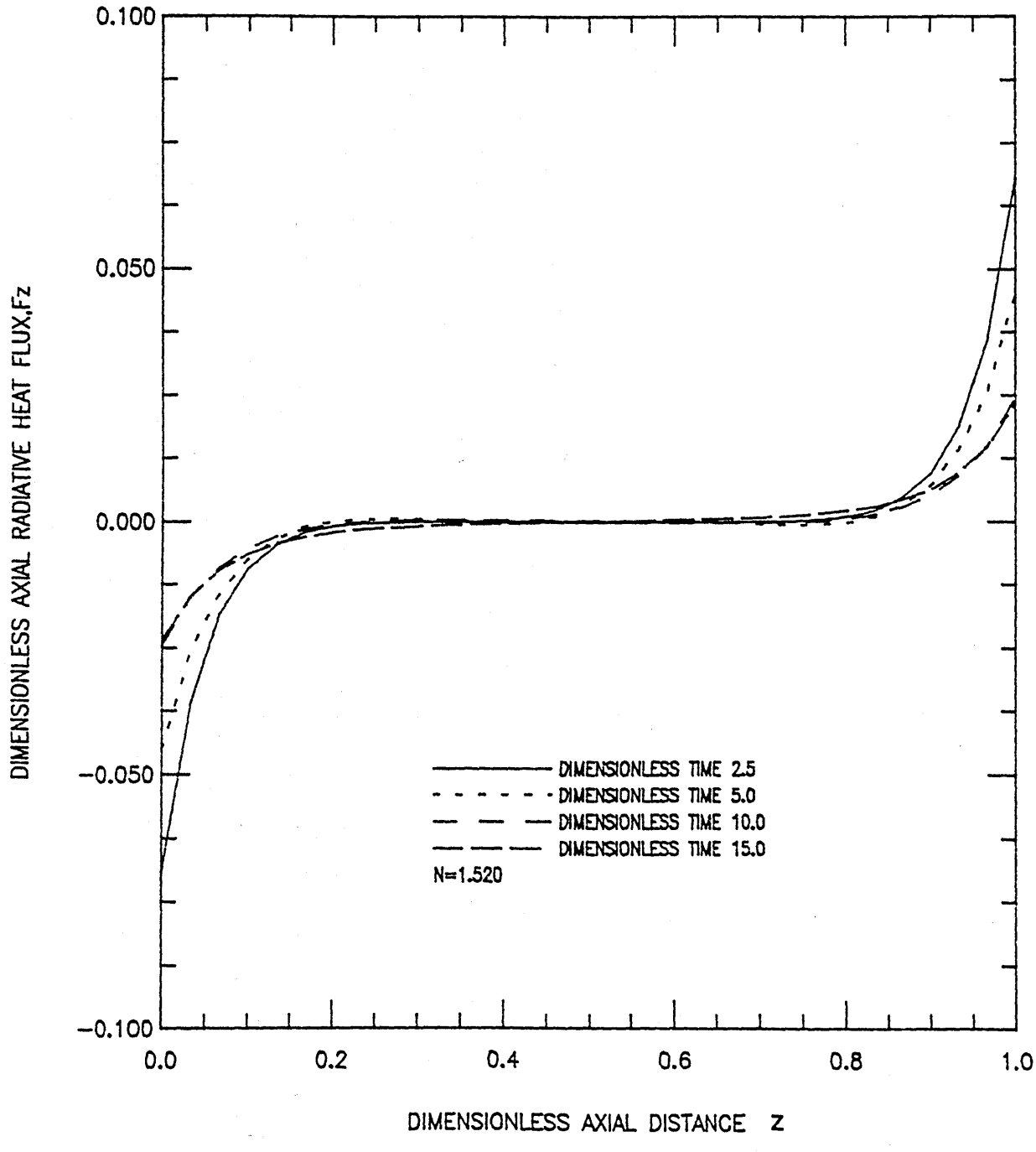

Figure 57 AXIAL RADIATIVE FLUX VS. DIMENSIONLESS AXIAL DISTANCE AT I=SLI/2

TI/TF=0.5, εw1= εw2=1.0, εw3= εw4=1.0,a=4.572 /m
ω =0.5,ri/ro=0.5,z/ro=1.0,Hsl=465.2kJ/kg
Ks=17.307W/mK, ρ=2803.2kg/m^3, αs=0.0307m^2/hr

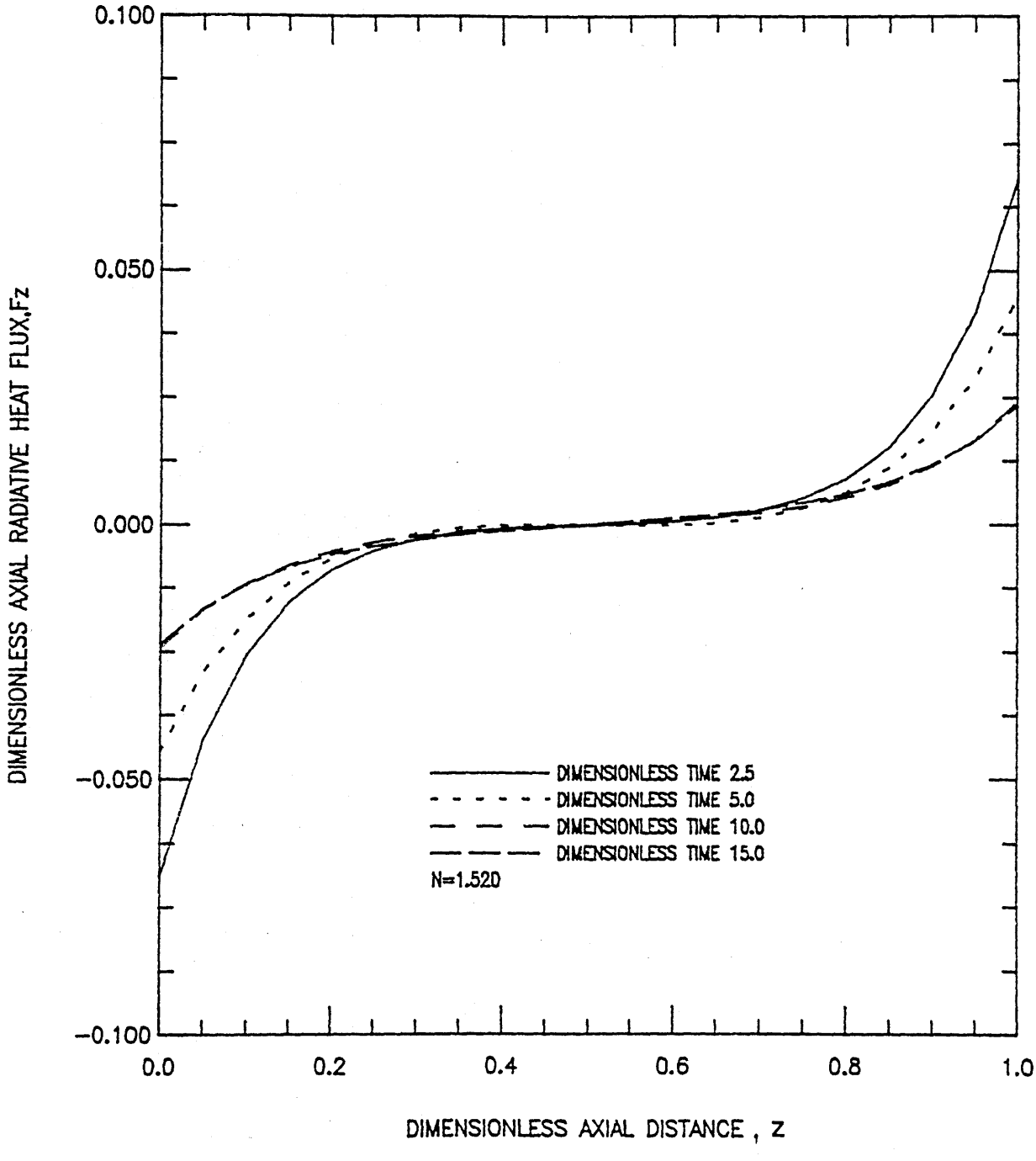

Figure 58 AXIAL RADIATIVE FLUX VS. DIMENSIONLESS AXIAL DISTANCE AT I=SLI/2

TI/TF=0.5, $\varepsilon w1 = \varepsilon w2 = 1.0$, $\varepsilon w3 = \varepsilon w4 = 1.0$, $a = 4.572$ /m
$\omega = 0.5$, $ri/ro = 0.5$, $z/ro = 0.5$, $Hsl = 465.2$ kJ/kg
$Ks = 17.307$ W/mK, $\rho = 2803.2$ kg/m^3, $\alpha s = 0.0307$ m^2 /hr

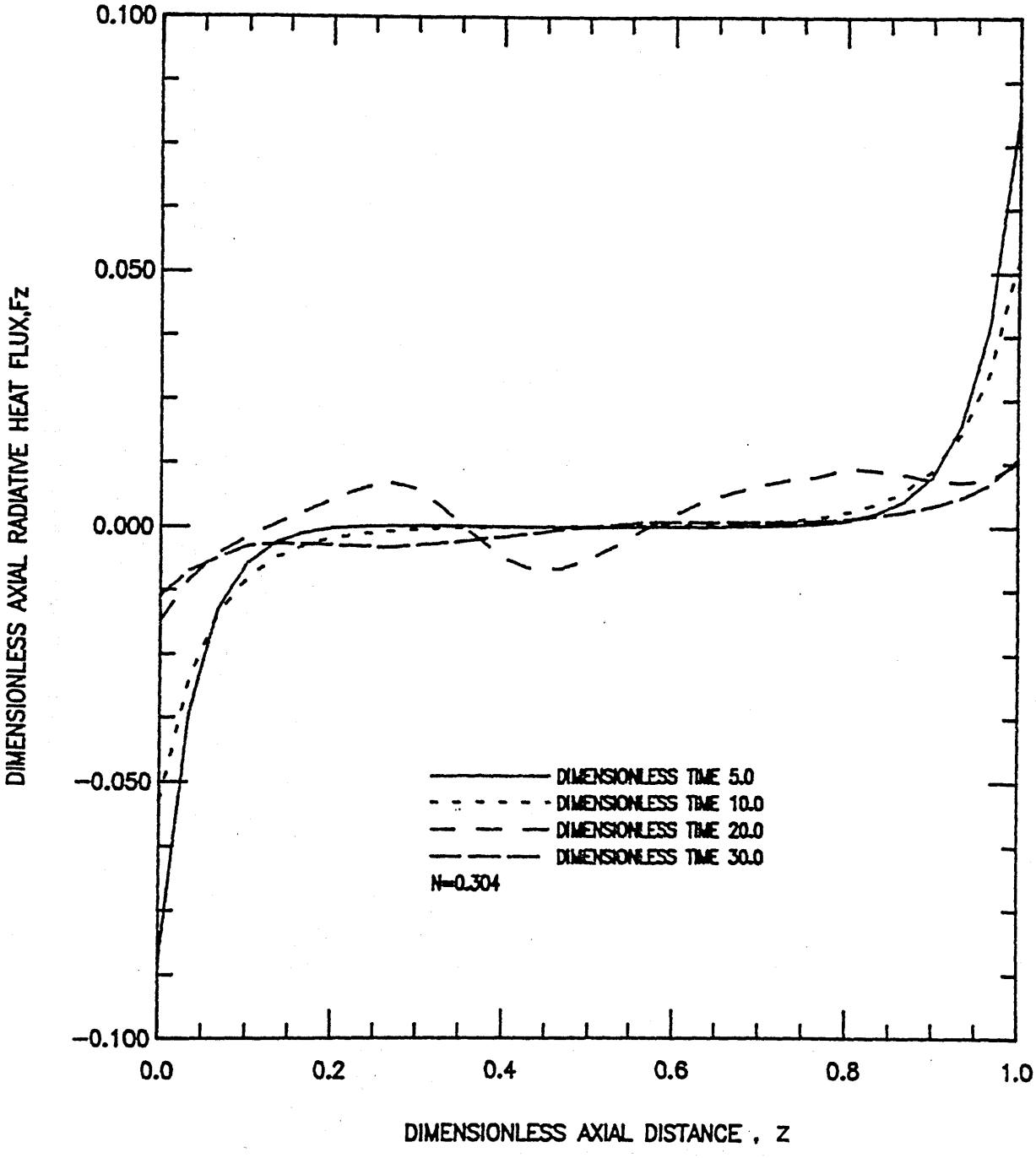

Figure 59 AXIAL RADIATIVE FLUX VS. DIMENSIONLESS AXIAL DISTANCE AT I=SLI/2

TI/TF=0.5, $\varepsilon w1 = \varepsilon w2 = 1.0$, $\varepsilon w3 = \varepsilon w4 = 1.0$, a=4.572 /m
ω =0.5, ri/ro=0.5, z/ro=1.0, Hsl=465.2kJ/kg
Ks=3.462W/mK, ρ=2803.2kg/m^3, αs=0.0307m^2/hr

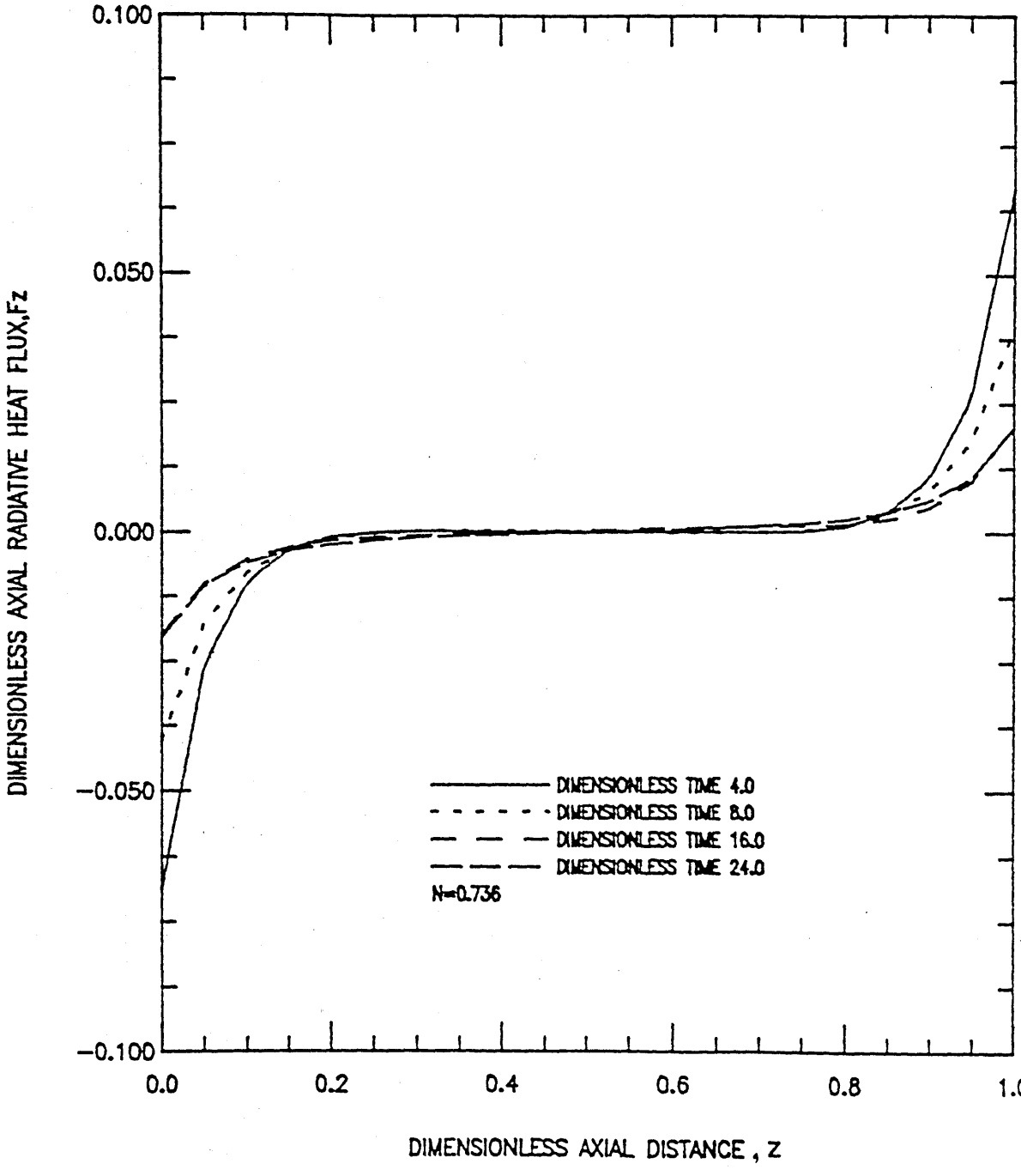

Figure 60 AXIAL RADIATIVE FLUX VS. DIMENSIONLESS AXIAL DISTANCE AT I=SLI/2

TI/TF=0.5, $\varepsilon w1 = \varepsilon w2 = 1.0$, $\varepsilon w3 = \varepsilon w4 = 1.0$, $a = 4.572$ /m
$\omega = 0.0$, ri/ro=0.5, z/ro=1.0, Hsl=465.2kJ/kg
Ks=8.654W/mK, $\rho = 2803.2 kg/m^3$, $\alpha s = 0.0307 m^2/hr$

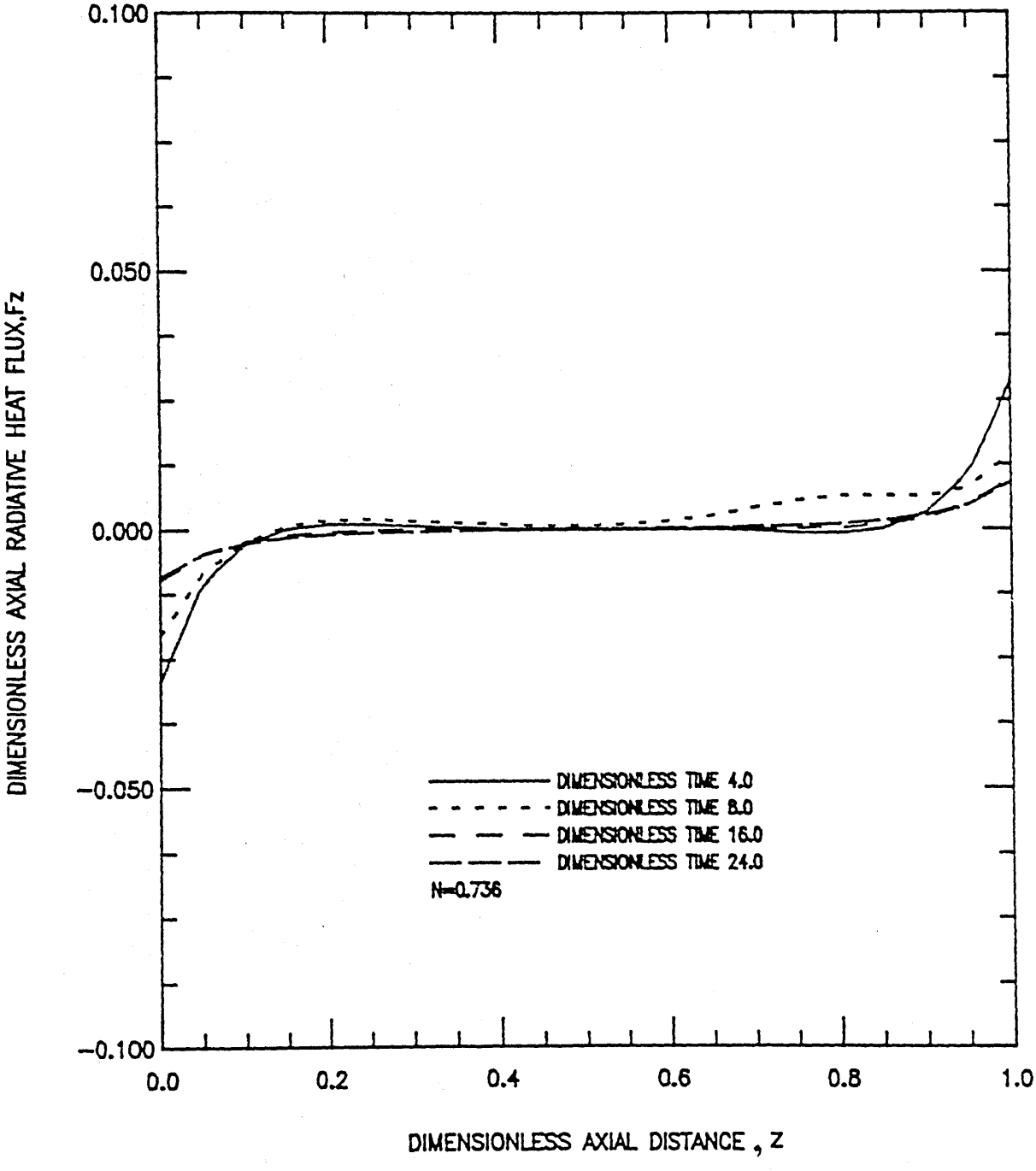

Figure 61 AXIAL RADIATIVE FLUX VS. DIMENSIONLESS AXIAL DISTANCE AT l=SLl/2

Tl/TF=0.5, εw1= εw2=0.5, εw3= εw4=0.5,a=4.572 /m
ω =0.0,ri/ro=0.5,z/ro=1.0,Hsl=465.2kJ/kg
Ks=8.654W/mK, ρ =2803.2kg/m^3, αs=0.0307m^2/hr

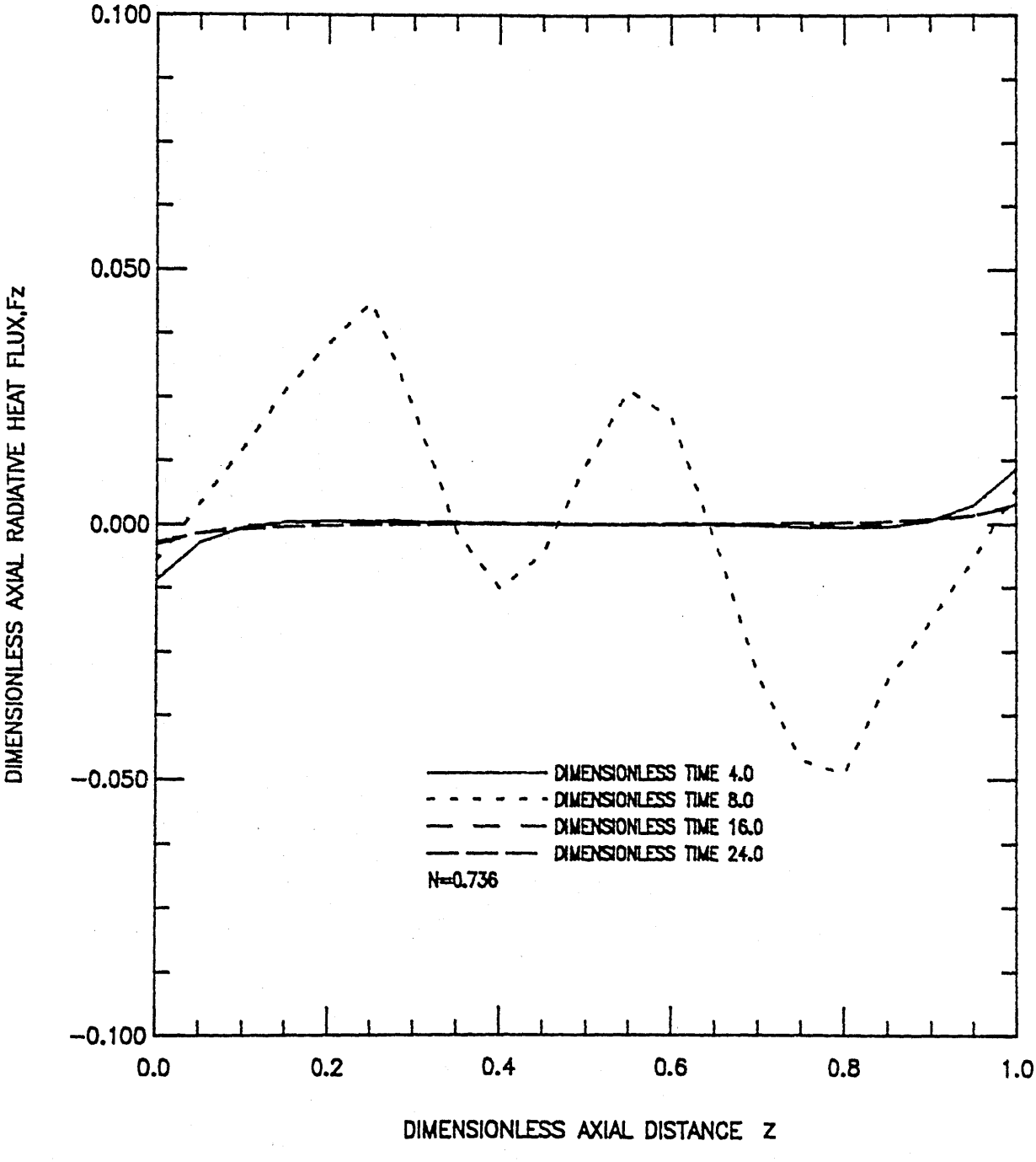

Figure 62 AXIAL RADIATIVE FLUX VS. DIMENSIONLESS AXIAL DISTANCE AT I=SLI/2

TI/TF=0.5, $\varepsilon w1 = \varepsilon w2 = 0.2$, $\varepsilon w3 = \varepsilon w4 = 0.2$, $a = 4.572$ /m
$\omega = 0.0$, ri/ro=0.5, z/ro=1.0, Hsl=465.2kJ/kg
Ks=8.654W/mK, $\rho = 2803.2 kg/m^3$, $\alpha s = 0.0307 m^2/hr$

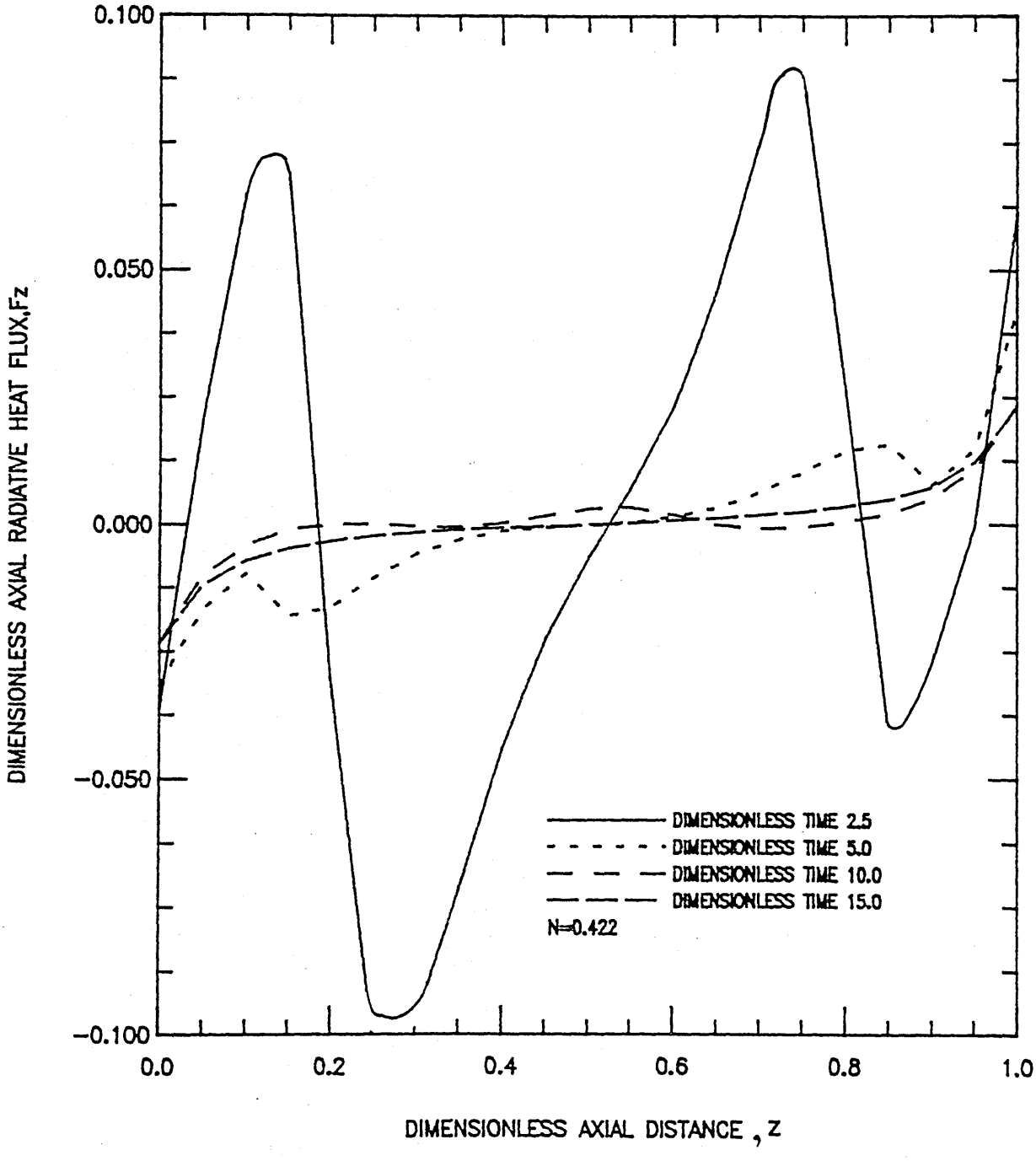

Figure 63 AXIAL RADIATIVE FLUX VS. DIMENSIONLESS AXIAL DISTANCE AT I=SLI/2

TI/TF=0.4, εw1= εw2=1.0, εw3= εw4=1.0,a=4.572 /m
ω =0.0,ri/ro=0.5,z/ro=1.0,Hsl=465.2kJ/kg
Ks=8.654W/mK, ρ =2803.2kg/m^3, αs=0.0307m^2/hr

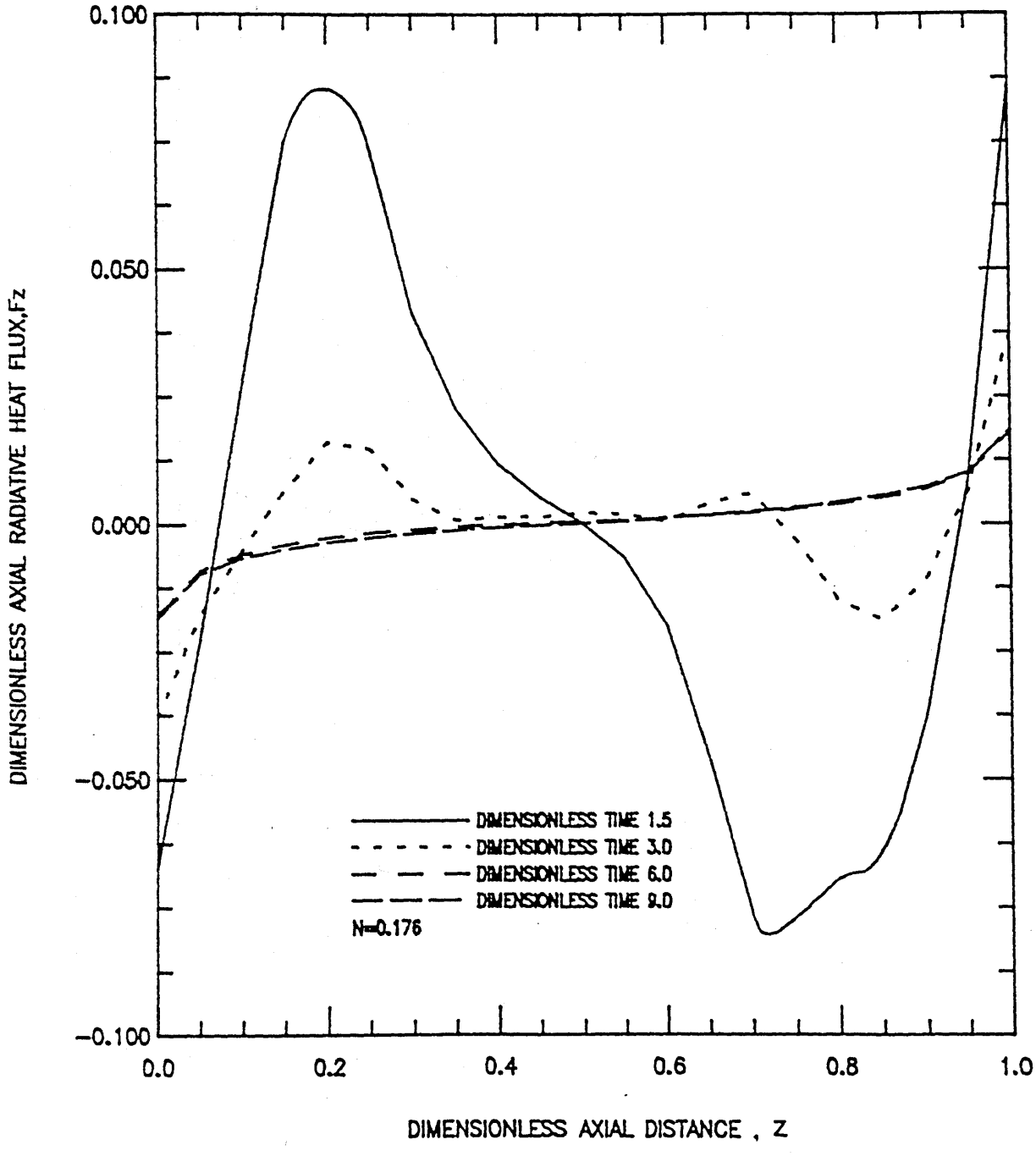

Figure 64 AXIAL RADIATIVE FLUX VS. DIMENSIONLESS AXIAL DISTANCE AT I=SLI/2

Tl/TF=0.286, εw1= εw2=1.0, εw3= εw4=1.0,a=4.572 /m
ω=0.0,ri/ro=0.5,z/ro=1.0,Hsl=465.2kJ/kg
Ks=8.654W/mK, ρ=2803.2kg/m^3, αs=0.0307m^2/hr

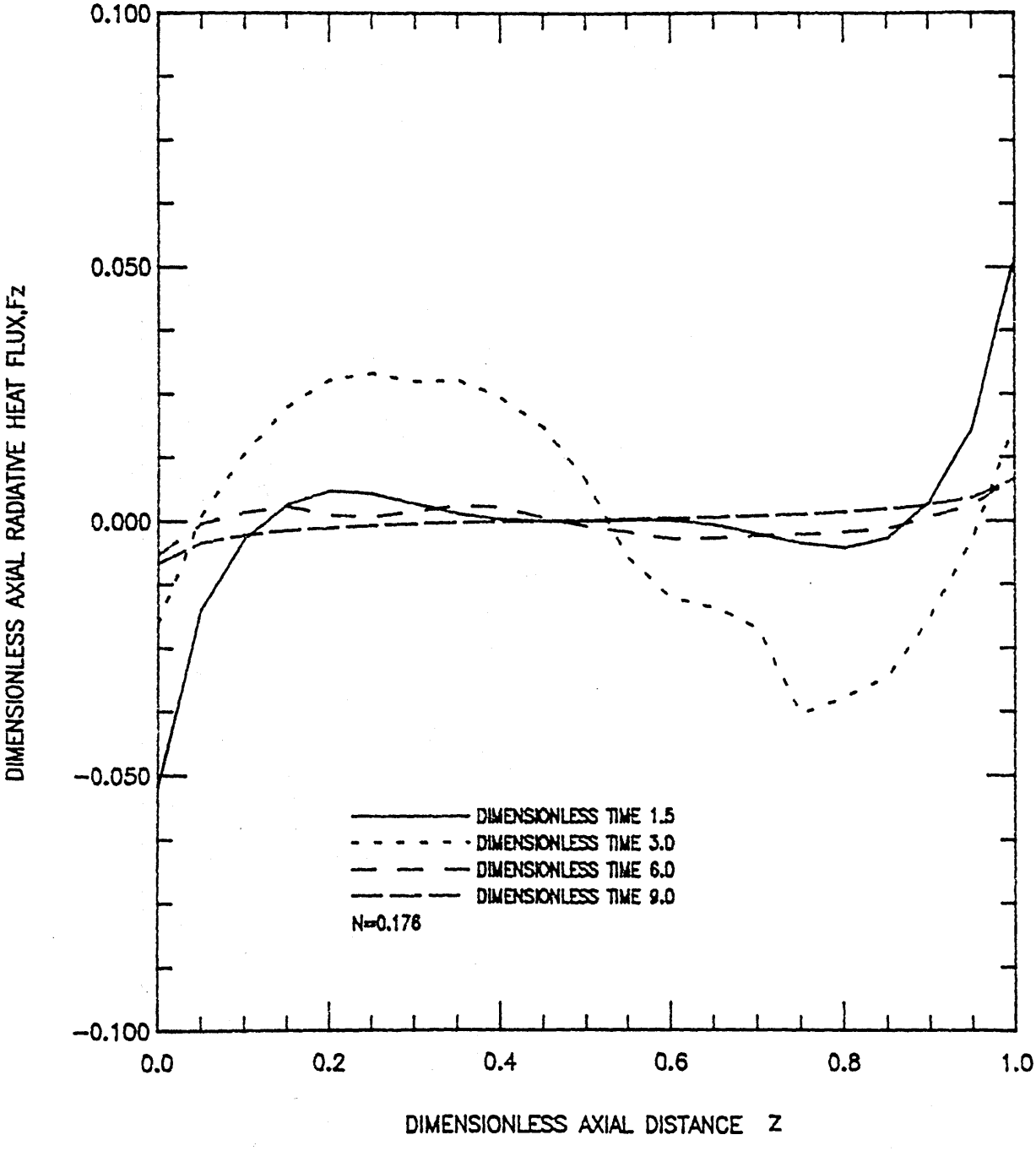

Figure 65 AXIAL RADIATIVE FLUX VS. DIMENSIONLESS AXIAL DISTANCE AT I=SLI/2

TI/TF=0.286, $\varepsilon w1 = \varepsilon w2 = 0.5$, $\varepsilon w3 = \varepsilon w4 = 0.5$, $a = 4.572$ /m
$\omega = 0.0$, $ri/ro = 0.5$, $z/ro = 1.0$, $Hsl = 465.2 kJ/kg$
$Ks = 8.654 W/mK$, $\rho = 2803.2 kg/m^3$, $\alpha s = 0.0307 m^2/hr$

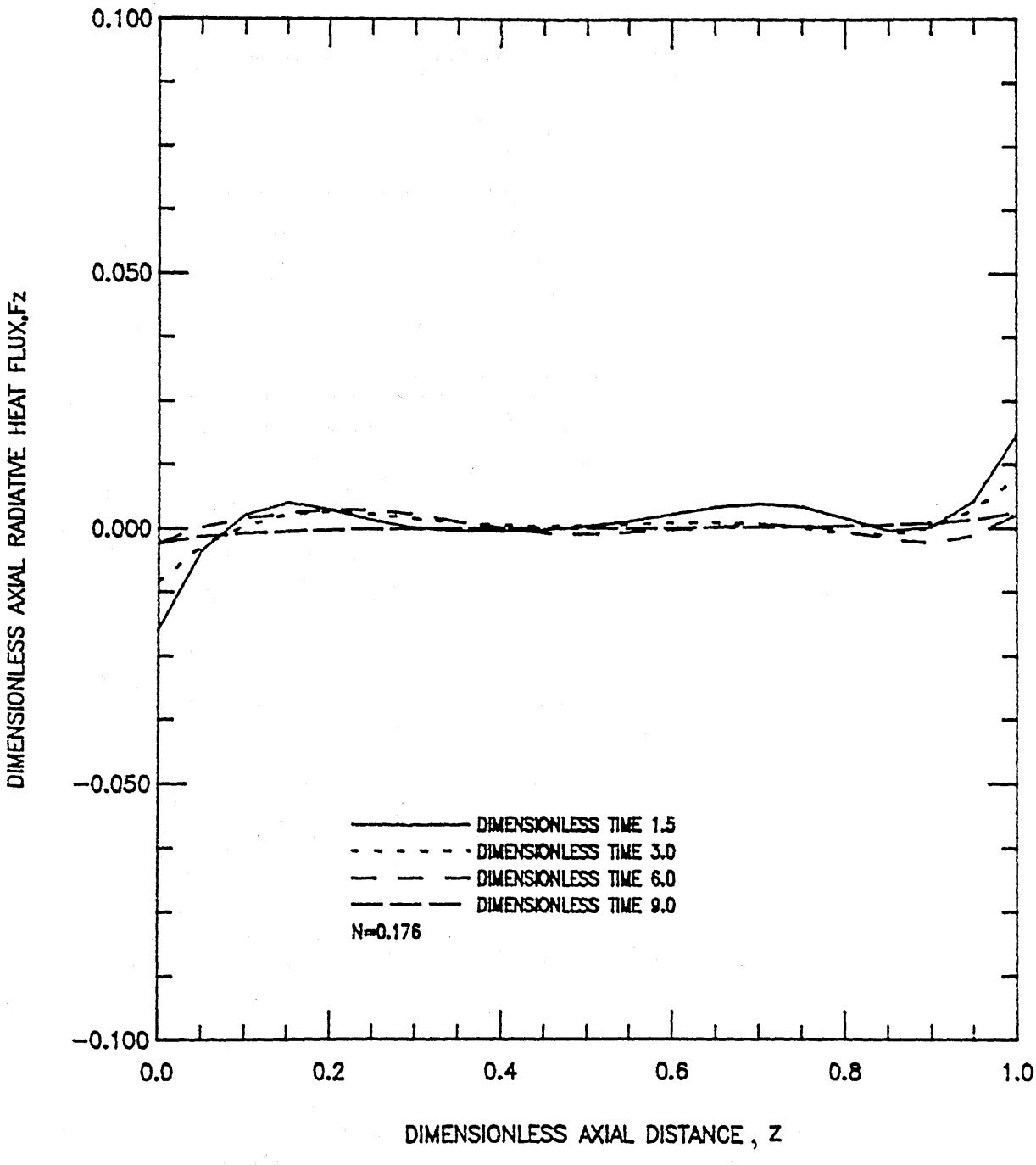

Figure 66 AXIAL RADIATIVE FLUX VS. DIMENSIONLESS AXIAL DISTANCE AT l=SLl/2

Tl/TF=0.286, εw1= ε w2=0.2, εw3= εw4=0.2,a=4.572 /m
ω=0.0,ri/ro=0.5,z/ro=1.0,Hsl=465.2kJ/kg
Ks=8.654W/mK, ρ=2803.2kg/m ^{3}, αs=0.0307m ^{2}/hr

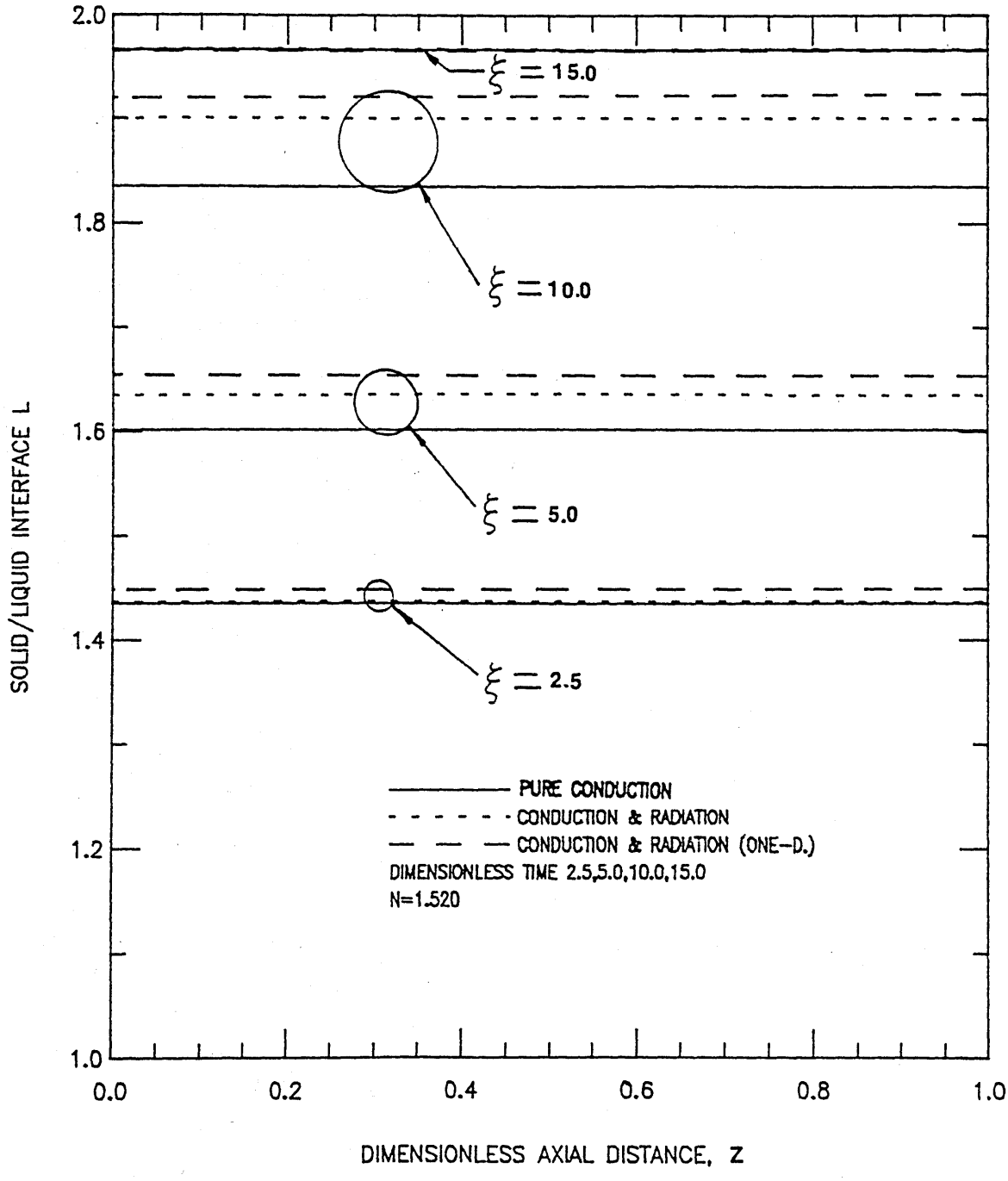

Figure 67 SOLID/LIQUID INTERFACE VS. DIMENSIONLESS AXIAL DISTANCE

Ti/Tf=0.5, εw1= εw2=1.0, εw3= εw4=1.0,a=4.572 /m
ω =0.5,ri/ro=0.5,z/ro=1.0,Hsl=465.2kJ/kg
Ks=17.307W/mK, ρ=2803.2kg/m^3, αs=0.0307m^2/hr

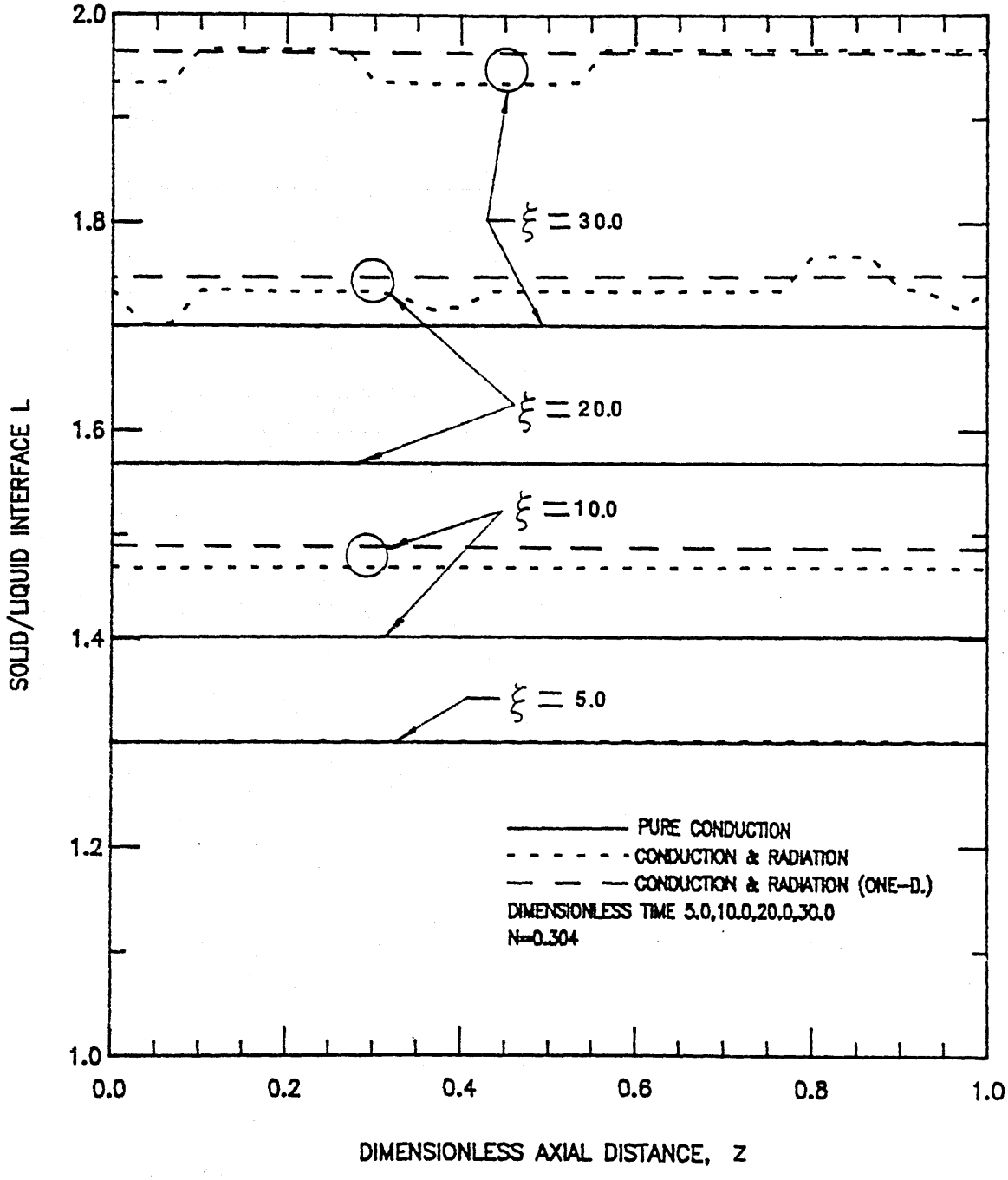

Figure 68 SOLID/LIQUID INTERFACE VS. DIMENSIONLESS AXIAL DISTANCE

$T_I/T_F=0.5$, $\varepsilon_{w1}=\varepsilon_{w2}=1.0$, $\varepsilon_{w3}=\varepsilon_{w4}=1.0$, $a=4.572$ /m
$\omega=0.5$, $r_i/r_o=0.5$, $z/r_o=1.0$, $H_{sl}=465.2$kJ/kg
$K_s=3.462$W/mK, $\rho=2803.2$kg/m^3, $\alpha_s=0.0307$m^2/hr

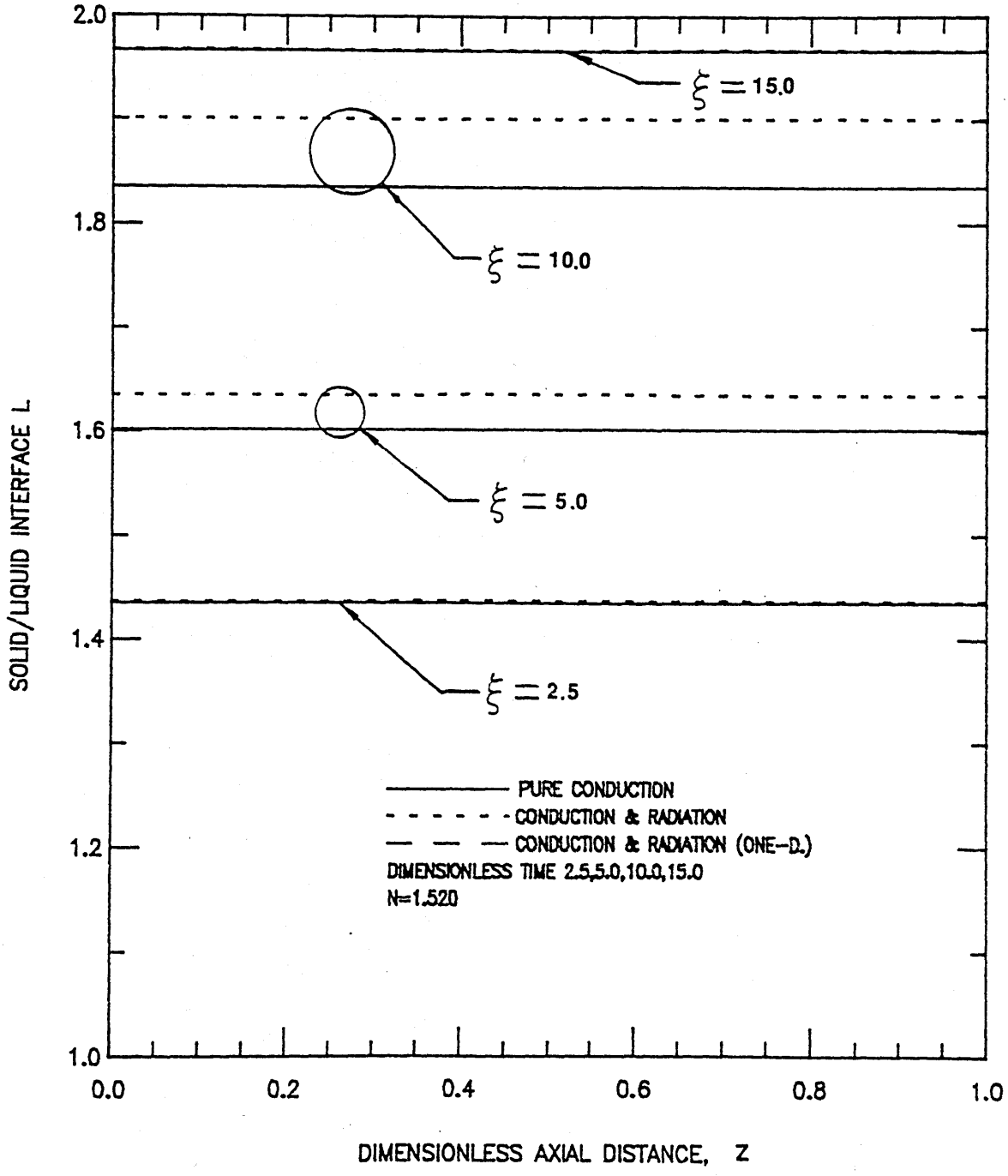

Figure 69 SOLID/LIQUID INTERFACE VS. DIMENSIONLESS AXIAL DISTANCE

$T_I/T_F=0.5$, $\varepsilon_{w1}=\varepsilon_{w2}=1.0$, $\varepsilon_{w3}=\varepsilon_{w4}=1.0$, $a=4.572$ /m
$\omega=0.5$, $r_i/r_o=0.5$, $z/r_o=0.5$, $H_{sl}=465.2$kJ/kg
$K_s=17.307$W/mK, $\rho=2803.2$kg/m^3, $\alpha_s=0.0307$m^2/hr

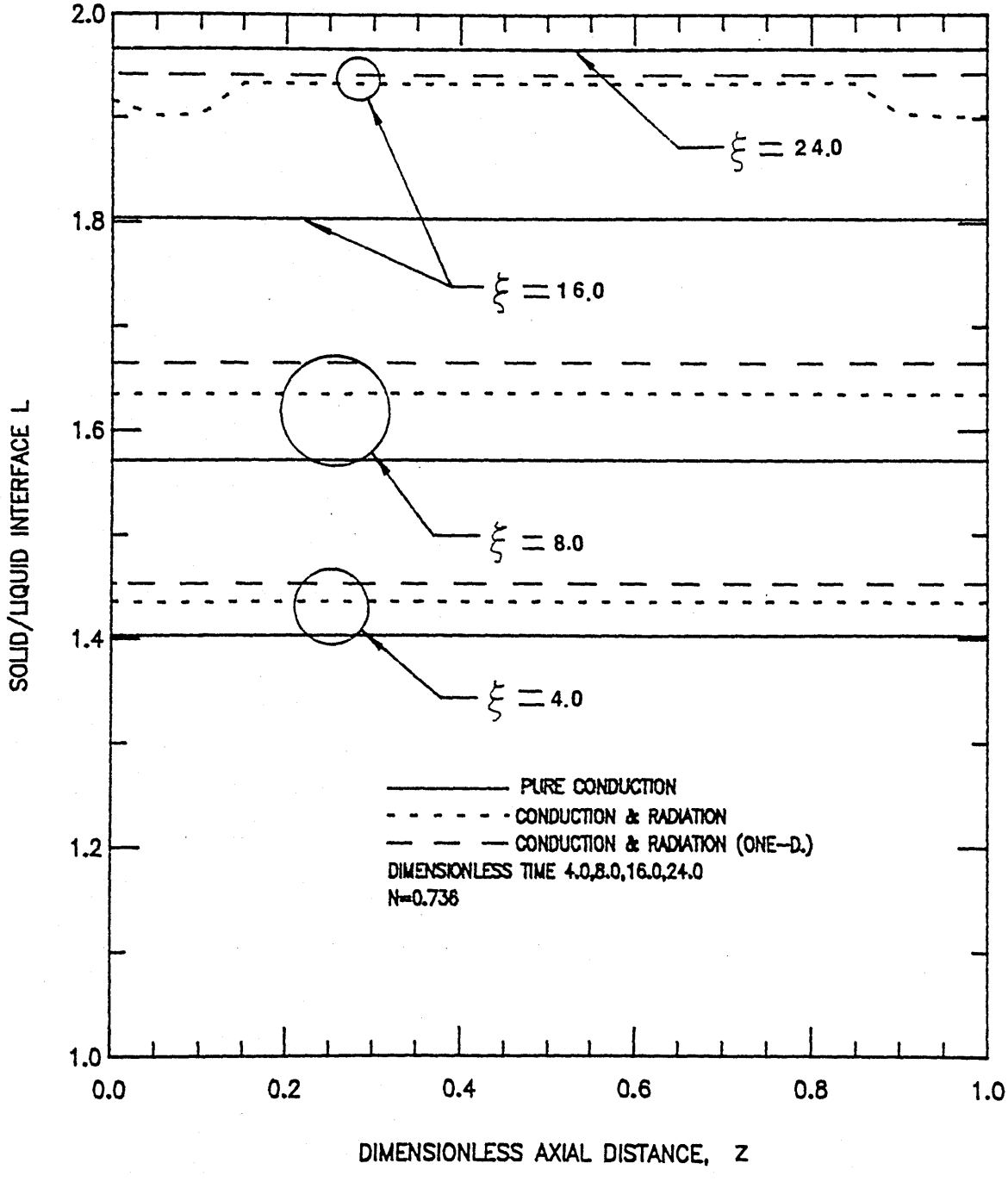

Figure 70 SOLID/LIQUID INTERFACE VS. DIMENSIONLESS AXIAL DISTANCE

TI/TF=0.5, $\varepsilon w1 = \varepsilon w2 = 1.0$, $\varepsilon w3 = \varepsilon w4 = 1.0$, $a = 4.572$ /m
$\omega = 0.0$, ri/ro=0.5, z/ro=1.0, Hsl=465.2kJ/kg
Ks=8.654W/mK, $\rho = 2803.2 kg/m^3$, $\alpha s = 0.0307 m^2/hr$

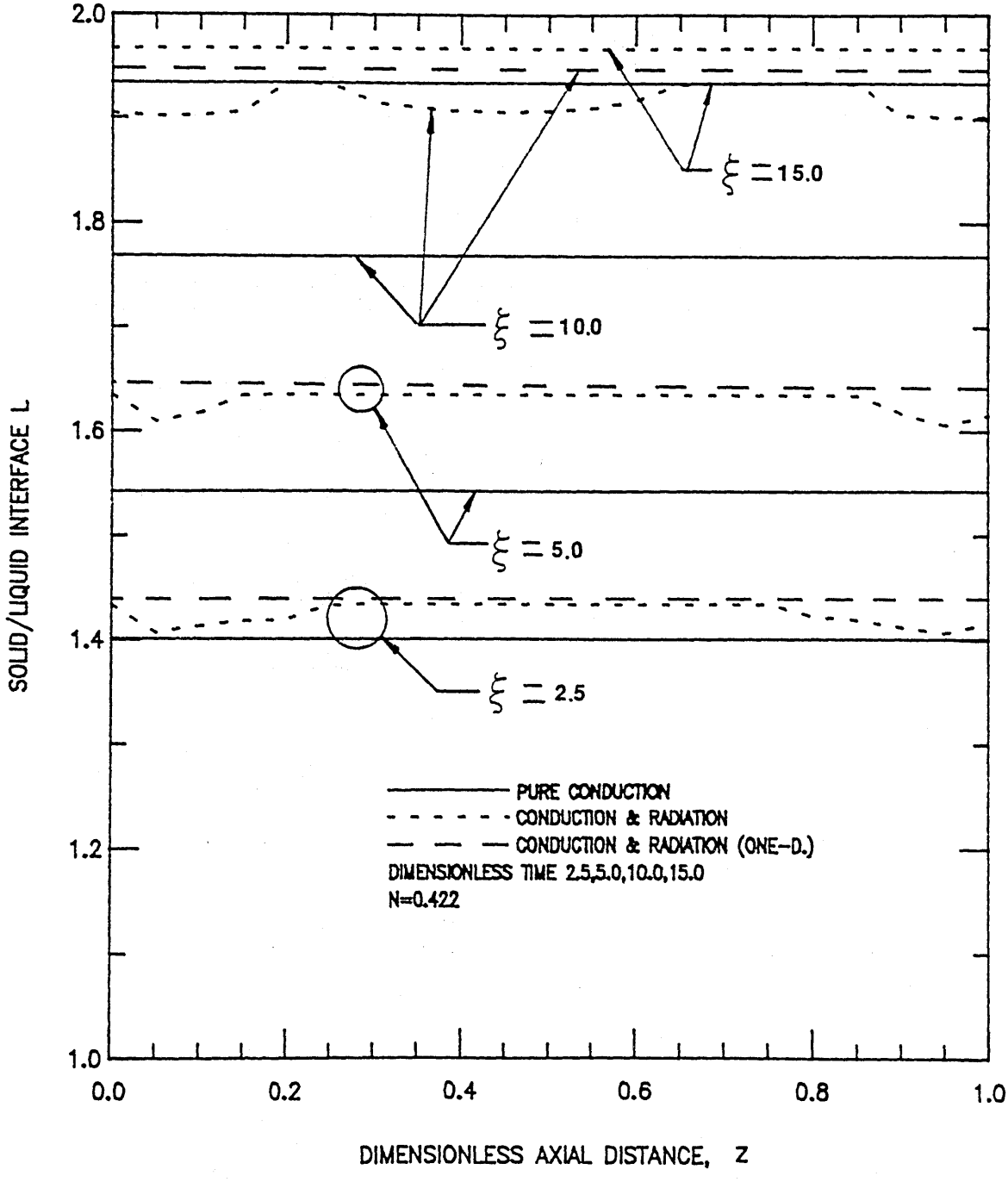

Figure 71 SOLID/LIQUID INTERFACE VS. DIMENSIONLESS AXIAL DISTANCE

TI/TF=0.4, εw1= εw2=1.0, εw3= εw4=1.0,a=4.572 /m
ω=0.0,ri/ro=0.5,z/ro=1.0,Hsl=465.2kJ/kg
Ks=8.654W/mK, ρ=2803.2kg/m^3, αs=0.0307m^2/hr

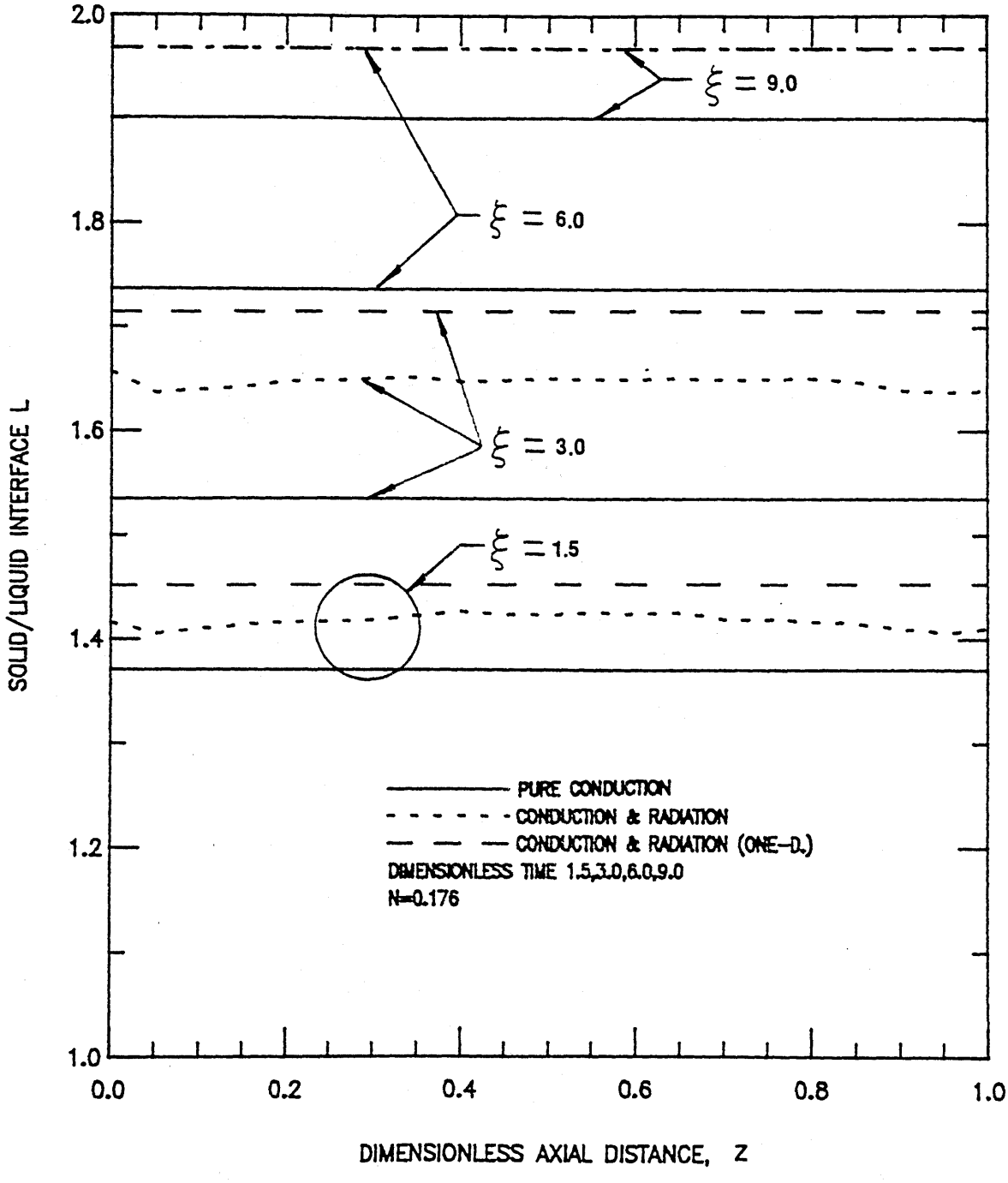

Figure 72 SOLID/LIQUID INTERFACE VS. DIMENSIONLESS AXIAL DISTANCE

Ti/TF=0.286, εw1= εw2=1.0, εw3= εw4=1.0,a=4.572 /m
ω=0.0,ri/ro=0.5,z/ro=1.0,Hsl=465.2kJ/kg
Ks=8.654W/mK, ρ=2803.2kg/m^3, αs=0.0307m^2/hr

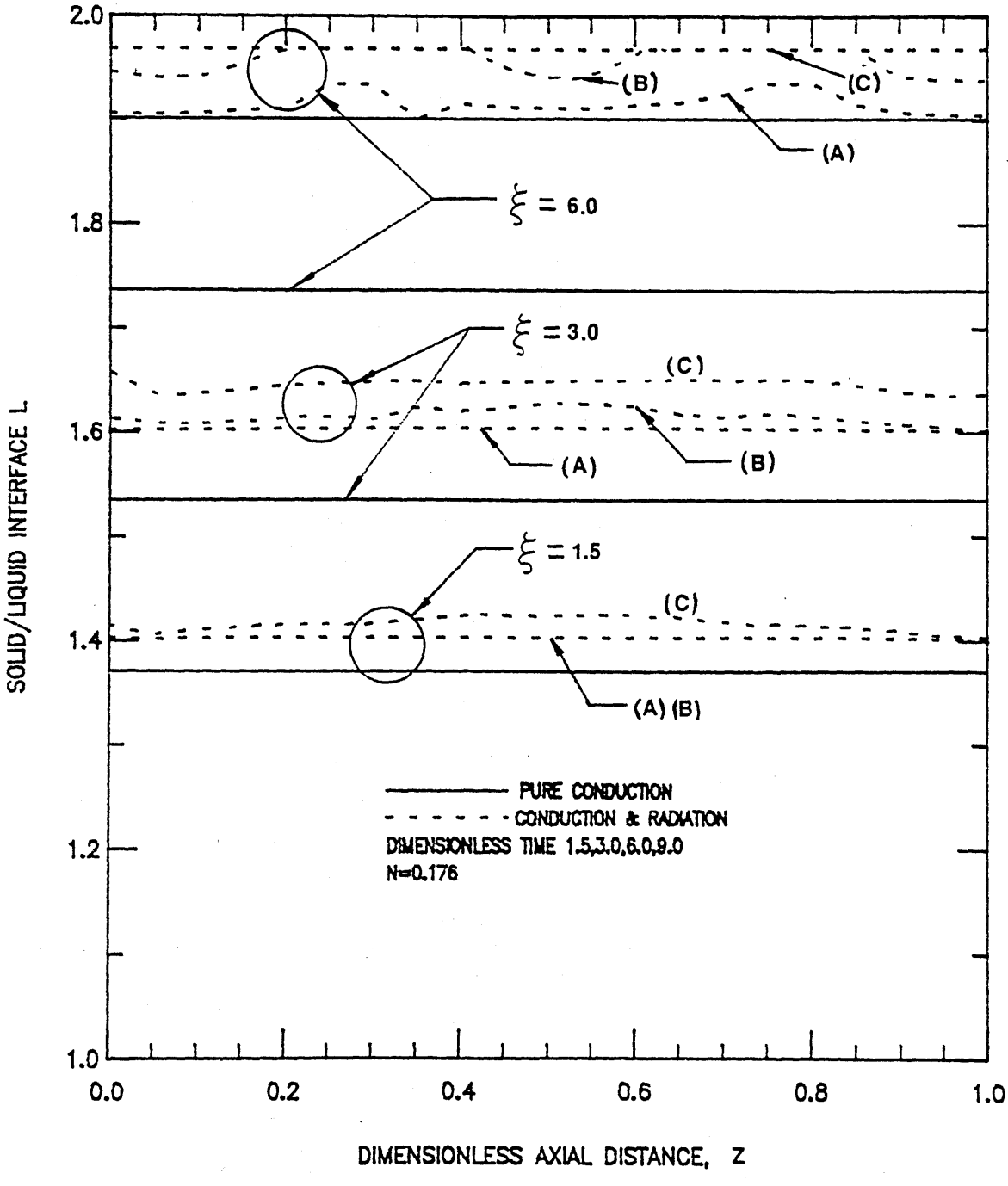

Figure 73 SOLID/LIQUID INTERFACE VS. DIMENSIONLESS AXIAL DISTANCE

TI/TF=0.5, $\epsilon w1 = \epsilon w2$=0.2(A),0.5(B),1.0(C),Ks=8.654W/mK
a=4.572 /m, ω=0.0,ri/ro=0.5,z/ro=1.0,Hsl=465.2kJ/kg
$\epsilon w3 = \epsilon w4$=0.2(A),0.5(B),1.0(C), ρ=2803.2kg/m^3, αs=0.0307m^2/hr

APPENDIX A

VERIFICATION OF ENTHALPY MODEL WITH RADIATIVE HEAT FLUX AT INTERFACE

APPENDIX A

VERIFICATION OF ENTHALPY MODEL WITH RADIATIVE HEAT FLUX AT INTERFACE

The equivalence between the enthalpy form and the conventional form of the energy equation for the case of a pure conductive substance with a discrete phase-change temperature has been demonstrated by Shamsundar and Sparrow [14]. The radiative heat flux will be included here to show the same equivalence for a semi-transparent phase change medium. The principle of conservation of energy for an arbitrary control volume was given in Chapter 3, as:

$$\frac{d}{dt}\iiint_{\forall} \rho h d\forall = \iint_{A} K \overrightarrow{\text{grad}}\, T \cdot \vec{n} dA - \iint_{A} \vec{q} \cdot \vec{n} dA \qquad (3.2)$$

Equation (3.2) can be mathematically shown to be equivalent to the convential differential form for a single phase region by simply applying the divergence theorem to the right hand side of it. For the control volume $\forall$ which contains the interface as shown in Figure A-1, the integral on the left side of (3.2) is investigated.

At time t,

$$\int_{\forall} \rho h dV = \int_{\forall_s} (\rho h)_s \, dV + \int_{\forall_\ell} (\rho h)_\ell \, dV$$

$$= \int_{\forall_s} (\rho h)_s \, dV + \int_{\forall_\ell - \delta V} (\rho h)_\ell \, dV + \int_{\delta_V} (\rho h)_\ell \, dV \qquad (A\text{-}1)$$

and at time t + δt,

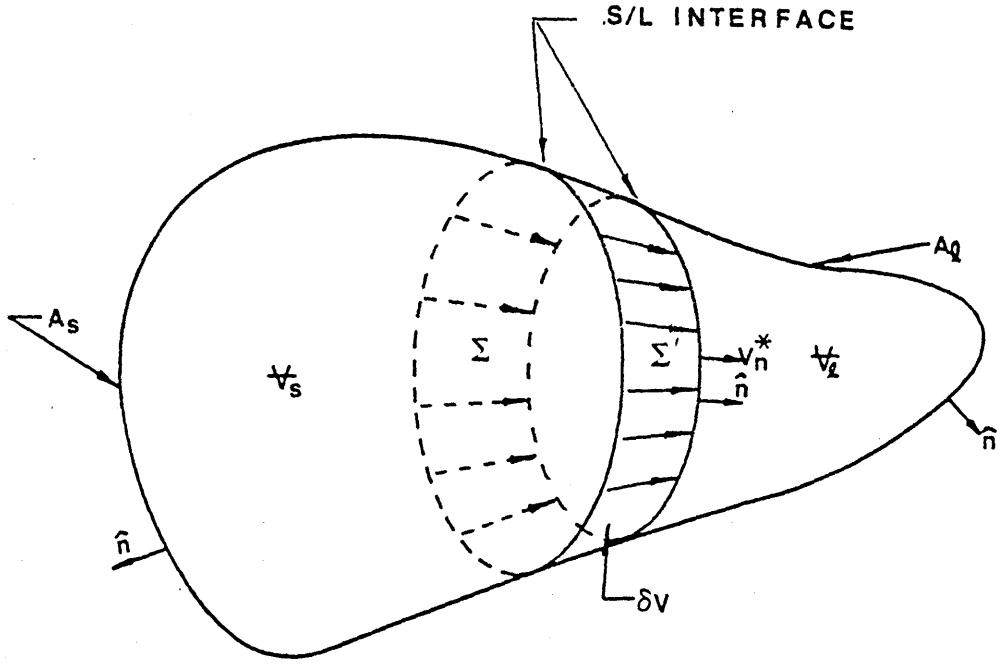

Figure A-1 Control Volume for a Two Phase Region

$$\int_{\forall} \rho h d\forall = \int_{\forall_s + \delta\forall} (\rho h)_s \, d\forall + \int_{\forall_\ell - \delta\forall} (\rho h)_\ell \, d\forall$$

$$= \int_{\forall_s} (\rho h)_s \, d\forall + \int_{\delta_\forall} (\rho h)_s \, d\forall + \int_{\forall_\ell - \delta\forall} (\rho h)_\ell \, d\forall \qquad \text{(A-2)}$$

The left-hand side of Equation (3.2) is obtained by subtracting (A-1) from (A-2), dividing by δt, and taking the limits as δt approaches zero. Remembering that as $\delta t \to 0$, $(\forall_\ell - \delta\forall) \to \forall_\ell$, we get

$$\frac{d}{dt} \int_{\forall} \rho h \, d\forall = \frac{d}{dt} \int_{\forall_s} (\rho h)_s \, d\forall + \frac{d}{dt} \int_{\forall_\ell} (\rho h)_\ell \, d\forall$$

$$+ \lim_{\delta t \to 0} \int_{\delta\forall} \frac{(\rho h)_{s,t+\delta t} - (\rho h)_{\ell,t}}{\delta t} \, d\forall \qquad \text{(A-3)}$$

As $\delta t \to 0$, the ratio $d\forall/\delta t$ at the last term in Equation (A-3) approaches $V_n^* \, d\Sigma$, where V_n^* is the local velocity of the interfacial surface element $d\Sigma$ normal to itself and toward the liquid region. Also, the space which is enclosed by $\delta\forall$ shrinks to the surface Σ, so that the region of integration becomes Σ. Simultaneously, h_s and h_ℓ approach their saturation values h_s^* and h_ℓ^*. Hence,

$$\frac{d}{dt} \int_{\forall} \rho h \, d\forall = \frac{d}{dt} \int_{\forall_s} (\rho h)_s \, d\forall + \frac{d}{dt} \int_{\forall_\ell} (\rho h)_\ell \, d\forall$$

$$+ \int_{\Sigma} \rho (h_s^* - h_\ell^*) \, V_n^* \, d\Sigma \qquad \text{(A-4)}$$

Then the substitution of Equation (3.2) into Equation (A-4) for the respective single phase region yields the equation

$$\frac{d}{dt}\int_{\forall} \rho h \, dV = \int_{A_s+\Sigma} K \overrightarrow{\text{grad}}\, T \cdot \vec{n} \, dA + \int_{A_\ell+\Sigma} K \overrightarrow{\text{grad}}\, T \cdot \vec{n} \, dA$$

$$- \int_{A_s+\Sigma} \vec{q}_r \cdot \vec{n} \, dA - \int_{A_\ell+\Sigma} \vec{q}_r \cdot \vec{n} \, dA - \int_{\Sigma} \rho hsl \, V_n^* \, d\Sigma \qquad \text{(A-5)}$$

where $hsl = h_s^* - h_\ell^*$ = latent heat of fusion.

For the solid region $\vec{n} = \vec{n}^*$ and for the liquid region $\vec{n} = -\vec{n}^*$, where $\vec{n}^*$ is the local normal to Σ toward the liquid region. Then split up the integrals of Equation (A-5) and recombine them to get

$$\frac{d}{dt}\int_{\forall} \rho h \, dV = \int_{A} K \overrightarrow{\text{grad}}\, T \cdot \vec{n} \, dA - \int_{A} \vec{q}_r \cdot \vec{n} \, dA$$

$$+ \int_{\Sigma} \left[\left(K \frac{\partial T}{\partial n^*}\right)_s - \left(K \frac{\partial T}{\partial n}\right)_\ell - (q_{r,s} - q_{r,\ell}) - \rho hsl \, V_n^* \right] d\Sigma \qquad \text{(A-6)}$$

where A is the sum of integrals over A_s and A_ℓ.

The subtraction of Equation (3.2) from Equation (A-6) produces the conventional interface condition

$$\left(K \frac{\partial T}{\partial n^*}\right)_s - \left(K \frac{\partial T}{\partial n^*}\right)_\ell - (q_{r,s} - q_{r,\ell}) = \rho hsl \, V_n^* \qquad \text{(A-7)}$$

APPENDIX B

BOUNDARY EMPLOYMENT FOR ONE-DIMENSIONAL RADIATIVE FLUX EQUATION

APPENDIX B

BOUNDARY EMPLOYMENT FOR ONE-DIMENSIONAL RADIATIVE FLUX EQUATION

For an infinite gray emitting and absorbing cylindrical medium of inside radium r_I and outside radius r_o illustrated in Figure 3.4, Equation (3.13) is rewritten as

$$q(r) = \frac{4r_o}{r} \left\{ \int_0^{\sin^{-1}(r_I/r_o)} \left[(q^i_{1d}/\pi)\ \varphi_1(r) + (q^i_{2d}/\pi)\ \varphi_2(r) + \varphi_3(r) \right] \cdot \cos\beta^* d\beta^* + \int_{\sin^{-1}(r_I/r_o)}^{\sin^{-1}(r/r_o)} \left[(q^i_{2d}/\pi)\ \psi_2(r) + \psi_3(r) \right] \cos\beta^* d\beta^* \right\} \quad \text{(B-1)}$$

Substitution of Equations (3.14) and (3.15) into Equation (B-1) yields

$$q(r) = \frac{4r_o}{r} \left\{ \int_0^{\sin^{-1}(R_1/R_2)} \left[\left[\varepsilon_1\sigma T_I^4 + (1 - \varepsilon_1)\ q(r_I) \right] /\pi \cdot \varphi_1(r) + \left[\varepsilon_2\sigma T_o^4 + (1 - \varepsilon_2)\ q(r_o)\right] /\pi \cdot \varphi_2(r) + \varphi_3(r) \right] \cdot \cos\beta^* d\beta^* + \int_{\sin^{-1}(r_I/r_o)}^{\sin^{-1}(r/r_o)} \left[\left[\varepsilon_2\sigma T_o^4 + (1 - \varepsilon_2)\ q(r_o)\right] /\pi \cdot \psi_2(r) + \psi_3(r) \right] \cos\beta^* d\beta^* \right\} \quad \text{(B-2)}$$

Equation (B-2) at $r = r_I$ and $r = r_o$ becomes respectively

$$q(r_I) = \frac{4r_o}{r_I} \int_0^{\sin^{-1}(r_I/r_o)} \{ [\, \varepsilon_1 \sigma T_I^4 + (1 - \varepsilon_1)\, q(r_I)\,] \cdot$$

$$\frac{\varphi_1(r_I)}{\pi} + [\, \varepsilon_2 \sigma T_o^4 + (1 - \varepsilon_2)\, q(r_o)\,] \cdot \frac{\varphi_2(r_I)}{\pi} + \varphi_3(r_I) \} \cos\beta^* d\beta^* \qquad \text{(B-3)}$$

and

$$q(r_o) = 4 \{ \int_0^{\sin^{-1}(r_I/r_o)} [\, [\, \varepsilon_1 \sigma T_I^4 + (1 - \varepsilon_1)\, q(r_I)\,] \cdot \frac{\varphi_1(r_o)}{\pi}$$

$$+ [\, \varepsilon_2 \sigma T_o^4 + (1 - \varepsilon_2)\, q(r_o)\,] \cdot \frac{\varphi_2(r_o)}{\pi} + \varphi_3(r_o)\,] \cos\beta^* d\beta^*$$

$$+ \int_{\sin^{-1}(r_I/r_o)}^{\pi/2} [\, [\, \varepsilon_2 \sigma T_o^4 + (1 - \varepsilon_2)\, q(r_o)\,] \cdot \frac{\psi_2(r_o)}{\pi}$$

$$+ \psi_3(r_o)\,] \cos\beta^* d\beta^* \, \} \qquad \text{(B-4)}$$

In order to solve the two Equations (B-3) and (B-4) by an iterative method for two unknowns $q(r_I)$ and $q(r_o)$, $q(r_I)$ may be expressed in terms of $q(r_o)$ and vice versa as

$$q(r_I) = -\, [\, \frac{4(1 - \varepsilon_1)}{\pi} \int_0^{\sin^{-1}(r_I/r_o)} \varphi_1(r_o) \cos\beta^* d\beta^* \,]^{-1}$$

$$\cdot \left[4 \left\{ \int_{0}^{\sin^{-1}(r_I/r_o)} \left[\frac{\varepsilon_1 \sigma T_I^4}{\pi} \varphi_1(r_o) + \left[\varepsilon_2 \sigma T_o^4 \right.\right.\right.\right.$$

$$\left. + (1 - \varepsilon_2)\, q(r_o) \right] \cdot \frac{\varphi_2(r_o)}{\pi} + \varphi_3(r_o) \left. \right] \cos\beta^* d\beta^*$$

$$+ \int_{\sin^{-1}(r_I/r_o)}^{\pi/2} \left[\left[\varepsilon_2 \sigma T_o^4 + (1 - \varepsilon_2)\, q(r_o) \right] \cdot \frac{\psi_2(r_o)}{\pi} \right.$$

$$\left. \left. + \psi_3(r_o) \right] \cos\beta^* d\beta^* \right\} - q(r_o) \left. \right] \tag{B-5}$$

and

$$q(r_o) = - \left[\frac{4r_o}{\pi r_I} (1 - \varepsilon_2) \int_{0}^{\sin^{-1}(r_I/r_o)} \varphi_2(r_I) \cos\beta^* d\beta^* \right] \cdot$$

$$\left[\frac{4r_o}{r_I} \int_{0}^{\sin^{-1}(r_I/r_o)} \left\{ \left[\varepsilon_1 \sigma T_I^4 + (1 - \varepsilon_1)\, q(r_I) \right] \cdot \right.\right.$$

$$\left. \left. \frac{\varphi_1(r_I)}{\pi} + \frac{\varepsilon_2 \sigma T_o^4}{\pi} \varphi_2(r_I) + \varphi_3(r_I) \right\} \cos\beta^* d\beta^* - q(r_I) \right] \tag{B-6}$$

The simultaneous solution of Equations (B-5) and (B-6) gives the local radiative heat flux in Equation (B-2). It may be seen that the employment of this local radiative heat flux in the energy equation, which includes the moving solid/liquid interface, is neither economical nor appropriate for the present investigation.

APPENDIX C

COMPUTER PROGRAM LISTING

ONE-DIMENSIONAL COMPUTER PROGRAM

THIS PROGRAM CALCULATES THE TRANSIENT TEMP. DISTRIBUTION AND ENTHALPY DISTRIBUTIONS IN THE RADIAL DIRECTION ONLY FOR ONE-D CONCENTRIC CYLINDERS IN THE STEFAN PROBLEM WITH CONDUCTION IN WHOLE REGION AND RADIATION IN SOLID REGION. THE LOCATION OF THE S/L INTERFACE, SOLIDIFIED VOLUME, AND HEAT EXTRACTED CAN BE OBTAINED AFTER SOME TIME STEPS. THE ENTHALPY MODEL EQUATION HAS BEEN SOLVED SIMULTANEOUSLY WITH RTE THAT HAS BEEN TRANSFORMED INTO CONVENIENT DIFFERENTIAL EQUATIONS BY USING P-1 APPROXIMATIONS.

DESCRIPTION OF MAIN PARAMETERS

A	=	ABSORPTION COEFFICIENT
BETA	=	EXTINCTION COEFFICIENT
C1,C2	=	CONDUCTIVITY OF MEDIUM
CND	=	CONDUCTIVITY OF SOLID AT FUSION TEMPERATURE
DEN	=	DENSITY OF SOLID AT FUSION TEMPERATURE
DIF	=	DIFFUSIVITY OF SOLID AT FUSION TEMPERATURE
ERR	=	ALLOWABLE ERROR
EW1,EW2	=	EMISSIVITY OF WALL
H	=	DIMENSIONLESS ENTHALPY
HSL	=	LATENT HEAT
IM	=	MAXIMUM ITERATIONS
IP	=	FLAG FOR PRINTING
NR	=	NUMBER OF RADIAL NODES
ORF	=	OVER RELAXATION FACTOR
PHI	=	DIMENSIONLESS EMISSIVE POWER
QF	=	DIMENSIONLESS RADIATIVE FLUX
RCP	=	RADIATION/CONDUCTION PARAMETER
RF	=	SOLID/LIQUID INTERFACE
S	=	DIMENSIONLESS RADIATIVE INTENSITY
SCAT	=	SCATTERING COEFFICIENT
SLI	=	DIMENSIONLESS SOLID/LIQUID INTERFACE
TAU	=	DIMENSIONLESS OPTICAL RADIUS
TF	=	TEMPERATURE OF FUSION
TH	=	DIMENSIONLESS TEMPERATURE
TSTP	=	TIME STEP

```
REAL TH(0:200),QF(0:200)
REAL TAU(200),S(200)
REAL TAU1(200)
REAL PHI(200),SI(200),PHII(200),QFI(200)
REAL C1(200, C2(200), H(200), T(200), DF(200), AK(200), PH(200)
REAL C5(200),C6(200),C7(200),C8(200),C9(200),C10(200)
REAL TFR(200)
INTEGER I,LL
LOGICAL L1
CALL BTIME
READ(20,*) DIF,CND, DEN, TF, HSL
READ(20,*)A,SCAT,BETA1
READ(20,*)EW1,EW2
READ(20,*) TI,TO
READ(20,*)RI,RO
READ(20,*)ORF,ERR
READ(20,*)HO,TSTP
READ(20,*)NR,MNTS
READ(20,*)IM,IP,ID,ICTRP
WRITE(21,*)'     '
WRITE(21,*)' OUTPUT OF CROP1T (P-1)'
WRITE(21,*)'     '
WRITE(21,*)'     '
WRITE(21,100) DIF,CND, DEN, TF, HSL
WRITE(21,105) A,SCAT
WRITE(21,107) EW1,EW2
WRITE(21,110) TI,TO
WRITE(21,120)RI,RO
WRITE(21,130)ORF,ERR
WRITE(21,140)HO,TSTP
WRITE(21,150)NR,MNTS
WRITE(21,160)IM,IP,ID
WRITE(21,*)' RADIATION TAKEN INTO ACCOUNT AFTER FOLLOWING NODES'
WRITE(21,*)ICTRP
IC=0
NTS=0
IP5=IP*10
SIGMA=0.1712E-08
AR=DIF*DEN*HSL/CND
TR=TO+460
BETA=A+SCAT
TAUI=RI*BETA
TAUO=RO*BETA
TAU(0)=TAUI
DTAU=(TAUO-TAUI)/NR
WRITE(21,*)' DTAU BECOMES'
WRITE(21,*)DTAU
DTAUS=DTAU*0.5
TH1=CND*(TI-TF)/DIF/DEN/HSL
TH2=CND*(TO-TF)/DIF/DEN/HSL
WRITE(21,*)' DMLESS INSIDE AND OUTSIDE WALL TEMPS. ARE:'
WRITE (21,*) TH1,TH2
DRT=DTAU*DTAU/TSTP
M=NR+1
```

```
      DO 10 I=1,M
      AK(I)=CND
      C1(I)=CND
      C2(I)=CND
   10 CONTINUE
      IF(ID.LT.1)GO TO 20
      WRITE(21,700) (C1(I), I=1,M)
      WRITE(21,700) (C2(I), I=1,M)
   20 CONTINUE
*    DO LOOP TO INITIALIZE TEMPERATURE, ENTHALPY, AND INTENSITY AT
*     ZERO TIME
      DO 30 I=1,M
      DF(I)=1.
      TH(I)=HO-1.
      T(I)=TH(I)*DIF*DEN*HSL/CND+TF+460.
      PH(I)=TH(I)*DF(I)+1.
      H(I)=PH(I)
      S(I)=0.
      QF(I)=0.
   30 CONTINUE
      IF (ID.LT.1) GO TO 35
      WRITE(21,700) (C1(I),C2(I), I=1,M)
      WRITE(21,700) (H(I), I=1,M)
      WRITE(21,700) (PH(I), I=1,M)
      WRITE(21,700) (TH(I), I=1,M)
      WRITE(21,700) (S(I),I=1,M)
      WRITE(21,700) (QF(I),I=1,M)
   35 CONTINUE
      WRITE(21,*)'      '
      WRITE(21,*)'      '
      WRITE(21,*)'   INITIAL DMLESS TEMP DISTRIBUTIONS ARE:'
      WRITE(21,700) (TH(I),I=1,M)
      WRITE(21,*)'   INITIAL DMLESS ENTHALPY DISTRIBUTIONS ARE:'
      WRITE(21,700) (PH(I), I=1,M)
      WRITE(21,*)'   INITIAL DMLESS INTENSITY DISTRIBUTIONS ARE:'
      WRITE(21,700) (S(I),I=1,M)
      WRITE(21,*)'      '
      WRITE(21,*)'      '
      RCP=0.25*CND*BETA/SIGMA/TR**3
      SR=CND**2*TR/DIF/DEN/HSL/4.
      WRITE(21,*)' CONDUCTION AND RADIATION INTERACTION PARAMETER IS'
      WRITE(21,*) RCP
      WRITE(21,*)' SR PARAMETER BECOMES'
      WRITE(21,*) SR
      WRITE(21,*)'    '
      WRITE(21,*)'    '
      DO 38 I=1,M
      TAU(I)=TAUI+(I-1)*DTAU
      TAU1(I)=TAU(I)/TAUI
      C5(I)=CND*DRT+1./DF(I)*((1.+0.5*DTAU/TAU(I))*C1(I)+(1.-0.5*DTAU/
     :      TAU(I))*C2(I))
      C6(I)=(1.+DTAU/2./TAU(I))*C1(I)
      C7(I)=(1.-0.5*DTAU/TAU(I))*C2(I)
      C8(I)=-0.5*DTAU*(1.+0.5*DTAU/TAU(I))
```

```
      C9(I)=-0.5*DTAU*DTAU/TAU(I)
      C10(I)=0.5*DTAU*(1.-0.5*DTAU/TAU(I))
   38 CONTINUE
      WRITE(21,*)' DMLESS RADIUS CO-ORDINATES FOR EACH NODE BECOME:'
      WRITE(21,700) (TAU1(I),I=1,M)
      WRITE(21,*)'      '
      LL=1
      LLI=1
      RF=TAUI
      TW2=TO+460
      TW1=TI+460
      PHW1=(TW1/TR)**4
      PHW2=TW2**4/TR**4
      PI=4.*ATAN(1.)
      E1=2./3.*(2.-EW1)/EW1
      E2=2./3.*(2.-EW2)/EW2
      F1=E2*0.5/DTAU
      F2=4.*PI*PHW2
      D1=0.5*E1/DTAU
      D3=4.*PI*PHW1
      ALAMDA=SCAT/(A+SCAT)
      AA=3.*(1.-ALAMDA)*DTAU*DTAU+2.
      BB=12.*PI*(1.-ALAMDA)*DTAU*DTAU
      DD=AA+(1.-0.5*DTAU/TAU(1))/D1
   40 IT=0
   95 CONTINUE
      EN=0
      ED=0
      DO 15 I=1,M
      IF(I.EQ.1.AND.LL.EQ.1)TH(I)=TH1
      IF(I.EQ.1) THEN
      TH(I)=TH1
      TH(I-1)=2.*TH1-TH(I+1)
      H(I)=TH(I)*DF(I)
      OH=H(I)
      GO TO 800
      END IF
      IF(I.EQ.M) THEN
      TH(I+1)=2.*TH2-TH(I-1)
      TH(I)=TH2
      END IF
      OH=H(I)
      L1=.FALSE.
      IF(I.GT.LL) THEN
      H(I)=(CND*DRT*PH(I)+C6(I)*TH(I+1)+C7(I)*TH(I-1))/C5(I)
      L1=.TRUE.
      END IF
      IF(L1) GO TO 65
      GO TO 910
      IF(LL.GE.2.AND.I.EQ.LL) THEN
      TH(I-1)=(TH(I)*(DTAU+DTAUS)-DTAU*TH2)/DTAUS
      END IF
  910 CONTINUE
      IF(I.EQ.LL.AND.LL.NE.LLI) QF(I+1)=0.
```

```
      H(I)=(CND*DRT*PH(I)+C6(I)*TH(I+1)+C7(I)*TH(I-1)+SR/RCP*(C8(I)*
     :     QF(I+1)+C9(I)*QF(I)+C10(I)*QF(I-1)))/C5(I)
   65 CONTINUE
      IF(H(I).LT.0.) GO TO 25
      H(I)=PH(I)+(C6(I)*TH(I+1)+C7(I)*TH(I-1))/CND/DRT
      IF(H(I).LT.0.) GO TO 25
      IF(H(I).LE.1.) GO TO 111
      H(I)=(PH(I)*CND*DRT+C6(I)*TH(I+1)+C7(I)*TH(I-1)+C5(I)-CND*DRT)
     :     /C5(I)
      TH(I)=(H(I)-1)/DF(I)
      GO TO 106
  111 TH(I)=0.
      GO TO 106
   25 IF(OH.LT.0.) H(I)=ORF*(H(I)-OH)+OH
      TH(I)=H(I)/DF(I)
      GO TO 800
      IP1=IP-1
      IF(IC.LT.IP1) GO TO 800
      WRITE(21,*)' DMLESS ENTHALPY AND TEMP ARE:'
      WRITE(21,*) H(I),TH(I)
  800 CONTINUE
      T(I)=TH(I)*DIF*DEN*HSL/CND+TF+460.
      PHI(I)=(T(I)/TR)**4
      IF(LLI.GE.ICTRP.AND.I.LE.LLI) GO TO 60
      GO TO 106
   60 CONTINUE
      L1=.FALSE.
      IF(I.EQ.1) THEN
      S(I)=(2.*S(I+1)+D3/D1*(1.-0.5*DTAU/TAU(I))+BB*PHI(I))/DD
      QF(I)=-1./6./DTAU/D1*S(I)+D3/6./DTAU/D1
      QF(I)=QF(I)/PI
      L1=.TRUE.
      END IF
      IF(L1) GO TO 106
      IF(I.EQ.LLI) THEN
      FF=AA+(1.+0.5*DTAU/TAU(I))/F1
      S(I)=((1.+0.5*DTAU/TAU(I))*F2/F1+2.*S(I-1)+BB*PHI(I))/FF
      QF(I)=-F2/F1/DTAU/6.+S(I)/6./F1/DTAU
      QF(I)=QF(I)/PI
      L1=.TRUE.
      END IF
      IF(L1) GO TO 106
      S(I)=((1.+0.5*DTAU/TAU(I))*S(I+1)+(1.-0.5*DTAU/TAU(I))*S(I-1)+
     :     BB*PHI(I))/AA
      QF(I)=-1./6./DTAU*(S(I+1)-S(I-1))
      QF(I)=QF(I)/PI
  106 CONTINUE
      EN=EN+ABS(H(I)-OH)
      ED=ED+ABS(H(I))
   15 CONTINUE
      IF(EN.LT.ED*ERR) GO TO 90
      GO TO 900
      WRITE(21,*)' WRITE ERROR AND ED*ERR FOR EACH ITERATION'
      WRITE(21,*) EN,ED*ERR
```

```
  880 CONTINUE
      WRITE(21,*)' DMLESS TEMPS,ENTHALPY,INTENSITY,HEAT FLUX'
      WRITE(21,700) (TH(I),I=1,M)
      WRITE(21,700) (H(I),I=1,M)
      WRITE(21,700)  (S(I),I=1,M)
      WRITE(21,700)  (QF(I),I=1,M)
  900 CONTINUE
      IT=IT+1
      IF(IT.LT.IM) GO TO 95
      WRITE(21,*)' CONVERGENCE HAS NOT BEEN ACHIEVED WITHIN ITERATIONS'
      CALL EXIT
   90 CONTINUE
      M1=M-1
C  THIS IS DO LOOP TO FIND SOLID/LIQUID INTERFACE :
      L1=.FALSE.
      DO 50 I=1,M1
      IF(H(I).LT.0..AND.H(I+1).GE.0.)THEN
      HI1=H(I+1)-H(I)
      RF=(TAU(I)*H(I+1)-TAU(I+1)*H(I))/HI1
      DTAUS=RF-TAU(I)
      LL=I
      LLI=I
      IF(DTAUS.GT.0.5*DTAU) LLI=I+1
      L1=.TRUE.
      END IF
      IF(L1) GO TO 45
   50 CONTINUE
      IF(H(M1-1).LT.0..AND.H(M1).LT.0.)THEN
      WRITE(21,*)' SOLIDIFICATION HAS BEEN COMPLETED'
      L1=.TRUE.
      CALL ETIME2(ISEC)
      WRITE(21,*)' THE ACCUMULATED CPU TIME BECOMES IN MSEC'
      WRITE(21,*) ISEC
      END IF
      IF(L1) CALL EXIT
   45 CONTINUE
      NTS=NTS+1
      IC=IC+1
      IF(IC.LT.IP) GO TO 2
      SM=0.
      HE=0.
      DO 1 I=1,M
      HI=HO
      HJ=AMAX1(0.,H(I))
      SM=SM+TAU(I)*DTAU*(HI-HJ)
      HE=HE+TAU(I)*DTAU*(HI-H(I))
    1 CONTINUE
      ER=EN/ED
      TP=TSTP*NTS
      TP1=TP*BETA1**2/BETA**2
      SLI=RF/TAUI
      QCI=-AR*BETA*CND*(TH(3)-TH1)*0.5/DTAU/SIGMA/TR**4
      QCRI=QCI+QF(1)
      WRITE(21,400) TP,IT,ER
```

```
      WRITE(21,*)' EQUIVALENT DMLESS TIME BECOMES'
      WRITE(21,*) TP1
      WRITE(21,500) RF
      WRITE(21,510) SLI
      WRITE(21,*)'  L AND DTAUS BECAME THE FOLLOWING  '
      WRITE(21,*), LLI,DTAUS
      WRITE(21,*)'     DMLESS TEMP DISTRIBUTIONS ARE :'
      WRITE(21,700) (TH(I),I=1,M,3)
      DO 6 I=1,M
      TFR(I)=TH(I)*AR/TR
    6 CONTINUE
      WRITE(21,*)' DMLESS TEMP (T-TF)/TR ARE:'
      WRITE(21,700) (TFR(I),I=1,M,3)
      WRITE(21,*)'    DMLESS ENTHALPY DISTRIBUTIONS ARE :'
      WRITE(21,700) (H(I),I=1,M,3)
      WRITE(21,*)' DMLESS RADIATIVE INTENSITIES BECOME:'
      WRITE(21,700) (S(I),I=1,M,3)
      WRITE(21,*)' DMLESS RAD. HEAT FLUX DISTRIBUTIONS ARE:'
      WRITE(21,700) (QF(I),I=1,M,3)
      WRITE(21,*)' DMLESS HEAT FLUXES FOR COND. ONLY,RAD. ONLY, AND
     :COND. & RAD. CASES AT INSIDE CYLINDER BECOME:'
      WRITE(21,*) QCI,QF(1),QCRI
      TIME=TP*BETA**2/DIF
      WRITE(22,*) TP1,SLI
      IF(TP.EQ.0.5*IP5*TSTP) THEN
      DO 9 K=1,M,3
      WRITE(58,*)TAU1(K),QF(K)
      WRITE(59,*)TAU1(K),TFR(K)
    9 CONTINUE
      END IF
      IF(TP.EQ.IP5*TSTP) THEN
      WRITE(21,710) IP5*TSTP
      DO 4 K=1,M,3
      WRITE(23,*) TAU1(K),TFR(K)
      WRITE(50,*) TAU1(K),S(K)
      WRITE(51,*) TAU1(K),QF(K)
    4 CONTINUE
      WRITE(21,700) (TFR(I),I=1,M,3)
      END IF
      IF(TP.EQ.2.0*IP5*TSTP) THEN
      DO 11 K=1,M,3
      WRITE(60,*)TAU1(K),QF(K)
      WRITE(61,*)TAU1(K),TFR(K)
   11 CONTINUE
      END IF
      IF(TP.EQ.4*IP5*TSTP) THEN
      WRITE(21,710) 3*IP5*TSTP
      DO 5 K=1,M,3
      WRITE(24,*) TAU1(K),TFR(K)
      WRITE(52,*) TAU1(K),S(K)
      WRITE(53,*) TAU1(K),QF(K)
    5 CONTINUE
      WRITE(21,700) (TFR(I),I=1,M,3)
      END IF
```

```
      IF(TP.EQ.5*IP5*TSTP) THEN
      DO 7 K=1,M,3
      WRITE(28,*) TAU1(K),TFR(K)
      WRITE(54,*) TAU1(K),S(K)
      WRITE(55,*) TAU1(K),QF(K)
    7 CONTINUE
      END IF
      IF(TP.EQ.6*IP5*TSTP) THEN
      DO 8 K=1,M,3
      WRITE(29,*) TAU1(K),TFR(K)
      WRITE(56,*) TAU1(K),S(K)
      WRITE(57,*) TAU1(K),QF(K)
    8 CONTINUE
      END IF
      WRITE(25,*) TP1,QCI*3.1546*SIGMA*TR**4
      WRITE(26,*) TP1,QF(1)*3.1546*SIGMA*TR**4
      WRITE(27,*) TP1,QCRI*3.1546*SIGMA*TR**4
      IC=0
    2 DO 3 I=1,M
      PH(I)=H(I)
    3 CONTINUE
      IF(NTS.LT.MNTS)GO TO 40
  100 FORMAT(' DIFFUSIVITY=',F10.3,'CONDUCTIVITY=',F10.3,'DENSITY=',
     C   F10.3,'FUSION TEMP=',F10.3,'LATENT HEAT=',F10.3)
  105 FORMAT(' ABSORPTION COEFF.=',F10.3,'SCATTERING COEFF.=',F10.3)
  107 FORMAT(' EMISSIVITY AT INSIDE WALL=',F10.3,' EMISSIVITY AT S/L
     : INTERFACE=',F10.3)
  110 FORMAT(' INSIDE TEMP=',F10.3,'OUTSIDE TEMP=',F10.3)
  120 FORMAT(' INSIDE RADIUS=',F10.3,'OUTSIDE RADIUS=',F10.3)
  130 FORMAT(' ORF=',F10.4,'ALLOWABLE ERROR=',F10.7)
  140 FORMAT(' INITIAL ASSUMED ENTHALPY=',F10.4,'TIME STEP=',F10.6)
  150 FORMAT(' NUMBER OF NODES=',I7,'MAX NO TIME STEP=',I7)
  160 FORMAT(' MAX ALLOWABLE INTER=',I5,'IPTH PRINT=',I5,'CONTROL TO
     CPRINT=',I5)
  200 FORMAT(5I5)
  400 FORMAT(1H1,'DMLESS TIME=',F8.4,3X,'ITERATIONS WITHIN CURRENT
     :TIME STEP=',I4,3X,'RELATIVE ERROR=',E12.5)
  460 FORMAT(1H1, ITER=',I4,3X,'ERROR=',E12.5)
  500 FORMAT(' SOLID/LIQUID INTERFACE R IS  ',F10.4)
  510 FORMAT(' DMLESS S/L INTERFACE RF/RI BECOME:',F10.4)
  700 FORMAT(1H ,16F8.4)
  710 FORMAT(' DMLESS TEMP (T-TF)/TR AT DMLESS TIME ',F8.4,' BECOME')
      CALL ETIME2(ISEC)
      WRITE(21,*)' THE ACCUMULATED CPU TIME BECOMES IN MSEC'
      WRITE(21,*) ISEC
      STOP
      END
EOF..
```

TWO-DIMENSIONAL COMPUTER PROGRAM

THIS PROGRAM CALCULATES THE TRANSIENT TEMP. DISTRIBUTION AND ENTHALPY DISTRIBUTIONS IN THE RADIAL/AXIAL DIRECTION FOR TWO-D CONCENTRIC CYLINDERS IN THE STEFAN PROBLEM WITH CONDUCTION IN WHOLE REGION AND RADIATION IN SOLID REGION. THE LOCATION OF THE S/L INTERFACE, SOLIDIFIED VOLUME, AND HEAT EXTRACTED CAN BE OBTAINED AFTER SOME TIME STEPS. THE ENTHALPY MODEL EQUATION HAS BEEN SOLVED SIMULTANEOUSLY WITH RTE THAT HAS BEEN TRANSFORMED INTO CONVENIENT DIFFERENTIAL EQUATIONS BY USING P-1 APPROXIMATIONS.

DESCRIPTION OF MAIN PARAMETERS

A	=	ABSORPTION COEFFICIENT
BETA	=	EXTINCTION COEFFICIENT
C1,C2		
C3,C4	=	CONDUCTIVITY OF MEDIUM
CND	=	CONDUCTIVITY OF SOLID AT FUSION TEMPERATURE
DEN	=	DENSITY OF SOLID AT FUSION TEMPERATURE
DIF	=	DIFFUSIVITY OF SOLID AT FUSION TEMPERATURE
ERR	=	ALLOWABLE ERROR
EW1,EW2		
EW3,EW4	=	EMISSIVITY OF WALL
H	=	DIMENSIONLESS ENTHALPY
HSL	=	LATENT HEAT
IM	=	MAXIMUM ITERATIONS
IP	=	FLAG FOR PRINTING
NR	=	NUMBER OF RADIAL NODES
NZ	=	NUMBER OF AXIAL NODES
ORF	=	OVER RELAXATION FACTOR
PHI	=	DIMENSIONLESS EMISSIVE POWER
QFR	=	DIMENSIONLESS RADIAL RADIATAIVE FLUX
QFZ	=	DIMENSIONLESS AXIAL RADIATIVE FLUX
RCP	=	RADIATION/CONDUCTION PARAMETER
RF	=	SOLID/LIQUID INTERFACE
S	=	DIMENSIONLESS RADIATIVE INTENSITY
SCAT	=	SCATTERING COEFFICIENT
SLI	=	DIMENSIONLESS SOLID/LIQUID INTERFACE
TAU	=	DIMENSIONLESS OPTICAL RADIUS
TF	=	TEMPERATURE OF FUSION
TH	=	DIMENSIONLESS TEMPERATURE
TSTP	=	TIME STEP
Z	=	AXIAL DISTANCE

```
REAL TH(0:50,0:50),QFR(0:50,0:50),QFZ(0:50,0:50)
REAL TAU(50),TAU1(50),ETA(50),ETA1(50)
REAL PHI(50,50),S(50,50)
REAL C1(50,50),C2(50,50),DF(50,50),AK(50,50)
REAL H(50,50),T(50,50),PH(50,50)
REAL C5(50,50),C6(50,50),C7(50,50),C8(50,50),C9(50,50),C10(50)
REAL RF(50),C3(50,50),C4(50,50),C11(50,C12(50)
REAL G3(50),P3(50),F2(50)
REAL TFR(50,50),SLI(50),QCI(50),QCRI(50)
INTEGER LL(50),LLI(50),L2(50)
LOGICAL L1
CALL BTIME
READ(20,*) DIF,CND, DEN, TF, HSL
READ(20,*)A,SCAT,BETA1
READ(20,*)EW1,EW2,EW3,EW4
READ(20,*) TI,TO
READ(20,*)RI,RO,Z
READ(20,*)ORF,ERR
READ(20,*)HO,TSTP
READ(20,*)NR,NZ,MNTS
READ(20,*)IM,IP,ID,ICTRP
WRITE(21,*)'       '
WRITE(21,*)' OUTPUT OF CRP12D (P-1)'
WRITE(21,*)'       '
WRITE(21,*)'       '
WRITE(21,100) DIF,CND, DEN, TF, HSL
WRITE(21,105) A,SCAT
WRITE(21,107) EW1,EW2
WRITE(21,108) EW3,EW4
WRITE(21,110) TI,TO
WRITE(21,120)RI,RO,Z
WRITE(21,130)ORF,ERR
WRITE(21,140)HO,TSTP
WRITE(21,150)NR,MNTS,NZ
WRITE(21,160)IM,IP,ID
WRITE(21,*)' RADIATION TAKEN INTO ACCOUNT AFTER FOLLOWING NODES'
WRITE(21,*)ICTRP
IC=0
NTS=0
IP5=IP*2
SIGMA=0.1712E-08
AR=DIF*DEN*HSL/CND
TR=TO+460
BETA=A+SCAT
TAUI=RI*BETA
TAUO=RO*BETA
TAU(0)=TAUI
DTAU=(TAUO-TAUI)/NR
ETAL=0.
ETAR=Z*BETA
DETA=(ETAR-ETAL)/NZ
DTZ2=(DTAU/DETA)**2
DTZ=0.5*DTAU**2/DETA
WRITE(21,*)' DTAU BECOMES'
```

```
      WRITE(21,*)DTAU
      DTAUS=DTAU*0.5
      TH1=CND*(TI-TF)/DIF/DEN/HSL
      TH2=CND*(TO-TF)/DIF/DEN/HSL
      WRITE(21,*)' DMLESS INSIDE AND OUTSIDE WALL TEMPS. ARE:'
      WRITE(21,*) TH1,TH2
      DRT=DTAU*DTAU/TSTP
      M=NR+1
      N=NZ+1
      DO 10 I=1,M
      DO 10 J=1,N
      AK(I,J)=CND
      C1(I,J)=CND
      C2(I,J)=CND
      C3(I,J)=CND
      C4(I,J)=CND
   10 CONTINUE
      IF(ID.LT.1)GO TO 20
      WRITE(21,700) ((C1(I,J),J=1,N),I=1,M)
      WRITE(21,700) ((C2(I,J),J=1,N),I=1,M)
      WRITE(21,700) ((C3(I,J),J=1,N),I=1,M)
      WRITE(21,700) ((C4(I,J),J=1,N),I=1,M)
   20 CONTINUE
*    DO LOOP TO INITIALIZE TEMPERATURE ,ENTHALPY,AND INTENSITY AT
*     ZERO TIME
      DO 30 I=1,M
      DO 30 J=1,N
      DF(I,J)=1.
      TH(I,J)=HO-1.
      T(I,J)=TH(I,J)*DIF*DEN*HSL/CND+TF+460.
      PH(I,J)=TH(I,J)*DF(I,J)+1.
      H(I,J)=PH(I,J)
      S(I,J)=0.
      QFR(I,J)=0.
      QFZ(I,J)=0.
   30 CONTINUE
      IF (ID.LT.1) GO TO 35
      WRITE(21,700) ((C1(I,J),C2(I,J),C3(I,J),C4(I,J), J=1,N),I=1,M)
      WRITE(21,700) ((H(I,J), J=1,N),I=1,M)
      WRITE(21,700) ((PH(I,J), J=1,N),I=1,M)
      WRITE(21,700) ((TH(I,J), J=1,N),I=1,M)
      WRITE(21,700) ((S(I,J),J=1,N),I=1,M)
      WRITE(21,700) ((QFR(I,J),J=1,N),I=1,M)
      WRITE(21,700) ((QFZ(I,J),J=1,N),I=1,M)
   35 CONTINUE
      WRITE(21,*)'      '
      WRITE(21,*)'      '
      WRITE(21,*)'   INITIAL DMLESS TEMP DISTRIBUTIONS ARE :'
      DO 31 I=1,M,2
      WRITE(21,700) (TH(I,J),J=1,N,2)
   31 CONTINUE
      WRITE(21,*)'   INITIAL DMLESS ENTHALPY DISTRIBUTIONS ARE :'
      DO 32 I=1,M,2
```

```
      WRITE(21,700) (PH(I,J),J=1,N,2)
   32 CONTINUE
      WRITE(21,*)'   INITIAL DMLESS INTENSITY DISTRIBUTIONS ARE:'
      DO 33 I=1,M,2
      WRITE(21,700) (S(I,J),J=1,N,2
   33 CONTINUE
      WRITE(21,*)'       '
      WRITE(21,*)'       '
      RCP=0.25*CND*BETA/SIGMA/TR**3
      SR=CND**2*TR/DIF/DEN/HSL/4.
      WRITE(21,*)'  CONDUCTION AND RADIATION INTERACTION PARAMETER IS'
      WRITE(21,*) RCP
      WRITE(21,*)'  SR PARAMETER BECOMES'
      WRITE(21,*) SR
      WRITE(21,*)'    '
      WRITE(21,*)'    '
      DO 36 J=1,N
      ETA(J)=ETAL+(J-1)*DETA
      ETA1(J)=ETA(J)/ETAR
   36 CONTINUE
      DO 38 I=1,M
      TAU(I)=TAUI+(I-1)*DTAU
      TAU1(I)=TAU(I)/TAUI
      DO 38 J=1,N
      C5(I,J)=CND*DRT+1./DF(I,J)*((1.+0.5*DTAU/TAU(I))*C1(I,J)
     :        +(1.-0.5*DTAU/TAU(I))*C2(I,J)+DTZ2*C3(I,J)+DTZ2*C4(I,J))
      C6(I,J)=(1.+DTAU/2./TAU(I))*C1(I,J)
      C7(I,J)=(1.-0.5*DTAU/TAU(I))*C2(I,J)
      C8(I,J)=DTZ2*C3(I,J)
      C9(I,J)=DTZ2*C4(I,J)
      C10(I)=-0.5*DTAU*(1.+0.5*DTAU/TAU(I))
      C11(I)=0.5*DTAU*(1.-0.5*DTAU/TAU(I))
      C12(I)=-DTAU**2*0.5/TAU(I)
   38 CONTINUE
      WRITE(21,*)'  DMLESS RADIUS CO-ORDINATES FOR EACH NODE BECOME:'
      WRITE(21,700) (TAU1(I),I=1,M,2)
      WRITE(21,*)'  DMLESS AXIAL CO-ORDINATES FOR EACH NODE BECOME:'
      WRITE(21,700) (ETA1(J),J=1,N,2)
      WRITE(21,*)'       '
      DO 39 J=1,N
      LL(J)=1
      LLI(J)=1
      RF(J)=TAUI
   39 CONTINUE
      TW2=TO+460
      TW1=TI+460
      PHW1=(TW1/TR)**4
      PHW2=TW2**4/TR**4
      PI=4.*ATAN(1.)
      E1=2./3.*(2.-EW1)/EW1
      E2=2./3.*(2.-EW2)/EW2
      E3=2./3.*(2.-EW3)/EW3
      E4=2./3.*(2.-EW4)/EW4
      F1=E2*0.5/DTAU
```

```
      D1=0.5*E1/DTAU
      D3=4.*PI*PHW1
      ALAMDA=SCAT/(A+SCAT)
      AA=3.*(1.-ALAMDA)*DTAU*DTAU+2.+2.*DTZ2
      BB=12.*PI*(1.-ALAMDA)*DTAU*DTAU
      DD=AA+(1.-0.5*DTAU/TAU(1))/D1
      G1=0.5*E3/DETA
      GG=AA+DTZ2/G1
      DDG=DD+DTZ2/G1
      P1=0.5*E4/DETA
      PP=AA+DTZ2/P1
      DDP=DD+DTZ2/P1
   40 IT=0
   95 CONTINUE
      EN=0
      ED=0
      DO 15 I=1,M
      DO 15 J=1,N
      IF(I.EQ.1.AND.LL(J).EQ.1)TH(I,J)=TH1
      IF(I.EQ.1) THEN
      TH(I,J)=TH1
      TH(I-1,J)=2.*TH1-TH(I+1,J)
      H(I,J)=TH(I,J)*DF(I,J)
      OH=H(I,J)
      GO TO 800
      END IF
      IF(I.EQ.M) THEN
      TH(I+1,J)=2.*TH2-TH(I-1,J)
      TH(I,J)=TH2
      H(I,J)=TH(I,J)*DF(I,J)+1.
      OH=H(I,J)
      GO TO 800
      END IF
      IF(J.EQ.1.AND.I.NE.M) TH(I,J-1)=TH(I,J+1)
      IF(J.EQ.N.AND.I.NE.M) TH(I,J+1)=TH(I,J-1)
      OH=H(I,J)
      L1=.FALSE.
      IF(I.GT.LL(J)) THEN
      H(I,J)=(CND*DRT*PH(I,J)+C6(I,J)*TH(I+1,J)+C7(I,J)*TH(I-1,J)
     :       +C8(I,J)*TH(I,J+1)+C9(I,J)*TH(I,J-1))/C5(I,J)
      L1=.TRUE.
      END IF
      IF(L1) GO TO 65
      GO TO 910
      IF(LL(J).GE.2.AND.I.EQ.LL(J)) THEN
      TH(I-1,J)=(TH(I,J)*(DTAU+DTAUS)-DTAU*TH2)/DTAUS
      END IF
  910 CONTINUE
      IF(I.EQ.LL(J).AND.LL(J).NE.LLI(J)) QFR(I+1,J)=0.
      H(I,J)=(CND*DRT*PH(I,J)+C6(I,J)*TH(I+1,J)+C7(I,J)*TH(I-1,J)
     :       +C8(I,J)*TH(I,J+1)+C9(I,J)*TH(I,J-1) +SR/RCP*(C10(I)*
     :       QFR(I+1,J)+C11(I)*QFR(I,J)-DTZ*QFZ(I,J+1)+DTZ*QFZ(I,J-1)))
     :       /C5(I,J)
   65 CONTINUE
```

```
      IF(H(I,J).LT.0.) GO TO 25
      H(I,J)=PH(I,J)+(C6(I,J)*TH(I+1,J)+C7(I,J)*TH(I-1,J)+C8(I,J)*
     :       TH(I,J+1)+C9(I,J)*TH(I,J-1))/CND/DRT
      IF(H(I,J).LT.0.) GO TO 25
      IF(H(I,J).LE.1.) GO TO 111
      H(I,J)=(PH(I,J)*CND*DRT+C6(I,J)*TH(I+1,J)+C7(I,J)*TH(I-1,J)
     :       +C5(I,J)-CND*DRT+C8(I,J)*TH(I,J+1)+C9(I,J)*TH(I,J-1))
     :       /C5(I,J)
      TH(I,J)=(H(I,J)-1)/DF(I,J)
      GO TO 106
  111 TH(I,J)=0.
      GO TO 106
   25 IF(OH.LT.0.) H(I,J)=ORF*(H(I,J)-OH)+OH
      TH(I,J)=H(I,J)/DF(I,J)
      GO TO 800
      IP1=IP-1
      IF(IC.LT.IP1) GO TO 800
      WRITE(21,*)'  DMLESS ENTHALPY AND TEMP ARE:'
      WRITE(21,*) H(I,J),TH(I,J)
  800 CONTINUE
      T(I,J)=TH(I,J)*DIF*DEN*HSL/CND+TF+460.
      PHI(I,J)=(T(I,J)/TR)**4
      IF(LLI(J).GE.ICTRP.AND.I.LE.LLI(J)) GO TO 60
      GO TO 106
   60 CONTINUE
      L1=.FALSE.
      IF(I.EQ.1) THEN
      IF(J.EQ.1) THEN
      G3(I)=4.*PI*PHI(I,J)
      S(I,J)=(2.*S(I+1,J)+D3/D1*(1.-0.5*DTAU/TAU(I))+2.*DTZ2*
     :       S(I,J+2)+G3(I)/G1*DTZ2+BB*PHI(I,J))/DDG
      QFR(I,J)=-S(I,J)/(6.*PI*D1*DTAU)+D3/(6.*PI*D1*DTAU)
      QFZ(I,J)=(-S(I,J)+G3(I))/(6.*PI*DETA*G1)
      L1=.TRUE.
      END IF
      IF(L1) GO TO 106
      IF(J.EQ.N) THEN
      P3(I)=4.*PI*PHI(I,J)
      S(I,J)=(2.*S(I+1,J)+D3/D1*(1.-0.5*DTAU/TAU(I))+2.*DTZ2*
     :       S(I,J-1)+DTZ2*P3(I)/P1+BB*PHI(I,J))/DDP
      QFR(I,J)=-S(I,J)/(6.*PI*D1*DTAU)+D3/(6.*PI*D1*DTAU)
      QFZ(I,J)=(S(I,J)-P3(I))/(6.*PI*DETA*P1)
      L1=.TRUE.
      END IF
      IF(L1) GO TO 106
      S(I,J)=(2.*S(I+1,J)+D3/D1*(1.-0.5*DTAU/TAU(I))+DTZ2*S(I,J+1)
     :       +DTZ2*S(I,J-1)+BB*PHI(I,J))/DD
      QFR(I,J)=-S(I,J)/(6.*PI*D1*DTAU)+D3/(6.*PI*D1*DTAU)
      QFZ(I,J)=-(S(I,J+1)-S(I,J-1))/(6.*PI*DETA)
      L1=.TRUE.
      END IF
      IF(L1) GO TO 106
      IF(I.EQ.LLI(J)) THEN
      IF(J.EQ.1) THEN
```

```
FF=AA+(1.+0.5*DTAU/TAU(LLI(J)))/F1
FFG=FF+DTZ2/G1
F2(J)=4*PI*PHW2
G3(I)=4*PI*PHI(I,J)
S(I,J)=(F2(J)/F1*(1.+0.5*DTAU/TAU(I))+2.*S(I-1,J)+2.*DTZ2*
:       S(I,J+1)+DTZ2*G3(I)/G1+BB*PHI(I,J))/FFG
QFR(I,J)=-F2(J)/(6.*PI*DTAU*F1)+S(I,J)/(6.*PI*DTAU*F1)
QFZ(I,J)=-S(I,J)/(6.*PI*DETA*G1)+G3(I)/(6.*PI*DETA*G1)
L1=.TRUE.
END IF
IF(L1) GO TO 106
IF(J.EQ.N) THEN
FF=AA+(1.+0.5*DTAU/TAU(LLI(J)))/F1
FFP=FF+DTZ2/P1
F2(J)=4.*PI*PHI(I,J)
P3(I)=4.*PI*PHI(I,J)
S(I,J)=((1.+0.5*DTAU/TAU(I))*F2(J)/F1+2.*S(I-1,J)+2.*DTZ2*
:       S(I,J-1)+DTZ2*P3(I)/P1+BB*PHI(I,J))/FFP
QFR(I,J)=-F2(J)/(6.*PI*DTAU*F1)+S(I,J)/(6.*PI*DTAU*F1)
QFZ(I,J)=(S(I,J)-P3(I))/(6.*PI*DETA*P1)
L1=.TRUE.
END IF
IF(L1) GO TO 106
FF=AA+(1.+0.5*DTAU/TAU(LLI(J)))/F1
F2(J)=4.*PI*PHI(I,J)
S(I,J)=((1.+0.5*DTAU/TAU(LLI(J)))*F2(J)/F1+2.*S(I-1,J)+
:       DTZ2*S(I,J+1)+DTZ2*S(I,J-1)+BB*PHI(I,J))/FF
QFR(I,J)=(-F2(J)+S(I,J))/(6.*PI*DTAU*F1)
QFZ(I,J)=(-S(I,J+1)+S(I,J-1))/(6.*PI*DETA)
L1=.TRUE.
END IF
IF(L1) GO TO 106
IF(J.EQ.1) THEN
G3(I)=4.*PI*PHI(I,J)
S(I,J)=((1.+0.5*DTAU/TAU(I))*S(I+1,J)+(1.-0.5*DTAU/TAU(I))
:       *S(I-1,J)+2.*DTZ2*S(I,J+1)+G3(I)/G1*DTZ2+BB*PHI(I,J))
:       /GG
QFR(I,J)=(-S(I+1,J)+S(I-1,J))/(6.*PI*DTAU)
QFZ(I,J)=(-S(I,J)+G3(I))/(6.*PI*DETA*G1)
L1=.TRUE.
END IF
IF(L1) GO TO 106
IF (J.EQ.N) THEN
P3(I)=4.*PI*PHI(I,J)
S(I,J)=((1.+0.5*DTAU/TAU(I))*S(I+1,J)+(1.-0.5*DTAU/TAU(I))
:       *S(I-1,J)+2.*DTZ2*S(I,J-1)+DTZ2*P3(I)/P1+BB*PHI(I,J))
:       /PP
QFR(I,J)=(-S(I+1,J)+S(I-1,J))/(6.*PI*DTAU)
QFZ(I,J)=(S(I,J)-P3(I))/(6.*PI*DETA*P1)
L1=.TRUE.
END IF
IF(L1) GO TO 106
S(I,J)=((1.+0.5*DTAU/TAU(I))*S(I+1,J)+(1.-0.5*DTAU/TAU(I))*
:       S(I-1,J)+DTZ2*S(I,J+1)+DTZ2*S(I,J-1)+BB*PHI(I,J))/AA
```

```
      QFR(I,J)=(-S(I+1,J)+S(I-1,J))/(6.*PI*DTAU)
      QFZ(I,J)=(-S(I,J+1)+S(I,J-1))/(6.*PI*DETA)
  106 CONTINUE
      EN=EN+ABS(H(I,J)-OH)
      ED=ED+ABS(H(I,J))
   15 CONTINUE
      IF(EN.LT.ED*ERR) GO TO 90
      GO TO 900
      WRITE(21,*)'  WRITE ERROR AND ED*ERR FOR EACH ITERATION'
      WRITE(21,*) EN,ED*ERR
  880 CONTINUE
      WRITE(21,*)'  DMLESS TEMPS,ENTHALPY,INTENSITY,HEAT FLUX'
      WRITE(21,700) ((TH(I,J),J=1,N),I=1,M)
      WRITE(21,700) ((H(I,J),J=1,N),I=1,M)
      WRITE(21,700) ((S(I,J),J=1,N),I=1,M)
      WRITE(21,700) ((QFR(I,J),J=1,N),I=1,M)
      WRITE(21,700) ((QFZ(I,J),J=1,N),I=1,M)
  900 CONTINUE
      IT=IT+1
      IF(IT.LT.IM) GO TO 95
      WRITE(21,*)' CONVERGENCE HAS NOT BEEN ACHIEVED WITHIN ITERATIONS'
      CALL EXIT
   90 CONTINUE
      M1=M-1
c  THIS IS DO LOOP TO FIND SOLID/LIQUID INTERFACE :
      DO 50 I=1,M1
      DO 50 J=1,N
      IF(H(I,J).LT.0..AND.H(I+1,J).GE.0.)THEN
      HI1=H(I+1,J)-H(I,J)
      RF(J)=(TAU(I)*H(I+1,J)-TAU(I+1)*H(I,J))/HI1
      DTAUS=RF(J)-TAU(I)
      LL(J)=I
      LLI(J)=I
      IF(DTAUS.GT.0.5*DTAU) LLI(J)=I+1
      END IF
   50 CONTINUE
      GO TO 45
      IF(H(M1-1,J).LT.0..AND.H(M1,J).LT.0.)THEN
      WRITE(21,*)'  SOLIDIFICATION HAS BEEN COMPLETED FOR ONE J'
      L1=.TRUE.
      CALL ETIME2(ISEC)
      WRITE(21,*)' THE ACCUMULATED CPU TIME BECOMES IN MSEC'
      WRITE(21,*) ISEC
      END IF
      IF(L1) CALL EXIT
   45 CONTINUE
      NTS=NTS+1
      IC=IC+1
      IF(IC.LT.IP) GO TO 2
      SM=0.
      HE=0.
      DO 1 I=1,M
      DO 1 J=1,N
      HI=HO
```

```
      HJ=AMAX1(0.,H(I,J))
      SM=SM+TAU(I)*DTAU*(HI-HJ)
      HE=HE+TAU(I)*DTAU*(HI-H(I,J))
    1 CONTINUE
      ER=EN/ED
      TP=TSTP*NTS
      TP1=TP*BETA1**2/BETA**2
      DO 12 J=1,N
      SLI(J)=RF(J)/TAUI
      QCI(J)=-AR*BETA*CND*(TH(3,J)-TH1)*0.5/DTAU/SIGMA/TR**4
      QCRI(J)=QCI(J)+QFR(1,J)
   12 CONTINUE
      WRITE(21,400) TP,ER
      WRITE(21,460) IT
      WRITE(21,*)' EQUIVALENT CMLESS TIME BECOMES'
      WRITE(21,*) TP1
      WRITE(21,500)
      WRITE(21,700) (RF(J),J=1,N,2)
      WRITE(21,510)
      WRITE(21,700) (SLI(J),J=1,N,2)
      WRITE(21,*)'  L AND DTAUS BECAME THE FOLLOWING  '
      WRITE(21,200) (LLI(J),J=1,N,2)
      WRITE(21,*)'    DMLESS TEMP DISTRIBUTIONS ARE :'
      DO 13 I=1,M
      WRITE(21,700) (TH(I,J),J=1,N,2)
   13 CONTINUE
      DO 6 I=1,M
      DO 6 J=1,N
      TFR(I,J)=TH(I,J)*AR/TR
    6 CONTINUE
      WRITE(21,*)' DMLESS TEMP (T-TF)/TR ARE;'
      DO 70 I=1,M,2
      WRITE(21,700) (TFR(I,J),J=1,N,2)
   70 CONTINUE
      WRITE(21,*)'    DMLESS ENTHALPY DISTRIBUTIONS ARE :'
      DO 71 I=1,M,2
      WRITE(21,700) (H(I,J),J=1,N,2)
   71 CONTINUE
      WRITE(21,*)'  DMLESS RADIATIVE INTENSITIES BECOME:'
      DO 72 I=1,M,2
      WRITE(21,700) (S(I,J),J=1,N,2)
   72 CONTINUE
      WRITE(21,*)' DMLESS RADIAL RAD. HEAT FLUX DISTRIBUTIONS ARE:'
      DO 73 I=1,M,2
      WRITE(21,700) (QFR(I,J),J=1,N,2)
   73 CONTINUE
      WRITE(21,*)'  DMLESS AXIAL RAD. HEAT FLUX DISTRIBUTIONS ARE:'
      DO 74 I=1,M,2
      WRITE(21,700) (QFZ(I,J),J=1,N,2)
   74 CONTINUE
      WRITE(21,*)' DMLESS HEAT FLUXES FOR COND. ONLY,RAD. ONLY, AND
     : COND. & RAD. CASES AT INSIDE CYLINDER BECOME:'
      WRITE(21,700) (QCI(J),J=1,N,2)
      WRITE(21,700) (QFR(1,J),J=1,N,2)
```

```
      WRITE(21,700)(QCRI(J),J=1,N,2)
      TIME=TP*BETA**2/DIF
      IF(TP.EQ.0.5*IP5*TSTP) THEN
      DO 51 J=1,N
      L2(J)=LLI(J)/2
      WRITE(22,*) ETA1(J),SLI(J)
      WRITE(50,*) ETA1(J),QCI(J)
      WRITE(54,*) ETA1(J),QFR(1,J)
      WRITE(58,*) ETA1(J),QCRI(J)
      WRITE(62,*) ETA1(J),QFZ(L2(J),J)
   51 CONTINUE
      DO 52 I=1,M
      J2=M/2
      WRITE(26,*) TAU1(I),TFR(I,J2)
      WRITE(66,*) TAU1(I),QFR(I,J2)
   52 CONTINUE
      END IF
      IF(TP.EQ.IP5*TSTP) THEN
      WRITE(21,710) IP5*TSTP
      DO 53 J=1,N
      L2(J)=LLI(J)/2.
      WRITE(23,*) ETA1(J),SLI(J)
      WRITE(51,*) ETA1(J),QCI(J)
      WRITE(55,*) ETA1(J),QFR(1,J)
      WRITE(59,*) ETA1(J),QCRI(J)
      WRITE(63,*) ETA1(J),QFZ(L2(J),J)
   53 CONTINUE
      DO 54 I=1,M
      J2=M/2
      WRITE(27,*) TAU1(I),TFR(I,J2)
      WRITE(67,*) TAU1(I),QFR(I,J2)
   54 CONTINUE
      DO 75 I=1,M,2
      WRITE(21,700) (TFR(I,J),J=1,N,2)
   75 CONTINUE
      END IF
      IF(TP.EQ.2.0*IP5*TSTP) THEN
      DO 55 J=1,N
      L2(J)=LLI(J)/2
      WRITE(24,*) ETA1(J),SLI(J)
      WRITE(52,*) ETA1(J),QCI(J)
      WRITE(56,*) ETA1(J),QFR(1,J)
      WRITE(60,*) ETA1(J),QCRI(J)
      WRITE(64,*) ETA1(J),QFZ(L2(J),J)
   55 CONTINUE
      DO 56 I=1,M
      WRITE(28,*) TAU1(I),TFR(I,J2)
      WRITE(68,*) TAU1(I),QFR(I,J2)
   56 CONTINUE
      END IF
      IF(TP.EQ.3*IP5*TSTP) THEN
      WRITE(21,710) 3*IP5*TSTP
      DO 57 J=1,N
      L2(J)=LLI(J)/2
```

```
      WRITE(25,*) ETA1(J),SLI(J)
      WRITE(53,*) ETA1(J),QCI(J)
      WRITE(57,*) ETA1(J),QFR(1,J)
      WRITE(61,*) ETA1(J),QCRI(J)
      WRITE(65,*) ETA1(J),QFZ(L2(J),J)
   57 CONTINUE
      DO 58 I=1,M
      WRITE(29,*) TAU1(I),TFR(I,J2)
      WRITE(69,*) TAU1(I),QFR(I,J2)
   58 CONTINUE
      DO 76 I=1,M,2
      WRITE(21,700) (TFR(I,J),J=1,N,2)
   76 CONTINUE
      END IF
      IC=0
    2 DO 3 I=1,M
      DO 3 J=1,N
      PH(I,J)=H(I,J)
    3 CONTINUE
      IF(NTS.LT.MNTS)GO TO 40
  100 FORMAT(1H ,'DIFFUSIVITY=',F10.3,'CONDUCTIVITY=',F10.3,'DENSITY=',
     C   F10.3,'FUSION TEMP=',F10.3,'LATENT HEAT=',F10.3)
  105 FORMAT(1H ,'ABSORPTION COEFF.=',F10.3,'SCATTERING COEFF.=',F10.3)
  107 FORMAT(1H ,'EMISSIVITY AT INSIDE WALL=',F10.3,'EMISSIVITY AT S/L
     : INTERFACE=',F10.3)
  108 FORMAT(1H ,'EMISSIVITY AT LEFT SURFACE=',F10.3,'EMISSIVITY AT
     "RIGHT SURFACE=',F10.3)
  110 FORMAT(1H ,'INSIDE TEMP=',F10.3,'OUTSIDE TEMP=',F10.3)
  120 FORMAT(1H ,'INSIDE RADIUS=',F10.3,'OUTSIDE RADIUS=',F10.3,
     : 'AXIAL LENGTH OF CYLINDER=',F10.3)
  130 FORMAT(1H ,'ORF=',F10.4,'ALLOWABLE ERROR=',F10.8)
  140 FORMAT(1H ,'INITIAL ASSUMED ENTHALPY=',F10.4,'TIME STEP=',F10.5)
  150 FORMAT(1H ,'NUMBER OF RADIAL NODES=',I7,'MAX NO TIME STEP=',I7,
     : 'NUMBER OF AXIAL NODES=',I7)
  160 FORMAT(1H ,'MAX ALLOWABLE ITER=',I5,'IPTH PRINT=',I5,'CONTROL TO
     CPRINT=',I5)
  200 FORMAT(16I8)
  400 FORMAT(1H1,'DMLESS TIME=',F8.4,3X,'RELATIVE ERROR=,'E12.5)
  460 FORMAT(1H ,'NUMBER OF ITERATIONS WITHIN CURRENT TIME STEP IS ',I4)
  500 FORMAT(1H ,'SOLID/LIQUID INTERFACE R IS  ')
  510 FORMAT(1H ,'DMLESS S/L INTERFACE RF/RI BECOME:')
  700 FORMAT(1H ,16F8.4)
  710 FORMAT(' DMLESS TEMP (T-TF)/TR AT DMLESS TIME ',F8.4,' BECOME')
      CALL ETIME2(ISEC)
      WRITE(21,*)' THE ACCUMULATED CPU TIME BECOMES IN MSEC'
      WRITE(21,*) ISEC
      STOP
      END
EOF..
```